Climate Monitoring and Diagnostics Laboratory

No. 19

Summary Report 1990

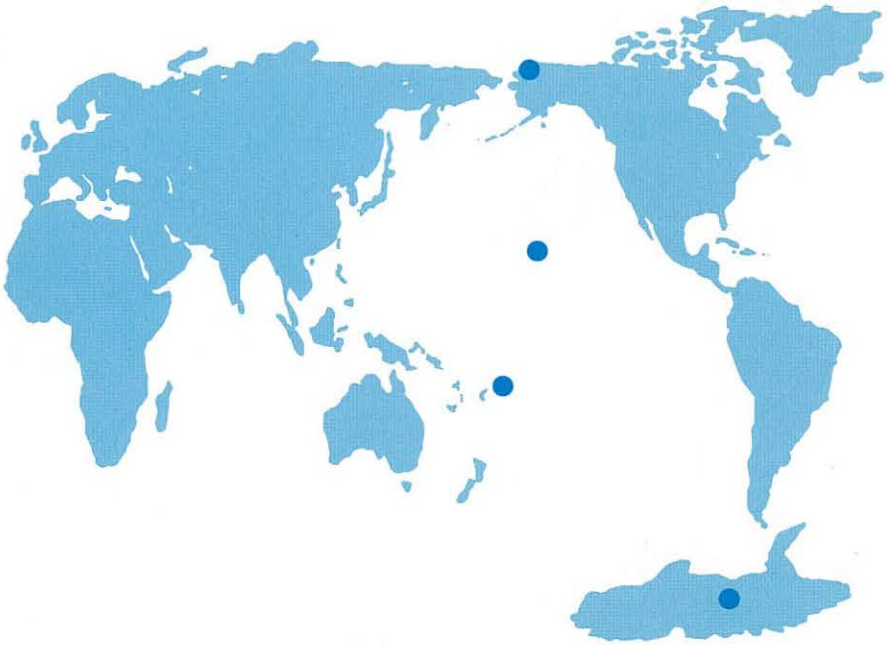

U.S. DEPARTMENT
OF COMMERCE

NATIONAL
OCEANIC AND
ATMOSPHERIC
ADMINISTRATION

ENVIRONMENTAL
RESEARCH
LABORATORIES

Climate Monitoring and Diagnostics Laboratory No. 19

Summary Report 1990

Eldon E. Ferguson, Editor
Rita M. Rosson, Assistant Editor

Boulder, Colorado

December 1991

U.S. DEPARTMENT OF COMMERCE
Robert A. Mosbacher, Secretary

National Oceanic and Atmospheric Administration
John A. Knauss, Under Secretary for Oceans and Atmosphere/Administrator

Environmental Research Laboratories
Joseph O. Fletcher, Director

NOTICE

Mention of a commercial company or product does not constitute an endorsement by NOAA Environmental Research Laboratories. Use for publicity or advertising purposes of information from this publication concerning proprietary products or the tests of such products is not authorized.

For sale by the National Technical Information Service, 5285 Port Royal Road
Springfield, VA 22161

Contents

DUPLICATE
WITHDRAWN

CMDL Staff, 1990 vi

CMDL Station Information vii

1. Introduction 1

2. Observatory Reports 2
   2.1. Mauna Loa 2
      2.1.1. Operations 2
      2.1.2. Programs 2
   2.2. Barrow 7
      2.2.1. Operations 7
      2.2.2. Programs 8
   2.3. Samoa 12
      2.3.1. Operations 12
      2.3.2. Programs 12
   2.4. South Pole 15
      2.4.1. Operations 15
      2.4.2. Programs 16
   2.5. References 19

3. Atmospheric Radiation Monitoring Group 20
   3.1. Continuing Programs 20
      3.1.1. Surface Radiation 20
   3.2. Special Projects 22
      3.2.1. Spectral Response Characteristics of Robertson-Berger Meters 22
   3.3. References 23

4. Carbon Cycle Group 24
   4.1. Continuing Programs 24
      4.1.1. In-Situ Carbon Dioxide Measurements 24
      4.1.2. Flask Sample Carbon Dioxide Measurements 24
      4.1.3. In-Situ Methane Measurements 27
      4.1.4. Flask Measurements of Methane 27
      4.1.5. Flask Measurements of Carbon Monoxide 30
   4.2 Reference Gas Standards 32
      4.2.1. Carbon Dioxide Standards 32
      4.2.2. Methane Standards 32
   4.3. Special Projects 33
   4.4. References 33

5. Aerosols, Ozone, and Water Vapor Group 34
   5.1. Continuing Programs 34
      5.1.1. Surface Aerosols 34
      5.1.2. Total Ozone Observations 36
      5.1.3. Umkehr Observations 37
      5.1.4. Calibration of NOAA-CMDL Dobson Spectrophotometers 38
      5.1.5. International Calibration of Dobson Instruments in Arosa 39
      5.1.6. Validation of TOMS and SBUV Satellite Instrument Ozone Data 39
      5.1.7. Tropospheric Ozone 41
      5.1.8. Ozonesonde Observations 43
      5.1.9. Stratospheric Water Vapor 44
      5.1.10. Long-Range Transport of Trace Gases 44

5.2. Special Projects 48
5.2.1. Nephelometer Comparison at MLO 48
5.2.2. Front Range Lidar, Aircraft, and Balloon Experiment 49
5.2.3. First Ground-Based Intercomparison of SBUV-2, S/N-2, and Dobson Spectrophotometer 83 51
5.2.4. Stratospheric Water Vapor Measurements in the Polar Regions 52
5.3. References 53

6. Acquisition and Data Management 55
6.1. Continuing Programs 55
6.1.1. Station Climatology 55
6.1.2. Data Management 58
6.2. References 62

7. Nitrous Oxide and Halocarbons Group 63
7.1. Continuing Programs 63
7.1.1. Flask Samples 63
7.1.2. RITS Continuous Gas Chromatograph Systems at CMDL Baseline Stations 64
7.1.3. Low Electron Attachment Potential Species 66
7.1.4. Gravimetric Standards 67
7.2. Special Projects 67
7.2.1. Alternative Halocarbon Measurements 67
7.2.2. Soviet-American Gas and Aerosol Experiment (SAGA III) 69
7.2.3. Airborne Gas Chromatograph For Atmospheric Species (ACATS) 70
7.3. References 71

8. Director's Office 72
8.1. Low-Level Temperature Inversions of the Eurasian Arctic and Comparisons With Soviet Drifting Station Data 72
8.1.1. Introduction 72
8.1.2. Results: Sea Ice/Land Comparisons 72
8.1.3. Summary and Conclusions 74
8.2. Boundary Layer Ozone Fluctuations Related to Organobromine Photochemistry in the Springtime Arctic 74
8.2.1. Introduction 74
8.2.2. Experimental 75
8.2.3. Results 76
8.2.4. Discussion and Summary 78
8.3. References 79

9. Cooperative Programs 81
Continuous Aerosol Monitoring with the Epiphaniometer at MLO
U. Baltensperger, H.W. Gäeggeler, and D.T. Jost 81
Antarctic Ultraviolet Spectroradiometer Monitoring Program
C.R. Booth, T. Lucas, J. Morrow, D. Neuschuler, J. Tusson, and J. Yeh 83
A Case Study of the Stable Lower Atmospheric Boundary Layer at Barrow, Alaska
T.K. Cheung 85
Artificial Windshielding of Precipitation Gauges in the Arctic
G.P. Clagett 87
UVB Monitoring Data from Mauna Loa
D.L. Correll, C. Clark, R. Goodrich, and D. Hayes 88
South Pole Lidar
G. Fiocco, M. Cacciani, P. DiGirolamo, A. DiSarra, and D. Fua 89
Total Nitrate Variations at Mauna Loa
B.J. Huebert and G.L. Lee 91

Temperature Inversions in the Canadian Arctic
J.D. Kahl, M.C. Serreze, and R.C. Schnell 92
The Historical Arctic Rawinsonde Archive
J.D. Kahl, M.C. Serreze, and R.C. Schnell 95
Trajectory Forecasting for Misers Gold
J.D. Kahl, R.C. Schnell, and P.J. Sheridan 99
Trace Gases Over Hawaii; Concentrations, Trends, and Vertical Gradients
M.A.K. Khalil and R.A. Rasmussen 102
Radioactivity in the Surface Air at BRW, MLO, SMO, and SPO
R.J. Larsen and C.G. Sanderson 105
Zonal Representativeness of Cape Grim CO_2 Measurements
G.I. Pearman, D.J. Beardsmore, R.J. Francey 107
Aerosol Constituents at American Samoa: May-June 1990
D.L. Savoie, J.M. Prospero, R. Arimoto, and R.A. Duce 109
Analysis of MSA and nss $SO_4^=$ at MLO
B.B. Shurtleff, X.Y. Cai, and W.H. Zoller 112
Stable Lead Isotope Ratios at Barrow, Alaska
W.T. Sturges, R.C. Schnell, J.F. Hopper, and L.A. Barrie 114
Atmospheric Bromine Measurements at Barrow, Alaska, using a Sequential Filter Pack and Carbon Tube Sampler
W.T. Sturges, R.C. Schnell, G.S. Duton, S.R. Garcia, and J.A. Lind 117
Radon as a Baseline Selection Criterion at Mauna Loa Observatory
S. Whittlestone, L.P. Steele, and S. Ryan 120
Seasonal Amplitude Variations in CO_2 in the Northern Hemisphere
T.P. Whorf and C.D. Keeling 124

10. International Activities, 1990 127

11. Publications and Presentations by CMDL Staff, 1990 129

12. Acronyms and Abbreviations 131

CMDL Staff, 1990

Director's Office

Eldon E. Ferguson, Director
James T. Peterson, Deputy Director
David Hofmann, Senior Scientist
Donna Leise, Administrative Officer
Sandra Howe, Administrative Assistant
Ellen Hardman, Secretary
Rita Rosson, Editorial Assistant

Special Projects

Russell Schnell, CIRES
Mark Serreze, CIRES
Scott Sewell, CU Grad Student
Patrick Sheridan, NRC Post Doctorate
Spencer Shiotani, CU Work Study
Donna Smith, CU Work Study
Matthew Steiman, CU Work Study
William Sturges, CIRES
Brett Taylor, CU Work Study

Acquistion & Data Management Group

Gary Herbert, Chief
Sheri Cox, Secretary
Pamela Grisham, Secretary
Mark Bieniulis, CIRES
Michael Ellis, Physical Science Aid
Joyce Harris, Computer Specialist
James McCutcheon, CIRES
Gregory Orleans, Physical Science Aid
Kenneth Thaut, Electronic Technician

Atmospheric Radiation Monitoring Group

John DeLuisi, Chief
Marilyn Van Asche, Secretary
Barry Bodhaine, Meteorologist
Paul Chilson, Physical Science Aid
Ellsworth Dutton, Meteorologist
Rudy Haas, Mathematician
Fred Kreiner, CIRES
David Longenecker, CIRES
Donald Nelson, Meteorologist
Gayland Pounder, Physical Science Aid
Patrick Reddy, CIRES
Kevin Schlatter, CIRES
Michael Shanahan, Physical Science Aid
Scott Siao, Physical Science Aid
Robert Stone, CIRES
Barbara Thomson, Physical Science Aid

Carbon Cycle Group

Pieter Tans, Chief
Lee Prendergast, Secretary
Thomas Conway, Research Chemist
Wyatt Coy, CIRES
Edward Dlugokencky, CIRES
Douglas Guenther, CIRES
Brian Hirsch, CO-OP
Duane Kitzis, CIRES
Patricia Lang, Physical Scientist
Terry Lesoing, CO-OP
Russell Martin, CIRES
Kenneth Masarie, CIRES
Paul Novelli, CIRES
Christopher Platt, CO-OP
L. Paul Steele, CIRES
Gregory Summers, CO-OP
Kirk Thoning, Physicist
Anthony Vaughan, Physical Science Aid
Lee Waterman, Research Chemist

Ozone Group

Walter Komhyr, Chief
Lee Prendergast, Secretary
Brandon Bird, WAE
Robert Evans, CIRES
Robert Grass, Physicist
Gloria Koenig, Computer Programmer
Jeffrey Lathrop, CO-OP
Kent Leonard, CIRES
Samuel Oltmans, Physicist
Michael O'Neill, CO-OP
Daniel Opperman, CO-OP
Christopher Platt, Physical Science Aid
Frank Polacek, III, Meteorological Technician
Brandon Strong, CU Student
Dorothy Quincy, CIRES
James Wendell, Electronic Technician

Nitrous Oxide and Halocarbons Group

James Elkins, Chief
Marilyn Van Asche, Secretary
Christina Brunson, CIRES
James Butler, Research Chemist
Thomas Baring, Physical Science Aid
Scott Cummings, Physical Science Aid
Timothy Gilpin, NRC Post Doctorate
Brad Hall, Research Chemist
Bradley Halter, CIRES
Garry Holcomb, CIRES
Thayne Thompson, Physicist
Jeffrey Sczechowski, CIRES
Thomas Swanson, CIRES

Observatory Operations

Bernard Mendonca, Chief
Sheri Cox, Secretary
Pamela Grisham, Secretary
Denise Theede, Program Clerk

Barrow - Daniel Endres, Station Chief
Christopher Churylo, Electronic Technician
Timothy Quakenbush, Electronic Engineer

Mauna Loa - Elmer Robinson, Director
Judith Pereira, Program Support Technician
John Chin, Physicist
Thomas DeFoor, Electronic Engineer
Barbara Kerecman, Data Clerk
Darryl Kuniyuki, NOAA Jr. Fellow
Steven Ryan, Physical Scientist
Mamoru Shibata, Electronic Technician
Tracie Yokoi, Physical Science Aid
Alan Yoshinaga, Chemist

Samoa - Carl Farmer, Station Chief
M. Emily Wilson-Godinet, Electronic Technician

South Pole - Carl Groeneveld, NOAA Corps
Fred Schrom, Electronic Technician
John Lowell, NOAA Corps
Michael O'Neill, Physicist

CMDL Station Information

Name:	**Barrow (BRW)**	**Mauna Loa (MLO)**
Latitude:	71.323	19.539
Longitude:	156.609	155.578
Elevation:	8 m	3397 m
Time Zone:	GMT -9	GMT -10
Office Hours:	8:00 am-5:00 pm	8:00 am-5:00 pm
Telephone		
Office hours:	(907) 852-6500	(808) 961-3788
Fax:	(907) 852-4622	(808) 961-3788
Postal Address:	Officer in Charge NOAA/ERL/CMDL Pouch 8888 Barrow, AK 99723	U.S. Dept. of Commerce NOAA - Mauna Loa Observatory P.O. Box 275 Hilo, HI 96720
Freight Address:	Same as above	U.S. Dept. of Commerce NOAA - Mauna Loa Observatory 154 Waianuenue Ave. Hilo, HI 96720

Name:	**Samoa (SMO)**	**South Pole (SPO)**
Latitude:	-14.232	-89.997
Longitude:	170.563	-102.0
Elevation:	77 m	2841 m
Time Zone:	GMT -11	GMT +12
Office Hours:	8:00 am-5:00 pm	8:00 am - 5:00 pm
Telephone:		
Office hours:	011 (684) 622-7455	Relayed through CMDL Boulder
After hours:	011 (684) 699-9953	
Fax:	011 (684) 699-4440	
Postal Address:	U.S. Dept. of Commerce NOAA - GMCC Samoa Observatory S-257 Pago Pago, American Samoa 96799	Officer in Charge, NOAA/CMDL Clean Air Facility South Pole, Antarctica PSC 468 Box 402 FPO AP 96598-5402
Freight Address:	Same as above	Same as above

CLIMATE MONITORING AND DIAGNOSTICS LABORATORY

NO. 19

SUMMARY REPORT 1990

1. Introduction

January 1990 marked the transition of the former Geophysical Monitoring for Climatic Change (GMCC) program into the Climate Monitoring and Diagnostics Laboratory (CMDL). CMDL was formed as part of an ERL reorganization, which combined the GMCC activities with those of the Climate Research Division of the Air Resources Laboratory. Dr. Eldon Ferguson was named the first Director of CMDL. Another significant personnel change was the recruitment of David Hofmann as the CMDL Chief Scientist. Dr. Hofmann, formerly with the University of Wyoming, brings added expertise to the Laboratory's aerosol and stratospheric ozone programs.

Significant new program activities continue to be supported by the developing NOAA Climate and Global Change (C&GC) Program. New funding has been received for development and preparation of primary gas standards for halocarbons, CO_2, CH_4, and CO. We are working with the University of Colorado to begin monitoring of the ^{13}C and ^{12}C isotopes of CO_2 and CH_4. Planning began for vertical profile measurements from aircraft and very tall television transmitting towers for CO_2, CO, and halocarbons. Finally, C&GC is also supporting research on monitoring of the replacement halocarbons, those species expected to see increasing use in place of the traditional CFC-11, CFC-12, and CFC-113 species. Regarding the Observatories, we are pleased that a new 5-year agreement with the National Science Foundation was accepted for continuation of our long-term monitoring program there.

This *Summary Report 1990, Number 19* continues the chronological numbering of the past, but includes the new Laboratory title. Similar to last year, this document does not include the activities of the Climate Research Division of the Laboratory.

2. Observatory Reports

2.1. MAUNA LOA OBSERVATORY

E. ROBINSON

2.1.1. OPERATIONS

An important addition to the MLO program occurred in December when a radon (Rn) concentration monitor was placed in operation as part of the permanent suite of monitoring instruments at the observatory. This radon monitor was constructed for CMDL and installed at MLO by personnel of the DOE Health and Safety Laboratory, New York. This CMDL Rn monitor joined the ANSTO Cooperative Rn monitoring program which has been operating at MLO since May 1989.

Another important instrumentation upgrade was made in July when the venerable G.E. CNC unit was finally retired and the CN monitoring task was taken over by the TSI CNC monitoring system. The TSI has undergone an extensive period of intercomparison with the G.E. CNC and the Pollak CNC before it was accepted as the MLO CNC for long term records. The substitution of the TSI for the G.E. CNC has simplified the required maintenance schedule for CN measurements.

Distinguished visitors in 1990 included Dr. John Knauss, Under Secretary of the Department of Commerce and Administrator of NOAA. He paid a 2-day visit to Hilo and MLO in July. November 30, 1990, marked the retirement of Mamoru "Al" Shibata after almost 30 years of government service. He started government service with ESSA (now NOAA) and the National Weather Bureau in 1961. Al had assignments in the South Pacific, in the Panama Canal Zone, and at ARL-Las Vegas before transferring back to Hawaii to work at MLO in 1972. The CMDL program will miss his dedication and many technical skills, while his associates at MLO will miss his warm disposition, subtle humor, and friendship.

March 1990 will be remembered as the month of the big snow at MLO. The storm hit on February 27 and continued through March 1. The storm left 0.5-1.0 m drifts across the upper portions of the MLO road. This was above about the 3.0 km level. Several attempts to reach the observatory (even by 4-wheel drive vehicles) were unsuccessful until Tuesday, March 6, when two MLO staff members hiked in and were able to check station conditions. The station facilities and instrumentation were in good condition and many observations had continued under CAMS control throughout the storm isolation period. CAMS tapes had switched although chart rolls had run out, operating filters had run extra time, and moisture traps on the CO_2 analyzers had frozen up. These were not unexpected. On Friday, March 9, a 4-wheel drive truck got within 100 m of the lower visitor parking area and then the crew walked the rest of the way in. At this time most of the remaining instruments were reset and restarted in a normal operational routine. On Monday, March 12, it was possible to drive to the observatory in the MLO station wagon, although it was necessary to use tire chains to get up the last hill above the lower parking area. Full operation of the MLO program was resumed on March 12. This storm was the most severe in the 34-year history of MLO. The "old timers" cannot remember a situation where snow blocked access to MLO for more than 2 consecutive days, compared to this storm's 1-2 weeks inaccessibility. It is encouraging to note that the MLO operations survived this event in good shape and with a high percentage of data recovery.

The east rift zone eruption of Kilauea Volcano continued during the year. Shifting areas of flow activity resulted in considerable property damage in the Kalapana and Kaimu areas. Because of the distance and direction to this eruption area, the local wind patterns, and the topography, this eruption activity is not believed to have any significant impact on the ongoing MLO monitoring program as was described previously [*Komhyr and Rosson*, 1990].

2.1.2. PROGRAMS

Table 2.1 summarizes the major CMDL and cooperative programs carried out at MLO during 1990. Although most of the programs listed in this table are continuations of similar listings in previous reports [e.g., see *Komhyr and Rosson*, 1990], there are several changes documented here. Perhaps the most important change, as noted in Section 2.1.1., was the addition of a continuous radon monitor in December 1990. This monitor was designed, constructed, and installed by the DOE, Health and Safety Laboratory. The sampling technique involves the collection of time-integrated samples. Samples of 30-minute duration have generally seemed to be optimum. The radon record provides information useful for the evaluation of long-range transport from distant land areas. A number of observations were also removed from the MLO schedule. The G.E. CNC was discontinued in July, and now the TSI CNC provides the MLO CN record. There was more than a year of parallel data for these two instruments prior to the discontinuance of the G.E. CNC. The sulfur monitoring program for both total sulfur and SO_2 was discontinued in February. This program had been supported with the cooperation of the ARL Air Quality Group. The hygro-thermograph at Kulani Mauka was also discontinued when the NWS lost interest in these data and in assisting in the maintenance of this station. Among the cooperative programs, the EPA support for programs of SO_2 bubbler sampling and high-volume filter sampling was discontinued. A modified total suspended particle sampling program was designed and begun using the available high-volume filter samplers and the MLO chemistry laboratory to continue the basic TSP data record. The NADP/ISWS program of ^{7}Be and ^{10}Be precipitation analyses was discontinued early in the year.

TABLE 2.1. Summary of Measurement Programs at MLO in 1990

Program	Instrument	Sampling Frequency
Gases		
CO_2	Siemens Ultramat-3 IR analyzer	Continuous
	3-L glass flasks†	1 pair wk^{-1}
	0.5-L glass flasks, through analyzer	1 pair wk^{-1}
CO_2, CH_4	0.5-L glass flasks, P^3 pump unit†	1 pair wk^{-1}
CH_4	Carle automated GC	1 sample $(24\ min)^{-1}$
Surface O_3	Dasibi ozone meter	Continuous
Total O_3	Dobson spectrophotometer no. 76	3 day^{-1}, weekdays
O_3 profiles	Dobson spectrophotometer no. 76 (automated Umkehr method)	2 day^{-1}
	Balloonborne ECC sonde	1 wk^{-1}
CFC-11, CFC-12, N_2O	300-mL stainless steel flasks	1 pair wk^{-1}
CFC-11, CFC-12, N_2O, CCl_4, CH_3CCl_3	HP5890 automated GC	1 sample $(h)^{-1}$
N_2O	Shimadzu automated GC	1 sample $(h)^{-1}$
Total sulfur gases	CSI flame photometric analyzer*	Discontinued 2/90
SO_2	TECO pulsed fluorescence analyzer*	Discontinued 2/90
Radon	2-filter system	Continuous
Aerosols		
Condensation nuclei	Pollak CNC	1 day^{-1}
	G.E. CNC*	Discontinued 7/31/90
	TSI CNC*	Continuous
Optical properties	Four-wavelength nephelometer*: 450, 500, 700, 850 nm	Continuous
Stratospheric aerosols	Lidar, 694.3 nm	1 profile wk^{-1}
Black carbon	Aethelometer	Continuous
Total suspended particles	High-volume sampler	2 samples $(mo)^{-1}$
Solar Radiation		
Global irradiance	Eppley pyranometers with Q, OG1, and RG8 filters	Continuous
Direct irradiance	Eppley pyrheliometer (2) with Q filter*	Continuous
	Eppley pyrheliometer with Q, OG1, RG2, and RG8 filters	3 day^{-1}
	Eppley/Kendall active cavity radiometer	1 mo^{-1}
Diffuse irradiance	Eppley pyrgeometer with shading disk and Q filter*	Continuous
Turbidity	J-202 and J-314 sunphotometers with 380-, 500-, 778-, 862-nm narrowband filters	3 day^{-1}
	PMOD three-wavelength sunphotometer*: 380, 500, 778 nm; narrowband	Continuous
Ultraviolet radiation	UV radiometer (erythema)	Continuous
Meteorology		
Air temperature	Aspirated thermistor*, 2- and 40-m heights	Continuous
	Max.-min. thermometers, 2-m height	1 day^{-1}
	Hygrothermograph	Continuous
Temperature gradient	Aspirated thermistors*, 2- and 40-m heights	Continuous
Dewpoint temperature	Dewpoint hygrometer*, 2-m height	Continuous
Relative humidity	Hygrothermograph	Continuous
Pressure	Capacitance transducer*	Continuous
	Mecurial barometer	5 wk^{-1}
Wind (speed and direction)	Bendix Aerovane*, 8.5- and 40-m heights	Continuous
Precipitation	Rain gauge, 8-in	5 wk^{-1}
	Rain gauge, 8-in‡	1 wk^{-1}
	Rain gauge, tipping bucket*	Continuous
Total precipitable water	Foskett IR hygrometer*	Continuous
Precipitation Chemistry		
pH	pH meter	Daily
Conductivity	Conductivity bridge	Daily
Chemical components	Ion chromatograph	Daily

TABLE 2.1. Summary of Measurement Programs at MLO in 1990—Continued

Program	Instrument	Sampling Frequency
Cooperative Programs		
CO_2 (SIO)	Applied Physics IR analyzer	Continuous
CO_2, ^{13}C, N_2O (SIO)	5-L evacuated glass flasks†	1 pair wk^{-1}
Surface SO_2 (EPA)	Chemical bubbler system	Discontinued 5/90
CO_2, CO, CH_4, $^{13}C/^{12}C$ (CSIRO)	Pressurized glass flask sample	1 mo^{-1}
CO_2, CH_4, other trace gases (NCAR)	Evacuated stainless steel flasks†	1 pair wk^{-1}
Total suspended particles (DOE)	High-volume sampler (1 filter wk^{-1})	Continuous
Turbidity (AES Canada)	Sonotek sunphotometer no. 5698	1-3 day^{-1}
CH_4 ($^{13}C/^{12}C$) (Univ. of Washington)	35-L evacuated flask	1 mo^{-1}
Total suspended particles (EPA)	High-volume sampler	Discontinued 5/90
Ultraviolet radiation (Smithsonian)	8-wavelength UV radiometer: 290-325 nm; narrowband	Continuous
Solar aureole intensity (CSU)	Multi-aperture tracking photometer: 2, 5, 10, 20, 30° fields of view	Continuous
Precipitation collection (DOE)	Exposed collection pails	Integrated monthly sample
Precipitation collection for ^{7}Be and ^{10}Be	Aerochemetric automatic collector	Discontinued 1/90
Precipitation collection for organic acid analysis (Univ. of Virginia)	Aerochemetric automatic collector	Collection after each rain event
Wet-dry deposition (ISWS, NADP)	Aerochemetric automatic collector and weighing-bucket rain gauge	Integrated 7-day sample
Aerosol chemistry, upslope-downslope discrimination (Univ. of Washington)	Nuclepore filters	Continuous
Aerosol chemistry (Univ. of Calif.-Davis)	Programmed filter sampler	Integrated 3-day sample 1 continuous and 1 downslope sample (3 days)$^{-1}$
Various trace gases (OGC)	Stainless steel flasks†	1 set wk^{-1} (3 flasks)
HNO_3, HCl vapor, aerosols (URI)	Filter system	Daily, 2000-0600 LST
Radon (ANSTO)	Aerosol scavenging of Rn	Continuous; integrated 30-min samples
Aerosol surface area (PSI)	Epiphaniometer	Continuous; integrated 30-min samples
Formation of ^{3}He (WHOI)	Closed cylinder	Continuous 12-mo ambient exposure from 1/90

All instruments are at MLO unless indicated.
*Data from this instrument recorded and processed by CAMS.
†MLO and Kumukahi.
‡Kulani Mauka

Carbon Dioxide

The CMDL Siemens Ultramat-3 IR CO_2 analyzer and the SIO Applied Physics IR CO_2 analyzer operated in parallel without major problems throughout the year. Routine maintenance and calibrations were done on both instruments on schedule. In May 1990, the air sampling pumps for the SIO CO_2 system were changed to Air Cadet pumps that use a plastic pump head and nitrile diaphragms. The original pumps used by SIO since 1958 were Dyna Pumps with neoprene diaphragms. In September a small precision temperature controller was added to the SIO Applied Physics analyzer. The preliminary provisional yearly average for MLO CO_2 concentration for 1990 was 354.3 ppm. The CO_2 annual growth rate between 1989 and 1990 was approximately 1.5 ppm. Outgassing from the volcanic vents at the Mauna Loa caldera and along the northeast rift zone at Mauna Loa continued to cause periodic observable disturbances in some of the CO_2 data record. As in prior years, these venting events occurred mostly between midnight and 0800 LST of the following day during the downslope wind regime. The erratic concentration data characterized by extreme variability resulting from venting events were easily identified by visually scanning the chart records or by setting up a computerized data screening procedure, and thus they have been separated from the clean-air record without difficulty. The frequency of monthly occurrences of observable outgassing from volcanic vents on Mauna Loa for 1990 are listed in Table 2.2. Such venting episodes were detected mainly on the basis of criteria for CO_2 concentration, CO_2 variability, and wind sector. The criterion for the CO_2 standard deviation screening was 1.0 ppm, which is the value suggested by *Thoning et al.* [1989]. The 1990 total venting of 48 hours as shown in Table 2.2 is significantly less than the 84 hours noted in 1989 [*Komhyr and Rosson*, 1990] and the 200 hours recorded in 1988 [*Elkins and Rosson*, 1989].

The weekly CO_2, CH_4 and other gas sampling programs using flasks at MLO and at Cape Kumukahi were carried out according to schedule through the year without problems.

TABLE 2.2. Estimated Frequency of MLO Venting Effects*

	Jan.	Feb.	March	April	May	June	July	Aug.	Sept.	Oct.	Nov.	Dec.	Year
Total time (hours)	7	3	5	2	4	6	0	3	3	5	9	1	48

*Criteria: CO_2 SD ≥1.0 ppm; wind direction sector 135°-225°; wind speed >1.35 m s^{-1}.

Methane

The Carle automated GC system was in continuous operation throughout the year and provided CH_4 data on the basis of a grab-air sample taken every 24 minutes. No major problems were encountered in this program. The CH_4 data continued to show clearly defined cycles of varying frequencies. The typical diurnal cycle was correlated with the up and downslope winds with the marine boundary layer air having the higher CH_4 concentrations. There were also multi-day or synoptic-scale cycles apparently related to air mass source regions. Finally, there is still a gradual upward trend in CH_4 concentrations throughout the year.

Ozone

The 1990 MLO O_3 monitoring program continued to consist of three phases: continuous MLO surface monitoring using a Dasibi model 1003-AH UV absorption ozone monitor; daily total ozone and Umkehr ozone profile measurements using a computer-based automated Dobson instrument (Dobson no. 76); and ozone profile measurements based on regular ascents of balloon-borne ECC ozonesondes from the NWS station at the Hilo airport.

The 1990 ozonesonde operations were programmed into a schedule of three flights per month. The program used 2000g rubber balloons from January 1 to July 5 and 1500g rubber balloons after July 5. In the first part of the year, 16 successful flights were made and in the latter period (i.e., after July 5), 15 flights were successful. During the year there was a total of 35 ozonesonde flights, but 4 failed after launch before useful data could be obtained resulting in a total of 31 successful ozonesonde launches. During the January through July 5 period when the larger 2000g balloons were used, the median altitude reached by the ozonesondes was 6.1 mb (34.6 km) and 75% of the flights rose to over 34 km. After July 5, when smaller 1500g balloons were used, the median flight altitude for the 15 successful flights was 7.5 mb (33.2 km). In this part of the program 75% of the flights went to an altitude of 32 km or higher. The maximum ozone concentration over Hawaii is typically found at around 25 km [*Bodhaine and Rosson*, 1988, pg 41]; thus these ozonesonde flights were able to provide good information on the ozone layer over Hawaii even though the 40 km flight altitudes reached in previous years could not be achieved by the smaller rubber balloons.

As noted above, total O_3 and Umkehr O_3 profiles using automated Dobson no. 76 were a regular part of the MLO observation routine in 1990. There were no major breaks in this record due to prolonged instrument problems. Weather conditions were favorable for Dobson direct sun observations on 75% of the observatory observation days. During the 1990 summer, a side-by-side calibration program was carried out using the WMO world standard Dobson no. 83 and the observatory Dobson instrument.

The third part of the MLO ozone monitoring program is the continuous operation of the Dasibi ozone monitor. This instrument performed in a very satisfactory manner throughout the year, and it provided a continuous record of station-level ozone concentrations for the year. The air inlet from the main sampling stack was unchanged from prior years.

Halocarbons and Nitrous Oxide

There was a major improvement in the RITS GC system in October when the newly developed RITS PLOT program was installed in the MLO system. With RITS PLOT it is possible to obtain a printout of GC results for the past 30 days and thus to review the performance of the system and to correlate RITS gas concentrations with other factors monitored at MLO. The RITS system was upgraded during the year to provide hourly ambient air concentrations in place of the once every 3-hour samples obtained previously. The RITS sample gases were expanded to include CFC-113 as well as N_2O, CFC-11, CFC-12, CCl_4, and CH_3CCl_3. Although this complex gas chromatographic system was not trouble free during the year, the problems that did occur could usually be corrected with little resulting downtime, and no catastrophic failures occurred. The RITS PLOT results appear to show both weak diurnal cycles and longer-term or multi-day synoptic scale concentration variations in the several CFC compounds, but not in N_2O. This is not unexpected.

Radon

The MLO radon program began in December with the installation of a radon monitor built by the DOE, Environmental Measurements Lab. The monitor operates on the two-filter principle using a 330-L delay tank and a 380-L minute flow rate. Air is sampled from the top of the 40-m tower via 7.5 cm diameter inlet tubing. In the monitor the air stream passes through a filter which removes all the ambient "daughters" but allows the inert radon gas to pass. The radon then enters the delay tank during which new daughters are produced. These are collected on a second filter, and the resulting alpha activity on the filter is monitored by a scintillation counter. The second filter consists of a filter roll that advances frame by frame. Successive frames are first exposed to the air stream and then monitored. Sampling and monitoring periods of 30

minutes have proven to be effective in tracking the radon concentration patterns at MLO.

Preliminary analysis of the data illustrated by Figure 2.1, shows periods of increased radon typically lasting several days, such as after December 25 that coincided with 700 mb isobaric back trajectories indicative of fast transport of air from Asia. Daytime radon increases were frequently coincident with periods of upslope winds. This probably indicated radon emanating from lower altitude island soils. December 15 is a clear example of this local or island-dominated pattern. The radon scale in Figure 2.1 is given in scintillation counts per 30-minute sample period. A calibration program is being carried out to convert this basic instrument output to more conventional radon concentration units.

Solar Radiation

The solar radiation measurement program in 1990 was unchanged from previous years. Tracking pyrheliometer no. 2119 was replaced by no. 16657 in April following a several month period of continuing sensitivity loss which reached 3%. Eight active cavity comparisons were performed in early 1990. The instrument was then shipped to Boulder and Switzerland for calibrations from August to December.

Sunphotometer calibrations were made on 15 days, during which 85 instrument calibrations were performed. Daily observations with the two MLO sunphotometers and the filter wheel NIP continued throughout the year.

Aerosol Monitoring

The MLO aerosol monitoring programs underwent a long anticipated change in July when the G.E. CNC was taken out of service, and the continuous MLO CN record was transferred to the TSI CNC. The TSI unit is a continuous expansion CNC in which condensation occurs in a butyl alcohol vapor chamber and single particle counting statistics are used as a basis for the CN concentration calculation. The TSI output is recorded by the ASR CAMS. The aethalometer unit, initially put into service in 1989 [*Komhyr and Rosson*, 1990] was modified in early 1990 so that both control and data recording were carried out by a dedicated lap-top computer. This computer setup substituted for CAMS control, which had proved to be unsatisfactory for the TSI instrument. With this change in the system, the aethalometer record began to exhibit very interesting features both in terms of short-term and long-term cyclic variations. The 4-wave length nephelometer was in continuous service during the year with a minimum of downtime.

The measurements of stratospheric aerosol concentrations and profiles using the MLO ruby lidar system continued throughout the year. During the year a total of 32 lidar aerosol profile observations were made. The lidar program was hampered to some extent in the months of September through December by a relatively high frequency of cloudy weather. During 1990 the stratosphere appeared to have approached a clean equilibrium background condition and no new injections of volcanic aerosol layers were detected. Figure 2.2 shows the MLO lidar record from its beginning in 1974 through 1990. Major volcanic eruptions causing probable stratospheric layers are also indicated. Note in particular the long decay time associated with the massive 1982 eruption of the Mexican volcano El Chichon. Figure 2.3 shows the 4-year lidar record from 1987 through 1990. The average stratospheric (16-33 km) non-Rayleigh backscatter, i.e., aerosol backscatter, exhibited little change during 1989 and 1990. The differences between 1989 and 1990 are not statistically significant and, as noted above, probably represent an equilibrium background aerosol concentration value during this 2-year period.

During a visit to Hilo by the Soviet research ship *Korolev* in February, it was possible to make an intercomparison of the Soviet lidar system on the ship and the MLO lidar. Although the two instruments were separated by both distance and altitude, the results of the intercomparison

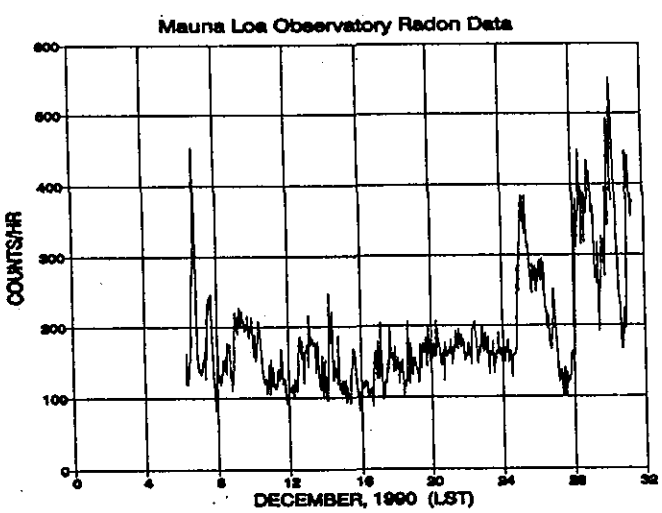

Fig. 2.1. Initial MLO radon concentration data from the CMDL/DOE two-filter monitor. Concentration scale is in relative units of scintillation counts per 30-minute sample.

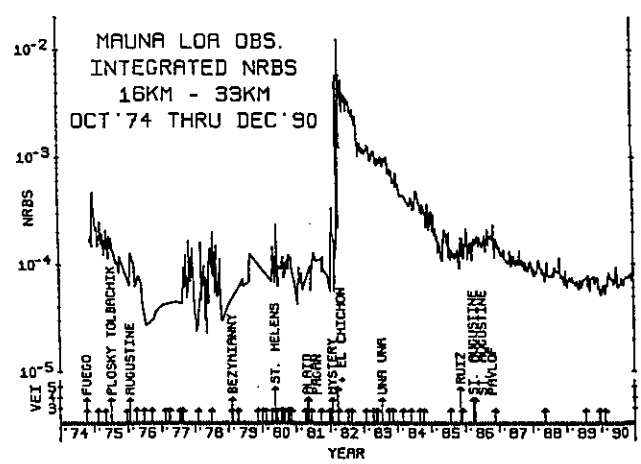

Fig. 2.2. MLO stratospheric aerosol lidar observations and major volcanic eruptions, 1974-1990.

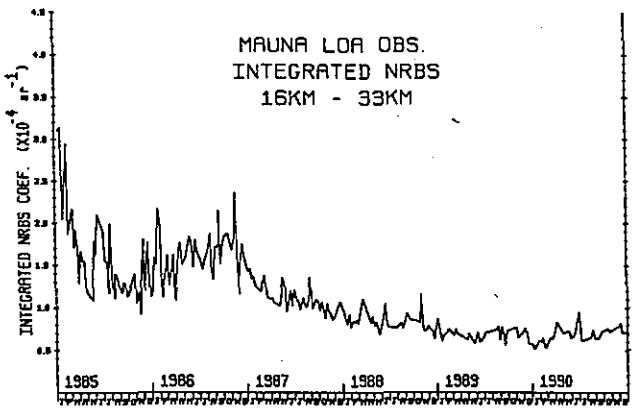

Fig. 2.3. MLO stratospheric aerosol lidar observations, 1985-1990. Note the relatively stable stratospheric background since about January 1989.

experiment were very favorable. Figure 2.4 shows the results of this experiment. The divergence below 16 km is not considered to be important and probably results from data processing variations.

Meteorology

The routine program of wind, temperature, dewpoint, and atmospheric pressure was carried out during 1990 with few problems. There were no major changes in the meteorological observation program. One minor change was the discontinuance of the hygrothermograph data at Kulani Mauka when the NWS dropped their support for temperature and humidity from this station. Rainfall data are still collected at Kulani Mauka on a weekly basis, however.

Precipitation Chemistry

Direction and support for the MLO precipitation chemistry program by ARL was discontinued this year. In June a modified program of precipitation chemistry collection and analyses was continued within the basic MLO operational routine. This program consists of a weekly integrated precipitation sample from the Hilo NWS station and the collection of precipitation event samples at MLO. Analyses of these samples are done in the Hilo laboratory for pH, conductivity, and several ions using currently available equipment.

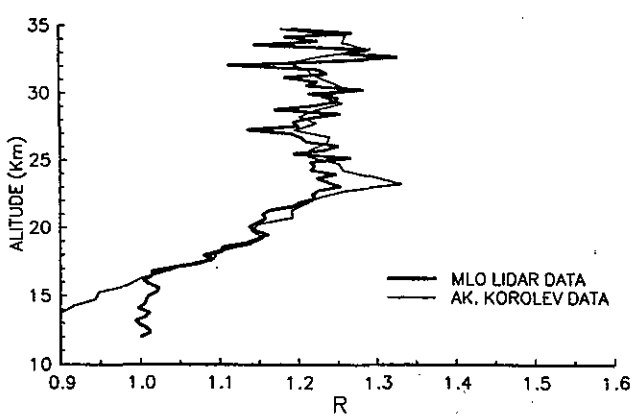

Fig. 2.4. Results of an intercomparison experiment between the MLO lidar system and the U.S.S.R. lidar system installed on the Soviet ship *Akademik Korolev*. The experiment was carried out on the evening of February 10, 1990.

Cooperative Programs

Table 2.1 lists a total of 20 long-term programs which were operated at MLO for other investigators and organizations. These are the cooperative programs. Most of the listed programs are continuations from 1989 and prior years. One new program was started. This was for the Woods Hole Oceanographic Institute to determine whether ^{3}He would be formed in water vapor contained in a closed cylinder when exposed for an extended time period to the cosmic ray radiation at MLO. A 1-year exposure is scheduled. The EPA programs of high-volume sampling for total suspended particles and SO_2 sampling using 24-hour bubblers, and the collection of weekly precipitation samples for the determination of ^{7}Be and ^{10}Be by ISWS were discontinued during the year. The University of Washington program of flask samples was expanded to include the periodic collection of 30-L flask samples at high (2000 psi) pressure.

As in most previous years, the MLO program also included several short period studies in which the investigators carried out programs of observations at MLO, usually with little need for assistance from MLO staff members. These programs are not listed in Table 2.1.

2.2. BARROW

D. ENDRES

2.2.1. OPERATIONS

A year of change best describes 1990 at BRW. A change in personnel took place in March with the arrival of a new electronics technician. A Fax machine was added to the station in January. The clean room was rewired during March to more evenly distribute the electrical load. The number of circuits in the clean room were doubled after several pieces of conduit were found to be warm from overloaded circuits. During the fall of 1989, a cutout on the power poles that supply power to the station exploded and had to be replaced. The local utilities company, BUECI, suggested that we upgrade the entire platform. We followed this recommendation in June after spring breakup and had the other two cutouts replaced along with the wiring between the transformers and the lines leading to the station.

Duct work for the observatory cooling system was modified in March to account for the greater heat load produced by the addition of several new projects throughout the observatory building.

A new telephone line was delivered and installed in May after the old line deteriorated to the point where repairs were no longer effective. The old line had been installed by

rolling a standard 6-pair phone line out on the ground from the BRW observatory building to the DEW Line hanger, a distance of about 3.2 km. After 18 years of exposure to the elements, the old line was showing severe wear from the ravages of time. Every spring during breakup, splices in the old line would fill up with water and telephone communications would degrade. GTE hung the new line on the power poles that run to UIC/NARL and it should last for a greater number of years since it cannot be run over by snowmachines or other tracked vehicles. Special thanks should be given to the USGS in Fairbanks for their help in obtaining the new line and working with GTE to write a contract to install it.

As in recent years, BRW was once again called on to serve as a training center for the new SPO crew. In the past, training time for each person was 2 weeks, this year it was increased to 1 month. In July, Boulder personnel from MASC and CMDL arrived to inspect the observatory building and collect data for a possible upgrade of the observatory facilities. At this time the road to the observatory was inspected and a local contractor was consulted as to the possibility of adding fill dirt to elevate the road which would improve road access during winter months. The current road is lower than the surrounding tundra and becomes impassable after most wind storms during the winter. A new contract to maintain the DEW Line was awarded to GEGS and on October 1 the new contractor arrived to take over operations. The old contractor, ITT, maintained a staff of 12 people on site; the new contractor uses 6 people, which for CMDL has resulted in less road maintenance. During the turnover to GEGS, several questions were raised about the actual boundaries of the DEW Line, NOAA, and USGS properties. As a result of these questions, a clerical error was discovered in the BLM files that brought to the attention of all agencies concerned, that the final transfer of property to NOAA and the USGS was still pending. The USGS in Fairbanks worked to resolve the problem and all paperwork effecting the transfer should be finalized at this writing.

A warehouse fire at Prudhoe Bay caused concern in the village of Barrow when it was discovered that the warehouse contained Xylene, organic polymers, a mixture of HCl and HFl, and instruments containing radioactive substances. The fire burned overnight but as the winds were from the west, the effluent was blown away from Barrow and no contamination was detected at BRW.

The BRW staff were called on to assist personnel from the North Slope Borough in technical and scientific matters. Technical expertise came in the form of repair and calibration of electronic equipment. BRW staff members appeared on locally-produced radio programs and answered questions concerning global climate change issues.

Station vehicles continued to be a major drain on time and resources of BRW personnel. Maintenance with the 1989 Chevrolet pick-up truck ran the gamut from a tune-up to major front-end work. Wrong shock absorbers installed on the truck by the factory were discovered and replaced by the BRW staff. Continuing problems with the front-end suspension indicated that it also may have been built incorrectly at the factory. The problem is still under investigation and review by GSA, the responsible government agency. Tires for the BRW vehicles were another major problem that hindered maintaining dependable transportation to and from the observatory. Tires on one truck became so weathered, that innertubes would squeeze out from cracks in the treads. Because of the cold arctic conditions, tires had to be ordered and replaced more frequently than in the lower 48 states. The 1979 GMC pick-up had a major tune-up and the carburetor was rebuilt by the BRW staff this year. After completing this maintenance on the 1979 truck, it was decided that it should be retired next summer and auctioned off by GSA. This is the last of the agency-owned vehicles at BRW; it has been in service for the past 11 years. Maintenance and repairs done on observatory vehicles are not inconsequential because of the lack of suitable working shelter and tools that are available to the BRW staff. The 1985 Chevrolet Suburban is awaiting shipment back to GSA in Anchorage after its 4-year stay in Barrow in accordance with our agreement with GSA.

With regards to the snowmachines, the suspension was rebuilt on the Skandic 503 snowmachine in October in preparation for winter. The Skandic 377 snowmachine continues to run well requiring only a tune-up and a new drive belt. The Honda Big Red 3-wheeler received a tune-up and a new battery. A new federal ban on the sale of 3-wheelers leaves us with doubts as to the number of years of service left in which we will be able to obtain parts.

2.2.2. PROGRAMS

Table 2.3 summarizes the 1990 measurement programs at BRW. Operational highlights were as follows:

Aerosols

A major change in the aerosol program was implemented in June with the addition of a TSI CNC. The TSI CNC is an alcohol-based CNC as opposed to the G.E. CNC which is water based. The G.E. CNC uses light attenuation by cloud formation due to particle growth from adiabatic expansion of CN in supersaturated air to measure CN. The TSI uses a single-particle-counting laser-diode optical detector to count individual droplets that have been supersaturated with n-butyl alcohol onto particles .014 microns and larger. By the end of the year, 6 months of a 12-month intercomparison had been completed with relatively few problems. The float which controls the alcohol level had to be reset to allow the TSI to run over a weekend without running out of alcohol. The only other occurrence of note was when a piece of insulation broke away from the condenser housing and entered the focusing nozzle, partiality blocking the flow that caused the TSI to give artificially low readings. The nozzle was cleaned and the instrument was returned to proper operation. The G.E. CNC ran well all year with only routine maintenance. The Pollak continues to serve as a field calibration standard for CNC measurements at BRW. The Pollak has been in operation at BRW since May 1976.

TABLE 2.3. Summary of Measurement Programs at BRW in 1990

Program	Instrument	Sampling Frequency
Gases		
CO_2	URAS-2T IR analyzer	Continuous
	3-L glass flasks	1 pair wk^{-1}
	0.5-L glass flasks, through analyzer	1 pair wk^{-1}
CO_2, CH_4, CO	0.5-L glass flasks, P^3 pump unit	1 pair wk^{-1}
CH_4	Carle automated GC	1 sample $(24\ min)^{-1}$
Surface O_3	Dasibi ozone meter	Continuous
Total O_3	Dobson spectrophotometer no. 91	3 day^{-1}
CFC-11, CFC-12, CFC-113, N_2O	300-mL stainless steel flasks	1 pair wk^{-1}
CFC-11, CFC-12, CFC-113, N_2O, CCl_4, CH_3CCl_3	HP5890 automated GC	1 sample $(3\ h)^{-1}$
N_2O	Shimadzu automated GC	1 sample $(3\ h)^{-1}$
Aerosols		
Condensation nuclei	Pollak CNC	1 day^{-1}
	G.E. CNC	Continuous
	T.S.I. CNC	Continuous
Optical properties	Four-wavelength nephelometer	Continuous
Black carbon	Aethalometer	Continuous
Solar and Terrestrial Radiation		
Global irradiance	Eppley pyranometers with Q and RG8 filters	Continuous
Direct irradiance	Tracking NIP	Continuous
	Eppley pyrheliometer with Q, OG1, RG2, and RG8 filters	Discrete
Terrestrial (IR) radiation	Eppley pyrgeometer	Continuous
Turbidity	Sunphotometers with 380-, 500-, 778-, and 862-nm narrowband filters	Discrete
Albedo	Eppley pyranometer and pyrgeometer	Continuous
Meteorology		
Air temperature	Thermistor, 2 levels	Continuous
	Max.-min. thermometers	1 day^{-1}
Dewpoint temperature	Dewpoint hygrometer	Continuous
Pressure	Capacitance transducer	Continuous
	Mercurial barometer	Discrete
Wind (speed and direction)	Bendix Aerovane	Continuous
Precipitation	Rain gauge, tipping bucket	
Precipitation Chemistry		
pH	pH meter (samples analyzed at MLO)	Discrete
Conductivity	Conductivity bridge (samples analyzed at MLO)	Discrete
Cooperative Programs		
Total surface particulates (DOE)	High-volume sampler (1 filter wk^{-1})	Continuous
Precipitation gauge (USDA)	Wyoming shielded precipitation gauge	2 mo^{-1}
Magnetic fields (USGS)	Magnetometer	Continuous
Various trace gases (OGC)	Stainless steel flasks	1 set wk^{-1} (3 flasks set^{-1})
CO_2, CH_4 (NCAR)	3-L stainless steel flasks	1 pair wk^{-1}
^{13}C, ^{18}O, CO_2 (CSIRO)	5-L glass flasks	1 pair $(2\ wk)^{-1}$
CO_2, ^{13}C, N_2O (SIO)	5-L evacuated glass flasks	1 pair wk^{-1}
CH_4 (Univ. of Calif., Irvine)	Various stainless steel flasks	1 set $(3\ mo)^{-1}$
Earthquake detection (Univ. of Alaska)	Seismograph	Continuous, check site 1 wk^{-1}, change tape 1 mo^{-1}
$^{13}CH_4$ ($^{13}C/^{12}C$) (Univ. of Washington)	35-L stainless steel flasks	1 $(2\ wk)^{-1}$
NO, NO_y (Univ. of Alaska)	Chemiluminscence	Continuous
Ultralow frequency waves (Univ. of Tokyo)	Magnetometer	Continuous
Air chemistry ions, organic acid, halogens, nitrous oxides (CIRES)	Sample tubes and filters	1 day^{-1}
UV monitor (NSF)	UV spectrometer	1 scan per 0.5 hour
Inversion meteorology (NOAA/WPL)	Acoustic sounder	Continuous
Air Chemistry O_3 destruction (CIRES/NAS)	Filter samples	1 day^{-1}

The aethalometer ran well all year except for a burned out light bulb that was replaced in September.

The nephelometer ran without any major problems for the entire year.

Solar Radiation

Solar radiation has been measured at BRW since 1976. The continuous downward global solar flux on a horizontal surface is measured in two spectral bands. In 1977 a normal incident pyrheliometer was added to measure the direct solar beam in four spectral bands. In 1988 an albedo rack was installed and measurements were made by a quartz pyranometer. The terrestrial IR budget, also started in 1988, is measured using an upward and a downward facing pyrgeometer.

A new 2-m high rack for the solar radiation equipment was installed on the roof of the observatory during June 1990. In 1986 and in 1990 it was noted that the albedo rack was used as a scratching post by caribou. The cyclic nature of the herd population, coupled with excessive snowfall throughout the North Slope during these 2 years, drove the herd far enough north to come in contact with BRW. There was no permanent damage to the rack and measurements were impacted minimally. All other equipment operated normally during the year.

CO_2

The weekly flask sampling program was accomplished throughout the year with no special problems. The URAS-2T IR analyzer operated without incident all year. The routine calibrations were performed on schedule and maintenance was performed as needed. A diaphragm was replaced in the pump used to supply ambient air to the CO_2 system. A Siemens Ultramat-3 IR analyzer is expected to be installed in 1991.

Meteorology

Continuous measurements of wind, temperature, dewpoint, pressure, and precipitation have been made at BRW since 1973. On June 25, 1990, the temperature at BRW was measured as 45°F. At the same time the temperature at the NWS office in the village of Barrow was measured at 71°F. This was the largest difference ever recorded between the two sites since measurements have been taken. Measuring equipment was checked at both sites to confirm the difference. The most likely cause was a heat island effect due to the wind direction and amount of ice still on the ocean. Wind was from the east and after passing over the relatively cold ice had only 0.8 km to pass over before it reached the observatory building and several miles over relatively warm land before it reached town. All equipment calibrations and maintenance were performed on schedule and without any problems of note.

CAMS

The Control, Acquisition, and Monitoring System (CAMS) was installed in the summer of 1984. It has worked with minimal problems since inception. During 1990 the only problems noted were during a power outage that caused start-up errors when power was restored and a separate incident of a bad monitor board. For a time the bad monitor board caused the aerosols and solar radiation acquisition box to quit several times per day. The board was changed and all autorestart problems were fixed.

Surface Ozone

Since the source of most of the ozone measured at the surface is from the stratosphere, a knowledge of the surface distribution can be useful in the study of transport processes in the atmosphere. Surface ozone has been measured at BRW since 1973 with an ECC. In 1974 a Dasibi chemiluminescent ozone analyzer was introduced and run in conjunction with the ECC. After a suitable side-by-side comparison, the Dasibi became the working station instrument and has been in use since then. The BRW instrument ran without problems all year. Routine cleaning of the optics was performed and weekly calibrations showed no problems.

Dobson

Dobson observations have been a part of the BRW operation since August 1973. With the exception of a break from 1983 to 1986, a continuous record of observations exists from 1973 to the present. The current instrument is Dobson no. 91. Over the years few problems have occurred with the Dobson instruments because of the long working history and the maintenance expertise that is available from personnel in Boulder. During this year, a clock drive motor was replaced in Dobson no. 91 in January after the old motor quit. Because of winter darkness, routine observations are started in February and continue through October. Boulder personnel visited the observatory in February to ascertain the condition of the instrument. The instrument was found to be in good shape. Minor maintenance of the Dobson was done during that visit.

Halocarbons

The halocarbons flask sampling project was initiated in September 1973 and has been carried out successfully since. There were no changes in this status during 1990. An automated HP-GC system was installed in October 1986 to measure N_20, CFC-11, CFC-12, CCl_4, and CH_3CCl_3. Since start up, the GC program has undergone several upgrades and minor modifications; most notable was the addition of a Shimadzu GC in 1987, which was optimized to measure N_2O. A column in the HP GC was changed to permit the measurement of CFC-113 in addition to the others mentioned above. During 1990 the majority of problems were either printer related or gas leaks due to the complex nature of the plumbing. During 1990 the sampling frequency was increased from one sample every hour to once every 0.5 hour. This has the advantage of greater precision by virtue of the larger statistical population used to calculate the concentration of the gases and a lower chance of electronic drifting between samples. The current sampling regime cycles through a calibration, an ambient air sample, a

calibration, and a second air sample for each species. The new system also employs a 2-point calibration for better accuracy.

Methane

To measure CH_4, an automated GC was installed in 1985. The automated GC measurements augmented prior CH_4 measurements obtained from flasks. CH_4 flask samples date back to 1983. Flasks for both the CO_2 and CH_4 are still being collected. Automated CH_4 GC samples are taken every 12 minutes using the following sampling scheme. Calibration gas, ambient air, calibration gas, etc. A 1-point calibration is used and very good accuracy is maintained. The system operated well all year with the only problem coming from the stream selection valve. The valve was replaced after it had become worn enough that it would no longer align itself with the ports.

Cooperative Programs

The cooperative program between CMDL and the USGS in Fairbanks has a long history that goes back to 1971-1972. For 1.5 years the USGS collected air samples for CMDL for a site suitability study. When it was determined that Barrow would be a good site, BRW was established and data collection began in January 1973. The Barrow Magnetic Observatory was started in 1949. In 1957 additional buildings were constructed at the present site. In 1975 all Barrow Magnetic Observatory functions were consolidated at the present site, approximately 0.4 km west the CMDL site and CMDL personnel began assisting in the operation.

Instrumentation in the magnetic observatory includes an EDA PPM-105 proton magnetometer and an EDA FM-100BR triaxial fluxgate magnetometer. The site is unmanned, and since the establishment of the observatory, BRW personnel check the operation once per week and report to the USGS as needed. A technician from USGS in Fairbanks performs an on-site inspection and collects data every 6 weeks. This cooperation between the two agencies has been beneficial over the years and it is expected to continue.

In 1978 the BRW staff assumed responsibility for reading and recording data from the University of Wyoming shielded rain gage. The gage is part of the Soil Conservation Service network of rain gages across the entire state of Alaska. In 1989 a program was established to study the collection efficiency of several types of collectors. BRW was chosen as one of the locations for this study because of the rapid service ability by CMDL staff members if any problems arise. Since then, the BRW staff have participated in the evaluation of five snow collectors.

A program was started in 1983 in cooperation with CSIRO to measure the $^{13}C/^{12}C$ ratio in ambient air. The theory is that the ratio should be decreasing due to the increased input of ^{13}C depleted CO_2 from combustion of fossil fuels. A pair of 5-L glass flasks are collected and shipped to Australia each month. Several broken flasks are noted throughout the year and steps have been taken to find the source of breakage.

The SIO CO_2 sampling program was one of the first flask sampling programs initiated at BRW in January 1974. Weekly samples have been taken since and continue up to the present. No problems have been reported and flasks were taken on a weekly basis.

A flask sampling program was initiated in 1983 with the University of California, Irvine, to measure CH_4. Personnel from the university are sent to Alaska each quarter to collect whole-air samples. A trip ending in BRW, consists of a transect across the state to collect samples. Samples are analyzed for CH_4.

The surface air sampling program started in August 1975. It is part of the 80th Meridian Program sponsored by the U.S. Naval Research Laboratory. The main objective was to study spatial and temporal distribution of radionuclides released by nuclear detonations and other nuclear events. Personnel also measured ^{210}Pb and ^{7}Be. The program at BRW consists of a weekly filter sample. The pump is checked once per month for proper flow and lubrication levels. Personnel from DOE visited the site in July to inspect and calibrate the pump and to train the SPO crew.

The Geophysics Research Laboratory of the University of Tokyo began measuring magnetic storm effects in 1985 at BRW. An audio-cassette recorder was modified to extend the life of a 90-minute audio cassette to 1 week and is used as a data logger. A series of three sensors were set up 70-m from the observatory building and are used to detect micro-pulsations of 0.001-5 Hz. In June 1990 the system was rewired by University of Tokyo personnel and the system was put into a standby mode.

The isotopic study of wetland and atmospheric CH_4 projects from the University of Washington continued through 1990, but there were problems with maintaining adequate supplies. BRW staff open 35-L evacuated flasks to the air, and samples are collected on a weekly basis. On several occasions the flasks were not available and several samples were missed. The project measures $^{13}C/^{12}C$ composition in CH_4 and was started in 1986.

The University of Washington also conducted an airplane aerosol project during June. In the course of the experiment, a TSI CNC was run at the station after it was discovered that it could not handle the rapid change in pressure in the airplane. There were no problems after it was installed as a ground-truth instrument.

BRW personnel collected whole-air samples for the OGC trace gas monitoring program. Using a metal bellows pump, a series of three stainless-steel flasks, 800-mL each, are filled with air and analyzed for halocarbons, CO_2, CO, and CH_4 at OGC. The program ran well all year and samples were collected on a weekly basis. This program was initiated in 1980.

During the winter of 1990, Biospherical Instruments, under NSF sponsorship, installed equipment in Barrow at UIC/NARL, to measure UV irradiance. The system consists of a high-spectral resolution scanning spectroradiometer optimized for UV light. BRW is part of the NSF spectroradiometer network. BRW personnel calibrate the equipment and troubleshoot any problems that arise in the hardware.

The University of Alaska, Fairbanks, maintains a chemiluminescent instrument used to measure NO, NO_y, HNO_3, and NO_3. The program has been operated in BRW in the past on a short-term basis. In February 1990 it was installed to run for at least 1 year. The only problem connected with the instrument was with the diaphragm pump. Several diaphragms showed signs of premature wear and subsequent failure. A GC for measuring PAN was also set up and was maintained by CMDL personnel for a 1-month period.

The Wave Propagation Laboratory in Boulder maintained a SODAR system in BRW for collecting inversion layer data. The system was augmented in March with a tethered balloon thermometer and an upward-looking radar antenna. The experiment was conducted, in part, to check out the equipment in an arctic environment. The project ended in April.

As in 1989, CIRES, under funding by the National Academy of Sciences, maintained a project to measure surface ozone and particulate and gaseous bromine at BRW to examine the causes of surface ozone destruction. A photochemical experiment was also performed to measure particulate bromine formation.

The University of Rhode Island filter sample was discontinued this year. It was started in 1976 and filters were collected until 1990.

The Naval Surface Warfare Center visited BRW to check on the viability of using the station as a base for data logging equipment used to record fluctuations in the earth's magnetic fields.

2.3. SAMOA OBSERVATORY

C.J. FARMER

2.3.1. OPERATIONS

During 1990 the major event in American Samoa was Hurricane Ofa. The hurricane passed near the island February 2-4, with the greatest intensity occurring during the afternoon of February 3; it was moving relatively slowly at 5-6 mph during that time. The hurricane had sustained winds of 65-75 mph with gusts at the observatory of over 100 mph. Over 6 inches of rainfall were recorded during this period and the minimum pressure at the observatory was 979 mb (986 mb at sea level).

Major damage at the observatory consisted of the loss of the walk-up tower at Matatula Point, the two buildings with all equipment that was contained in them, and the stair railings. There was also some damage to the main observatory building shingles and some of the rooftop instruments. For the most part, the only sampling program that was affected by the damage was the continuous CO_2 sampling. To get the program running again, a temporary sampling mast was installed at Matatula Point and new lines put in place to the bottom of the stairs. This was completed by the middle of April and sampling continued with this temporary setup until the middle of October.

The generator failed during the hurricane due to a bad fuel transfer pump from the underground tank to the "day" tank. It stopped around the peak of the hurricane. The photovoltaic system did keep the meteorological and solar instruments running throughout the hurricane passage.

The major work to repair the Hurricane Ofa damage began in June. A new Matatula Point building was constructed using concrete blocks with a concrete roof. This is expected to be a more permanent building if another hurricane passes near the area. Repairs were then made to the stairs with many of the support posts and planks and all the railings being replaced. The carport and main building were then reshingled and after a delay to wait for wood to arrive, a new roof cap was put in place. Later in the year this new wood began to warp badly and it was brought to the attention of the contractor. A solution had not been worked out by the end of the year. After all the other work was completed, the outside of the observatory building and the surrounding concrete were repainted. There were also some repairs necessary on the houses due to the damage done by the hurricane. The roofs both needed to be reshingled and the garages needed repair. This work was not completed by the end of the year. Other work on the houses included remodeling of the kitchen in T-7 and preparation of the house T-11 for new personnel. The carpets were steam-cleaned, a new stove was purchased for the house, and some small repairs were performed. Other repairs were made once the new person arrived. Estimates were also obtained for a couple of larger jobs that needed to be done.

The diesel tank for the generator was tested for leaks in November. This was part of an island-wide testing program to check all underground storage tanks instituted as a result of action by the Environmental Protection Agency. The tank showed no leaks. Testing of this nature will have to be done on a bi-annual basis to conform with the new regulations.

A new computer was purchased for the observatory. The new unit is a Compaq 386S and should provide us with enough computing power for several years.

The observatory was broken into during the year on at least one occasion. The major item taken was a camera belonging to the Station Chief that was being used to take pictures of the repair work at the observatory.

The government pickup was involved in an accident in early October. It went off the road and flipped upside down in shallow water. There was no serious injury, but the vehicle was a total loss. A replacement vehicle (1986 Dodge pickup) arrived by the end of November.

There was a staff change at the observatory during the year. The electronics technician was replaced by an electrical engineer. There was temporary help by the electronics technician from MLO to fill the gap between the technician's departure and the engineer's arrival.

2.3.2. PROGRAMS

Table 2.4 summarizes the programs at the observatory for 1990. Further discussion of some of the programs follows.

TABLE 2.4. Summary of Measurement Programs at SMO in 1990

Program	Instrument	Sampling Frequency
Gases		
CO_2	URAS-2T IR analyzer	Continuous
CO_2, CH_4	3-L glass flasks	1 pair wk^{-1}
	0.5-L glass flasks, through analyzer	1 pair wk^{-1}
	0.5-L glass flasks, P^3 pump unit	1 pair wk^{-1}
Surface O_3	Dasibi ozone meter	Continuous
Total O_3	Dobson spectrophotometer no. 42	4 day^{-1}
O_3 profiles	Balloonborne ECC sonde	2 mo^{-1}
CFC-11, CFC-12, N_2O	300-mL stainless steel flasks	1 pair wk^{-1}
CFC-11, CFC-12, N_2O, CCl_4, CH_3CCl_3	HP5890 automated GC	1 sample $(2\ h)^{-1}$
N_2O	Shimadzu automated GC	1 sample $(2\ h)^{-1}$
Aerosols		
Condensation nuclei	Pollak CNC	1 day^{-1}
	G.E. CNC	Continuous
Optical properties	Four-wavelength nephelometer	Continuous
Solar Radiation		
Global irradiance	Eppley pyranometers with Q and RG8 filters	Continuous
	Eppley pyranometers with Q filters on tilted mounts	Continuous
Direct irradiance	Eppley pyrheliometer with Q filter	Continuous
	Eppley pyrheliometer with Q, OG1, RG2, and RG8 filters	Discrete
Turbidity	Sunphotometers with 380-, 500-, 778-, and 862-nm narrowband filters	Discrete
Meteorology		
Air temperature	Thermistors (2)	Continuous
	Max.-min. thermometers	1 day^{-1}
Dewpoint temperature	Polished mirror	Continuous
Pressure	Capacitance transducer	Continuous
	Mercurial barometer	1 wk^{-1}
Wind (speed and direction)	Bendix Aerovane	Continuous
Precipitation	Rain gauge, weighing bucket	Continuous
	Rain gauge, tipping bucket	Continuous
	Rain gauge, plastic bulk	1 day^{-1}
	Aerochem wet/dry collector	1 day^{-1}
Precipitation Chemistry		
pH	Fisher model 805 meter	1 day^{-1} (CMDL); 1 wk^{-1} (NADP)
Conductivity	Beckman model RC-16C meter	1 day^{-1} (CMDL); 1 wk^{-1} (NADP)
Cooperative Programs		
CO_2, ^{13}C, N_2O (SIO)	5-L evacuated glass flasks	3 flasks wk^{-1}
GAGE project: CFC-11, CFC-12, N_2O, CH_3CCl_3, CCl_4 (SIO)	HP5880 gas chromatograph	1 h^{-1}
Various trace gases (OGC)	Stainless steel flasks	3 flasks wk^{-1} (3 flasks set^{-1})
Wet-dry deposition (NADP)	HASL Chemetrics wet-dry collector	1 wk^{-1}, wet; discrete, dry
Bulk deposition (EML)	Plastic bucket	Continuous (1 bucket mo^{-1})
Hi-vol sampler (EML)	High-volume sampler	Continuous (1 filter wk^{-1})
Hi-vol sampler (SEASPAN Project)	High-volume sampler	Continuous (1 filter wk^{-1})
CO_2, CH_4, trace gases (NCAR)	Evacuated stainless steel flasks	1 pair wk^{-1}
$^{13}C/^{12}C$ ratio (Univ. of Wash.)	30-L pressurized cylinder	2 mo^{-1}
Light hydrocarbons (UCI)	1-L evacuated stainless steel flasks	3-4 flasks qtr^{-1}

Carbon Dioxide

The continuous measurements were most affected by the hurricane. The loss of the tower at Matatula Point and the buildings to house the water removal system resulted in these measurements being discontinued until the middle of April. The installation of new sampling lines to the Point had been completed prior to the hurricane and testing the new lines against the old lines was underway. A temporary sampling mast and a small building were erected at the Point in April so that continuous measurements could be restarted. The measurements from this temporary mast were in agreement with those just before the hurricane. This setup ran until October. The problem with the cracked pump heads on the CO_2 air pumps continued.

In October a new sampling mast was installed and the moisture removal system for the CO_2 sampling line was moved into the new building at the Point. The sampling mast is now a 13-m tall aluminum mast. New CO_2 sampling lines were installed from the mast to the bottom of the stairs at this time as well. The air cadet pumps were moved from the main building to the Point building in an attempt to cure the problem of the cracked heads. This has taken care of the problem.

During this same time period, a new Siemens continuous analyzer was installed in the main building to monitor CO_2.

A new flask sampling unit was put into use in October. The so-called MAKS unit is used to fill the 0.5-L flasks and is designed to also accept 3-L flasks with two sampling ports when they become available. A problem with water vapor content of the air caused a significant disagreement between the flask pairs at first. This was solved by reducing the pressure to which the flasks were filled.

Surface Ozone

Observations continued during 1990 with no significant problems or downtime. Occasional loss of data occurred when the CAMS unit failed to recognize the signal from the Dasibi.

Total Ozone

Observations were conducted throughout the year without difficulty. The measurements were changed for awhile during August through October to a CDADC sequence instead of the normal ADADA sequence.

Ozone Profiles

In January two launches were made before the ozonesonde program was discontinued due in part to the hurricane, but also lack of funding.

Nitrous Oxide and Halocarbons

The GC operated during the year with only a few problems. There was a continuation of the problem with the Shimadzu GC not coming up on line after a power failure. The stream select valve failed in November and caused some loss of data. The most puzzling problem was the presence of a contamination peak on channel B that was affecting the methyl chloroform peak on one of the calibration standards.

In late October a new operating program was installed. This program provides the capability of plotting out the data from the previous 30 days for any of the gases sampled. This has not only increased the interest of the observatory personnel in the results, but could also prove to be an important diagnostic tool.

A new printer was also installed during the year. This has cured the problems with the paper jams that seemed to be occurring quite often. The paper handling system was also arranged so that an entire box of paper can be put into service at a time. This not only decreases the chance of running out of paper, but also saves a great deal also.

Flask sampling continued on a weekly basis when flasks were available. LEAPS flasks were substituted for the 300-mL flasks once per month when available.

Aerosols

The G.E. CNC had problems with a high background after it was greased in July. It was taken apart and boiled out and the problem was taken care of. The only other problem was condensation accumulating in fairly large amounts in the inlet line. The line was shortened as much as possible and any sags were removed and later insulation was added to cure the problem. There were no significant problems with the nephelometer during the year. All calibrations were performed as necessary.

Solar Radiation

The pyrheliometer suffered from tracking problems during part of the year. Realignment and leveling in September alleviated most of this problem. A bad cable on the tracking NIP went undetected for a couple weeks in December causing some loss of data for this instrument. The RG8 pyranometer was swapped out during the year. The filter-wheel NIP was compared with the standard NIP during June. The sun photometers began having problems during the latter part of the year, but apparently the program had been discontinued and no replacements were sent to the observatory.

Meteorology

The meteorology program had no significant changes during the year. The cable running from the observatory to the Aerovane was replaced in July and August. Wind data was lost for about a month as a result of this problem. A new Aerovane was installed shortly before this problem had occurred. Instrumentation ran well during the hurricane with the wind record being pegged (100 mph) on at least two occasions. The temperature board on the dewpoint hygrometer went bad resulting in bad air temperature readings with this instrument, however the dewpoint measurements continued in agreement with sling psychrometer measurements (within 1°C).

Precipitation Chemistry

Daily precipitation samples continued to be analyzed for pH and conductivity during the year. These samples were then sent to MLO for further analyses. SMO began

analyzing some of the samples at the observatory for several different ions. No major problems with the wet/dry collector occurred during the year.

Cooperative Programs

There were no changes in cooperative programs at the observatory during the year. The most significant involvement during the year was the participation in the NASA Globe Program through the SEASPAN project of the University of Miami. During the months of May and June daily filter changes were made to provide ground measurement support for the program. The operation of the GAGE gas chromatograph was taken over by SIO. This system was down for almost the entire year, due first to the loss of a calibration tank and then to the change of principal investigators on the project. The observatory also provided support for the Combined Release and Radiation Effects Satellite Program. The University of Alaska, Fairbanks, conducted measurements on two evenings at the observatory studying the ionization of gases released from a satellite passing overhead using a low-light camera.

A new measurement program was begun in early May that includes sampling for formic, acetic, and nitric acids, and sulfur dioxide. It utilizes a condensation sampling technique and analysis by ion chromatography. The results are to be compared with other measurements performed on the marine boundary layer during the past several years and will also be used to study direct emission of the organic acids from vegetation. The long-term measurements of the nitric acid and sulfur dioxide will be used to detect local effects from the nearby villages well as long-range transport into the area.

2.4. South Pole Observatory

C. Groeneveld

2.4.1. Operations

The normal schedule of deployment of personnel to SPO does not conform to the calendar year, instead it covers the period from about November 1, 1989, to November 1, 1990, and consequently this report will review this period of operations.

SPO staffing for the winter totaled 20 people, 6 scientists, and 14 support personnel hired by the NSF contractor. During the summer, the station population varied from 40 to 100 people.

The CMDL 1989-1990 SPO staff arrived at the South Pole on November 1, 1989. CMDL Boulder personnel spent November and December at the SPO to assist in the station turnover helping in operations and maintenance tasks, as well as to upgrade the NOAH GC's.

In the spirit of South Pole cooperation, help from other winter-over scientific and technical personnel was obtained for CMDL operations when needed. CMDL's balloon program was expanded to include a cooperative effort with the University of Wyoming.

The SPO operation is located in the Clean Air Facility (CAF) upwind of the main Amundsen-Scott South Pole Station. The CAF is a wood frame building, 5 m × 10 m, with the long axis of the building lined up approximately grid north and south (the Greenwich Meridian is grid north at the South Pole). CMDL's operations are part of NSF's total science complement that uses the CAF. The CMDL programs occupy about one third of the building, while the remaining two thirds of the CAF are occupied by summer science programs that have NSF grants, CMDL cooperative projects, several NSF winter-science projects, and a joint CMDL and CAF electronics shop.

The CAF was built and suspended above the snow surface on steel "H" beams to prevent it from being drifted over and to keep the air sampling stacks above the blowing surface snow. Built in 1977, the CAF was raised once in 1987 and the base of the building is presently about 2 m above the snow surface.

Two major projects were planned for the CAF during the 1990 austral summer: removal and replacement of the fiberglass insulation in the roof with blue board and a complete rewiring of the CAF electric distribution. Both projects were put on hold due to delays in other SPO projects. These other projects included the raising and repairing of the dome over the main station and the replacement of the powerplant generators. The dome project that included the removal of a large snow drift that had formed downwind of it was completed as planned. However, only one generator was replaced which caused some minor power conservation inconveniences during the year.

The problem of summer overheating inside the CAF was solved by reducing passive solar heating inside of the building by covering the windows in the main room with silvered opaque plastic. The window coverings and an upgrading of the exhaust fan in the main instrument room wall helped to reduce the disruptive CAF temperature variations that have been experienced in other years. The building still experiences cold inside temperatures in the winter, but this cooling impacts human habitation more than it interferes with operating equipment. In winter the inside building temperature varies from about 65°F to 45°F and is a function of the wind direction and speed and the outside ambient air temperature. The silvered opaque plastic was removed at sunrise to allow the new crew to install reflective film.

Data transmission was improved this year due to the installation of a Novell Network line from the COMMS office to the CAF and the addition of LES-9 satellite transmissions from SPO to the continental United States.

Message traffic is relayed via satellite from SPO to Florida and then by telephone line transmission to Boulder. An alternate route that is sometimes used goes by HF radio to McMurdo and then via satellite to Malabar, Florida. The ASA Communications Coordinator is the first contact in this process, transmitting all outgoing traffic and receiving and sorting all incoming messages. Messages are handled as either data or text and all traffic to or from SPO is accessible to NSF, ASA, CMDL, and the other PI's.

Data transmission can be limited in the summer when the summer increase in science projects results in an increase of data transmission to the continental United States; however, no limit was imposed on the science projects during the winter. The communications coordinator was able to send out as much traffic as satellite time and weather conditions would allow during the winter. There were occasional delays of a day or two but all data would eventually get sent out. Blowing snow can create enough static charge on the outdoor ground antennas that there were periods when receiving or transmitting messages were not possible at SPO.

Typical message traffic for CMDL included monthly CAMS data, NOAH GC data every 5 days, BSI UV data daily, and general text messages to Boulder. The entire suite of CMDL projects continued and remained in operation throughout the year. They are listed in Table 2.5. A summary of the major upgrades for each project follows:

2.4.1. PROGRAMS

Aerosols

The CMDL operator makes two sets of three discrete observations each day with the Pollak CNC. The Pollak observations are used to calibrate the G.E. CNC and the TSI CNC. The microamperes meter was replaced at opening and then the lamp power supply was rebuilt in November. After that, the Pollak operated normally.

The TSI CNC makes continuous aerosol measurements and was installed during the summer of 1989 to replace the G.E. CNC. When the supply of butyl alcohol ran out several months before station opening, the TSI was turned off and remained on inactive status until station opening when more butyl could be brought in. After receiving the butyl alcohol, the TSI was back on line by November 22 and ran problem free for the rest of the year.

The G.E. CNC has been the primary instrument used to make continuous aerosol measurements at SPO since 1975. Both G.E.s on station were rebuilt during the summer and continued operation until about March when one G.E. began to drift from calibration to calibration. The valve seized on one instrument and the spare G.E. would not settle out or stabilize from one calibration to another. The inter-comparison with the TSI was terminated in August, after adequate overlap data with the TSI was obtained. The G.E. counters were retrograded back to Boulder on opening in November 1990 and continuous CNC measurements will now be obtained with the TSI counter.

The optical properties of submicron aerosols are determined with the nephelometer by measuring the difference in light scattering between a control air sample and the ambient air sample. The nephelometer ran trouble free all year. A CO_2 calibration was performed in April. In September the four channels began to stair step on the chart recorder, but normal operations were achieved by checking and refurbishing all the control boards in the instrument.

The aethalometer measures the carbon content of submicron aerosols by measuring light absorption on aerosols collected on a filter substrate. The aethalometer ran without problems for most of the year. In July the light source became intermittent for about 2 weeks but normal operations were achieved by reseating and aligning the light source on top of the filter chamber. This problem occurred once more before station opening and was solved by the same method.

CAMS

The CAMS has been collecting data at SPO since 1984. It uses 250 Kbyte DEC tapes to record data. No records of CAMS BRAM lost or autorestarts were kept. Most autorestarts were the result of keypad lock-ups due to improper or too rapid entries. The rest were due to temporary power losses by either routine maintenance or occasional malfunctions in the SPO power plant. The CO2 CAMS lost a BRAM board on August 1, probably due to a static discharge. The BRAM board was replaced and normal operations resumed by August 8.

Carbon Dioxide

The CO_2 program consists of a continuous infrared analyzer that makes in situ measurements and a flask sampling program that augments and provides for independent checks on the continuous sampling program. Both programs began in 1975. New station gas standards were installed and instrument calibrations were run in early January. In late January the continuous analyzer's relay board malfunctioned and the CO_2 standard gas and air lines would not switch through its normal cycle. A spare board was located, installed, and normal continuous analyzer operations resumed. The air sampling pump diaphragm was replaced in May and once again in June. During the May diaphragm replacement, the pump lines were inadvertently reversed. This reversal of lines occurred on May 19 and was not discovered and fixed until May 20. Working gases were replaced in May and again in October.

Meteorology

The standard meteorology measurements of wind direction and speed, 2-m and 20-m temperature, 2-m humidity, and station pressure continued as in years past. The more complicated hygrothermometer was removed from the roof of CAF and installed at 2-m AGL on the meteorological tower in December. After the tower installation, the instrument was checked out and calibrated. During the winter the air intake orifice of the hygrothermometer would become packed with snow and frost, especially during humid or windy conditions at which time such accumulations in the line would occur more often. This accumulation of snow and ice increased the maintenance required for the hygrothermometer significantly.

The T_a and T_b winter calibration was conducted during March 10-April 13. The length of comparison was mainly due to inexperience and difficulty with communication to and from Boulder in trying to resolve procedural problems. The calibration was eventually completed and resolved at the South Pole but 1 month of T_a - T_b data were lost.

TABLE 2.5. Summary of Measurement Programs at SPO in 1990

Program	Instrument	Sampling Frequency
Gases		
CO_2	URAS-2T IR analyzer	Continuous
CO_2, CH_4	0.5-L glass flasks, through analyzer	1 pair twice mo^{-1}
	0-5L glass flasks, P^3 pump unit	1 pair twice mo^{-1}
Surface O_3	Dasibi ozone meter	Continuous
Total O_3	Dobson spectrophotometer no. 80 and no. 82	3 day^{-1}
Ozone profiles	Balloonborne ECC sonde	1 wk^{-1}, summer, autumn, winter; 1 $(3\ day)^{-1}$, spring
CFC-11, CFC-12, N_2O, CH_3CCl_3, CCl_4	Shimadzu automated mini-2 gas chromatographs	1 sample $(3\ h)^{-1}$
	300-mL stainless steel flasks	1 pair wk^{-1}, summer
CFC-11, CFC-12, N_2O	300-mL stainless steel flasks	3 wk^{-1}, summer
Aerosols		
Condensation nuclei	Pollack CNC	1 day^{-1}
	G.E. CNC	Continuous
	TSI CNC	Continuous
Optical properties	Four-wavelength nephelometer	Continuous
Carbon aerosols	Aethalometer	Continuous
Solar and Terrestrial Radiation		
Global irradiance	Eppley pyranomters with Q and RG8 filters	Continuous, summer
Direct irradiance	Eppley pyrheliometer with Q, OG1, RG2, and RG8 filters	Discrete, summer
Turbidity	Sunphotometers with 380-, 500-, 778-, and 862-nm narrowband filters	Discrete, summer
Albedo	Eppley pyranometers with Q and RG8 filters, downward facing	Continuous, summer
Meteorology		
Air temperature	Platinum resistor, 2- and 20-m heights	Continuous
Pressure	Capacitance transducer	Continuous
	Mercurial barometer	2 times wk^{-1}
Wind (speed and direction)	Bendix Aerovane	Continuous
Frost-point temperature	Hygrometer	Continuous
Cooperative Programs		
CO_2, ^{13}C, N_2O (SIO)	5-L evacuated glass flasks	2 mo^{-1} (3 flasks $sample^{-1}$)
Total surface particulates (DOE)	High-volume sampler	Continuous (4 filters mo^{-1})
Various trace gases (OGC)	Stainless-steel flasks	Twice mo^{-1} (3 flasks set^{-1})
^{14}C (NOAA/ARL)	1,500 and 3,000 psi spheres	250 or 500 psi day^{-1}
Snow aciditiy (NOAA/ARL)	125-mL Nalgene flasks	1 $(2\ wk)^{-1}$
Interhemispheric $^{13}C/^{14}C$ (CSIRO)	5-L glass flasks	1 or 2 flasks mo^{-1}
Ultraviolet radiation (NSF)	UV radiometer, data logger	Periodic
Polar stratospheric clouds (Univ. of Rome)	Optical lidar	Instrument inoperative

A nagging and persistent problem with the take-up reel on the wind recorder caused the paper to jam in the recorder. The problem was traced to the aluminum gears on the take-up reel. The problem was solved by shifting the drive gear over about 1 mm and filing the burrs off the take-up reel.

Halocarbons

Two Shimadzu automated mini-2 GCs analyze ambient samples twice each hour and a summer flask sampling program collects ambient air sample pairs once per week.

The GC in situ sampling of N_2O, CFC-12, and CFC-11 began in 1983, and CH_3CCl_3 and CCl_4 were added at a later date. Flask sampling measurements for N_2O, CFC-12, and CFC-11 began in 1977.

Both GC's were upgraded and rephumbed in January. Argon-methane carrier gas was added to GC1 at that time. Both GCs ran all year without a mole sieve change. GC1 experienced a steady decrease in peak height throughout the year, possibly caused in part by a sensitivity loss because the mole sieve was not changed. By September, the F12 peak on GC1 was below the threshold set for recording the peaks to the PC; this in turn caused the data integrator to revert to a default mode and stop recording data. The F12 peak, however, was still showing up on

the GC chart recorder. When this was discovered and rectified on September 27, data was once again recorded on the PC by lowering the threshold value on Integrator 1.

Solar Terrestrial Radiation

This surface-based program measures several components of the solar and terrestrial radiation budget at the snow surface using Eppley pyranometers and pyrgeometers that measure global and albedo radiation, pyrheliometers for direct solar radiation, and J-series sunphotometers for turbidity. Solar radiation measurements have been made since 1976.

The solar radiation rack inside the CAF was upgraded and rewired in early December. During this period all experiments were off line.

An experiment was conducted to determine the effectiveness of snow and frost removal by aspiration on Eppley pyranometer RG8 domes in the summer and quartz domes in the winter. While the aspiration works, it does not always keep the domes free of frost buildup especially when temperature, humidity, and cloud cover conditions combine to create persistent frost buildup on the domes.

Ozonesondes

The balloon sonde program that was started in 1986 to investigate the destruction of stratospheric ozone over SPO, continued throughout the year with 50 successful flights. ECC ozonesondes were used with a VIZ radiosonde and a GMD radiotheodolite receiving system to make each sounding. The GMD tracking system is used jointly with the South Pole Meteorology Office. Flights were occasionally postponed due to high winds.

Surface Ozone

Surface ozone measurements have been made at SPO since 1975 and have provided an uninterrupted data set of tropospheric ozone in one of the cleanest places on earth. Dasibi 1328 was replaced by a 5000 series instrument (the most up-to-date version of Dasibi ozone measurement instruments) in January and normal SPO operations continued throughout the year. The Dasibi-CAMS interface problem continued intermittently throughout the year.

Total Ozone

Dobson total ozone measurements at SPO were started in November 1961 and have continued to the present. Dobson instrument no. 82 was replaced by no. 80 in December 1989. Dobson no. 82 was returned to Boulder for calibration and refurbishment. During shipment to SPO, Dobson no. 80 was inadvertently handled as regular cargo and left outside at subfreezing temperatures. The freezing of the instrument contributed to some initial calibration problems. To remedy this, two calibrations per month were conducted until October 1990 to monitor the situation. At that time it was determined that Dobson no. 80 had completely stabilized.

Frostpoint Sondes

This year a new frostpoint sounding program was initiated at SPO to obtain preliminary measurements of stratospheric water vapor. Most of the equipment for the frostpoint-backscatter project didn't arrive until the middle of January and then due to end of season activities, didn't get inventoried until late February. The telemetry didn't become operational until April and instrument preparation took much longer than anticipated. The biggest setback to this program was the final requirement to inflate the balloons outside because no sheltered area opening was large enough to exit with a fully inflated balloon. Because of this, we could only fill and release balloons when wind speeds were less than 10 kts from the northeast or less than 7 kts when winds were from the east. Ten soundings were planned for the year, but due to the initial equipment delays and weather problems only seven flights were completed.

Cooperative Programs

The CMDL program conducted eight cooperative research programs with other independent PIs during the year (Table 2.5). These programs are carried out with NSF approval and provide a way for CMDL and NSF to participate in additional research projects that are closely related to the CMDL and NSF missions with minimum cost and logistical support. These research projects have their own funding and principal investigators, and the CMDL program usually provides manpower for their operation, maintenance, and data collection.

SCRIPPS-CO_2 Flask Sampling. No problems occurred this year. This program continued the long-term monitoring of CO_2, $^{13}C/^{12}C$ ratio, and N_2O.

OGC Flask Sampling. No problems occurred this year. This program continued to determine the seasonal cycles and annual trends in CH_4, CO, CH_3Cl, CH_3I, CH_3Br, F-113, CH_3CCl_3, C_2Cl_4, F-22, SF_6, F-11, F-12, F-114, N_20, and other trace species.

ARL ^{14}C Atmospheric Monitoring. No problems. 1500 PSI spheres were used through September and then the 3000 PSI spheres were used for the rest of the year. This program continues to monitor ^{14}C in the atmosphere as part of a world-wide network to monitor debris from nuclear explosions.

CSIRO Flask Sampling. No problems. This program obtains values of the ratio of $^{13}C/^{12}C$ in atmospheric CO_2. This information is used in the constraints of a 2-D global carbon cycle model which will determine the magnitudes of the different carbon sources in atmospheric CO_2 that are involved in the fluxes in the global carbon cycle.

NZARP Remote Atmospheric Sampling. This experiment was discontinued and removed from clean air in early December.

CMDL Snow Samples (MLO). Two samples per month were collected during the summer months and one sample per month was collected during the winter months. Several

samples were removed by station personnel from their usual storage place and were subsequently misplaced. These samples were never found.

DOE Atmospheric Aerosol Sampling-Filter Samples. No problems. The primary objective of this program was to study the spatial and temporal distribution of specific natural and man-made radionuclides in the surface air.

Backscattersondes. This experiment incurred many of the same problems encountered with the frostpoint project. Four of the instruments were found to be inoperative after the initial set up. The purpose of this program is to understand the formation of polar stratospheric clouds in the Antarctic and their role in ozone destruction.

2.5. REFERENCES

Bodhaine, B.A., and R.M. Rosson (Eds.), *Geophysical Monitoring for Climatic Change, No. 16: Summary Report 1987*, 110 pp., NOAA Air Resources Laboratory, Boulder, CO , 1988.

Elkins, J.W., and R.M. Rosson (Eds.), *Geophysical Monitoring for Climatic Change, No. 17: Summary Report 1988*, 142 pp., NOAA Air Resources Laboratory, Boulder, CO, 1989.

Komhyr, W.D., and R.M. Rosson (Eds.), *Climate Monitoring and Diagnostics Laboratory, No. 18: Summary Report 1989*, 141 pp., NOAA Environmental Laboratories, Boulder, CO, 1990.

Thoning, K.W., P.P. Tans, and W.D. Komhyr, Atmospheric carbon dioxide at Mauna Loa Observatory, 2, Analysis of the NOAA GMCC Data, 1974-1985, *J. Geophys. Res., 94(D6)*, 8549-8565, 1989.

3. Atmospheric Radiation Monitoring Group

J. J. DELUISI (Editor), E.G. DUTTON, F. KREINER, D.W. NELSON, AND R. STONE

3.1. CONTINUING PROGRAMS

3.1.1 SURFACE RADIATION

Surface radiation budget, atmospheric transmission, and aerosol remote sensing measurement projects at the four CMDL observatories continued through the year with no significant modifications in the measurement systems until year's end when sunphotometer measurements were discontinued at all sites but MLO. Table 3.1 shows the current baseline observatory measurement projects being overseen by the ARM Group. Other ongoing projects maintained are the surface radiation budget measurements made at the top and at the base of the 300 m BAO tower near Erie, Colorado, and down-welling broadband solar and thermal irradiance measurements at Kwajalein and Bermuda. Results of these and other ARM measurement projects during past and preceding years have been used in studies of surface radiation budget characteristics, light-sensitive atmospheric chemical reactions, satellite algorithm verification, climatic impact of volcanic eruptions, climatic trends and variability, errors in ozone remote sensing, surface optical properties, cloud optical properties, radiative transfer calculation verification, instrument development and improvement, and solar energy assessment and utilization. A summary of significant results from the ARM baseline radiation projects follows.

A dramatic trend in solar irradiance in the late summer at SPO was detected in the 14-year CMDL global pyranometer record and was shown to be caused by a related trend in cloudiness, *Dutton et. al.* [1991]. The annual forcing of diurnal cycles in the near-surface radiation budget as measured at BAO are discussed in *Dutton* [1990]. Surface radiation measurements made at the BAO site were used to verify satellite determinations of the surface radiation budget as discussed by *Cess et. al.* [1991]. The BRW surface solar albedo record was used by *Dutton and Endres* [1991] to better define the data of spring snow melt in the Alaskan arctic and improve knowledge of possible related climatic trends.

Kwajalein, Bermuda, and BAO as well as BRW and SPO, are candidate sites for participation in the WMO World Climate Research Program's Baseline Surface Radiation Network (BSRN). The BSRN will consist of approximately 20 sites globally with participation from several nations. The purpose of the BSRN is similar to CMDL's surface radiation project, but with emphasis on satellite validation as well as better resolution of regional and global variability.

Beginning in 1989 a different procedure for assuring the long-term calibration stability of the solar radiation sensors was implemented for the four CMDL sites. The new procedure involves swapping instruments once every 2 years with an instrument recently calibrated at the Boulder Solar Radiation Facility. This procedure replaces the system where the instruments' calibrations were monitored on site by a traveling standard. Some on-site visits by traveling standards will continue as a secondary check on the instruments' calibration.

TABLE 3.1. Current Radiation Measurements at CMDL Observatories

	SWD	SWU	LWD	LWU	RG8D	DIRQ	FWNIP	SPHTM	MISC
BRW	X	X	X	X	X	X	X	X	O
MLO	X	O	O	O	X	X	X	X	X
SMO	X	O	O	O	X	X	X	X	O
SPO	X	X	X	X	X	X	X	X	X

X, measurements made; O, measurements not made; SWD, shortwave downward solar irradiance; SWU, shortwave upward (reflected) solar; LWD, longwave downward (sky emitted); LWU, longwave upward (earth emitted); RG8D, downward solar (RG8 filter, 0.7 to 3.0 μm) irradiance; DIRQ, direct solar; FWNIP, filter wheel normal incidence pyrheliometer (discrete observations, four solar bands); SPHTM, multiwavelength sunphotometer; MISC, miscellaneous—MLO: global diffuse solar, downward solar (OG1 filter, 0.53 to 3.0 μm), 2-channel sunphotometer (water vapor), 3-channel sunphotometer (calibration standard); SPO: RG8 albedo, direct sun (RG8 filter).

Observatory Activities

An Eppley computer-controlled tracker was sent to BRW to replace the aging LiCor tracker. The BRW installation is the harshest environment in which these new computer-controlled trackers have been field tested. Also at BRW, the pyrgeometers now operate without temperature compensating batteries. The battery circuit data were only used for real-time monitoring, but tended to interfere with other signals. Air ventilating systems are scheduled to be added to the upward facing pyrgeometer to reduce solar heating errors and prevent ice accumulation on the dome. Pyrgeometer no. 27407 went online October 1, 1990, replacing the upfacing instrument, no. 23896.

After nearly two decades of field service, the MLO tracking pyrheliometer no. 2119 began to show serious signs of sensitivity loss and was replaced on April 4, 1990, by NIP no. 16657.

SMO continues to be a severe testing site for radiation instrumentation where weather-tight instruments absorb moisture, spectral filter material provides a culture for apparent fungus and bacterial decay, and calibration constants drift three to four times faster than normal. However, the program is maintained with relatively frequent instrument exchanges and calibration corrections. The SMO pyrheliometer was swapped in April with instrument no. 16229 replacing no. 11947.

The new SPO albedo rack served well during its 2 years of operation. The rack was designed to keep the downfacing instruments 2.0-2.5 m above the surface, but must be rotated onto the upfacing position on occasion for cross comparison with other sensors. Instrument icing, particularly on the upfacing pyrgeometers, is attended to on a nearly daily basis by the observer; but, ice still accumulates on the instrument to the extent that some data is lost. Beginning in December 1990 dome ventilation, similar to that used on the PSPs, was added to the upfacing pyrgeometer and helps greatly in keeping the ice off the dome. The effect of adding the blower to the pyrgeometer was thoroughly tested and no resulting additional error was detected. Data that are determined to be contaminated by icing are edited from the data base during post processing.

Example Results

Examination of the year-to-year variation of monthly mean global solar irradiance at SPO has revealed large significant trends for the months of February and March. The irradiance during these months has decreased between 1976 and 1988; however, the most recent data indicated that this trend is currently subsiding. Figure 3.1 shows the SPO solar irradiance trends for each month. The decrease in solar irradiance is attributed to increased cloudiness and is discussed further by *Dutton et al.* [1991].

The long-term atmospheric transmission record from MLO is shown in Figure 3.2. The transmission is calculated after the technique introduced by *Ellis and Pueschel* [1971]. The earliest data in the record suggested that a biennial cycle in the transmission may exist. The possibility of the presence of such an obvious signal was masked by numerous volcanic eruptions after 1963. However, complex demodulation of the record and subsequent coherency analysis revealed a high level of coherency between a quasi-biennial cycle, the transmission record, and the well-known QBO in the equatorial stratospheric zonal wind field. Figure 3.3 shows a plot of the coherency between the amplitude of the transmission annual cycle and the QBO. This result is further discussed by *Dutton* [1991].

Surface solar albedo data collected at BRW have been used to help establish the long-term date of spring snow melt. Earlier work of *Foster* [1989] suggested that significant trend was present in the date of snow melt near BRW. The CMDL albedo record provided evidence to the contrary as discussed by *Dutton and Endres* [1991].

As of press time for this publication, the optical and radiation budget effects of the 1991 eruption of Mt. Pinatubo are being assessed in the radiation data collected at MLO.

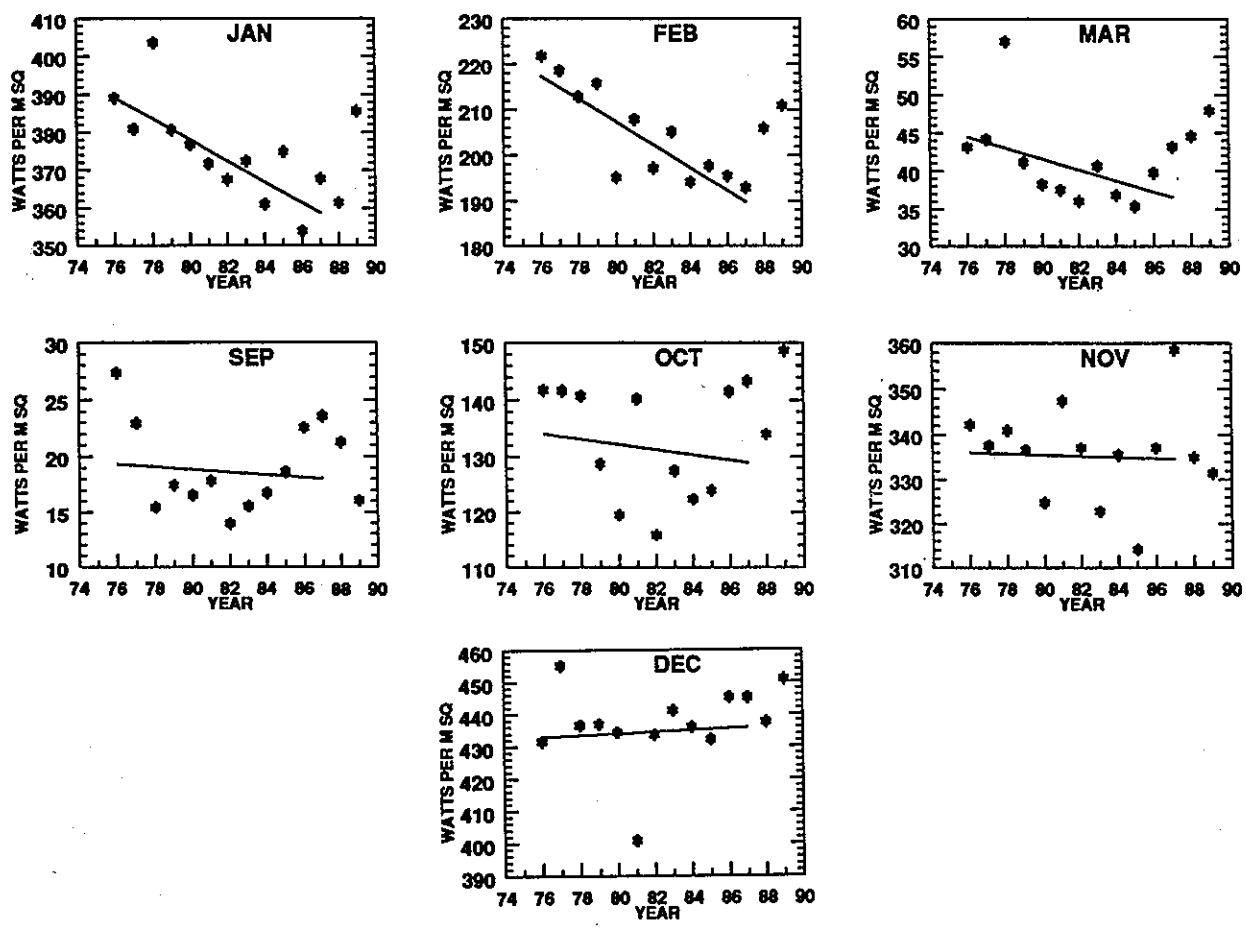

Figure 3.1. The month-by-month year-to-year variation is surface global solar irradiance at SPO. Significant trends are seen for January and February with a clear lack of any indication of a trend in most other months.

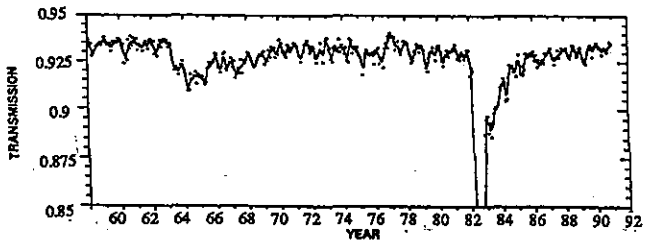

Figure 3.2. MLO direct solar transmission with a 7-month lowess smoother. The solid line plotted for the smoother reveals a persistent annual cycle, the instantaneous amplitude of which can be determined by complex demodulation.

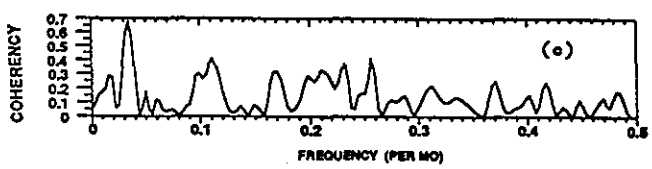

Figure 3.3. The coherency between the equatorial zonal winds and the amplitude of the annual cycle in the MLO transmission record. The peak near a frequency of 0.037 (period of 27 months) corresponds to the dominant quasi-biennial oscillation in the equatorial zonal wind field.

Although the total amount of material ejected from Pinatubo is believed to be greater than that from El Chichon, the impact at MLO will be less for Pinatubo primarily because the horizontal dispersion of the material is substantially different as seen by satellite.

3.2. Special Projects

3.2.1. Spectral Response Characteristics of Robertson-Berger Meters

Introduction

Concern over the possible depletion of atmospheric ozone by high-flying supersonic aircraft emissions (Climatic Impact Assessment Program, U.S. Department of Transportation), and an associated predicted increase in biologically damaging UV radiation inspired the construction, installation, and operation of a network of R-B meters, to measure UV radiation on a continuous basis. The design of these instruments was essentially that of *Robertson* [1972]. They were placed at different latitudes and longitudes in the United States in the early 1970s such that the gross seasonal and regional variations in UV exposure could be studied and related to human skin cancer. A few were placed outside the mainland United States. NOAA presently operates 17 U.S. instruments, 2 of which are on the Hawaiian Islands.

These instruments sense a broad wavelength band that is meant to simulate the sunburning action spectrum of caucasian skin, similar to that of *Coblentz and Stair* [1934]. However, the design of the instrument did not accurately meet this requirement [*Berger*, 1976], and for this reason it has been criticized [e.g., *NAS*, 1979]. The instrument possesses a spectral response function (SRF) that is similar in shape to the human skin erythemal action spectrum at wavelengths greater than 300 nm, but the solar UV band it senses is shifted toward longer wavelengths several nanometers beyond the human skin erythemal action spectrum. The bandwidth of solar UV radiation actually sensed by the instrument is ≅13 nm at half-power wavelengths, and at a solar zenith angle of 30°, the band's maximum power wavelength is ≅311 nm; whereas, it should be ≅307 nm if the instrument were to accurately simulate the response to the human skin action spectrum [*DeLuisi and Harris*, 1983]. Nevertheless, the band extends sufficiently far into the wavelength region of the Huggins ozone absorption band such that the meter is sensitive to atmospheric ozone absorption of UV radiation, although, not as sensitive as it would be if it accurately simulated that of the human skin action spectrum.

Since the SRFs were not measured for each instrument in the network until this investigation, it would not be possible to directly determine whether changes in their characteristics occurred. Nevertheless, by examining the characteristics of a sample of several R-B meters that served in the network (about one-half the number in the network) it should comprise a sufficient set for determining the degree of their mutual consistency, and perhaps yield information that would bear upon their stability while operating in the network.

The R-B meter sensor unit is sensitive to temperature changes. *Blumthaler and Ambach* [1986] reported a sensitivity change of 8% per 10°C change in sensor temperature. The instruments should be temperature stabalized to improve their accuracy. Details in the construction and design principles of the R-B meter are given by *Berger* [1976].

To obtain a representative measure of the SRF of an R-B meter optical head, the SRFs of five sections of an R-B meter optical head are measured and averaged. A few tests have shown that more than one run on a specific area is repeatable to better than 2%. The most important region is within the range between 300 and 330 nm, wherein lies the meter's greatest sensitivity to the spectral distribution of the incident solar UV radiation. Below 300 nm UV is cut off by ozone and above 330 UV is cut off by the instrument SRF.

Figure 3.4 contains six plots representing the SRFs of six R-B meters. Numerical tabulations of these plots and their standard deviations will be given in a later report. Some interesting differences are noted in the 300-330 nm wavelength region, although all shapes in this region are quite similar. This wavelength region is essentially the band of atmospheric UV radiation that is sensed by the instrument. No explanation is given for the differences at this time except that variations in instrument construction (e.g., filters and substrate thickness) are likely to be a cause, combined with experimental error in determining the SRFs. Aging from long-term field use may also be responsible; however, this cannot be assessed because, as mentioned earlier, no previous characterization data exist. Nevertheless, these instruments have operated in the field for several years for more than a decade, and it is quite remarkable that their SRFs have retained shape similarity. The CMDL plot in Figure 3.5 is the average of the seven R-B meter SRFs. This plot is compared with the SRFs obtained from the literature.

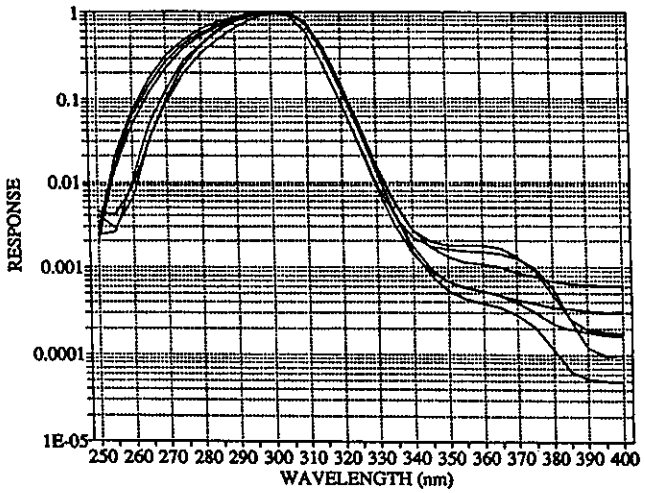

Fig. 3.4. Spectral response functions of six R-B meters plotted as response versus wavelength.

The present SRFs are consistent with those of *Berger* [1976] and *CIAP* [1976] also plotted in Figure 3.5. The fact that the SRFs presently measured are so close to earlier determinations, especially Berger's, strongly suggests a possible verification of the long-term stability of the R-B meter network's sensor SRFs.

Discussion

Seven R-B meters were subjected to an examination of their spectral response characteristics. The SRFs thus far measured were found to be quite similar in shape in the UV wavelength region sensed by the instrument, i.e., 300-330

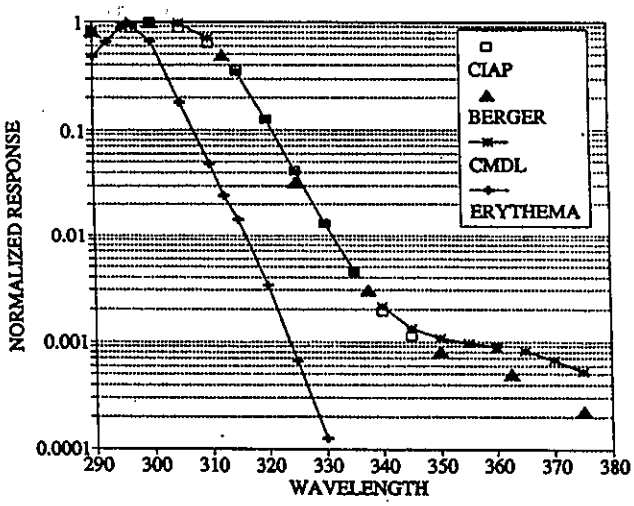

Fig. 3.5. Average of seven R-B meter spectral response functions (CMDL), the human erythemal action spectrum (ERYTHEMA), *Berger's* [1976] spectral response function (BERGER), and the *NAS* [1979] spectral response function (CIAP) [after *Robertson*, 1972].

believed to be partially responsible. The displacements have only a small impact on the agreement among the instruments when they are calibrated to agree with a standard as is done for the network meters. The results of this investigation are nm. However, the wavelength positions among them varied by a few nanometers. Experimental error is partially responsible for this variation. Variations in the optical components, such as filter and substrate thicknesses, are also further described in *DeLuisi et al.* [1992]. Determination of the SRFs of all R-B meters in the NOAA network were recently completed. All instruments were subjected to a maintenance update including cleaning, repainting, electronic repair, and calibration and then returned to their respective sites.

3.3. References

Berger, D., The sunburning ultraviolet meter: Design and performance, *Photochem. and Photobiol.*, *24*, 187-192, 1976.

Blumthaler, M., and W. Ambach, Messungen der temperatur koeffizienten des Robertson-Berger sunburn meters und des Eppley UV-radiometers, *Arch. Met. Geophys. Biol., Ser. B, 36*, 357-373. 1986.

Cess, R.D., E.G. Dutton, J.J. DeLuisi, and F. Jiang, Determining surface solar absorption from broadband satellite measurements for clear skies: comparison with surface measurements, *J. Clim.*, *4*, 2367-247, 1991.

CIAP (Climatic Impact Assessment Program), Monograph 5, Part 1, U.S. Department of Transportation, Washington, DC, 1976.

Coblentz, M.W., and R. Stair, Data on the spectral erythemic reaction of untanned human skin to ultraviolet radiation, *J. Res. (Natl. Bur. Stand.)*, *13*, 13-14, 1934.

DeLuisi, J., and J. Harris, A determination of the absolute energy of a Robertson-Berger meter sunburn unit, *Atmos. Environ.*, *17*, *4*, 751-758, 1983.

DeLuisi, J., J. Wendell, and F. Kreiner, Spectral response characteristics of seven Robertson-Berger meters after long-term field use, *Photochem. and Photobiol.*, in press, 1992.

Dutton, E.G., R.S. Stone, D.W. Nelson, and B. Mendonca, Recent interannual variations in solar radiation, cloudiness, and surface temperature at the South Pole, *J. Clim.*, *4*, 848-858, 1991.

Dutton, E.G., and D.J. Endres, Date of snowmelt at Barrow, Alaska, USA, *Arct. Alp. Res.*, *23*, 115-119, 1991.

Dutton, E.G., A Coherence between the QBO and the amplitude of the Mauna Loa atmospheric transmission annual cycle, *Int. J. Climatol.*, in press, 1991.

Dutton, E.G., Annual forcing of the surface radiation balance diurnal cycle measured from a high tower near Boulder, Colorado, *J. Climate*, *3*, 1400-1408, 1990.

Ellis, H.T., and R.F. Pueschel, Solar radiation: Absence of air pollution trends at Mauna Loa, *Science*, *172*, 845-846, 1971.

Foster, J.L., The significance of the date of snow disappearance on the Arctic tundra as a possible indicator or climate change, *Arct. Alp. Res.*, *21*, 60-70, 1989.

NAS (National Academy of Science), *Protection Against Depletion of Stratospheric Ozone by Chlorofluorocarbons*, National Academy of Sciences, Library of Congress Card Catalog Number 79-57247, 392 pp., 1979.

Robertson, D., Solar ultraviolet radiation in relation to human skin burn and cancer, Ph.D. Thesis, No. THE4866, University of Queensland, Australia, 1972.

4. Carbon Cycle Group

P.P. TANS (Editor), T.J. CONWAY, E.J. DLUGOKENCKY, D.R. KITZIS,
P.C. NOVELLI, K.W. THONING, AND L.S. WATERMAN

4.1. CONTINUING PROGRAMS

4.1.1. IN SITU CARBON DIOXIDE MEASUREMENTS

The concentration of atmospheric CO_2 was measured with continuously operating NDIR analyzers at the four CMDL observatories during 1990 as in previous years. Monthly and annual mean CO_2 concentrations are given in Table 4.1. These values are provisional, pending final calibrations of station standards. Revised values for 1988 and 1989 are also included. Preliminary selected daily average CO_2 concentrations for 1990 are plotted versus time for the four observatories in Figure 4.1.

On February 3, the in situ CO_2 measurements at SMO were halted due to damage to the sample air intake system on Matatula Point from Hurricane Ofa. The sampling tower holding the intake lines was destroyed as was a building in which a refrigeration system for removing water vapor from the sample air was located. Sampling resumed on May 4, with a temporary sampling intake mast. During the period when the continuous measurements were not being made, the frequency of collecting flask samples was increased to approximately twice a week. By October, a new building and a new sampling mast were installed. The new mast is a fiberglass flagpole, 77 feet high, 10 inches in diameter at the base, located approximately 30 feet from the original tower further out on the Point on a little knoll. The new intake is about 20 feet higher than the old one. On October 14, the CO_2 NDIR analyzer was changed from a Hartmann-Braun URAS-2T to a Siemens ULTRAMAT-5F. This new analyzer shows better stability than the URAS-2T. On December 5, the analyzer at SPO was also changed from a URAS-2T to an ULTRAMAT-5F.

4.1.2. FLASK SAMPLE CARBON DIOXIDE MEASUREMENTS

In 1990 the measurement of the global distribution of atmospheric CO_2 continued. CO_2 mixing ratios were measured in samples collected at 29 sites of the CMDL cooperative flask sampling network (Table 4.2). Provisional annual mean CO_2 mixing ratios for 1990 and revised values for 1988 and 1989 are also given in Table 4.2. Sampling at the U.S. Virgin Islands site (AVI) was discontinued in 1990 because the cooperating institution, the West Indies Laboratory of Fairleigh Dickinson University, ceased operations. In anticipation of this closure, sampling was begun in Barbados in 1987, so there is an overlap and continuing measurements in the Caribbean. Sampling on voyages of the containership *Southland Star* in the Pacific Ocean continued in 1990. To increase the temporal resolution of the shipboard data, sampling on a second ship, the *Wellington Star*, was begun in 1990.

TABLE 4.1. Provisional Monthly Mean CO_2 Concentrations from Continuous Analyzer Data (ppmv, Relative to Dry-Air X85 Mole Fraction Scale)

	BRW	MLO	SMO	SPO
		1988		
Jan.	354.87	350.19	349.24	348.06
Feb.	356.23	351.50	349.70	347.92
March	356.56	352.11	349.35	347.98
April	357.40	353.51	350.27	348.18
May	356.83	354.16	349.63	348.28
June	355.27	353.60	349.66	348.50
July	348.43	352.61	349.94	348.89
Aug.	343.10	350.32	349.81	349.33
Sept.	345.87	348.81	348.94	349.63
Oct.	350.59	348.96	349.26	349.70
Nov.	354.28	350.09	349.72	349.70
Dec.	357.86	351.32	350.58	349.69
Annual	353.11	351.43	349.67	348.82
		1989		
Jan.	360.88	352.72	351.29	349.62
Feb.	358.16	353.16	351.62	349.68
March	359.15	353.71	351.38	349.60
April	359.27	355.42	351.40	349.68
May	358.74	355.67	351.66	349.92
June	357.04	355.14	350.73	350.22
July	349.34	353.81	351.04	350.58
Aug.	344.48	351.40	351.07	351.00
Sept.	346.18	349.80	350.62	351.08
Oct.	351.19	350.04	350.21	351.24
Nov.	355.81	351.28	350.63	351.29
Dec.	358.29	352.63	350.60	350.87
Annual	354.88	352.90	351.02	350.40
		1990		
Jan.	359.81	353.64	351.68	350.76
Feb.	359.85	354.81	353.24	350.57
March	361.24	355.56	--	350.64
April	361.04	356.10	--	350.91
May	360.48	357.04	352.22	351.25
June	356.77	356.06	352.92	351.58
July	349.49	354.45	352.76	352.06
Aug.	345.74	352.67	352.82	352.40
Sept.	346.37	350.97	352.88	352.70
Oct.	353.81	351.28	352.74	352.74
Nov.	356.63	352.73	352.90	352.74
Dec.	359.21	354.16	353.43	352.30
Annual	355.87	354.12	352.76	351.72

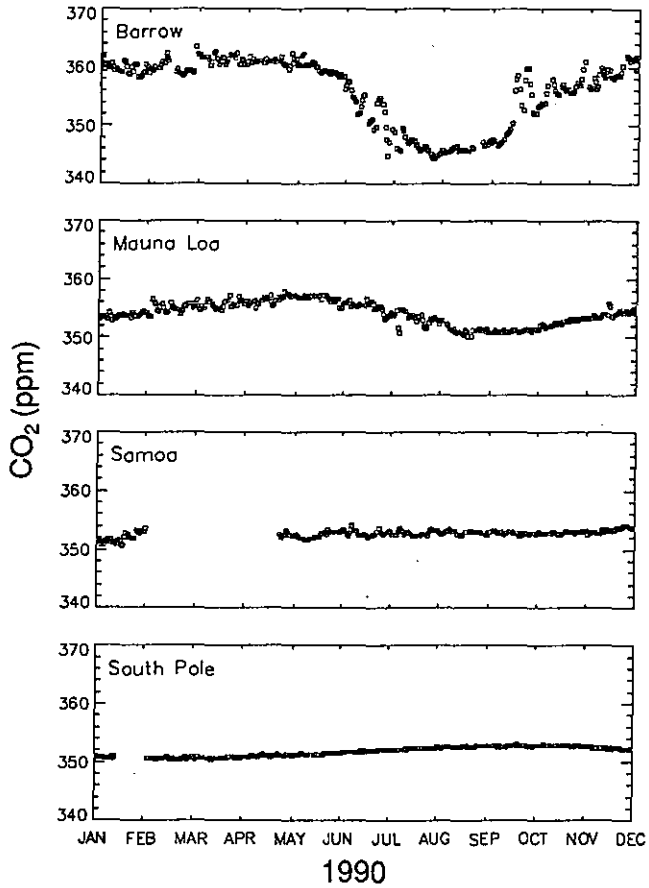

Fig. 4.1. Preliminary selected 1989 daily average CO_2 concentrations from the in situ measurements at BRW, MLO, SMO, and SPO.

TABLE 4.2. Provisional 1988-1990 Annual Mean CO_2 Concentrations From the Flask Network Sites

Code	Station	CO_2 (ppm) 1988	1989	1990
ALT	Alert, N.W.T., Canada	353.0	355.1	355.5
AMS	Amsterdam Island	349.5	350.5	[ ]
ASC	Ascension Island	350.4	351.6	352.9
AVI	St. Croix, Virgin Islands	351.5	353.5	[ ]
AZR	Terceira Island, Azores	351.6	351.1	353.9
BME	Bermuda (east coast)			355.2
BMW	Bermuda (west coast)			355.3
BRW	Barrow, Alaska	353.4	354.9	356.0
CBA	Cold Bay, Alaska	352.3	354.4	355.3
CGO	Cape Grim, Tasmania	348.9	350.3	351.6
CHR	Christmas Island	351.3	353.3	354.3
CMO	Cape Meares, Oregon	352.6	354.4	355.4
GMI	Guam, Mariana Islands	352.1	353.5	354.2
HBA	Halley Bay, Antarctica	349.7	[ ]	[ ]
KEY	Key Biscayne, Florida	352.7	354.4	356.3
KUM	Cape Kumukahi, Hawaii	351.4	352.9	354.3
MBC	Mould Bay, Canada	353.5	355.5	356.0
MID	Midway Island	352.9	354.1	355.1
MLO	Mauna Loa, Hawaii	351.3	352.8	354.1
NWR	Niwot Ridge, Colorado	351.9	353.3	354.7
PSA	Palmer Station, Antarctica	349.6	350.9	351.9
RPB	Ragged Point, Barbados	351.5	352.9	354.7
SEY	Mahé Island, Seychelles	350.3	352.2	353.2
SGI	South Georgia Island	[ ]	[ ]	[ ]
SHM	Shemya Island, Alaska	353.1	354.5	355.0
SMO	American Samoa	350.2	351.7	352.8
SPO	South Pole, Antarctica	349.0	350.6	351.8
STM	Ocean Station M	352.4	354.0	354.8
SYO	Syowa Station, Antarctica	349.3	[ ]	[ ]

Square brackets indicate insufficient data to calculate annual mean.

As noted in last year's *Summary Report* we have begun the conversion to 2.5-L flasks equipped with Teflon O-ring stopcocks. Laboratory and field tests have shown that CO_2, CO, and isotopic ratios are more stable in these flasks. In 1990 flasks with Teflon O-rings were in use at 15 sites. Also during 1990, we began routine deployment of a new portable sampler (Martin and Kitzis Sampler, abbreviated MAKS) to replace the design in use since 1980 (the P^3). The new design includes a more powerful pump and battery, and several modifications intended to increase the probability that a person with little or no technical background can collect an uncontaminated sample. Whenever possible, we are providing face-to-face training for sample collectors when we deploy the new sampler. Training takes place preferably in Boulder or at the sampling site if travel to Boulder is impractical.

The new sampling unit weighs 24 pounds, and can be used with the old 0.5-L and the new 2.5-L flask pairs. A light shield is incorporated into the unit to reduce the possibility of any CO photochemistry during the sampling procedure. The air intake is now 16 feet above the unit to reduce CO_2 contamination from the sample taker and from vegetation in the immediate surroundings. Final pressure is held constant by a backpressure regulator so that the integrity of the connections can be checked. We are starting to employ Teflon connectors to the 14/35 tapered glass joints to eliminate the use of, and possible contamination by, vacuum grease. These connectors were developed and tested extensively by the Carbon Cycle Group. Further development of the MAKS is continuing. We are currently testing a thermo-electric cooling stage to dry the air stream before it enters the flasks.

The CMDL flask network CO_2 data are summarized in Figure 4.2 where annual means for each site are plotted versus latitude for the period 1981-1990. Two important features of this figure are the interannual and spatial variability of the CO_2 growth rate, and the shift in the North Pole-to-South Pole CO_2 difference from ≈3 ppmv during 1981-1987 to ≈4 ppmv during 1988-1990. The variations in emissions of CO_2 from fossil fuel combustion [*Marland et al.*, 1990] are too small to explain the changes observed in the atmosphere. Therefore, these data reflect significant temporal and spatial variability in the exchanges of carbon between the atmosphere and oceans, and between the atmosphere and the marine and terrestrial biospheres.

To investigate this variability, we have used a 2-dimensional (latitude and height, 2-D) atmospheric transport model [*Tans et al.*, 1989] to calculate the CO_2 sources and

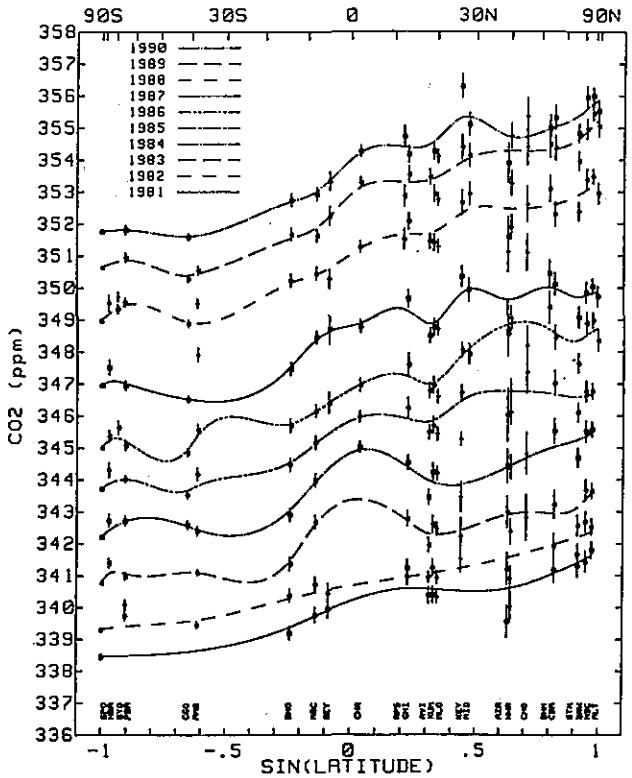

Fig. 4.2. Annual mean CO_2 mixing ratios for sampling sites of the NOAA/CMDL flask sampling network plotted versus sine of latitude for the period 1981-1990. The curves are cubic splines fitted to the data for each year as a visual aid. The high altitude sites at MLO and NWR are not used in the curve fits. Annual means considered unreliable due to infrequent sampling or poor sampling technique are not included in the curve fits. The excluded points are plotted with plus symbols. The error bars represent 65% confidence intervals.

sinks needed to produce the spatial CO_2 gradients observed in the atmosphere. The annual global net CO_2 source to the atmosphere (fossil fuels plus natural sources and sinks) calculated by the model is plotted in Figure 4.3. The pattern of the net CO_2 source is, of course, very similar to the smoothed, de-seasonalized, global average CO_2 growth rate determined from the flask network data (Figure 4.4). The net CO_2 source ranges from less than 40% (1982) to greater than 80% (1988) of fossil fuel emissions. Although the 2-D model cannot identify the processes responsible for these variations, it can give us some idea of the temporal variability of major global scale sources and sinks.

The model results grouped into four equal area latitudinal bands are shown in Figure 4.5. The model is run with 20 equal area latitudinal zones, but aggregating the output into four bands is more robust, considering the number and distribution of sampling sites. It is clear from Figure 4.5 that the global net sink is dominated by the mid-to-high latitude northern hemisphere sink and that there is a smaller sink at mid-to-high southern latitudes. On average, the tropical regions in both hemispheres are a source of CO_2 to the atmosphere.

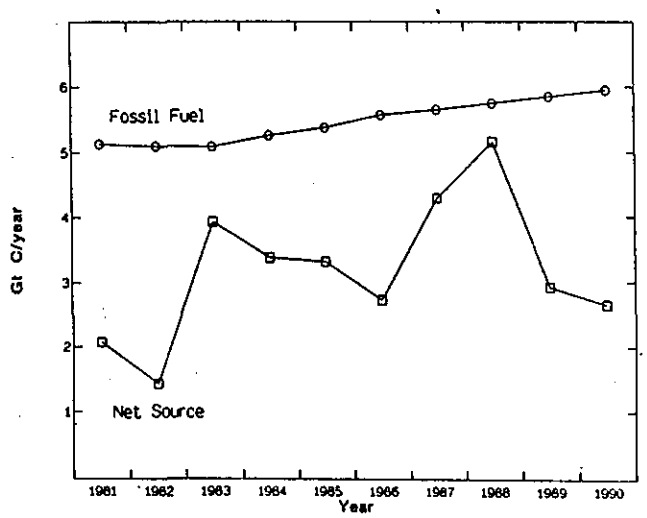

Fig. 4.3. The annual net source of CO_2 to the atmosphere, in Gt of carbon yr^{-1}, calculated from the 1981-1990 NOAA flask data using the 2-D model of *Tans et al.* [1989] (squares). The annual fossil fuel CO_2 emissions are also plotted (circles). The fossil fuel data for 1981-1986 are from *Marland et al.* [1990]. For 1987-1990 we have assumed an increase in the fossil fuel combustion of 2% yr^{-1}.

The major variations in the global growth rate plot (Figure 4.4) occur in 1982-1983 and 1986-1988 in association with El Niño/Southern Oscillation events, but the source/sink patterns for the two cases are different. The low growth rate in 1982 resulted from a decrease in the northern tropical source combined with relatively large sinks in both the northern and southern mid- and high latitudes. The growth rate peak in 1983 results mainly from a decrease in the northern and southern hemisphere sinks; the tropical sources were still relatively low. In 1986 the tropical sources drop to approximately 0, but a decrease in the high latitude northern hemisphere sink partially counteracts this effect, preventing

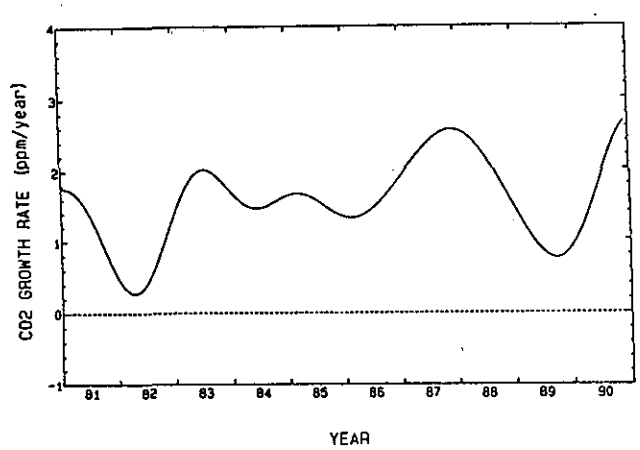

Fig. 4.4. The variation of the CO_2 growth rate for the period 1981-1990. The curve is the time derivative of the deseasonalized, latitudinally weighted, globally averaged, smoothed data from the CMDL flask network.

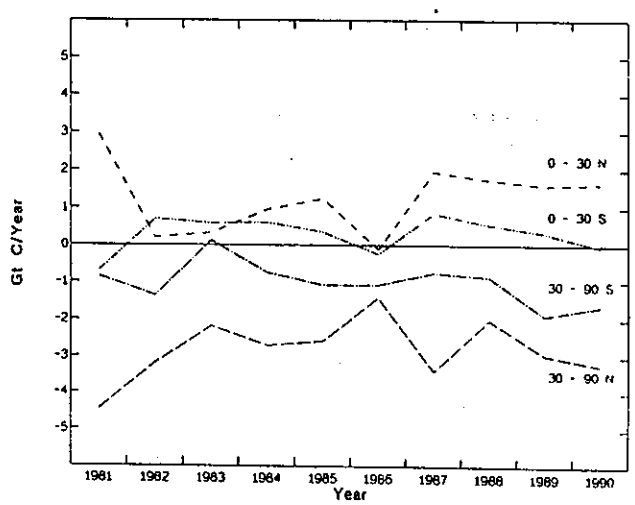

Fig. 4.5. Annual average sources (excluding fossil fuels) of CO_2 to the atmosphere calculated using the NOAA/CMDL flask data and the 2-D model of *Tans et al.* [1989]. Negative values represent sinks for atmospheric CO_2. The model calculates sources in 20 equal area latitude bands that we have grouped into four bands for increased clarity and robustness. The sum of these four curves and the fossil fuel emissions gives the net CO_2 source shown in Figure 4.3.

the growth rate from becoming as low as in 1982. In 1987 the tropical sources rebounded but the northern hemisphere sink also increased. In 1988 the tropical sources decreased only slightly, while the northern hemisphere sink decreased significantly leading to a peak in the CO_2 growth rate.

The tropical sources of CO_2 derived by the model from our flask data cast doubt on the estimates of biomass burning in the tropics (2-5 Gt C yr^{-1} [*Crutzen and Andreae*, 1990]). Outgassing of CO_2 from the tropical oceans is a well-known phenomenon, and it is partly responsible for our derived tropical sources. It has been estimated to be in the vicinity of 1 Gt C yr^{-1} [e.g., *Tans et al.*, 1990]. That would leave only a small net annual CO_2 source from biomass burning, as seems to be the case during El-Niño years when the equatorial oceans don't lose much CO_2 to the atmosphere. If the majority of the burning is seasonal, in which case the CO_2 is fixed again by plants outside of the burning season, no net annual source would result. However, we do not find a marked seasonality in our flask data from the tropics either. If tropical biomass burning is such a large phenomenon, why does it remain almost totally hidden from our tropical network sites?

The 2-D model results also suggest where to search for the reasons that the mean CO_2 latitude gradient changed. In 1987 the tropical sources increased but the northern hemisphere sink also increased and no change in the pole-to-pole gradient was observed. In 1988 the tropical sources remained high (especially in the northern tropics) while the northern sink decreased, leading to an increase in the gradient from ≈3 ppmv to ≈4 ppmv. In 1989 and 1990 the northern tropical source remained steady, the southern tropical source declined to ≈0, and the high latitude southern hemisphere sink increased. This combination appears to have maintained the pole-to-pole difference at the ≈4 ppmv level it reached in 1988.

These results show that with 10 years of flask network data, we are beginning to be able to identify changing source/sink patterns on a very broad scale. We are still unable to identify processes or even to distinguish between marine or terrestrial effects, particularly in the northern hemisphere. The addition of isotopic ratios, continental regions, and vertical profiles to our measurement program will increase our ability to quantify the global carbon cycle and possibly enable us to finally balance the carbon budget.

4.1.3. In Situ Methane Measurements

Quasi-continuous measurements of CH_4 at BRW and MLO continued during 1990 with a frequency of 60 samples per day. A modification to the analytical systems was performed at both observatories. The measurement systems came equipped with a catalyst which, in the presence of H_2, reduces CO_2 and CO to CH_4, followed by quantitative detection with the FID. A change to the analytical systems microprocessor software has eliminated routing of CO_2 and CO to the catalyst, so now only CH_4 is quantitatively measured with better reproducibilty than before.

Raw data from the in situ analytical systems are processed in Boulder using a rule-based expert system. This rule-based expert system (AMIE: Automated Methane Instrument Evaluation) was developed and implemented to assess the quality of the in situ data. The algorithm determines the validity of an ambient measurement by evaluating the stability of the gas chromatograph (GC) system about the time of the analysis. If the GC system is not operating optimally, the measurement is considered invalid and the ambient sample is assigned a flag indicating how the system instability was detected. In 1990, 5.1% of the data from BRW were flagged by AMIE, while 19.6% were flagged from MLO. The reasons for the large percentage of flagged data from MLO are unknown.

Daily mean CH_4 mixing ratios in ppbv (where 1 ppbv = 1 part in 10^9 by volume) for 1990 are shown in Figures 4.6*a* (BRW) and 4.6*b* (MLO). These daily means exclude all data flagged by the expert system, but they are not constrained for wind speed and direction. Large, short-term variations in the CH_4 mixing ratio at BRW (Figure 4.6*a*) result from local contamination of air masses reaching the sampling site. Much, but not all, of this variability is removed when the wind direction is constrained to a clean air sector defined as 20° to 110°. Changes in the CH_4 mixing ratio of up to 50 ppbv at MLO occurring on synoptic time scales are due to large-scale air movements rather than local contamination. Relationships among CH_4 source/sink regions, flow patterns for MLO, and CH_4 variations on a synoptic time scale at MLO are described in section 5.1.10 of this report.

4.1.4. Flask Measurements of Methane

The determination of the global distribution of CH_4 continued during 1990. Measurements of the atmospheric

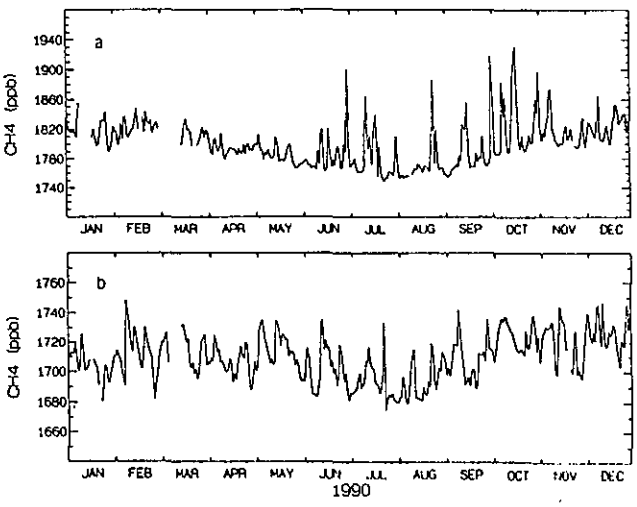

Fig. 4.6. Edited, unselected daily average methane mixing ratios for 1990: *a*-BRW and *b*-MLO. Gaps in the data are due to instrument malfunction.

CH_4 mixing ratio were made from flask samples collected approximately weekly at 28 sites in the CMDL cooperative flask sampling network. Also, flask samples were collected from aboard the container ship *Southland Star* every 5° in latitude from 35°S to 30°N. Provisional annual mean mixing ratios from the flask data are shown in Table 4.3 and Table 4.4. Some sites do not have annual means listed. At Amsterdam Island we have only received and analyzed samples which were collected through May. At Azores, sampling problems continued; 6 months of data are missing due to U.S. Air Force commitments for Operation Desert Shield. A new station is under construction up-wind from the current sampling site at Halley Bay. This may be the reason for severe contamination in almost all of the samples collected at that site during 1990. For Seychelles and Syowa, 2 months at each site had insufficient data to calculate monthly means. Mean values for those months were determined by interpolation and combined with the remainder of the data to calculate the annual means listed.

A new flask measurement system, Carle 7, was put into service in 1990. This system allows for simultaneous measurement of CH_4, CO, and H_2 on two different gas chromatographs. Previously CH_4 and CO were measured on separate analytical systems, and the CO system was not automated. Currently, all three species are measured with a single manipulation of the flasks, and the chromatography for each species can be optimized independently of the other. The measurement techniques are the same as before; CH_4 is detected by flame ionization, and CO and H_2 are detected by first producing Hg atoms by the reactions $CO + HgO \rightarrow CO_2 + Hg$ and $H_2 + HgO \rightarrow H_20 + Hg$, and then detecting the Hg atoms by resonance absorption. The carousel is still used to set up eight flasks for unattended analysis. A comparison between Carle 4 and Carle 7 was made using test flask samples flushed and filled in series from a tank of natural air. Eight flasks were measured on each system for CH_4. In addition to the test flasks, numerous tank calibrations were made on Carle 7. No systematic difference was observed between Carle 4 and Carle 7 suggesting that switching to Carle 7 for routine flask analysis would not result in any bias

TABLE 4.3. Provisional 1990 Annual Mean CH_4 Mixing Ratio Concentrations From the Flask Network Sites

Code	Station	CH_4, ppbv
ALT	Alert, N.W.T., Canada	1783.7
AMS	Amsterdam Island	[ ]
ASC	Ascension Island	1656.7
AZR	Terceira Island, Azores	[ ]
BME	Bermuda (east coast)	1756.7
BMW	Bermuda (west coast)	1744.9
BRW	Barrow, Alaska	1798.2
CBA	Cold Bay , Alaska	1778.3
CGO	Cape Grim, Tasmania	1644.3
CHR	Christmas Island	1668.9
CMO	Cape Meares, Oregon	1759.8
GMI	Guam, Mariana Islands	1708.6
HBA	Halley Bay, Antarctica	[ ]
KEY	Key Biscayne, Florida	1741.4
KUM	Cape Kumukahi, Hawaii	1723.4
MBC	Mould Bay, Canada	1790.3
MID	Midway Island	1742.2
MLO	Mauna Loa, Hawaii	1711.5
NWR	Niwot Ridge, Colorado	1733.0
PSA	Palmer Station, Antarctica	1641.0
RPB	Ragged Point, Barbados	1716.8
SEY	Mahé Island, Seychelles	1670.0
SGI	South Georgia Island	[ ]
SHM	Shemya Island, Alaska	1784.7
SMO	American Samoa (Matatula Point)	1648.1
SPO	South Pole, Antarctica	1642.4
STM	Ocean Station M	1778.4
SYO	Syowa Station, Antarctica	1642.4

Square brackets indicate insufficient data to calculate annual mean.

TABLE 4.4. Provisional 1990 Annual Mean Mixing Ratios From the *Southland Star* Shipboard Flasks

Latitude	CH_4 (ppb)
35°S	1643.4
30°S	1641.7
25°S	1643.6
20°S	1647.0
15°S	1644.9
10°S	1656.0
5°S	1665.9
Equator	1669.9
5°N	1681.6
10°N	1669.8
15°N	1721.3
20°N	1724.1
25°N	1729.1
30°N	1744.1

in our CH_4 data. An important aspect of these measurement systems is the precision. The mean difference between the two aliquots measured from 857 flasks on Carle 7 was (-0.32 ± 3.4) ppbv. This is an improvement over Carle 4. Finally, combining the CO/H_2 measurement with CH_4 on the same system has made us more efficient; Carbon Cycle Group personnel now spend approximately 20 staff-hours less per week on flask analysis.

The average seasonal cycles for CH_4 over the period 1983 through 1990 determined from the flask sample data, with the trends removed, are shown in Figures 4.7*a* for BRW and 4.7*b* for SPO. At BRW, the seasonal cycle is mostly due to seasonality in the natural wetland sources and the photochemical sink. The peak-to-peak amplitude is ≈54 ppbv. The large decrease in CH_4 during summer months is due to chemical destruction by reaction with hydroxyl (OH) radical $OH + CH_4 \rightarrow H_2O + CH_3$; k(298 K) = 6.35×10^{-15} cm^3 $molecule^{-1}s^{-1}$. The multiple maxima are unexplained, but some possibilities exist. For example, the fall maximum in October and November may be due to CH_4 released when high northern latitude wetland lakes turn over due to sinking cold water just before freeze over. The sinking water may disturb sediments which trap bubbles of CH_4 produced by anaerobic bacteria. At SPO, a seasonal sink term and transport of CH_4 from the northern hemisphere are responsible for the seasonal cycle observed there, ≈30 ppbv peak-to-peak.

Over the entire period of the CMDL CH_4 measurements, the average increase in CH_4 has been ≈11.9 ppbv yr^{-1}. Detailed analysis has shown that the growth rate has not been constant over time. The flask data can be averaged using the techniques described in *Steele et al.* [1987], to determine global monthly means for CH_4. The data fitting routines of *Thoning et al.* [1989], have been applied to these monthly values. Briefly, a function consisting of a quadratic polynomial plus four seasonal harmonic terms is fit to the global monthly means. The residuals are then filtered with a low-pass filter in the frequency domain to separate variability occurring on time-scales of the order of 1 year and longer, and these values are added back to the quadratic trend portion of the original function. The resulting composite shows the trend in CH_4, including long-term variations in that trend. The derivative of this curve gives the instantaneous smoothed growth rate, and it is shown for the flask data through 1990 in Figure 4.8. Not all sites listed in Table 4.3 are included; those with limited data and the high altitude sites at MLO and NWR are excluded. Two features apparent in Figure 4.8 are: 1) The growth rate of CH_4 has decreased over the period of our measurements. This decrease is due to long-term changes in the sources or sinks of CH_4. From our data, it is impossible to determine which is the most important contributor. 2) Significant interannual variations in the CH_4 growth rate appear to exist. This is most likely due to interannual variations in the strengths of CH_4 sources, but at this time, we cannot rule out the possibility that it may, in part, be due to an artifact of our data analysis procedures.

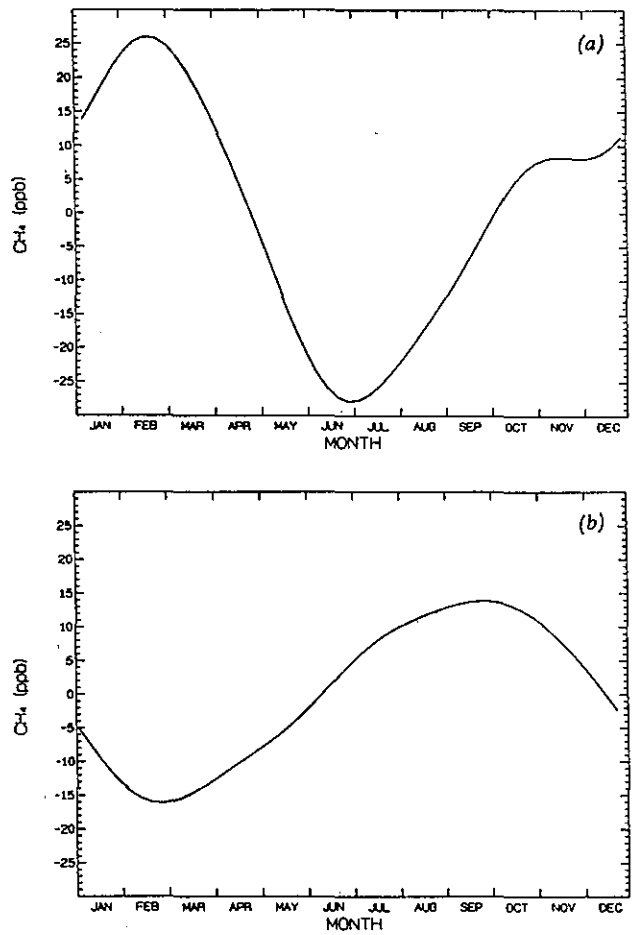

Fig. 4.7. Average seasonal cycles, with trend removed, for the period 1983 through 1990 for *a*-BRW and *b*-SPO. Seasonal cycle is extracted using the techniques from *Thoning et al.* [1989].

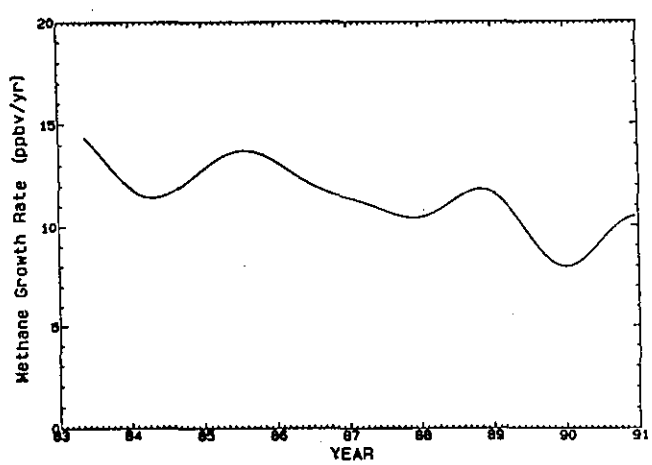

Fig. 4.8. Globally averaged instantaneous growth rate, with the seasonal cycle removed, for atmospheric CH_4 determined from CMDL flask network data for 1983-1990.

4.1.5. FLASK MEASUREMENTS OF CARBON MONOXIDE

During 1990 the measurement of CO concentrations in air samples continued. Samples were collected in flasks having two different volumes, either 0.5 L or 3 L. Samples in 0.5-L flasks were collected using our portable pumping system, which filled a pair of glass flasks, fitted with two Teflon O-ring stopcocks, with air to a final pressure of about 1.5 atm. The 3-L samples were collected in previously evacuated flasks having one Teflon O-ring stopcock, which were opened to the atmosphere at the site. The sampling methods used are detailed in *Steele et al.* [1987]. Air samples were analyzed for CO using the mercuric oxide reduction technique. Until November 1990, we used a semi-automated instrument for flask analysis. In December we began analyzing CO using a more fully automated system (see section 4.1.4). The CO working standards are secondary standards to the NOAA/CMDL CO gravimetric standards [*Novelli et al.*, 1991].

Laboratory experiments have previously shown that the concentration of CO in air contained in the 0.5-L and 3-L flasks was stable (to within 1 ppbv or about 1%) over the course of 2 weeks and at least 4 weeks, respectively. Experiments also showed that air in flasks exposed to even a few minutes of sunlight exhibited an increase in CO over time, probably as a result of the photo-oxidation of organic molecules which coat the inside walls of the flask. To minimize light-enhanced CO levels, all flasks used for CO sampling were coated with two layers of white adhesive tape. Additional experiments that compared the growth of CO in taped 0.5-L and 3-L flasks indicated that the smaller flasks were somewhat more susceptible to light-induced CO growth. In the field, sample takers were instructed to minimize the exposure of the flasks to sunlight. The new MAKS sampling unit minimizes light exposure during flask filling (see section 4.1.2).

CO concentrations were measured in samples from eight stations during 1990 (see Table 4.5). These sites were chosen based on their geography, and from a more practical standpoint, upon the basis of how long a time it took for the flask to return to Boulder after sampling. At all stations except CHR, samples were collected in 0.5-L glass flasks. At CHR, samples were collected only in 3-L flasks. At three sites (BRW, KUM, and SMO), we collected air samples in both 0.5-L and 3-L glass flasks. Samples were collected approximately once per week at all stations other than GMI. At GMI, air samples were collected twice weekly.

The 1990 provisional annual mean CO concentrations measured in 0.5-L glass flasks and referenced to the CMDL reference scale, are provided in Table 4.5. The data have been selected to remove erroneous values due to sampling and instrumental problems. Table 4.6 compares the calculated annual mean concentrations determined in 0.5-L flasks to those measured in 3-L flasks. Monthly mean concentrations were calculated directly from the measured weekly CO concentrations, and the annual values are the arithmetic means of the monthly means. Figure 4.9 compares the CO concentrations determined in 0.5-L flasks and 3-L flasks at BRW. This comparison gives us an estimate for the repeatability of the sampling and measurement procedure, plus the effects of natural atmospheric variability on a time scale of minutes. For data collected at BRW, the standard deviation of the individual samples from the linear fit is 2.4 ppbv.

In addition to the arithmetic calculation of monthly means, we also used a curve-fitting method to calculate the monthly mean concentrations. Whereas the arithmetic calculations could be biased by missing data, the curve-fitting approach interpolates over periods of absent data. Specifically, the smoothing routine uses the flask data to characterize the seasonal CO cycle as a linear combination of four harmonics, and then uses the curve to calculate monthly means. The annual means calculated using the two averaging methods differed by at most 1.5% for each station and were not significantly different from one another. Figure 4.10 presents the relationship for the curve fit monthly mean and the arithmetic mean CO concentrations determined at BRW. This figure suggests that the uncertainty of the monthly means due to collecting weekly samples is in the vicinity of 1.5% at BRW (annual average).

TABLE 4.5 Provisional 1990 Annual Mean CO Concentrations From the 0.5 l Flasks[1]

Code	Station	CO (ppbv)
ASC	Ascension Island	88.6 (10.3)
BRW	Barrow, Alaska	152.3 (22.9)
CHR*	Christmas Island	79.6 (5.8)
GMI	Guam, Mariana Islands	104.7 (8.5)
KUM	Cape Kumakahi, Hawaii	109.9 (12.8)
MLO[2]	Mauna Loa, Hawaii	101.6 (11.4)
NWR†	Niwot Ridge, Colorado	122.5 (8.7)
SMO	American Samoa	64.4 (5.2)

*Concentrations are reported in units of parts per billion by mole fraction, values in parentheses are the pooled standard deviations. Samples at Christmas Island were collected only in 3-L flasks, all other values were determined from samples collected in 0.5-L flasks.

†MLO and NWR are mountain sites, all others are in the boundary layer.

TABLE 4.6 Comparison of Annual Mean CO Concentrations Determined in 0.5- and 3-L Glass Flasks

Station	CO Concentration (ppbv) 0.5 l	3 l
BRW	152.3 (22.9)*	152.9 (24.0)
KUM	109.9 (12.8)	108.3 (12.5)
SMO	64.4 (5.2)	64.2 (4.5)

*Values in the parentheses are pooled standard deviations around the mean.

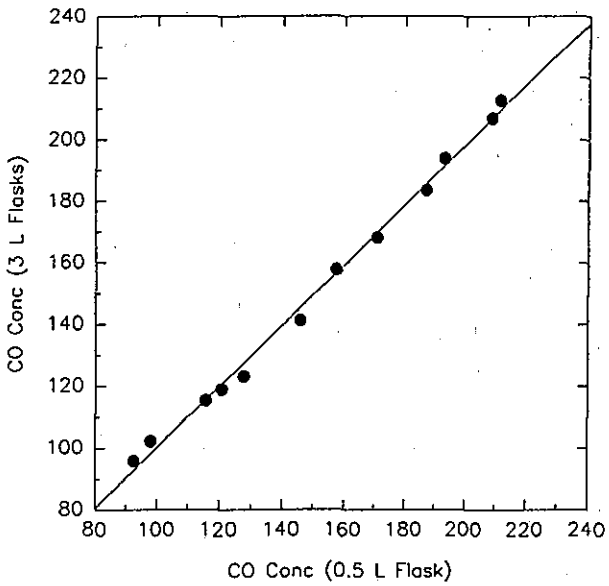

Fig. 4.9. Comparison of monthly mean CO concentrations determined in 0.5-L and 3-L glass flasks collected at BRW. Both types of flasks were taped with white adhesive tape to minimize light effects. Monthly means were calculated simply as the mean of the weekly concentrations. The line is described by Y = -0.97 (0.038) + 1.012 (0.016)X. Values in parentheses are the standard error.

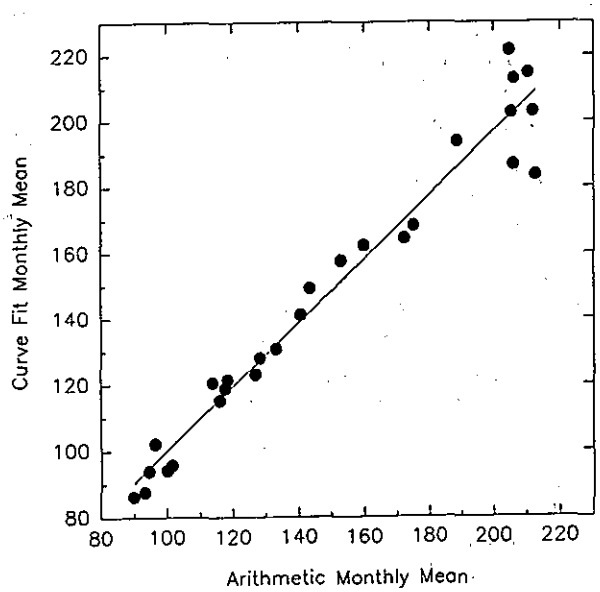

Fig. 4.10. Comparison of monthly mean CO concentrations for BRW calculated arithmetically to those calculated using a curve fitting technique. The line is described as Y = 2.69 (0.182) + 0.991 (0.015)X. Values in parentheses are the standard error.

Figure 4.11 plots the 1990 CO concentration time series at BRW. The monthly mean concentrations determined for samples collected in both 0.5-L and 3-L flasks are shown. The seasonal cycle is clearly evident, with highest concentrations in the winter and with lower levels observed in the summertime. This seasonal cycle has been observed previously in both hemispheres [*Dianov-Klokov and Yurganov*, 1981, among others] and is believed to reflect the seasonal CO oxidation via the reaction with OH.

Figure 4.12 presents the 1990 annual mean CO concentrations plotted as a function of latitude. For comparison, the 10-year average annual mean determined at Cape Point, South Africa, by Seiler and coworkers is also plotted. The concentration of CO clearly decreases from north to south. Concentrations at the high altitude sites, NWR and MLO, are slightly lower than might be expected for ground-level sites at the corresponding latitudes (also compare annual mean concentrations for KUM and MLO in Table 4.4). This reflects the general decrease in CO mixing ratios with altitude observed in the northern hemisphere [*Seiler*, 1974]. The annual mean CO concentration at ASC (8°S) is about 15 ppbv higher than might be expected in comparison to that of CHR (2°N) and SMO (14°S). Model calculations have indicated that this site will be influenced by transport from emissions due to biomass burning on the African continent (J. Logan, personal communication, 1991), and enhanced ozone levels measured at ASC have been attributed to African fires [*Fishman et al.*, 1991]. However, we observe no apparent elevation of CO_2 at ASC relative to other stations at similar latitudes, as would be expected if ASC were affected by combustion emissions.

The CO concentration gradient between 71°N and 34°S calculated from the data presented in this work is approximately 100 ppbv. This estimate agrees well with data collected previously by other groups [*Seiler*, 1974; *Dianov-Klokov et al.*, 1989].

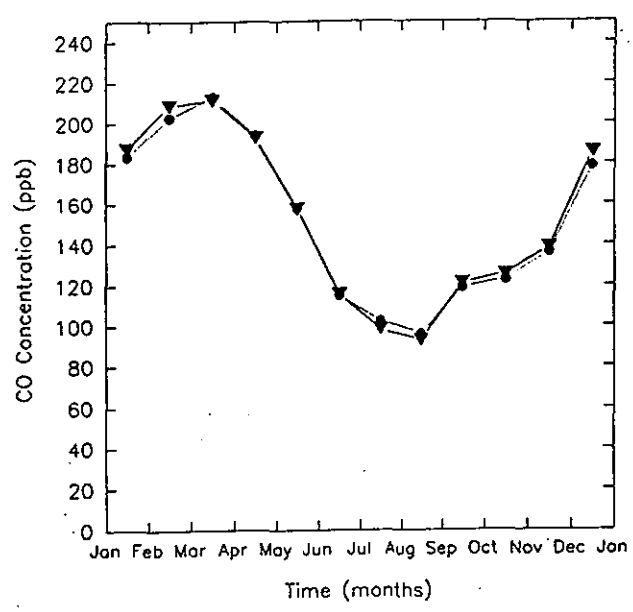

Fig. 4.11. 1990 monthly mean CO at BRW. Dashed line and solid circles represent 0.5-L flasks. Solid line and inverted triangles indicate 3-L flasks.

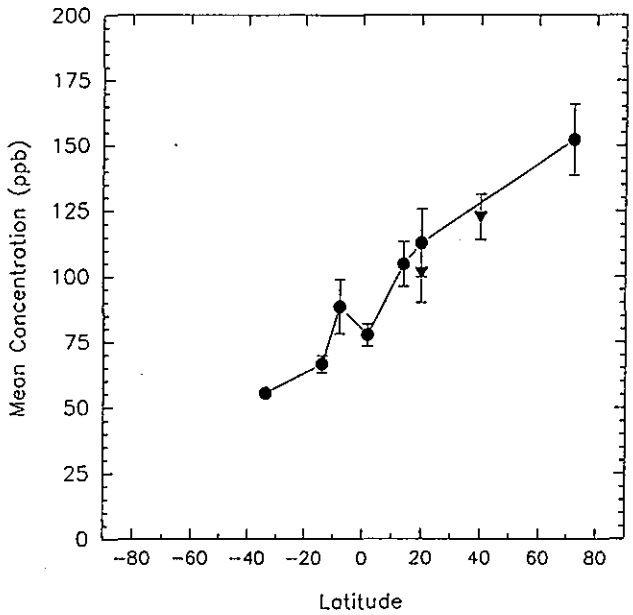

Fig. 4.12. Provisional 1990 annual mean CO concentrations at the eight sites where CO is measured as a function of latitude. Inverted triangles are high elevation sites (MLO and NWR). Data for 34°S are the 8-year annual average (1979-1987, excluding 1985) mean CO concentration at Cape Point, South Africa, from *Brunke et al.* (1990). Error bars indicate the pooled standard deviation around the mean.

4.2. Reference Gas Standards

4.2.1. Carbon Dioxide Standards

The calibrations of CO_2-in-air reference gas tanks continued in 1990; on 116 days, 236 tanks were calibrated. All CO_2-in-air reference gas tanks used by CMDL are now being filled with dry ambient air from Niwot Ridge (NWR), Colorado, in aluminum tanks. The aluminum tanks show better stability for CO_2 than the steel tanks that have been used previously. In 1990, 121 tanks were filled in 47 days at NWR. Included among these were 15 large aluminum cylinders that will eventually replace the current set of secondary standard gases. These 15 tanks were filled in 1989, but a problem with the stability of the CO_2 concentration for several minutes after the tank valve was opened was noticed. The valves on all these tanks were changed from packless stainless steel to packless brass valves, since this problem did not occur with previous aluminum cylinders using brass valves. The new set of 15 gases range from 250 to 500 ppmv CO_2 and will be calibrated by the central CO_2 laboratory at SIO in 1991.

Construction of a system for performing primary calibrations of the mole fraction of CO_2 in reference gases began in 1990. A 12-L volume is filled with a sample of reference gas from a compressed gas cylinder, and the pressure and temperature are measured. After the CO_2 in the sample has been separated from the air by pumping the sample through a trap cooled with liquid nitrogen, the CO_2 is transferred to a ≈4 cc volume, and the pressure and temperature of the collected CO_2 is measured. The pressure and temperature data and the precise volume ratio of the 12 L and 4 cc volumes, along with corrections for the non-ideality of the gases, are used to calculate the mixing ratio of the CO_2 in the sample. Pressure is measured with a high precision quartz-spiral pressure gauge manufactured by RUSKA. Temperature is measured using platinum resistance thermometers. The volumes and pressure gauge are contained in a cabinet that is temperature controlled to less than 0.1°C. The system is highly automated with valve switching and pressure and temperature measurements controlled by computer in order to reduce the time and skill required by the operator, as well as to increase the repeatability of each measurement.

4.2.2. Methane Standards

All standards used to determine CH_4 mixing ratios reported by CMDL are natural air. It is critical to any long-term time series of measurements that the trace gas composition of the standards does not change over the period of the measurements. Figure 4.13 shows the calibration history of the primary standards used since the start of the CH_4 measurement program in 1983. All cylinders are referenced against cylinder number 259 that was purchased from the Biospherics Company in 1983. Each of these cylinders has sufficient air remaining in it so that if they are used wisely, they may be calibrated twice a year for the next 30 years.

Three different cylinder materials are represented in Figure 4.13: aluminum, steel, and stainless steel. The air in the aluminum and steel cylinders is natural air which was dried to less than 1 ppmv of water before being pumped into the tank. The stainless-steel cylinders are also natural air, but the air in them was collected without drying. It is highly unlikely that the trace gas composition of all six cylinders could be changing in exactly the same manner. Therefore, we feel confident that our CH_4 time series is free from bias due to the calibration tanks used, and the trends we report are not affected by changes in the composition of our reference gases with time.

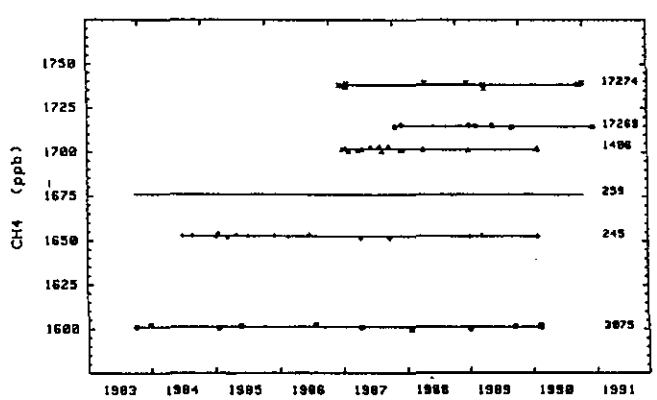

Fig. 4.13. Calibration history of NOAA/CMDL primary CH_4 standards.

In addition to the primary standards, secondary standards are used for in situ measurements at the observatories. These are extensively calibrated against the primaries in Boulder and the secondaries at the observatories. Once a secondary standard is nearly exhausted, it is returned to Boulder for further comparison with the primaries. Unlike the primaries, the secondaries are not retained indefinitely.

In 1990, Carle 4 was retired from flask analysis and dedicated to standard calibrations. A subset of our primary standards is calibrated periodically on Carle 7 to insure that the consistency of our calibration scale is maintained on that instrument.

4.3. SPECIAL PROJECTS

During May and June, with the cooperation of the Blue Star Line (London and San Francisco), regular sampling at 5° latitude intervals was initiated on the *M/V Wellington Star* to complement the ongoing program started in 1986 on the *M/V Southland Star* [*Schnell and Rosson*, 1987]. L. Waterman sailed on Voyage 1281 (May 20-June 13) from Los Angeles to Auckland, New Zealand, to investigate the suitability of using a MAKS unit aboard the ship with 2.5-L flasks and the standard flushing technique and to train the deck officers to operate the equipment. On the basis of this experience, it was decided to go back to the simpler evacuated flask technique that was being used on the first vessel. The possibility of extending the sampling south of 30°S latitude was also investigated. The idea was discarded because the sailing times between ports, Auckland to Wellington to Lyttelton, are brief and the ship stays close to land. A total of 239 samples was collected on the *M/V Wellington Star* during the first year (May-December) of operation.

4.4. REFERENCES

Brunke, E.G., H.E. Scheel, and W. Seiler, Trends of tropospheric CO, N_2O, and CH_4 as observed at Cape Point, South Africa, *Atmos. Environ., 24A*, 585-595, 1990.

Crutzen, P.J., and M.O. Andreae, Biomass burning in the tropics: Impact on atmospheric chemistry and biogeochemical cycles, *Science, 250*, 1669-1678, 1990.

Dianov-Klokov, V.I., and L.N. Yurganov, Spectroscopic study of the global time-space distribution of atmospheric CO, *Tellus, 33*, 262-273, 1981.

Dianov-Klokov,V.I., L.N. Yurganov, E.I. Grechko, and A.V. Dzhola, Spectroscopic measurements of atmospheric carbon monoxide and methane. 1. Latitudinal Distribution, *J. Atmos. Chem., 8*, 139-151, 1989.

Fishman, J., K. Fakhruzzaman, B. Cros, and D. Nganga, Identification of widespread pollution in the southern hemisphere deduced from satellite analyses, *Science, 252*, 1693-1696, 1991.

Marland, G., T.A. Boden, R.C. Griffin, S.F. Huang, P. Kanciruk, and T.R. Nelson, Estimates of CO_2 emissions from fossil fuel burning and cement manufacturing, based on the United Nations energy statistics and the U.S. Bureau of Mines cement manufacturing data. ORNL/CDIAC-25, *Numerical Data Package NDP-30*, 712 pp, Oak Ridge National Laboratory, Oak Ridge, TN, 1990.

Novelli, P.C., J.W. Elkins, and L.P. Steele, The development and evaluation of a gravimetric reference scale for measurements of atmospheric carbon monoxide, *J. Geophys. Res., 96*, 13,109-13,122, 1991.

Schnell, R.C., and R.M. Rosson (Eds.), *Geophysical Monitoring for Climatic Change, No. 15: Summary Report 1986*, 155 pp., NOAA Air Resources Laboratory, Boulder, CO, 1987.

Steele, L.P., P.J. Fraser, R.A. Rasmussen, M.A.K. Khalil, T.J. Conway, A.J. Crawford, R.H. Gammon, K.A. Masarie, and K.W. Thoning, The global distribution of methane in the troposphere, *J. Atmos. Chem., 5*, 125-171, 1987.

Seiler, W., The atmospheric cycle of CO, *Tellus, 26B*,118-135, 1974.

Tans, P.P., T.J. Conway, and T. Nakazawa, Latitudinal distribution of the sources and sinks of atmospheric carbon dioxide derived from surface observations and an atmospheric transport model, *J. Geophys. Res., 94*, 5151-5172, 1989.

Thoning, K.W., P.P. Tans, and W.D. Komhyr, Atmospheric carbon dioxide at Mauna Loa Observatory, 2, Analysis of the NOAA/GMCC data, 1975-1985, *J. Geophys. Res., 94*, 8549-8565, 1989.

5. Aerosol, Ozone, and Water Vapor Group

D. HOFMANN, B. BODHAINE, R.D. EVANS, R.D. GRASS, J. HARRIS, W. KOMHYR, AND S. OLTMANS

5.1. CONTINUING PROGRAMS

5.1.1. SURFACE AEROSOLS

Barrow

The aerosol monitoring program at BRW was initiated in 1976 with the installation of a Pollak CN counter as the CN calibration standard, a G.E. automatic CN counter for routine operations, and a four-wavelength nephelometer for the measurement of aerosol scattering extinction coefficient (σ_{sp}) at 450-, 550-, 700-, and 850-nm wavelengths. A TSI (butanol-based) CN counter was installed in March 1990 and will undergo a 1-year comparison with the existing G.E. CN counter before the G.E. counter is permanently retired. Aerosol absorption coefficient (σ_{ap}) has been measured continuously with an aethalometer since April 1988. The BRW data record was presented by *Quakenbush and Bodhaine* [1986] and *Bodhaine* [1989].

Mauna Loa

The aerosol program at MLO was initiated in 1974 with the installation of Pollak and G.E. CN counters and a four-wavelength nephelometer. A TSI CN counter was installed in May 1988 and, after a 1-year overlap with the G.E. automatic CN counter, the G.E. counter was retired. The comparison between the TSI and G.E. CN counters at MLO was reported in the *Summary Report* for 1989 [*Komhyr and Rosson*, 1990]. Aerosol absorption has been measured with an aethalometer since April 1990. The MLO data record was presented by *Massey et al.* [1987].

Samoa

The aerosol program at SMO was initiated in 1977 with the installation of Pollak and G.E. CN counters, and a four-wavelength nephelometer. A TSI CN counter will be installed in 1991 and will undergo an overlap period with the G.E. CN counter before the G.E. counter is retired. There are no current plans for installing an aethalometer at SMO. The SMO data record was presented by *Bodhaine and DeLuisi* [1985].

South Pole

The aerosol program at SPO was initiated in 1974 with the installation of Pollak and G.E. CN counters. A four-wavelength nephelometer was installed in January 1979; a TSI CN counter was installed in January 1989; and an aethalometer was installed in December 1986. The SPO data record was presented by *Bodhaine et al.* [1986, 1987] and *Bodhaine and Shanahan* [1990].

Discussion of Data

CN concentration was measured continuously with G.E. and/or TSI CN counters, and daily calibration points were provided by Pollak CN counters at all stations (twice daily at SPO). After a TSI CN counter is installed at a station, a 1-year overlap with the existing G.E. CN counter is performed. All G.E. CN data have been scaled to agree with the Pollak CN counter observations. Since the TSI instrument is a single particle counter and is considered to be an absolute instrument, its data are not scaled to agree with the Pollak counter. However, Pollak counter observations are being continued at all stations to maintain the continuity of the record and to serve as quality control for the TSI instrument.

Figure 5.1 shows daily geometric means of CN concentration (lower portion of each plot), σ_{sp} (middle portion of each plot), and Ångström exponent (upper portion of each plot) at the CMDL stations for 1990. Three independent values of Ångström exponent (α) were calculated from the four channels of σ_{sp} data using the relation $\alpha = -\Delta\sigma_{sp}/\Delta\lambda$ where λ is the wavelength of light. The interpretation of α in terms of aerosol size distribution was discussed by *Bodhaine and DeLuisi* [1985]. Monthly geometric means of the 1990 aerosol data are listed in Table 5.1. A graphical presentation of the monthly geometric means of the entire data record for the four stations is shown in Figure 5.2.

The BRW data in Figure 5.1 show a σ_{sp} maximum of about 2×10^{-5} m^{-1} during winter and spring, typical of the well-known arctic haze. The BRW long-term record shown in Figure 5.2 clearly shows this annual cycle in σ_{sp}. The 850-nm data for BRW for January-May are omitted from Table 5.1 because of instrument problems that required deletion of much of the data. The BRW CN record shows a more variable semiannual cycle with a maximum that usually coincides with the maximum in σ_{sp} and a relative maximum in late summer or early spring.

The MLO σ_{sp} data shown in Figure 5.1 are fairly typical with large values in April and May, and smaller values in fall and winter. Events in April and May, caused by the long-range transport of Asian desert dust in the upper troposphere to the vicinity of Hawaii, dominate the record. σ_{sp} values have been generally higher since the installation of the new nephelometer in 1985 and have not reached the low values expected in winter. A nephelometer comparison experiment was performed in the spring of 1990 in order to determine if σ_{sp} has generally increased at MLO or if reduced instrument sensitivity is responsible for the higher values (see section 5.2.1). The MLO CN record shown in Figure 5.1 is fairly typical, giving an annual geometric mean concentration of 203 cm^{-3}, compared with 218 cm^{-3} for the previous year. Note that all MLO aerosol data presented here are in the form of geometric means during 0000-0800 HST (1000-1800 UT) in order to include data for downslope wind conditions only.

The SMO σ_{sp} and CN data continue as in previous years with no significant annual cycle or long-term trend. The SMO 1990 annual mean is about 1.77×10^{-5} m^{-1} for σ_{sp} (550) and about 218 cm^{-3} for CN concentration (compared

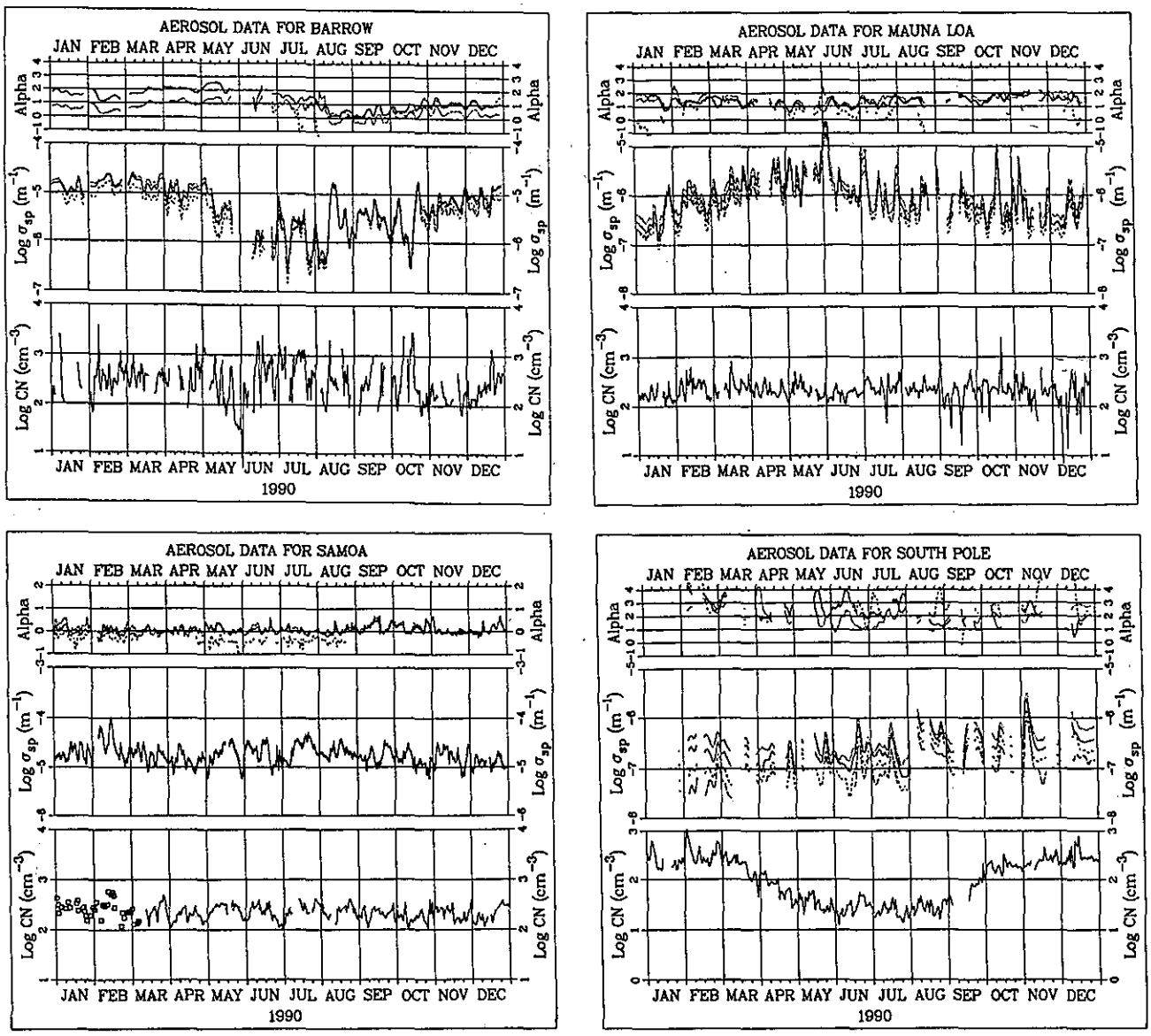

Fig. 5.1. Daily geometric means of σ_{sp} and CN data at BRW, MLO, SMO, and SPO for 1989. Data for MLO are included only for 0000-0800 LST. For each station, CN concentration (lower) is shown as a solid line. σ_{sp} data (middle) are shown for 450 (dotted), 550 (solid), 700 (dashed), and 850 nm (long-dashed). Ångström exponents were calculated from 450- and 550-nm (dotted), 550- and 700-nm (solid), and 700- and 850-nm (dashed) σ_{sp} data.

with 1.80×10^{-5} m^{-1} and 229 cm^{-3} last year), representative of the background marine boundary layer in that region. The CN data were filled with daily Pollak counter observations when available. A detailed analysis of the entire SMO data record was presented by *Bodhaine and DeLuisi* [1985].

The SPO CN data from the TSI CN counter are shown in Figure 5.1. These data show a strong annual cycle reaching a maximum exceeding 200 cm^{-3} in the austral summer and a minimum approaching 10 cm^{-3} in the winter; the CN data appear to be higher than in previous years. Shown on the same graph are daily means from the Pollak CN counter (squares). The CN data shown in Figure 5.2 were filled with Pollak counter data when continuous data were missing. The σ_{sp} data in Figure 5.1 generally show intermediate values in the austral summer, a minimum in May, and large events, sometimes exceeding 10^{-6} m^{-1}, in late winter. These large aerosol events are caused by the transport of sea salt in the upper troposphere from stormy regions near the Antarctic coast to the interior of the continent.

The least-squares trend lines shown in Figure 5.2 were calculated using the common logarithms of the monthly means of the entire data record, and the results are given in Table 5.2. Similar trend lines have been calculated and presented in previous *Summary Reports*.

TABLE 5.1. Monthly Geometric Means of CN Concentration (cm^{-3}) and σ_{sp} (m^{-1}) at 450, 550, 700, and 850 nm, for BRW, MLO, SMO, and SPO, During 1990

	Jan.	Feb.	March	April	May	June	July	Aug.	Sept.	Oct.	Nov.	Dec.
						BRW						
CN	192	294	366	310	217	305	582	350	284	272	155	243
σ_{sp}(450)	1.40-5	1.84-5	1.85-5	1.31-5	7.00-6	1.53-6	2.21-6	2.60-6	3.09-6	3.25-6	6.91-6	1.14-5
σ_{sp}(550)	1.23-5	1.67-5	1.56-5	1.06-5	5.42-6	1.21-6	1.89-6	2.53-6	3.20-6	3.04-6	6.25-6	1.06-5
σ_{sp}(700)	8.19-6	1.17-5	9.99-6	6.52-6	3.13-6	7.63-7	1.36-6	2.20-6	2.93-6	2.47-6	4.77-6	8.29-6
σ_{sp}(850)						7.01-7	1.73-6	2.74-6	2.90-6	2.21-6	3.94-6	6.72-6
						MLO						
CN	166	238	252	207	218	173	240	221	175	230	190	155
σ_{sp}(450)	4.57-7	9.01-7	1.69-6	2.96-6	3.22-6	2.89-6	1.67-6	8.59-7	9.19-7	7.12-7	8.65-7	6.92-7
σ_{sp}(550)	3.38-7	6.44-7	1.22-6	2.22-6	2.62-6	2.28-6	1.21-6	6.30-7	6.74-7	5.08-7	5.85-7	4.91-7
σ_{sp}(700)	2.39-7	4.58-7	8.84-7	1.62-6	2.11-6	1.79-6	8.73-7	4.54-7	4.58-7	3.52-7	3.86-7	3.42-7
σ_{sp}(850)	2.96-7	6.44-7	7.83-7	1.39-6	1.92-6	1.68-6	9.93-7	5.69-7	5.04-7	4.61-7	4.66-7	4.30-7
						SMO						
CN			253	183	254	210	253	243	208	179	214	201
σ_{sp}(450)	1.90-5	2.68-5	1.79-5	1.38-5	1.73-5	1.96-5	2.35-5	2.04-5	1.80-5	1.47-5	1.62-5	1.29-5
σ_{sp}(550)	1.82-5	2.67-5	1.79-5	1.39-5	1.70-5	1.93-5	2.32-5	2.01-5	1.71-5	1.41-5	1.62-5	1.27-5
σ_{sp}(700)	1.82-5	2.70-5	1.80-5	1.37-5	1.65-5	1.93-5	2.31-5	2.01-5	1.64-5	1.35-5	1.60-5	1.23-5
σ_{sp}(850)	1.94-5	2.95-5	2.27-5	1.48-5	1.94-5	2.21-5	2.59-5	2.24-5	1.85-5	1.54-5	1.87-5	1.36-5
						SPO						
CN	234	332	180	69	34	29	23	29	68	180	236	281
σ_{sp}(450)	2.47-7	4.12-7	2.73-7	2.34-7	2.45-7	2.56-7	2.19-7	6.56-7	4.65-7	4.66-7	5.78-7	6.80-7
σ_{sp}(550)	1.30-7	2.33-7	1.70-7	1.47-7	1.62-7	1.90-7	1.50-7	5.04-7	3.36-7	3.26-7	3.85-7	3.89-7
σ_{sp}(700)	5.97-8	1.03-7	8.84-8	8.48-8	8.45-8	9.83-8	8.46-8	3.31-7	2.27-7	1.97-7	2.19-7	2.54-7
σ_{sp}(850)	3.77-8	5.31-8	4.87-8	6.89-8	9.23-8	9.48-8	6.55-8	2.23-7	1.54-7	1.16-7	1.22-7	1.58-7

A compact exponential format is used for σ_{sp} such that 1.40-5 = 1.40×10^{-5}.

5.1.2. TOTAL OZONE OBSERVATIONS

Total ozone observations were continued throughout 1990 at 15 of the 16 stations that comprise the U.S.A. Dobson spectrophotometer network (Table 5.3). Of the 15 stations, 5 are operated by CMDL personnel, 4 are operated by the NWS, 2 are domestic cooperative stations, and 4 are foreign cooperative stations. The Dobson spectrophotometer operated at Florida State University, Tallahassee, Florida, until November 1989 is being relocated to the Municipal Airport in Tallahassee and will be operated by NWS staff.

Daily 1990 total ozone amounts applicable to local noon for stations listed in Table 5.3 have been archived at the World Ozone Data Center, 4905 Dufferin Street, Downsview, Ontario M3H 5T4, Canada, in *Ozone Data for the World*. Table 5.4 lists the provisional mean monthly total ozone amounts measured at the various stations during 1990.

Figure 5.3 plots mean total ozone amounts measured at SPO during October 15-31 of 1962-1990. (Mid-October is when Dobson spectrophotometer total ozone observations first become possible each year at South Pole following the polar night.) Least squares linear regressions fitted to the data for 1962-1979 and 1979-1990 show an initial moderate downward trend in ozone not statistically significant at the 95% confidence level (t-statistic), followed by a large, statistically significant downward ozone trend during 1979-1990 of −4.35% yr^{-1}. During October 1988, ozone at SPO recovered to a value comparable to October values observed there in 1965, 1969, 1975, and 1977. *Komhyr et al.* [1991] attributed this recovery to increased transport from the tropics of heat, momentum, and ozone to SPO during June-October 1988 following a drop in sea-surface temperatures in the eastern equatorial Pacific to low values last observed there prior to 1976. Polar vortex breakdown and stratospheric warming occurred 3-4 weeks earlier in Antarctica in 1988, compared to the time of occurrence of these phenomena in other recent years, thereby causing early disruption of heterogeneous photochemical processes that destroy ozone during austral springtime in the presence of polar stratospheric clouds. During 1989 and 1990, June-August SSTs in the eastern equatorial Pacific recovered to above normal values. October total ozone at SPO declined successively during these 2 years for the first time since 1980.

Figure 5.4 plots provisional total ozone anomaly data (i.e., monthly mean ozone deviations from monthly normals) for SMO, MLO, as well as for the contiguous U.S.A. stations of Fresno, Boulder, Bismarck, and Caribou. Least square linear regression trend lines are fitted to the data for 1979-1990 for

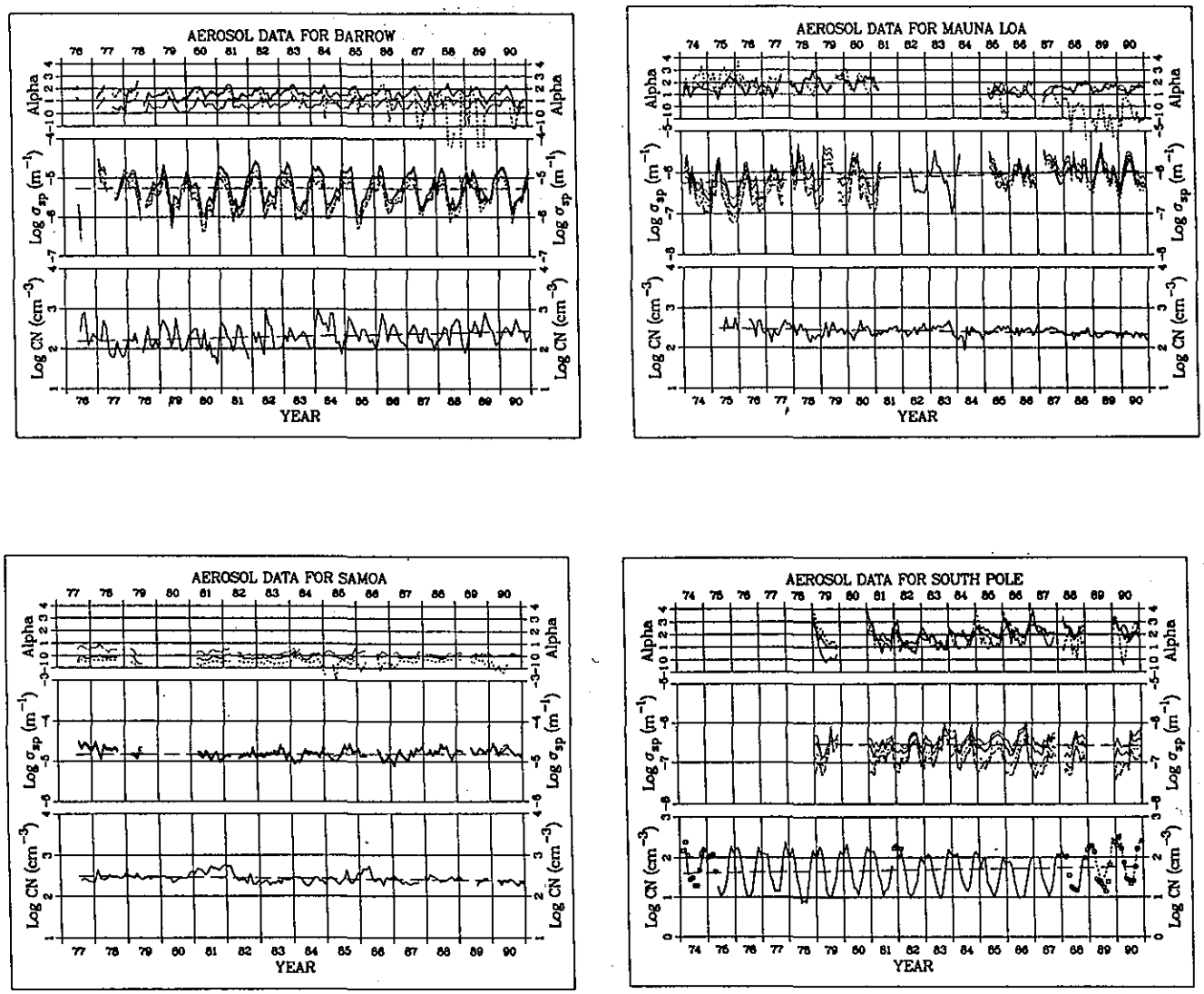

Fig. 5.2. Monthly geometric means of σ_{sp} and CN data for the entire data record. Details of the trend lines are given in Table 5.2.

all stations except 1984-1990 for Fresno where the record is of shorter duration. No significant linear trends are evident in 12-year SMO and MLO ozone data records, and in the shorter (7-year) Fresno ozone data record. Significant downward ozone trends averaging 4.9%/decade are present, however, in the ozone data from Boulder, Bismarck, and Caribou. While the provisional data are subject to additional refinement, it is unlikely that the ozone trends shown in Figure 5.4 are in error by more than ±1%/decade.

5.1.3. UMKEHR OBSERVATIONS

Umkehr observations with automated Dobson ozone spectrophotometers were continued during 1990 at Boulder; MLO; Haute Provence, France; Perth, Australia; and Lauder, New Zealand. Table 5.5 lists the number of Umkehr observations made at each station during the year, as well as the number that yielded useful data. Not useful Umkehr observations are those exhibiting excessive cloud interference. The relatively fewer observations made at Poker Flat reflect the station's high latitude location where wintertime observations cannot be made.

Because of political and economic problems, Umkehr observations at CMDL's seventh automated Dobson station at Huancayo, Peru, are no longer being made.

All provisional 1990 Umkehr data have been archived at the WMO World Ozone Data Centre, Atmospheric Environment Service, Downsview, Canada, from where they are received by NOAA-NESDIS (and other users) for comparison with NOAA-11 satellite SBUV-2 ozone profile measurements. Umkehr layer aerosol corrections [*DeLuisi*, 1989], as a function of latitude and time, are routinely

TABLE 5.2. Least-Squares Trend Analysis of the Common Logarithms of the Data Shown in Figure 5.2*

	Parameter	Slope	Intercept	S.E.	Trend (% yr^{-1})
BRW	CN	0.0179	0.828	0.277	4.21%
	σ_{sp}	-0.00130	-5.16	0.377	-0.30%
MLO	CN	-0.00820	3.09	0.119	-1.87%
	σ_{sp}	0.0171	-7.51	0.311	4.02%
SMO	CN	-0.00949	3.23	0.109	-2.16%
	σ_{sp}	0.00166	-4.96	0.116	0.38%
SPO	CN	0.00899	0.948	0.436	2.09%
	σ_{sp}	-0.00163	-6.42	0.194	-0.37%

*The time axes in Figure 5.2 are in fractional years, with a data point centered at the center of a month; e.g., Jan. 1974 = 74.042, Feb. = 74.125, etc.

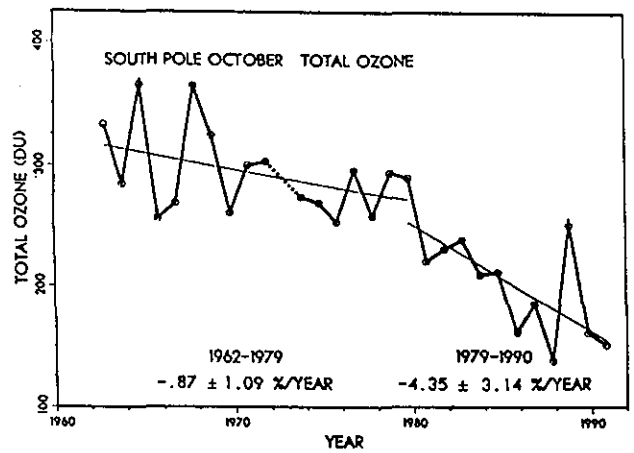

Fig. 5.3. South Pole October 15-31 mean total ozone amounts (DU) for 1962-1990. Trend lines fitted to the data are linear least-squares regressions.

provided to NESDIS. C.L. Mateer (Scarborough, Ontario, Canada) is currently improving existing Umkehr observation reduction algorithms by incorporating into them improved ozone absorption and primary scattering coefficients.

5.1.4. Calibration of NOAA-CMDL Dobson Spectrophotometers

Because considerable effort was spent during 1990 in organizing, preparing for, and conducting international Dobson ozone spectrophotometer comparisons in Arosa, Switzerland, there was time to perform calibration checks on only three NOAA-CMDL Dobson instruments. The calibration level of Dobson instrument 65, used as the reference spectrophotometer at the Arosa comparisons, was checked relative to World Primary Standard Dobson instrument 83, and it was found to agree with instrument 83 to within 0.3%. Optical wedges of instruments 65 and 83 were recalibrated, and instrument 83 was sent to MLO where special observations were conducted during June-August to check its calibration using the Langley method. These showed that the calibration level of instrument 83 was unchanged from that determined for it at MLO in 1989, to within several tenths of a percent experimental error.

Enroute to the Dobson instrument comparisons in Arosa, a detour was made to Haute Provence Observatory in France, to recalibrate NOAA-CMDL automated Dobson spectrophotometer 85 which had last been calibrated in 1986. No significant change with time was detected in the calibration of instrument 85 whose total ozone values agreed with those of secondary standard Dobson instrument 65 in the mean to 0.2%.

TABLE 5.3. U.S. Dobson Ozone Spectrophotometer Station Network for 1990

Station	Period of Record	Instrument No.	Agency
Bismarck, ND	Jan. 1, 1963-present	33	NOAA
Caribou, ME	Jan. 1, 1963-present	34	NOAA
Wallops Is., VA	July 1, 1967-present	38	NOAA; NASA
SMO	Dec. 19, 1975-present	42	NOAA
Tallahassee, FL	May 2, 1964-Nov. 30, 1989	58	NOAA; Florida State University
Boulder, CO	Sept. 1, 1966-present	61	NOAA
Poker Flat, AK	March 6, 1984-present	63	NOAA; University of Alaska
Lauder, New Zealand	Jan. 29, 1987-present	72	NOAA; DSIR
MLO	Jan. 2, 1964-present	76	NOAA
Nashville, TN	Jan. 2, 1963-present	79	NOAA
Perth, Australia	July 30, 1984-present	81	NOAA; Australian Bureau Meteorology
SPO	Nov. 17, 1961-present	82	NOAA
Haute Provence, France	Sept. 2, 1983-present	85	NOAA; CNRS
Huancayo, Peru	Feb. 14, 1964-present	87	NOAA; IGP
BRW	June 6, 1986-present	91	NOAA
Fresno, CA	June 22, 1983-present	94	NOAA

TABLE 5.4. Provisional 1990 Monthly Mean Total Ozone Amounts (m-atm-cm)

Station	Jan.	Feb.	March	April	May	June	July	Aug.	Sept.	Oct.	Nov.	Dec.
Bismarck, ND	331	374	362	356	353	328	313	304	288	299	286	334
Caribou, ME	335	393	394	381	382	350	339	325	317	287	289	321
Wallops Is., VA	298	315	337	373	357	342	-	326	314	285	286	282
SMO	261	256	254	250	252	244	241	252	254	258	257	262
Tallahassee, FL												
Boulder, CO	322	338	338	345	338	305	304	299	283	286	274	313
Poker Flat, AK			385	384	370	344	317	299	322	321		
Lauder, New Zealand	288	267	275	281	300	303	324	339	353	343	321	301
MLO	250	250	265	278	286	279	276	276	270	264	260	257
Nashville, TN	295	304	329	351	339	320	322	318	311	287	285	293
Perth, Australia	280	276	271	277	280	277	298	304	320	329	307	295
SPO	272	291	-	198	243	261	248	233	208	151	186	273
Haute Provence, France	325	290	333	380	359	338	335	326	318	287	304	312
Huancayo, Peru	258	251	253	251	245	255	252	253	264	265	263	256
BRW			378	405	379	355	315	294	344			
Fresno, CA	319	337	332	344	346	320	311	311	304	297	280	307

TABLE 5.5. Umkehr Observations Frequency During 1990

Station	Station Coordinates	Total No. Obs. Made	Total No. Useful Obs.
Boulder	40°N, 105°W	508	205
Haute Provence	43°N, 6°E	459	246
Lauder	45°S, 170°E	620	151
MLO	20°N, 156°W	599	385
Perth	32°S, 116°E	504	284
Poker Flat	65°N, 147°W	379	90

While at Haute Provence, France, French Dobson spectrophotometer 49 was calibrated. It was found to measure ozone too low by 1.89%.

5.1.5. International Calibration of Dobson Instruments in Arosa

International Dobson spectrophotometer comparisons were conducted by NOAA-CMDL ozone project scientists at Arosa, Switzerland, July 21-August 9, 1990, under auspices of the WMO. Seventeen countries including the U.S.A. participated with 18 instruments. Table 5.6 lists the participants and instruments. Results of the comparisons are summarized in Table 5.7

Of the 17 instruments calibrated in Arosa relative to U.S.A. secondary standard Dobson instrument 65, 15 had previous calibrations traceable to CMDL's World Primary Standard Dobson Spectrophotometer 83. Calibration errors were determined to be less than 1% for 12 of these 15 instruments. Of the three instruments with larger calibration errors, one (Iceland's instrument 50) had not been calibrated since 1977.

Two instruments had not been calibrated previously by CMDL. They were instruments 15 (Switzerland) and 118 (Greece), with calibration errors of -4.96% and -5.94%.

As indicated in Table 5.7, additional work was performed on 13 instruments to recalibrate optical wedges, or to correct optical or electronic problems.

Comparison Umkehr observations were made one morning during the Arosa instrument comparisons with 15 instruments. Observational data from C-wavelength observations were processed by the standard Umkehr technique [*Mateer and Dütsch*, 1964], and Umkehr layer mean ozone amounts were computed. Figure 5.5 plots the layer mean ozone amount differences in percent from Umkehr layer ozone values measured with secondary standard Dobson instrument 65. A maximum difference of 9% is evident for Umkehr layer 9. In an attempt to determine a possible cause of the differences, Umkehr layer 9 differences were plotted as a function of the ozone measurement residual (Figure 5.6), a statistical measure of observation quality derived during data processing. Note the correlation (Figure 5.6) between the residuals and percent ozone differences, indicating that instruments with low ozone measurement residuals yielded Umkehr layer ozone values that agreed more closely with Dobson instrument 65 values than did instruments having higher measurement residuals.

5.1.6. Validation of TOMS and SBUV Satellite Instrument Ozone Data

NOAA-CMDL World Primary Standard Dobson spectrophotometer 83 was operated in June-August 1990 at MLO in an ongoing program to assess the quality of total ozone data obtained with the TOMS and SBUV spectrometers aboard the Nimbus 7 satellite. Relative to Dobson instrument 83, whose long-term ozone measurement precision has been maintained at ±0.5% [*Komhyr et al.*, 1989], the calibration of the TOMS instrument has continued to drift (Figure 5.7*a*), at a rate now approaching 0.9% yr^{-1}.

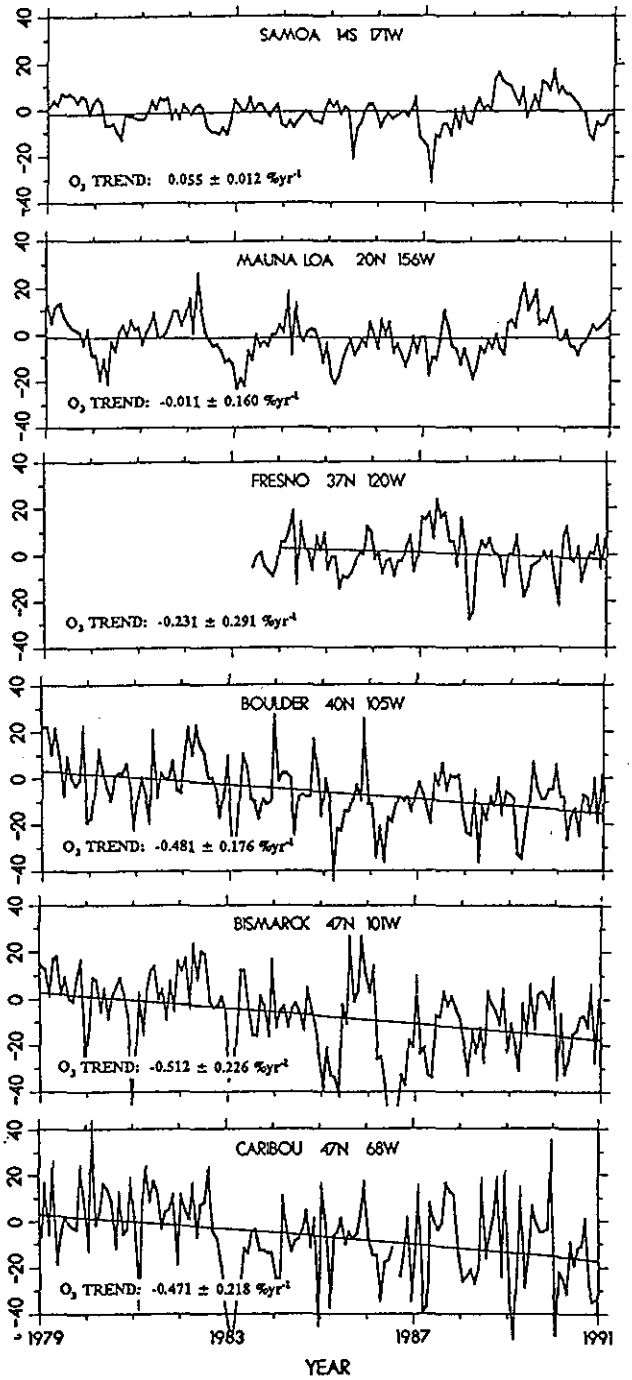

Fig. 5.4. Provisional total ozone anomaly data derived from Dobson spectrophotometer observations. Least squares linear regression trend lines are fitted to 12 years of data for all stations except 7 years of data for Fresno. Indicated uncertainties in the trends are 95% confidence limits (student's t-statistic).

Dobson instrument 83 has been used since the mid-1970's to calibrate Dobson instruments of the global Dobson spectrophotometer station network. While in the past the

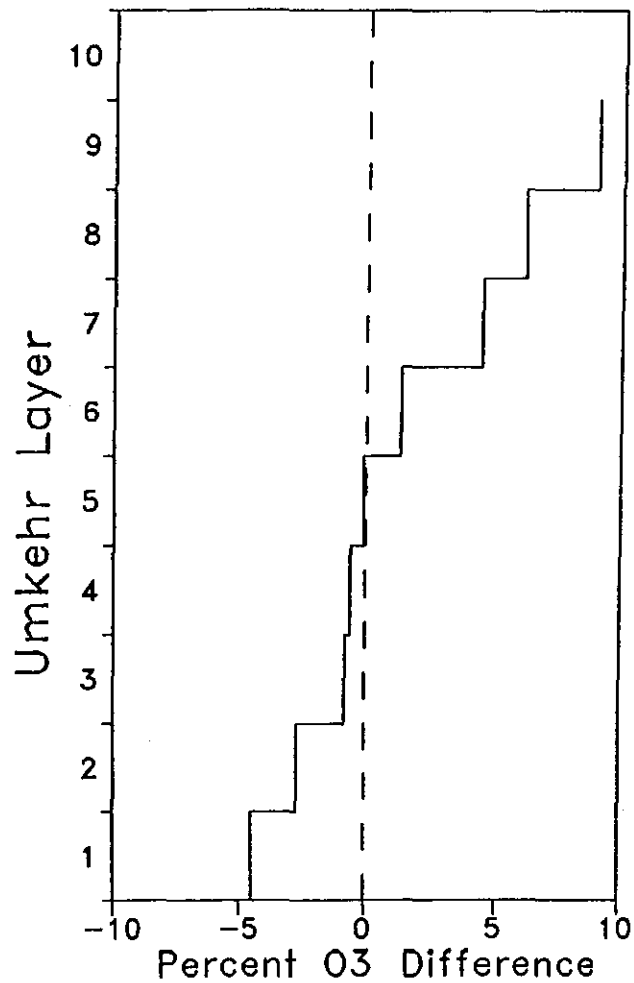

Fig. 5.5. Differences in percent of mean Umkehr layer ozone derived from measurements with 15 Dobson spectrophotometers from Umkehr layer ozone measured with secondary standard Dobson instrument 65.

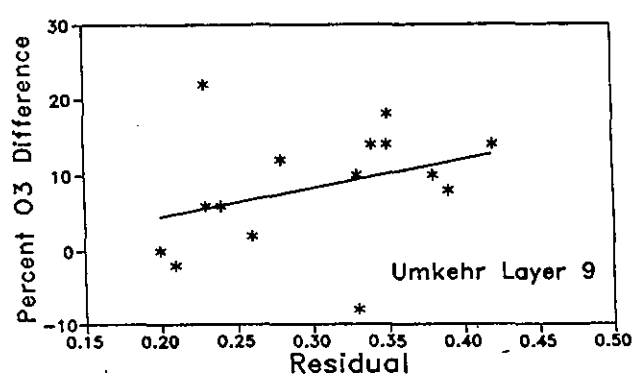

Fig. 5.6. Variation of Umkehr layer 9 ozone differences in percent for 14 Dobson instruments from secondary standard Dobson instrument no. 65 Umkehr layer 9 value as a function of observation quality (residual). The lowest value residual shown is that obtained with instrument 65.

TABLE 5.6. Arosa Dobson Instrument Comparison Participants

Country	Dobson Instrument	Participants
United States	65	W. Komhyr, R. Grass, R. Evans
Portugal	13	D. Henriques, J. Cacho
Norway	14	K. Henriksen
Switzerland	15	K. Aeshbacher
Belgium	40	D. De Muer, H. De Bacher
United Kingdom	41	A. Lapworth
France	49	J. de La Noe
Iceland	50	B. Thorkelsson
German Democratic Republic	64	U. Feister, P. Plessing
Czechoslovakia	74	K. Vanicek
Poland	84	M. Degorska, B. Rajewska-Wiech
Denmark	92	P. Eriksen
Switzerland	101	J. Staehelin, B. Hogger
Federal Republic Germany	104	U. Köhler, R. Hartmannsgruber
U.S.S.R.	107	V. Dorokhov
Hungary	110	F. Miskolczi, Z. Nagy, G. Luska
Greece	118	D. Asimakopoulos, C. Varotsos
Spain	120	J. Cacho, A. Diaz
Romania	121	M. Frimescu

TOMS and SBUV data have been corrected by normalization to Dobson spectrophotometer total ozone values [*World Meteorological Organization,* 1988], a pair wavelength justification technique has been recently developed by NASA scientists as an independent means of correcting the satellite data. Data thus corrected are referred to as Version 6 data. As shown in Figure 5.7*b* [see also *McPeters and Komhyr,* 1991], the agreement between the corrected TOMS data and Dobson instrument 83 data is now highly satisfactory.

To investigate the possibility of instrument stray light affecting the MLO Dobson instrument 83 observations that involve A-wavelength (305.5/325.0-nm) observations, an analysis was conducted in 1990 using longer, C-wavelength (311.5/332.4-nm) observations made at MLO since 1979. Stray light effects at the longer wavelengths are negligible. As shown in Figure. 5.7*c* relative to TOMS data, observations with Dobson instrument 83 on AD and C wavelengths yield highly similar results, lending credance to the validity of the MLO Dobson instrument 83 and the TOMS and SBUV instrument comparisons.

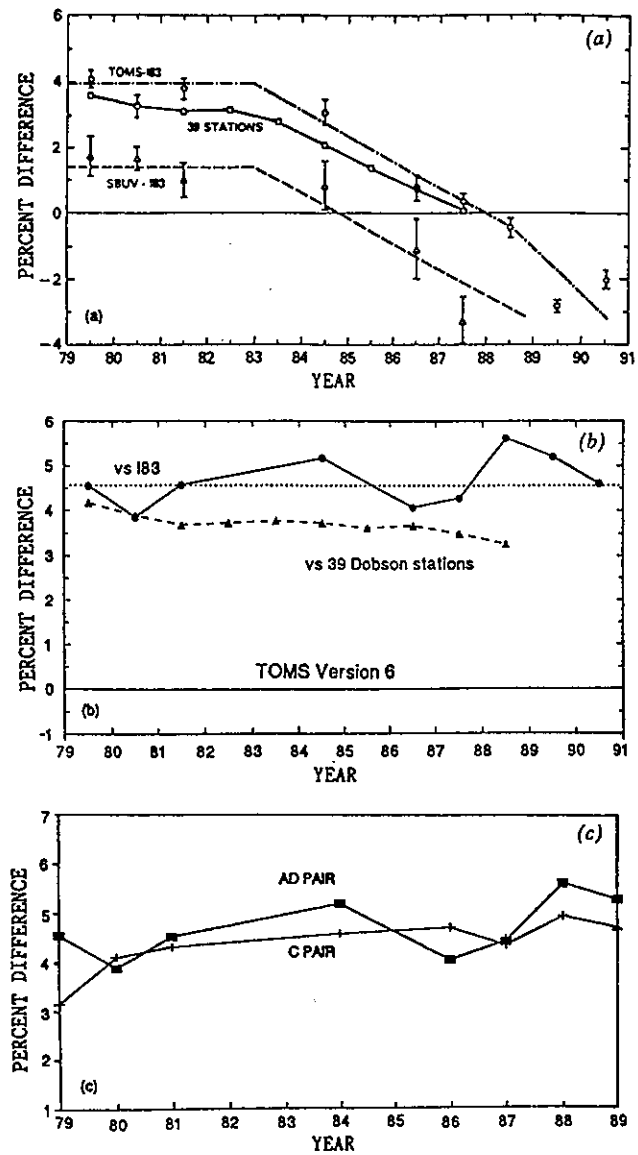

Fig. 5.7. (*a*) TOMS and SBUV total ozone data compared with Dobson instrument 83 total ozone data at MLO and total ozone data from 39 select Dobson instrument stations showing calibration drift with time of the satellite instruments due to diffuser plate degradation. (*b*) TOMS version 6 total ozone data corrected by means of a pair-wavelength justification technique, compared with Dobson instrument 83 data and data from 39 select Dobson instrument station. (*c*) Corrected TOMS total ozone data, compared with Dobson instrument 83 data derived from observation on AD as well as C wavelengths.

5.1.7. TROPOSPHERIC OZONE

Surface ozone measurements continued at the four CMDL observatories as well as the AEROCE sites at Bermuda, Barbados, and Mace Head, Ireland. In addition, observations started in July at Niwot Ridge in conjunction with the CFC measurements of the NOAH Group. Monthly mean ozone mixing ratios for 1990 at each site are given in Table 5.8. At SPO there has been a long-term decrease in the surface ozone concentration during the spring and summer [*Schnell et al.*, 1991]. Figure 5.8 shows the long-term monthly means (1975-1989) compared with the averages over the 5 years (1985-1989). The percentage departures of the 5-year mean from the long-term mean show decreases of 5% or more

TABLE 5.7. Results of The 1990 Arosa International Comparisons of Dobson Ozone Spectrophotometers

Inst. No.	Country	Last Calib.	Initial Calib. Error (%)	Initial Error Range (%)	Final Calib. Error (%)	Final Error Range (%)	Wedge Calib.	Optics Adjjustment	Electronics Adjustment
13	Portugal	1987	0.28	1.40	-0.16	1.32			
14	Norway	1977	-0.99	2.85	-0.19	1.69			Yes
15	Switzerland	*	-4.96	2.85	0.82	5.95*	Yes		
40	Belgium	1986	-0.60	1.68	-0.15	1.33			
41	United Kingdom	1985	0.59	0.39	0.15	1.03			
50	Iceland	1977	-3.16	0.50	0.05	0.32	Yes	Yes‡	
64	GDR	1977	0.22	0.52	-0.09	0.78			
74	Czechoslovakia	1986	-0.66	1.01	-0.07	0.75	Yes		
84	Poland	1986	0.35	1.15	-0.05	0.85	Yes		Yes
92	Denmark	1986	-0.50	1.10	-0.05	0.75	Yes		
101	Switzerland	1986	0.37	0.51	0.09	1.16			
104	FRG	1986	-2.40	1.19	-0.04	1.04	Yes	Yes§	
107	USSR	1988	-0.95	0.67	0.00	0.60		Yes**	
110	Hungary	1988	0.93	1.12	-0.24	1.95	Yes		
118	Greece		-5.94†	11.71	0.03	0.78	Yes		Yes
120	Spain	1989	-1.92	1.33	0.20	1.30			Yes
121	Rumania	1988	-0.06	0.64	0.04	1.54			Yes
65	USA	1990							

Observations were made over the μ-range 1.15-3.2.
*Better calibration not possible, as instrument needs optical alignment.
†Calibration error in the observing interval $1.15 < \mu < 1.5$ was -2.27%.
‡New mirrors installed.
§Phototube adjusted, mirrors adjusted, and rocking cover problem corrected.
**New mirror M1 installed.

TABLE 5.8. Monthly Mean Surface Ozone Concentrations in PPB During 1990

	Jan.	Feb.	Mar.	April	May	June	July	Aug.	Sept.	Oct.	Nov.	Dec.
BRW	32.5	29.1	27.1	19.6	24.6	23.5	21.1	25.6	32.3	33.0	34.4	32.7
Mace Head	31.7	34.3	35.6	40.4	41.1	34.7	32.7	29.3	36.1	33.6	31.2	33.2
NWR							46.9	46.7	44.3	43.6	41.8	42.1
Bermuda	22.3	35.5	41.1	43.5	39.9	25.0	20.2	25.9	30.3	31.2	38.2	36.4
MLO	37.2	37.6	47.6	47.6	49.9	42.6	32.5	31.5	29.1	35.0	28.4	38.5
Barbados	29.4	26.7	24.6	19.9	19.8	18.5	18.0	16.2	16.5	19.1	22.7	28.4
SMO	11.1	10.9	11.1	10.6	16.4	15.8	19.6	19.0	13.2	12.4	12.9	12.9
SPO	20.4	20.1	23.2	24.7	27.9	31.3	32.4	29.9	28.2	27.1	27.6	24.0

during the spring and summer. The December-January-February trends are significant at the 95% confidence level. These data suggest that this decrease is associated with the mechanisms responsible for producing the seasonal minimum.

Much of the southern hemisphere is thought to have low NO_x concentrations. Under such conditions, ozone will be lost in the lower troposphere by the action of UV radiation penetrating to the surface [*Crutzen*, 1989]. Such losses will be largest during the summer and at latitudes where sunlight is most abundant. At SPO the seasonal cycle appears to be driven by decreasing ozone concentrations on the periphery of Antarctica that are transported poleward during the spring and summer [*Schnell et al.*, 1991]. Both the degree of ozone destruction and the transport into the Pole have probably contributed to the changes seen in Figure 5.8. The decrease in stratospheric ozone during the spring over Antarctica has been dramatic since the early 1980s. This loss has extended into midlatitudes of the southern hemisphere [*Stolarski et al.*, 1989]. The reduction of overhead column ozone amounts has allowed greater penetration of UV radiation to the surface with the resulting greater tropospheric ozone loss [*Schnell et al.*, 1991].

It has also been found that during the summer (January-February) that there has been an increase at the South Pole in cloudiness that parallels the decline in surface ozone. Since

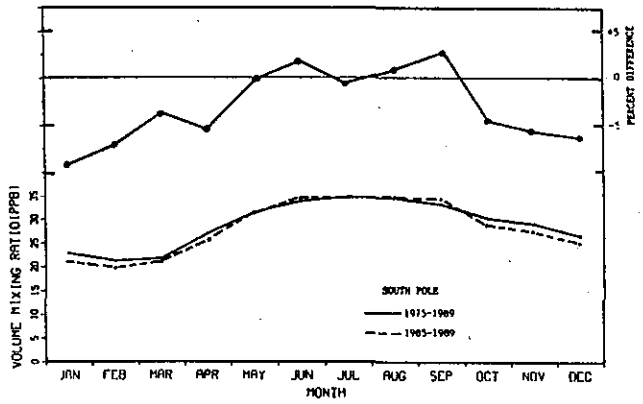

Fig. 5.8. Lower curves. Mullti-year averages of surface ozone mixing ratio at SPO for the periods 1975-1989 and 1985-1989. Upper curve. Percent difference between the two periods.

the primary source of the cloudiness is the transport of moist air from the edges of Antarctica, the enhanced transport of ozone-poor air to SPO has also been an important contributor to the long-term decline [*Schnell et al.*, 1991].

At Bermuda there is a springtime peak in the seasonal cycle with lower summertime values [*Komhyr and Rosson*, 1990]. The spring peak results from strong pulses of ozone advected to Bermuda during this time of year. This behavior is illustrated in Figure 5.9 which shows the hourly concentrations during May 1990. The high values (over ~45 ppb) are associated with flow from the midtroposphere over North America. The low values occur under weak flow conditions with the air often originating south of Bermuda and generally

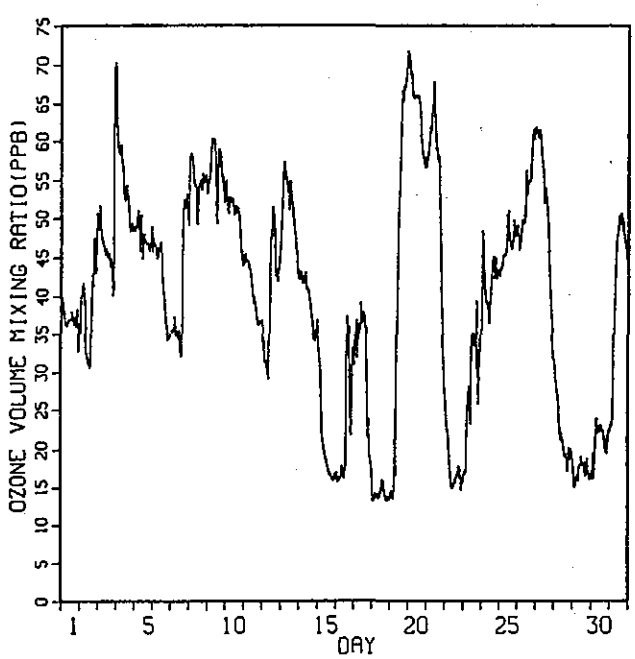

Fig. 5.9. Hourly ozone concentrations (ppb) at Bermuda for May 1990.

confined to lower altitudes. This can be seen dramatically in the strong event beginning on May 19 where ozone values go from less than 15 ppb to over 65 ppb in a few hours. The isentropic back trajectories from Bermuda for 00 and 12 UTC on May 19 (Figure 5.10*a* and *b*) show a pronounced change with low-level flow from south of Bermuda shifting to midtropospheric flow that traveled from western North America in the 10-day period represented. During the summer when the Bermuda anticyclone dominates, the high ozone events virtually cease, leading to gradually decreasing ozone concentrations through the summer.

5.1.8. Ozonesonde Observations

A digital ozonesonde system for obtaining vertical profiles of ozone was installed at SPO in November 1990. This system provides an automated, low initial cost method for obtaining ozone vertical profiles from balloonborne ozonesondes. The balloon flight package consists of an ECC ozonesonde mated to a Vaisala 403MHz radiosonde through a microprocessor-based interface. The three components of the system are purchased commercially and integrated into a flight package. This integration was carried out under a contract with the University of Wyoming. In addition, each of the air pumps on the ozonesonde was individually calibrated to determine the pumping efficiency loss at altitudes above 15 km (100 mb).

The operation of the ozonesonde sensor has been described previously in several publications [*Komhyr*, 1969, 1986]. The microprocessor-based interface (TMAX) measures six frequencies of the Vaisala RS-80 radiosonde along with the current output of the ECC sensor and the temperature of the ozonesonde pump. These parameters are formatted into a hexadecimal, ASCII serial data stream every 6 seconds. This data stream is converted to an audio frequency shift keyed (AFSK) signal which modulates the Vaisala transmitter in place of its standard frequency output.

The ground station for the system consists of an FM radio receiver capable of obtaining a signal at the 403 MHz carrier transmitting frequency of the radiosonde, an antenna with a preamplifier, a modem, and a lap-top computer. A printer and a cassette tape recorder for recording the audio output of the receiver are optional equipment used to provide backup for the data acquisition.

The computer software package developed by the University of Wyoming records the telemetered data, processes the raw data, and provides for tabular and graphical presentation (Figure 5.11) of the information. The digital form of the data allows for rapid processing and transmittal of the complete profile information for planning and research purposes.

The austral spring of 1990 marked the second consecutive year of very strong depletion over Antarctica of the stratospheric ozone layer. Since the early 1980s there has been a pattern of alternating years of larger and smaller ozone amounts in the springtime stratosphere with smaller amounts in 1985, 1987, and 1989. In 1990 values in the stratosphere approached the very low values seen in 1987 and 1989. In addition, low amounts persisted into December

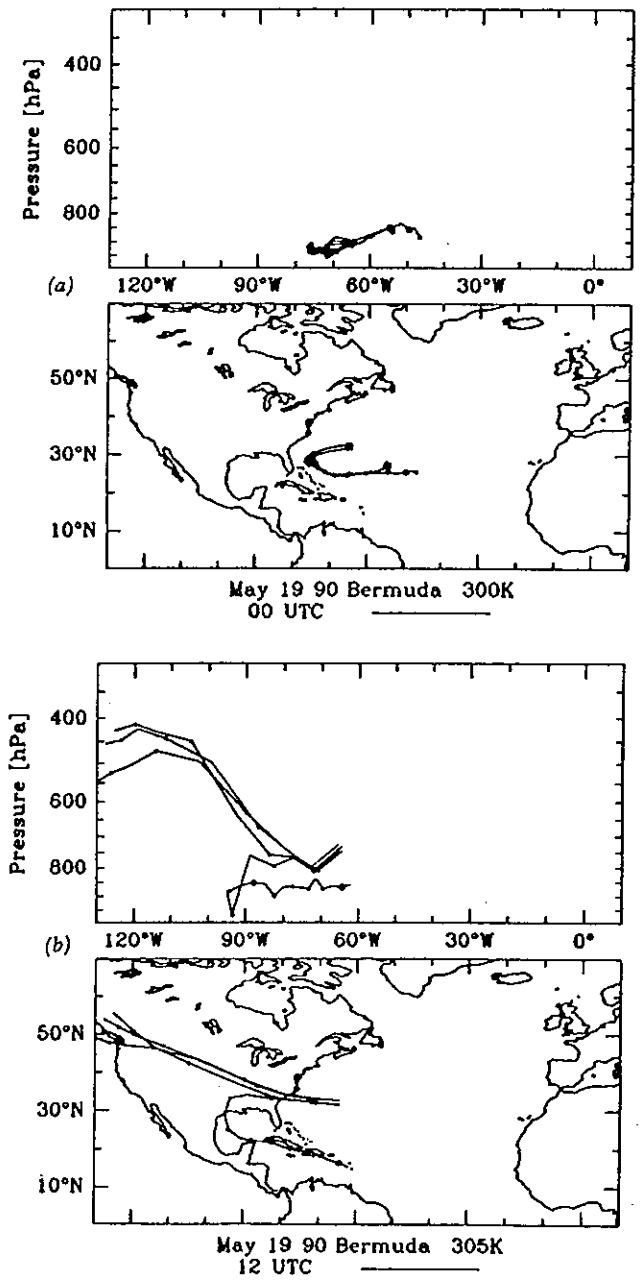

Fig. 5.10. Isentropic back trajectories to Bermuda for May 19, 1990 (*a*) 00 UTC and (*b*) 12 UTC.

at SPO. These year-to-year differences in the degree of ozone depletion appear to be related to variations in circulation patterns associate with the changes in SST and the tropical stratospheric quasibiennial wind oscillation [*Angell*, 1990; *Komhyr et al.*, 1991].

A limited program of ozonesonde measurements was done in Hilo, Hawaii, with approximately three soundings per month. Ozonesonde measurements were discontinued at SMO after January 1990, and only occasional training flights were made in Boulder during the year.

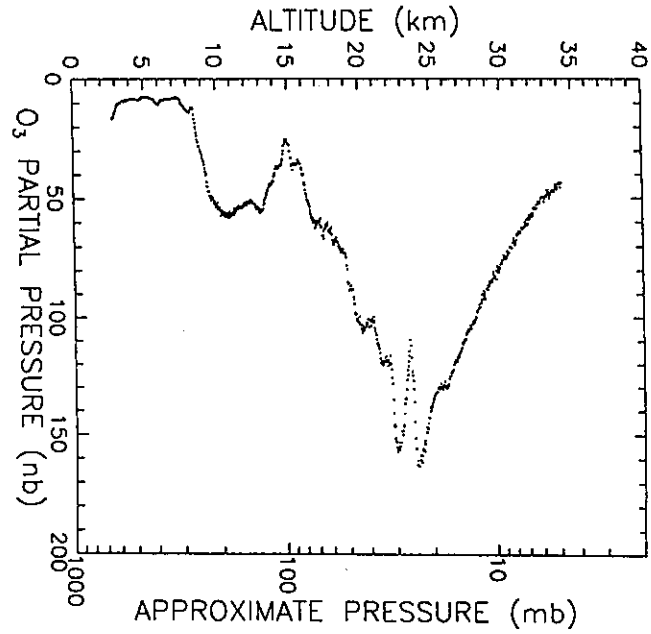

Fig. 5.11. Profile of ozone partial pressure (nb) at SPO obtained from the digital ozonesonde system.

5.1.9. STRATOSPHERIC WATER VAPOR

Monthly balloon soundings of the water vapor content of the upper troposphere and stratosphere continued in Boulder. This data set now includes the 10-year period 1981-1990. The mixing ratio from each sounding at three stratospheric levels (25 mb, 50 mb, 80 mb) is shown in Figure 5.12. The greater variability at 80 mb is associated with the seasonal change in the local tropopause height. The lowest mixing ratios (<3 ppmv) are associated with the appearance of water-vapor concentrations in the late winter and spring reflecting the drying of the stratosphere that takes place in the western tropical Pacific. At 50 mb the variability is relatively low and a possible long-term increase may be taking place. This may, however, reflect the low values measured early in the program. At the highest level shown (25 mb) a trend is not apparent. The mean value (solid line) shows a noticeable increase with altitude.

5.1.10. LONG-RANGE TRANSPORT OF TRACE GASES

Isobaric and isentropic trajectory models have been developed and used within CMDL over the past decade. The isobaric model is documented by *Harris* [1982], while the methodology for isentropic trajectories is described in *Harris and Bodhaine* [1983]. In addition, most Summary Reports contain an article describing the latest developments in and studies using atmospheric trajectories.

This year the isentropic model was modified to accept the consolidated GRIB data set supplied by ECMWF. This data set consists of global meteorological data at 14 mandatory levels from 1000 to 10 hPa. Atmospheric transport studies

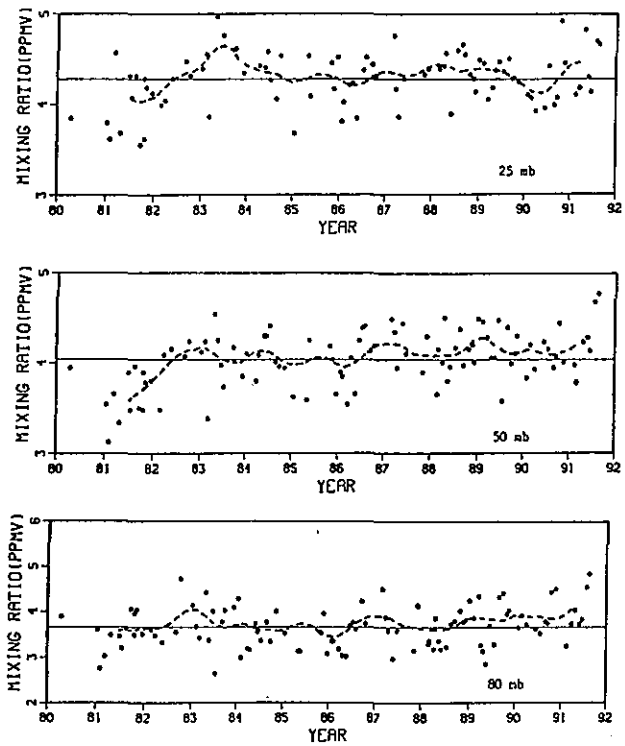

Fig. 5.12. Water vapor volume mixing ratios (ppm) at three levels in the stratosphere over Boulder. Each circle is the mixing ratio at the given level from a balloon descent profile. Note the scale difference at 80 mb.

relating to stratospheric ozone depletion are now possible with these analyses extending into the stratosphere. The domain of the isentropic model was expanded by using extended memory, so that cases with flow from outside the polar vortex can be diagnosed. Temperature and illumination along the trajectory path were features added to aid in determining conditions favorable to chemical ozone depletion.

Stratospheric ozone variations above Heiss Island (80.5°N, 57.5°E) were investigated in collaboration with scientists from the U.S.S.R. and the University of Milwaukee-Wisconsin. Figure 5.13 is a time-height cross-section of temperature (°C) for Heiss Island during winter 1988-1989. At around 20 km in the lower stratosphere, very low temperatures, often below -80°C, were measured in January and early February. During the last half of February, a pronounced warming of at least 40° occurred at this level. Figure 5.14 is a time-height cross section of ozone concentration (nb) showing a corresponding change in ozone over Heiss Island. At 20 km the ozone concentration was low and steady at about 140 nb until the warming. By February 20, ozone concentration at this level had surpassed 250 nb.

Backward isentropic trajectories for Heiss Island show that before the major warming, flow was confined to a tight path within the vortex and wind speeds were low (i.e., February 2, Figure 5.15). Trajectories for February 20 (Figure 5.16) confirm that the vortex had eroded. It appears

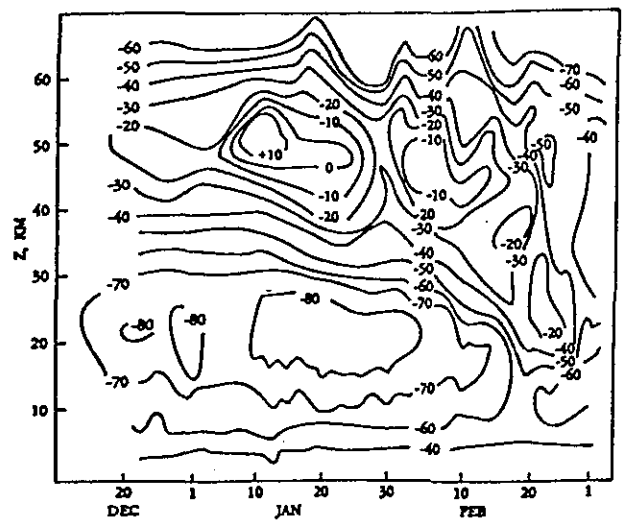

Fig. 5.13. Time-height cross-section of temperature (°C) over Heiss Island during winter 1988-1989.

that strong southerly flow transported the warmer, ozone-rich air from lower latitudes. This is an example where atmospheric dynamics appear to have played a major role in determining ozone concentration.

Ozone variations were also investigated over Kiruna, Sweden (68.0°N, 21.0°E) during winter 1989-1990 [*Hofmann and Deshler*, 1991]. Isentropic trajectories for the lower stratosphere (500 K) were calculated. Figure 5.17 shows ozone profiles for several balloon flights. A "notched" area from 20-25 km is suggestive of the beginnings of ozone chemical destruction. Figure 5.18 shows 550 K isentropic trajectories arriving above Kiruna on January 26, 1990. Flow appears to be confined within an elliptical vortex. The temperature history along the trajectories (lower plot, Figure 5.18) confirms that during the day prior to arrival, temperatures were below -80°C, which is required for the formation of polar stratospheric clouds. In addition, symbols plotted along the temperature plot indicate that the air parcel was illuminated. Sunlight is necessary to free Cl before destruction of ozone can occur. This example supports the possibility of ozone chemical depletion.

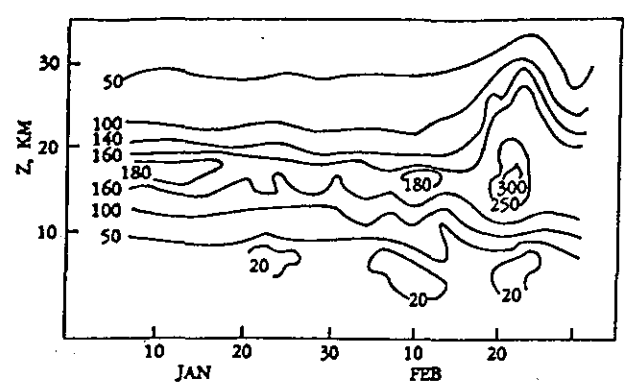

Fig. 5.14. Time-height cross-section of ozone concentration (nb) over Heiss Island, January and February 1989.

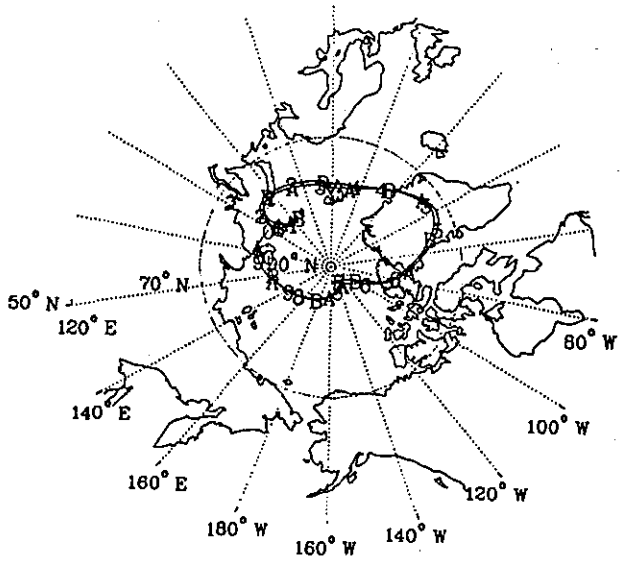

Fig. 5.15. Heiss Island trajectories (500 K) arriving February 2, 1989: A = 0000 UT, B = 1200 UT.

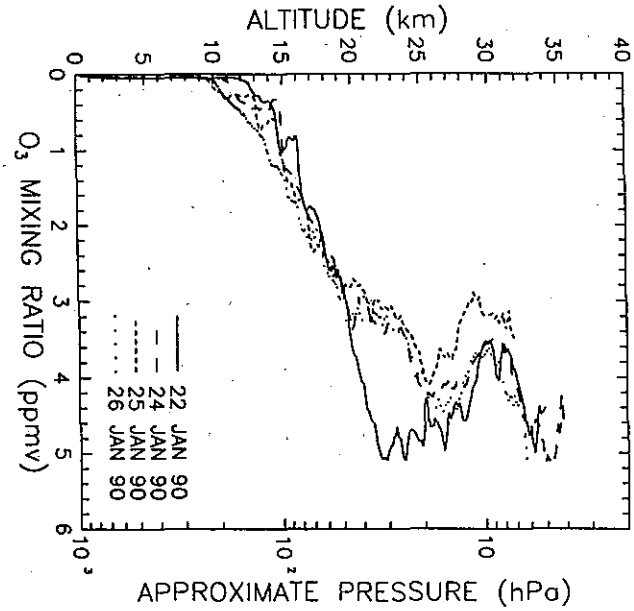

Fig. 5.17. Ozone mixing ratio profiles for four balloon flights from January 22-26, 1990 over Kiruna, Sweden.

Isobaric back trajectories and radon data were used to determine air parcel origins for a study of CH_4 variability at MLO. Scientists from CMDL's Carbon Cycle Group, CSIRO, and ANSTO were co-investigators. Six common flow patterns were determined for the 3-year period July 1987-June 1990 using the cluster analysis method described in *Harris and Kahl* [1990]. Only 1200 UT trajectories were considered to insure free tropospheric sampling conditions during downslope flow. Figure 5.19 shows the six cluster means that represent groups of similar 10-day back trajectories. The percent of trajectories falling in each cluster appears with the cluster number (1-6) 10 days upwind of MLO. To explore the hypothesis that flow patterns (and hence possible source/sink areas) directly affect the CH_4

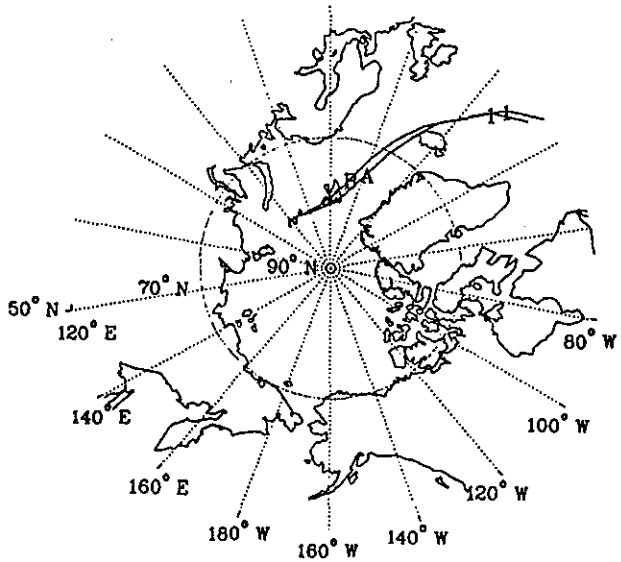

Fig. 5.16. Heiss Island trajectories (500 K) arriving February 20, 1989: A = 0000 UT, B = 1200 UT.

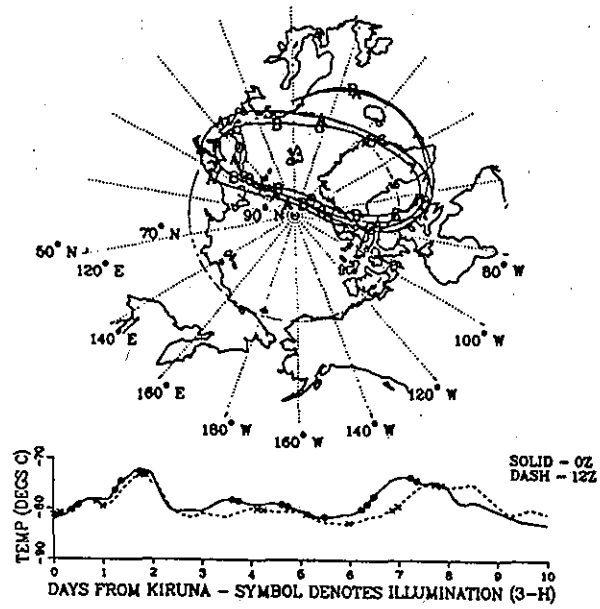

Fig. 5.18. Kiruna isentropic trajectories (550 K) arriving January 26, 1990: A = 0000 UT, B = 1200 UT. The lower plot depicts temperature (°C) along the trajectories. Symbols (o for 0000 UT, x for 1200 UT) denote illumination of the air parcel during the 3-hour time step.

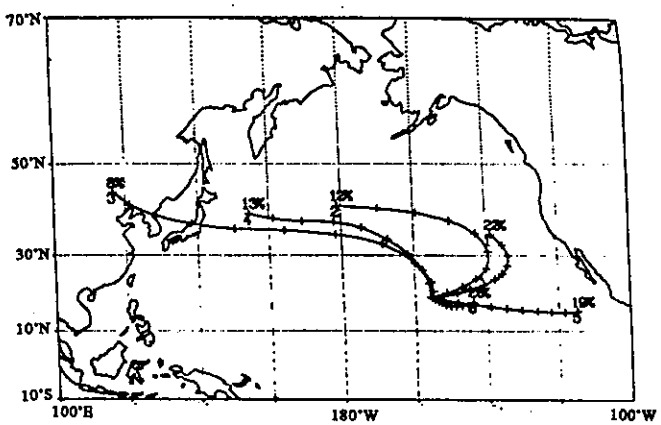

Fig. 5.19. Atmospheric transport regimes for MLO, depicted by cluster mean back trajectories at 700 hPa for the period July 1987-June 1990. Plus signs indicate 1-day upwind intervals. The numbers 10 days upwind of MLO show the percent of complete trajectories occurring in that cluster (top) and an arbitrary cluster number used for identification (bottom).

mixing ratio at MLO, an hourly average (1100-1200 UT) detrended CH_4 value was paired with each trajectory. Figure 5.20 shows the distribution of detrended CH_4 according to the six transport clusters. Note that cluster 3 has a median CH_4 value (1699.5 ppbv) that is 17.2 ppbv higher than that of cluster 5 (1682.3 ppbv). Cluster 3 corresponds to strong westerly flow from Asia where rice cultivation, ruminants, and other CH_4 sources are concentrated [*Fung et al.*, 1991]. Cluster 5 trajectories have 10-day origins mostly in tropical regions of the eastern Pacific. This area is postulated as a

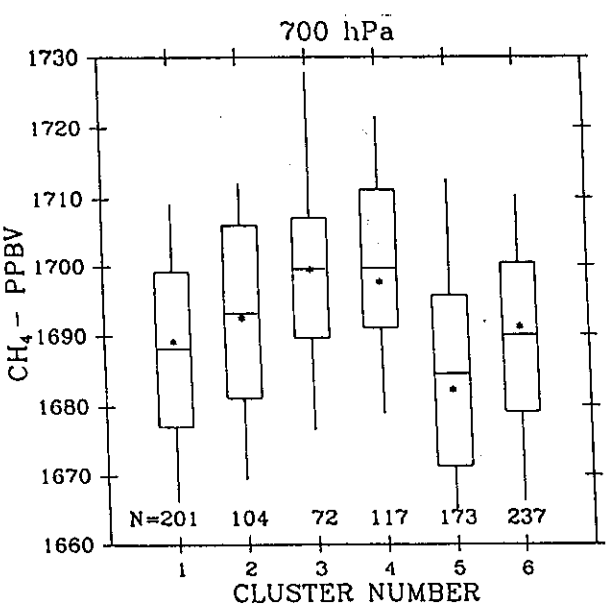

Fig. 5.20. Distribution of detrended CH_4 mixing ratio (ppbv) according to transport cluster. The asterisk is the median; the line across the box is the mean; the bottom and top of the box are the 25th and 75th percentiles; the ends of the whiskers are the 5th and 95th percentiles The cluster number refers to the transport regimes shown in Figure 5.19.

net sink for CH_4 because of the presence of OH radicals [*Spivakovsky et al.*, 1990] and the absence of CH_4 sources. Two factors besides direct transport that could contribute significantly to the difference in CH_4 distribution between clusters 3 and 5 are transport across the CH_4 latitudinal gradient and seasonality of flow patterns.

Case studies compared individual trajectories, radon data (a tracer of continental air), and the MLO CH_4 record. Examination of synoptic scale events in the CH_4 data revealed that transport from the proposed source area was reflected in CH_4 values up to 50 ppbv higher than CH_4 values during flow from the Pacific sink area. Trajectories also provided evidence that transport affects the CH_4 mixing ratio on the seasonal time scale. Figure 5.21 shows cluster means describing MLO transport patterns for (*a*) February and (*b*) August. These plots are excerpted from the 8-year climatology of *Harris and Kahl* [1990]. During winter the changing synoptic situation results in alternation among very different flow types at MLO: strong westerlies, anticyclonic curving flows arriving from the northeast, easterly trades (including southeast flow), and sometimes, southwest flow as seen in a case study for February 1990 (not shown). In addition, the region of highest OH concentration migrates to the south [*Spivakovsky et al.*, 1990], so that MLO is situated on the northern edge of the strong sink area. The changing flow patterns, combined with the influences of the source and sink regions, result in a more variable CH_4 record in winter than in summer (especially July and August).

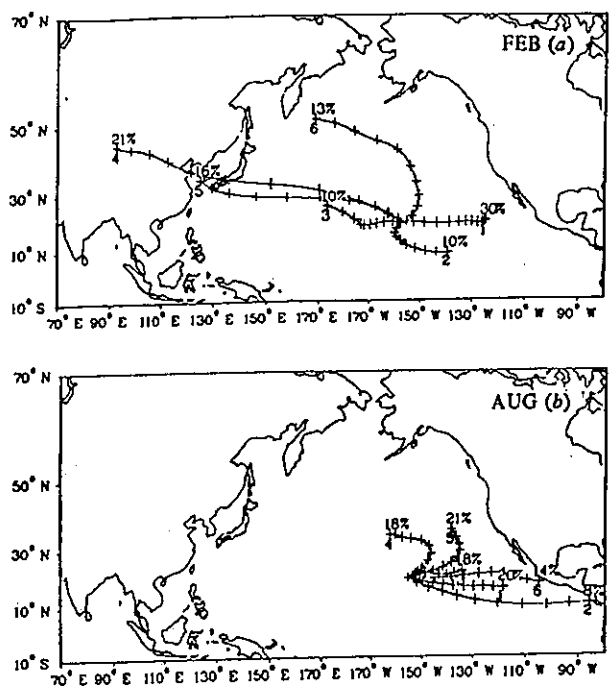

Fig. 5.21. Atmospheric transport regimes for MLO for *a*) February and *b*) August, depicted by cluster-mean back trajectories at 700 hPa for the period 1981-1988. Plus signs indicate 1-day upwind intervals.

Figure 5.21*b* indicates air parcel origins in the sink region and no contact with Asia at a time when CH_4 reaches the lowest levels of the year. Variability in the CH_4 record is reduced as the flow patterns in summer become more homogeneous and the region of peak OH concentration moves northward, so that MLO is centrally located with respect to the methane sink region. A publication detailing these results is planned for 1991.

5.2. SPECIAL PROJECTS

5.2.1. NEPHELOMETER COMPARISON AT MLO

Introduction

A four-wavelength (4-λ) nephelometer, model 1559B manufactured by MRI, was installed at MLO in January 1974. This instrument operated admirably until the beginning of 1981 when it was sent in for repairs. Because of continuing problems for the next 3 years, the instrument was returned to Boulder to be upgraded with electronics to match that used in the nephelometers at the other three baseline stations. The instrument was put back into operation at MLO in early 1985.

The new electronics allowed better control over the operation of the instrument because it allowed the operator control over instrument cycle times, averaging times, and calibration procedures. However, the instrument retained the same optics. The operation of the original instrument was described in the *Summary Report* for 1974 [*Miller*, 1975] and the operation of the new instrument was described by *Bodhaine* [1982]. An important difference between the two designs is that the original instrument used a geometric averaging technique, and the new design uses an arithmetic averaging process. Because long averaging times (about 1 hour) are necessary to recover an inherently noisy signal during clean conditions, it is expected that the geometric mean may be significantly lower than the arithmetic mean. An additional concern has been that, because of the diurnal effects at MLO, the instrument may not fully settle to the clean background values during the night.

Examination of the MLO σ_{sp} record in Figure 5.2 suggests that the clean values in the winters of 1985-1990 are higher than those in 1974-1980. This could be caused by three possible effects: 1) σ_{sp} at MLO is larger in recent years than it was in the early years of the program; 2) instrument sensitivity is poorer for the new design than in the original instrument; or 3) the geometric averaging performed by the instrument produced lower values during clean conditions in the original design than the arithmetic averaging scheme in the new design.

An experiment was performed at MLO during October 15, 1990-January 16, 1991, to compare the existing 4-λ nephelometer with a new high sensitivity three-wavelength (3-λ) nephelometer [*Bodhaine et al.*, 1991*a*]. Because of its high sensitivity, the 3-λ instrument could be operated at a shorter time constant, thus eliminating the settling-time problem during diurnal events and giving better sensitivity during clean background conditions.

Data

Hourly means for the existing 4-λ nephelometer and the new 3-λ nephelometer (both at 550 nm) for the entire period of the experiment are shown in Figure 5.22. The new instrument (dashed lines) reaches significantly lower values during the clean downslope flow events and occasionally reaches higher values during large upslope events. Figure 5.23 shows the monthly means for October-January (ordinarily the cleanest time of the year) of the 4-λ instrument for the 1974-1981 and 1985-1990 time periods. The values during the earlier time period are lower by a factor of 2-3. Figure 5.24 shows a comparison of monthly means of the new 4-λ and the new 3-λ nephelometer data during the period of the experiment. Figure 5.25 shows the means of 4-λ and 3-λ nephelometer data for October-January for the

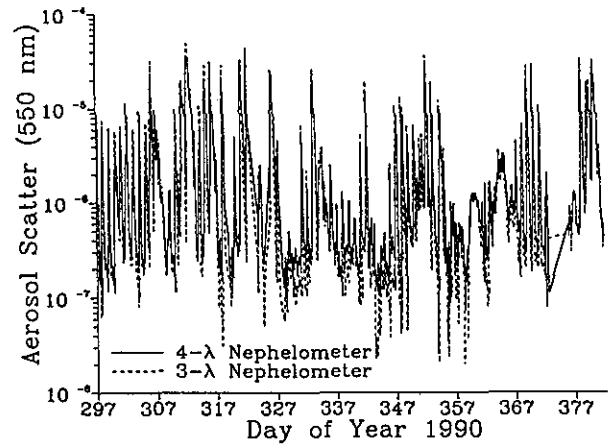

Fig. 5.22. Hourly means of σ_{sp} for the four-wavelength (solid) and three-wavelength nephelometers at MLO during the period October 24, 1990-January 16, 1991 (DOY 297-381).

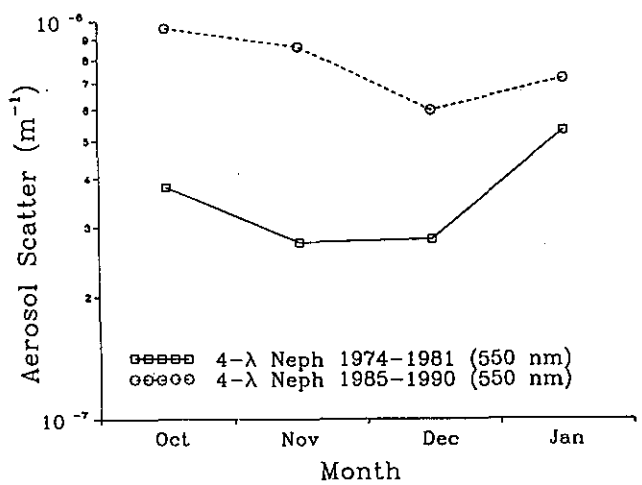

Fig. 5.23. Monthly geometric means of the original 4λ nephelometer data (solid) for 1974-1981, and the modified 4λ nephelometer data (dashed) for 1985-1990 at MLO.

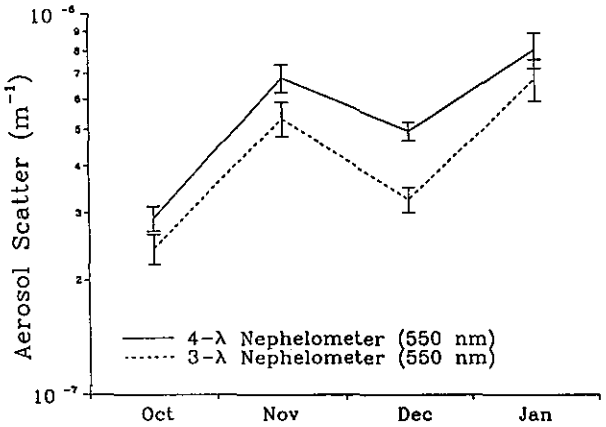

Fig. 5.24. Monthly geometric means of the 4λ and 3λ nephelometer data for the period of the experiment, October 24, 1990-January 16, 1991. The error bars are 1 standard deviation on either side of the mean.

period of the experiment, and the October-January means for the long-term record during 1974-1981 and 1985-1990 (for the two versions of the 4-λ nephelometer). All long-term average data shown here are nighttime data only (1000-1800 UT).

Conclusion

The data presented here show that the existing 4-λ nephelometer is not sensitive enough to measure the background nighttime aerosol at MLO. However, even though the new 3-λ nephelometer is sensitive enough to do the job, it still did not record values during the 1990-1991 period that were as low as those measured during the beginning period of data at MLO (1974-1981). This could be due to the fact that the 3-λ instrument and the existing 4-λ instrument (1985-1990) perform an arithmetic mean, whereas the original 4-λ instrument (1974-1981) performed a

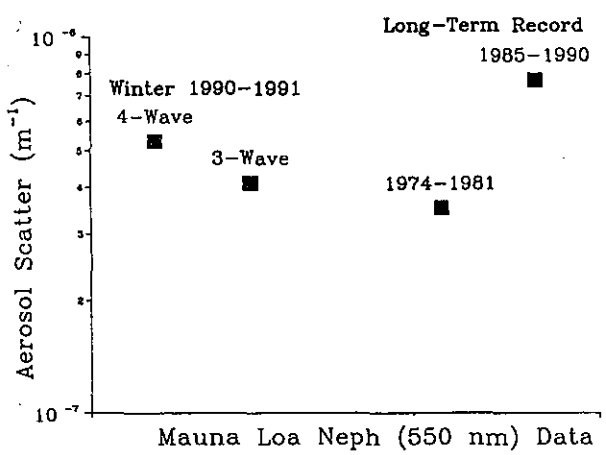

Fig. 5.25. Geometric means of the October-January, 4λ and 3λ nephelometer data during the entire winter 1990-1991 experiment, and the long-term geometric means of the original 4λ nephelometer data (1974-1981) and the modified 4-λ nephelometer data (1985-1990).

geometric mean. Or, it is possible that the actual background scattering coefficient at MLO has increased by about 10% since the beginning of the record. This is seen as the difference between the "3-Wave" point and the "1974-1981" point in Figure 5.25.

5.2.2. FRONT RANGE LIDAR, AIRCRAFT, AND BALLOON EXPERIMENT

Introduction

The first FRLAB experiment was conducted on July 26, 1989, and the second was conducted on May 23-24, 1990. For these experiments, NOAA's CMDL and ARL scientists flew the NOAA King Air aircraft instrumented with a CN counter, a three-wavelength nephelometer operating at 449, 536, and 690 nm, and an aethalometer; NOAA's WPL scientists operated CO_2 (10.59 μm) and ruby (694.3 μm) lidars; and the University of Wyoming scientists flew a balloon carrying a two-wavelength backscattersonde capable of operating at 480, 700, or 940 nm. Results of the two experiments were presented by *Bodhaine et al.* [1990, 1991*b*].

Logistics

Because of the occurrence of high cirrus clouds, the ruby lidar was used to test the atmosphere until clear conditions were observed. Test shots began at about 2100 LDT on the night of each flight and continued at 30-minute intervals until satisfactory conditions were obtained (usually at about midnight when the high cirrus clouds dissipated). Regular shots by both lidars commenced at this time.

The NOAA King Air aircraft, which was standing by at the Jefferson County Airport (just south of Boulder), took off at just after midnight on all 3 days, and the balloon carrying the backscattersonde was launched from the Marshall field site at about the same time.

Lidars

The CO_2 lidar operates primarily at a wavelength of 10.59 μm, has a 0.3-m aperture, and typically transmits 10 pulses s^{-1}, averaging 1000 pulses to compute backscattering profiles. However, it is grating-tunable and can be made to operate at other nearby wavelengths. For FRLAB we took data at three wavelengths: 10.59, 9.57, and 9.28 μm. Signals at these wavelengths arise solely from particulates and are much weaker than signals at the ruby wavelength (694.3 μm); hence coherent detection is employed, and the retrieved profiles are referenced to internally generated shot noise and a hard-target calibration. The CO_2 lidar can also measure the Doppler shift of the backscattered energy and, therefore, the radial component of the wind. By scanning its beam in a vertically oriented conical pattern, it can determine the horizontal wind profiles averaged over the diameter of the cone at the altitude in question.

The WPL systems were located near the intersection of Broadway Avenue and Baseline Street in Boulder (39.991-1°N, 105.2594°W, 1.677 km), and data were acquired nearly simultaneously. The CO_2 and ruby lidar profiles obtained on May 23, 1990, are shown in Figure 5.26. The boundary

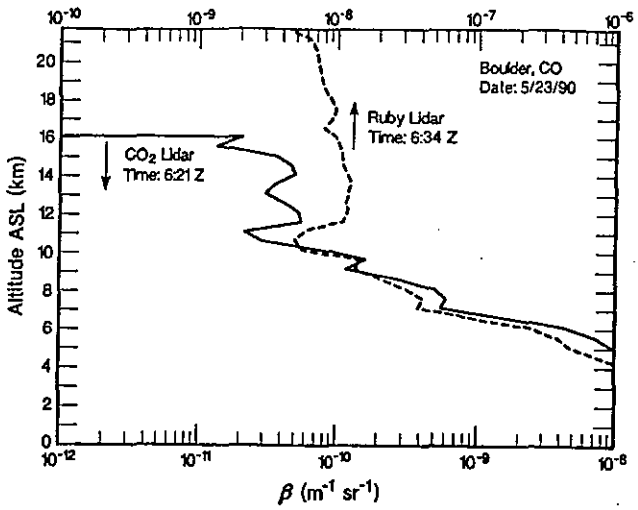

Fig. 5.26. Backscatter profile at 10.59 μm for the May 23, 1990, balloon flight (lower scale) with 0.5-km range averaging and 0.5-km vertical spacing. Also shown is the concurrent ruby lidar backscatter profile (upper scale) at the same 0.5-km spacing and resolution.

layer extends to about 6 km, where a small relatively clean region appears; the backscatter signal then decreases until about 12-km altitude, the region of the tropopause.

Aircraft

The NOAA King Air research aircraft (Beechcraft C-90) was used to measure meteorological parameters, aerosol concentration, size distribution, and scattering coefficient of atmospheric aerosols during FRLAB [*Wellman et al.*, 1989]. A LORAN system is installed aboard the aircraft for determination of aircraft position.

Data from all instruments are digitized using an aircraft data acquisition system (Science Engineering Associates, Model M200) and are recorded on a 40-MB tape drive. Data are sampled every 0.5 seconds and recorded to a tape cartridge. Most aspects of the Model M200 data acquisition system are controlled by user-modifiable text tables. These user tables control acquisition, computation, display, and storage of measured data.

Aerosol measurements were performed using an ASASP-100X, FSSP-100, CN counter, three-wavelength nephelometer, and an aethalometer. The aethalometer has been described by *Hansen and Rosen* [1984]. Figures 5.27 and 5.28 show the temperature and humidity profiles for May 23, 1990. The σ_{sp} profile for May 23, 1990, is shown in Figure 5.29; note the boundary layer extending up to the 500-mb level and the clean region between 500 and 550 mb.

Balloon

The backscattersonde is a balloonborne instrument that measures the amount of light backscattered from a xenon flash lamp triggered about once every 7 seconds. The sensitive volume is on the order of 1 m^3 within a few meters of the balloonborne package. The instrument is sufficiently sensitive to measure the scattering at 30-km altitude with a

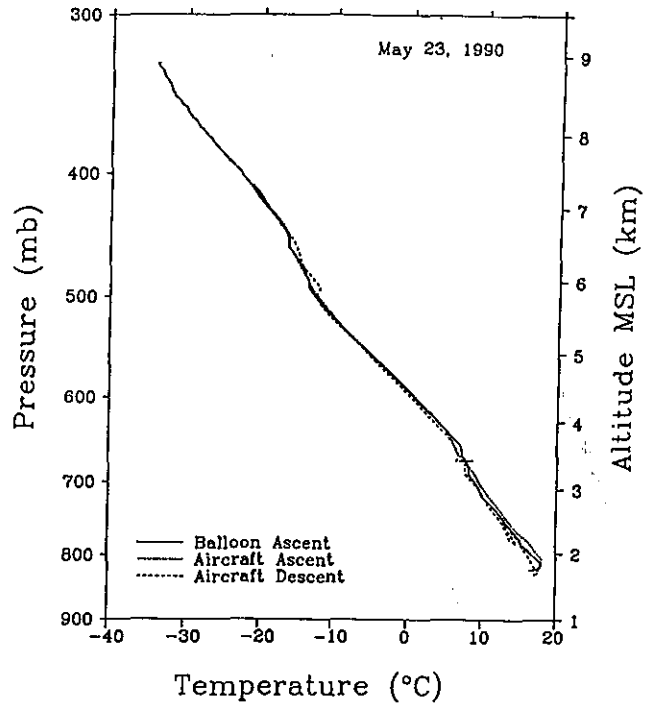

Fig. 5.27. Balloonborne and aircraft measurements of temperature on May 23, 1990.

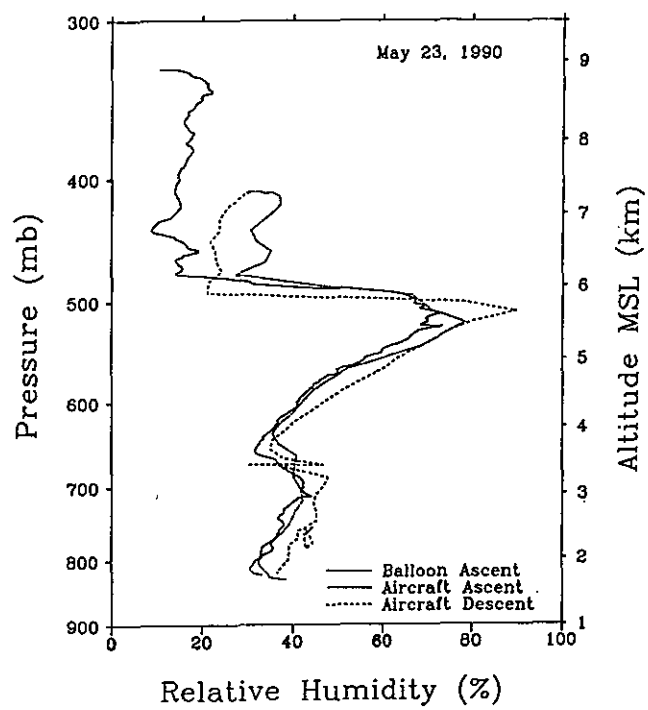

Fig. 5.28. Balloonborne and aircraft measurements of relative humidity on May 23, 1990. Aircraft relative humidity was calculated using the Goff-Gratch relations given by *List* [1949].

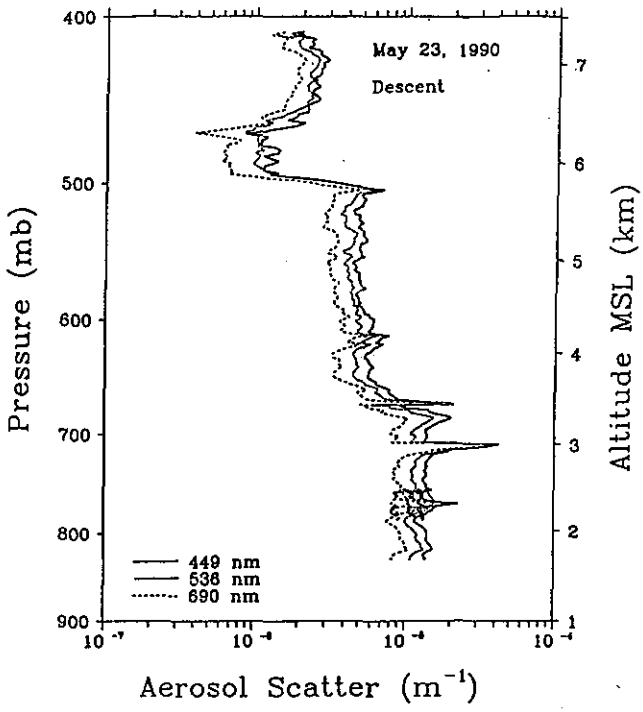

Fig. 5.29. Aircraft descent measurements of aerosol scattering extinction at 449, 536, and 690 nm on May 23, 1990.

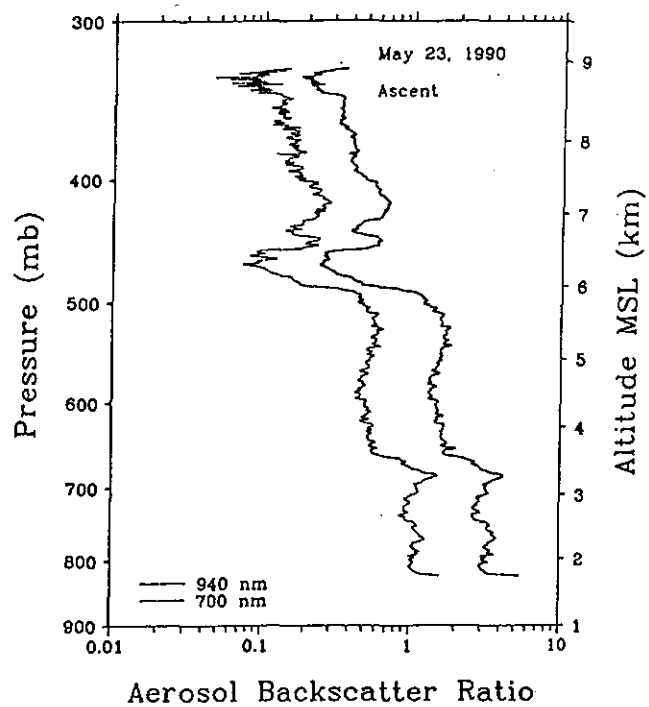

Fig. 5.30. Balloonborne measurements up to 300 mb of aerosol backscatter ratio, aerosol/Rayleigh, at 940 and 700 nm on May 23, 1990.

signal-to-noise ratio of about 50-1. The data product is similar to that produced by a typical lidar system. Standard meteorological parameters are also measured in a sounding including pressure, air temperature, and relative humidity. This instrument has been described in detail by *Rosen and Kjome* [1991].

The backscattersonde data profile for May 23, 1990, is shown in Figure 5.30; the boundary layer below 500 mb and the clean region between 500 and 550 mb appear as seen similarly in the lidar and aircraft data.

Conclusion

Lidar profiles obtained routinely are difficult to calibrate because the return signal is the sum of both aerosol and molecular backscatter, and it is difficult to assign an absolute value to a point on the profile. A common calibration method involves locating the cleanest region of the profile and then assigning an aerosol backscatter value, usually zero or some small, climatologically obtained value. Furthermore, in the absence of a simultaneous radiosonde ascent, a standard atmosphere must be assumed in order to estimate molecular scatter. The FRLAB experiment was designed to perform absolute aerosol scattering measurements in conjunction with lidar measurements in order to characterize a calibration for lidar data.

The ASASP and FSSP probes provided aerosol size distribution data that could be used to calculate aerosol backscatter. The nephelometer measured the aerosol scattering properties directly, allowing an estimate of backscatter. Finally, the backscattersonde measured the aerosol scatter directly in a manner similar to the lidar; however, the sonde also measures temperature and pressure, allowing a more accurate estimate of air density and molecular scatter. Work is presently in progress to accurately characterize the lidar profiles using data from this experiment.

5.2.3. First Ground-Based Intercomparison of SBUV-2, S/N-2, and Dobson Spectrophotometer 83

In early April 1990, comparison total ozone and ozone vertical distribution (Umkehr) observations were made for the first time with Dobson spectrophotometer 83 and with satellite ozone spectrometer SBUV-2, S/N-2 operated at ground level [*Komhyr et al.*, 1990; *Heath and Komhyr*, 1991]. The work was conducted at CMDL in Boulder and at the research and instrument manufacturing facility of the Ball Aerospace System Division located 3 km east of Boulder. The SBUV-2, S/N-2 instrument, built by Ball Aerospace Systems Division, is scheduled for launch in November 1991 aboard the NOAA-13 satellite. It is one of a series of SBUV-2 instruments being flown on the TIROS-N series of NOAA satellites. Two satellites of the series, NOAA-9 carrying SBUV-2 S/N-1 and NOAA-11 carrying SBUV-2 S/N-4, were launched in October 1984 and October 1989, respectively.

Comparison total ozone observations were made with Dobson spectrophotometer 83 and with the ground-based SBUV-2, S/N-2 satellite ozone instrument on April 7 between 8:22 and 11:40 MST. Observations with both instruments were made on standard A and D Dobson instrument wavelengths. Effective ozone absorption coefficients from the two instruments used in processing the observational data were based on the laboratory measurements of *Bass and Paur* [1985].

Total ozone amounts obtained with Dobson spectrophotometer 83 and with ground-based SBUV-2, S/N-2 satellite ozone instrument agreed in the mean to 0.8%, but exhibited an air mass dependency (Figure 5.31) with the SBUV-2 measuring 1.5% more ozone at an air mass of 1.95, but 2.8% less ozone at an air mass of 1.2. The reason for this discrepancy in results is not known. TOMS overpass data over Boulder April 7 agreed with Dobson instrument 83 data to within about 0.5%. This agreement is better than that which has been observed during similar observations made in the past at MLO (where TOMS ozone values were on average about 4% higher than Dobson instrument 83 values), but falls within the variability of the MLO comparison data. The NOAA-11 SBUV-2 satellite ozone instrument measured 1.4% more ozone over Boulder on April 7 than did Dobson instrument 83.

Comparison Umkehr observations were made April 4, 1990, in Boulder with Dobson spectrophotometer 83 and with ground-based SBUV-2, S/N-2 operated at Dobson instrument wavelengths. Inversions of the C-wavelength observational data for both instruments to obtain ozone vertical distributions in Umkehr layers 1-9 were performed by C. L. Mateer (Scarborough, Ontario, Canada) who recently devised an improved data reduction algorithm.

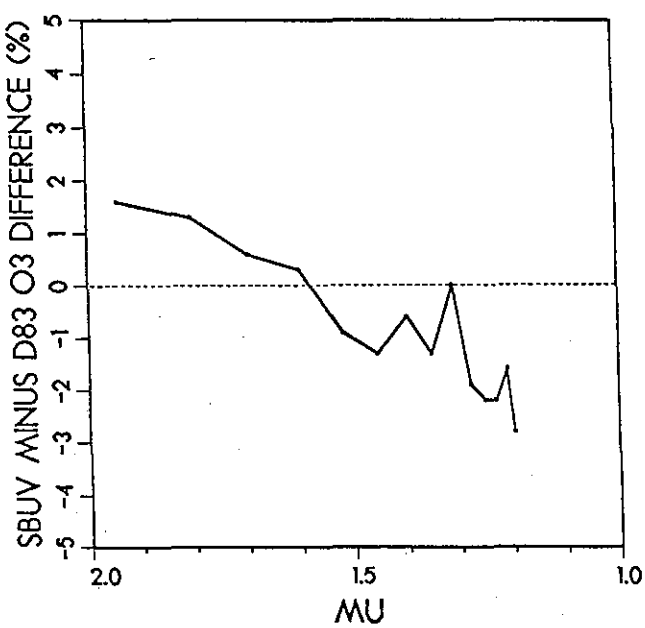

Fig. 5.31. Total ozone differences measured April 7, 1990, in Boulder, Colorado, with Dobson spectrophotometer 83 and ground-based satellite ozone instrument SBUV-2, S/N-2.

Results in Umkehr layers 3-9 agreed to within ±7%, with an agreement of 1.1% in the region of ozone maximum (Umkehr layer 4). A skewness in the comparison data was evident, however, with the SBUV-2 ozone values somewhat larger at the higher altitudes and smaller at the lower altitudes than Dobson instrument 83 data. Agreement was poor in Umkehr layers 1 and 2 where the sensitivity of the Umkehr method to ozone is poor.

5.2.4. Stratospheric Water Vapor Measurements in the Polar Regions

Measurements to investigate the role of PSCs in ozone depletion were carried out as part of two cooperative programs. At Alert, Northwest Territories, Canada, and at SPO, profiles were obtained as part of a joint effort with the University of Wyoming [*Komhyr and Rosson*, 1990]. At McMurdo, Antarctica, two profiles were obtained in September and October in a collaborative effort also with the University of Wyoming.

At Alert the concurrent measurements of water vapor and aerosol backscatter confirmed the formation of PSCs in the Arctic polar vortex at temperatures warmer than the frost point of water. This result shows that the particles are not water ice crystals but $HNO_3 \cdot 3H_2O$ [*Rosen et al.*, 1989, 1990]. Because of the lack of ice crystal formation, there appears to be little dehydration in the Arctic vortex associated with the formation of PSCs. This is consistent with aircraft-based measurements in other parts of the Arctic [*Fahey et al.*, 1990].

In Antarctica several stratospheric water vapor profiles were obtained in the period from May to November (Figure 5.32). In May and June mixing ratios are still relatively high with a dryer region centered about 13 km. These profiles are similar to what is seen in the spring at Boulder but with slightly higher average mixing ratios. During May frost-point temperatures in the region above 10 km are 5°-10°C cooler than the ambient temperature so that the stratosphere is not close to saturation at any point. Although water vapor mixing ratios by June are nearly identical to those in May, the stratosphere has cooled greatly and saturated conditions prevail from 16-22 km. By August (a flight in July was not successful) the stratosphere from 11-22 km is -80°C or colder, reaching -90°C at 20 km. Saturated conditions prevail throughout the stratosphere to about 20 km. Throughout the winter the decrease in water vapor closely follows the drop in temperatures. Backscatter sonde profiles in July and August [*Rosen et al.*, 1991] show that during July there were extensive PSCs in the region of temperatures below -80°C at altitudes between 15-20 km. By late August the PSCs were primarily in the region below 15 km and the strong backscatter signal extends well into the troposphere suggesting that the particles are precipitating out of the stratosphere into the troposphere. The saturated conditions of the troposphere appear to prevent these particles from evaporating.

By October, stratospheric temperatures have warmed considerably with no regions colder than about -75°C but the

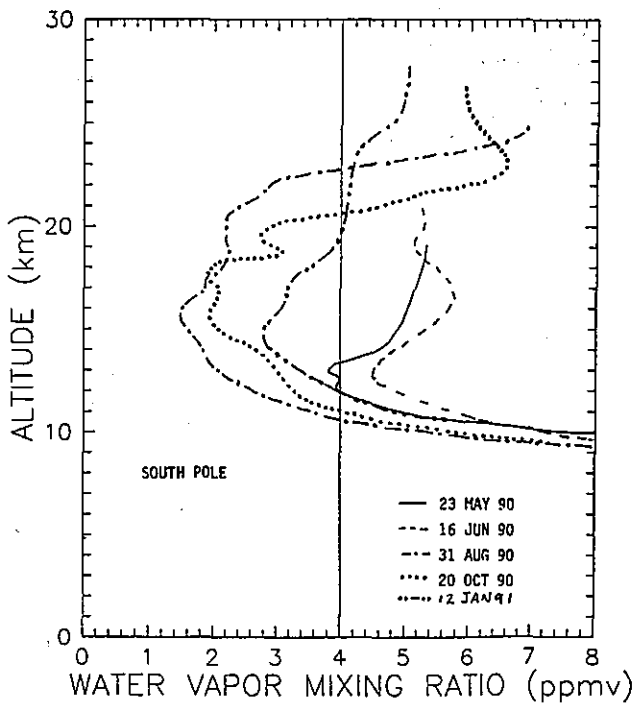

Fig. 5.32. Water vapor mixing ratio (ppmv) profiles in the stratosphere over SPO from five balloonborne frost-point hygrometer flights.

stratosphere remains extensively dehydrated (Figure 5.32) with much of the region between 11-20 km as dry as in August. By November temperatures above 15 km had warmed by 10°C, but the stratospheric water vapor content is essentially unchanged from October. This suggests that even in November the antarctic vortex continues to retain the material and prevents the rapid exchange of air from outside the vortex at these altitudes. Also in November (and even October) temperatures appear too warm to allow continuing water vapor removal.

A mid-austral summer (January) profile (Figure 5.32) shows drier conditions above 20 km than during the winter but somewhat wetter values between 10-20 km. In January conditions above 12 km are still drier than at the beginning of the winter (May-June). Evidently significant rehydration takes place from January to May.

The two profiles obtained at McMurdo about 2 weeks apart in September and October show that the strong dehydration of the stratosphere seen at SPO extends to much of Antarctica. During the 2 weeks between the profiles, the boundary of the vortex pushed south of McMurdo [*Hofmann et al.*, 1991] and then moved north once again before the flight of October 1.

5.3. References

Angell, J.K., Influence of equatorial QBO and SST on polar total ozone and the 1990 Antarctic ozone hole, *Geophy. Res. Lett., 17*, 1569-1572, 1990

Bass, A.M., and R.J. Paur, The ultraviolet cross-sections of ozone: 1. The measurements, in *Atmospheric Ozone*, edited by C.S. Zerefos and A. Ghazi, pp. 606-610 D. Reidel, Dordrecht, Holland, 1985.

Bodhaine, B.A., The GMCC four-wavelength nephelometer, in *Light Absorption by Aerosol Particles*, H.E. Gerber and E.E. Hindman, (Eds.), Spectrum, Hampton, VA, 149-168, 1982.

Bodhaine, B.A., Barrow surface aerosol: 1976-1986, *Atmos. Environ., 23*, 2357-2369, 1989.

Bodhaine, B.A., and J.J. DeLuisi, An aerosol climatology of Samoa, *J. Atmos. Chem., 3*, 107-122, 1985.

Bodhaine B.A., and M.K. Shanahan, Condensation nucleus and aerosol scattering extinction measurements at the South Pole Observatory: 1979-1988, *NOAA Data Rep. ERL CMDL-1*, Climate Monitoring and Diagnostics Laboratory, Boulder, CO, 148 pp., 1990.

Bodhaine, B.A., J.J. DeLuisi, J.M. Harris, P. Houmere, and S. Bauman, Aerosol measurements at the South Pole, *Tellus, 38B*, 223-235, 1986.

Bodhaine, B.A., J.J. DeLuisi, J.M. Harris, P. Houmere, and S. Bauman, 1987, PIXE analysis of South Pole aerosol, *Nuclear Instr. Meth., B22*, 241-247, 1987.

Bodhaine, B.A., J.J. DeLuisi, J.F. Boatman, M.J. Post, and J.M. Rosen, The front range lidar, aircraft, and balloon experiment, *NOAA Data Rep. ERL CMDL-2*, Climate Monitoring and Diagnostics Laboratory, Boulder, CO, 27 pp., 1990.

Bodhaine, B.A., N.C. Ahlquist, and R.C. Schnell, Three-wavelength nephelometer suitable for aircraft measurement of background aerosol scattering coefficient, *Atmos. Environ., 25A*, 2267-2276, 1991*a*.

Bodhaine, B.A., J.J. DeLuisi, J.F. Boatman, Y. Kim, D.L. Wellman, R.L. Gunter, M.J. Post, R.E. Cupp, T. McNice, J.M. Rosen, P.J. Sheridan, R.C. Schnell, D.M. Garvey, A.E. Wade, and R.G. Steinhoff, The second front range lidar, aircraft, and balloon experiment, *NOAA Data Rep. ERL CMDL-8*, Climate Monitoring and Diagnostics Laboratory, Boulder, CO, 142 pp., 1991*b*.

Crutzen, P.J., Tropospheric ozone: An overview, in *Tropospheric Ozone*, edited by I.S.A. Isaksen, Reidel, New York, 3-32, 1989.

DeLuisi, J.J., D.U. Longenecker, C.L. Mateer, and D.J. Webbles, An analysis of northern middle-latitude Umkehr measurements corrected for stratospheric aerosols for 1979-1986, *J. Geophys. Res., 94(D7)*, 9837-9846, 1989.

Fahey, D.W., K.K. Kelly, S.R. Kawa, A.F. Tuck, M. Lowenstein, K.R. Chan, and L.E. Heidt, Observations of denitrification in the winter polar stratosphere, *Nature, 344*, 321-324, 1990.

Fung, I., J. John, J. Lerner, E. Matthews, M. Prather, L.P. Steele, and P.J. Fraser, Three-dimensional model synthesis of the global methane cycle, *J. Geophys. Res. 96*, 13,033-13,065, 1991.

Hansen, A.D.A., and H. Rosen, The aethalometer—an instrument for the real-time measurement of optical absorption by aerosol particles, *Sci. Total Environ., 36*, 191-196, 1984.

Harris, J.M., The GMCC atmospheric trajectory program, *NOAA Tech. Memo., ERL ARL-116*, 30 pp., NOAA Environmental Research Laboratories, Boulder, CO, 1982.

Harris, J.M., and B.A. Bodhaine (eds.), *Geophysical Monitoring for Climatic Change, No. 11: Summary Report 1982*, pp. 67-75, NOAA Environmental Research Laboratories, Boulder, CO, 1983.

Harris, J.M., and J.D. Kahl, A descriptive atmospheric transport climatology for the Mauna Loa Observatory using clustered trajectories, *J. Geophys. Res., 95(D9)*, 13,651-13,667, 1990.

Heath, D.F., and W.D. Komhyr, Preliminary ground-based intercomparison of SBUV-2, S/N-2 and world standard Dobson spectrophotometer 83, paper presented at the meeting of the 20th General Assembly of the International Union of Geodesy and Geophysics, Vienna, Austria, August 11-24, 1991.

Hofmann, D.J., and T. Deshler, Evidence from balloon measurements for chemical depletion of stratospheric ozone in the Arctic winter of 1989-90, *Nature, 349*, 30-305, 1991.

Hofmann, D.J., S.J. Oltmans, and T. Deshler, Simultaneous balloonborne measurements of stratospheric water vapor and ozone in the polar regions, *Geophys. Res. Lett., 18*, 1011-1014, 1991.

Komhyr, W.D., Operations handbook-ozone measurements to 40 km, altitude with model 4A electrochemical concentration cell (ECC) ozonesondes (used with 1680-MHz radiosondes), *NOAA Tech. Memo ERL ARL 149*, NOAA Environmental Research Laboratories, Boulder, CO, 49 pp., 1986.

Komhyr, W.D., Electrochemical concentration cells for gas analysis, *Annals de Geophysique, 25*, 203-210, 1969.

Komhyr, W.D., and R.M. Rosson (Eds.), *Climate Monitoring and Diagnostics Laboratory, No. 18; Summary Report 1989*, 141 pp., NOAA Environmental Research Laboratories, Boulder, Colorado, 1990.

Komhyr, W.D., R.D. Grass, and R.K. Leonard, Dobson spectrophotometer 83: A standard for total ozone measurements, 1962-1987, *J. Geophys. Res., 94(D7)*, 9847-9861, 1989.

Komhyr, W.D., S.J. Oltmans, R.D. Grass, and R.K. Leonard, Possible influence of long-term sea surface temperature anomalies in the tropical Pacific on global ozone, *Can. J. Phys., 69*, 1093-1102, 1991.

Komhyr, W.D., R.D. Evans, R.D. Grass, G.L. Koenig, J.A. Lathrop, and D.M. Quincy, Dobson spectrophotometer, ECC ozonesonde, and ground-based NOAA SBUV-2, S/N-2 satellite instrument comparison observations, NOAA Data Report ERL CMDL-6, 17 pp., 1990.

List, R.J., *Smithsonian Meteorological Tables*, Smithsonian Institution Press, Washington, DC, 1949.

Massey, D.M., T.K. Quakenbush, and B.A. Bodhaine, Condensation nuclei and aerosol scattering extinction measurements at Mauna Loa Observatory: 1974-1985, *NOAA Data Rep. ERL ARL-14*, NOAA Air Resources Laboratory, Silver Spring, MD, 174 pp., 1987.

Mateer, C.L., and H.U. Dütsch, *Uniform evaluation of Umkehr observations from the world ozone network: Part I, Proposed standard Umkehr evaluation technique*, National Center for Atmospheric Research, Boulder, CO, 105 pp., 1964.

McPeters, R.D., and W.D. Komhyr, Long-term changes in SBUV/TOMS relative to world primary standard Dobson spectrophotometer 83, *J. Geophys. Res., 96(D2)*, 2987-2993, 1991.

Miller, J.M., (Ed.), *Geophysical Monitoring for Climatic Change, No. 3: Summary Report 1988*, NOAA/ERL Air Resources Laboratory, Boulder, CO, 1975.

Quakenbush, T.K., and B.A. Bodhaine, Surface aerosols at the Barrow GMCC observatory: data from 1976 through 1985, *NOAA Data Rep. ERL ARL-10*, NOAA Air Resources Laboratory, Silver Spring, MD, 1986.

Rosen, J.M., and N.T. Kjome, The backscattersonde: A new instrument for atmospheric aerosol research, *Appl. Opt.*, in press, 1991.

Rosen, J.M., N.T. Kjome, and S.J. Oltmans, Balloonborne observations of backscatter, frostpoint, and ozone in polar stratospheric clouds at the South Pole, *Geophys. Res. Lett., 18*, 171-174, 1991.

Rosen, J.M., N.T. Kjome, and S.J. Oltmans, Observations of backscatter, particle concentration, and frostpoint in north polar vortex stratospheric clouds, *Geophys. Res. Lett., 17*, 1271-1274, 1990.

Rosen, J.M., S.J. Oltmans, and W.F. Evans, Balloonborne observations of PSCs, frostpoint, ozone, and nitric acid in the north polar vortex, *Geophys. Res. Lett., 16*, 791-794, 1989.

Schnell, R.C., S.. Liu, S.J. Oltmans, R.S. Stone, D.J. Hofmann, E.G. Dutton, T. Deshler, W.T. Sturges, J.W. Harder, S.D. Sewell, M. Trainer, and J.M. Harris, Decrease of summer tropospheric ozone concentrations in Antarctica, *Nature, 351*, 726-729, 1991.

Spivakovsky, C.M., R. Yeich, J.A. Logan, S.C. Wofsy, M.B. McElroy, and M.J. Prather, Tropospheric OH in a three-dimensional chemical tracer model: An assessment based on observations of CH_3CCl_3, *J. Atmos. Res., 95*, 18,441-18471, 1990.

Stolarski, R.S., A.J. Krueger, and M.R. Schoeberl, Total ozone trends from TOMS data, in *Atmospheric Ozone*, edited by R.D. Byokov and P. Fabian, 185-188, 1989.

Wellman, D.L., M. Luria, C.C. Van Valin, and J.F. Boatman, The use of an airborne air sampling platform for regional air quality studies, *NOAA Tech. Rep. ERL 437-ARL 10*, Air Resources Laboratory, Boulder, CO, 1989.

World Meteorological Organization, *Report of the International Ozone Trends Panel-1988, Volume 1, Rpt. No. 18*, 441 pp., WMO Global Ozone Research and Monitoring Project, Washington, D.C., 1988.

6. Acquisition and Data Management

G. HERBERT (Editor), M. BIENULIS, AND J. MC CUTCHEON

6.1. CONTINUING PROGRAMS

6.1.1. STATION CLIMATOLOGY

The climatology of surface weather observations at the CMDL observatories is based on hourly-average measurements of the wind direction, wind speed, station pressure, air and dewpoint temperature, and precipitation amount. The 14-year station climatologies are an important record for the interpretation of measured values of aerosols, trace gases, and climatic change. The sensors currently in use were selected not only for high accuracy but also for ruggedness, to minimize failures in the extreme conditions of the polar region (Table 6.1). To the extent that it is practical, WMO siting standards are followed.

Table 6.1 describes the disposition of the sensors as of January 1, 1990. The following changes were made throughout the year: MLO anemometer 782 replaced 931 on DOY 200 only to be replaced again by 931 on DOY 212. Also at MLO, anemometer 883 was replaced by 876 on DOY 200. Later on DOY 230 anemometer 876 was replaced by 782. Thermometer 8805 replaced 8807 on DOY 293. In SMO anemometer 458 replaced 782 on DOY 109. Thermometers 7 and 9 were replaced by 8803 and 8806 respectively on DOY 20. Thermometer 2 was replaced by 8008 on DOY 95. On DOY 109 the new hygrometer was installed, thus dewpoint sensor 1 was replaced by 50. At SPO, anemometer 585 was replaced by 168 on DOY 340.

Barrow

Descriptions of the BRW station and its climate are given in previous *CMDL Summary Reports* [e.g., *DeLuisi*, 1981]. Wind roses of hourly average resultant wind direction and speed are presented in 16 direction classes and 4 speed classes (Figure 6.1). Winds from the "clean-air" sector, north-northeast-southeast directions, occurred 61% of the time as compared to 65% for the 13-year climatology. As was the case in 1989, the distribution of wind by direction for the 1990 wind rose shows a higher percentage of winds from the southwest quadrant (25%) compared to the 13-year climatology (19%). The anomalous southwest winds were recorded during the months January-March. The year's maximum hourly-average wind speed of 24 m s^{-1} occurred on December 18.

New maximum wind speeds were measured during October and December (Table 6.2), and the maximum pressure for April and the minimum in August exceeded the 13-year climatology. The average temperature for 1990 was within 0.5°C of the climatological average of -12.7°C. A record minimum temperature was reported for November. The year's minimum temperature of -42.1°C occurred on February 23, and the maximum of 17.9°C on July 16 ties the record high temperature for July. Unlike 1989 when monthly mean temperatures were above normal for 9 months out of the year, in 1990 the monthly mean temperatures and pressures, as well, were not significantly different from normal.

Instrument heights: wind, 16.7 m; pressure, 9 m (MSL); air and dewpoint temperature, 2.5 m. Wind and temperature instruments are on a tower 25 m northeast of the main building. Precipitation amounts are only valid for the period May-September.

Mauna Loa

In this report the climatology of MLO is regarded as consisting of two distinct regimes because the bimodal

TABLE 6.1. CMDL Meteorological Sensor Deployment 1990

Sensor	BRW		MLO		SMO		SPO	
	Serial No.	Elevation, m	Serial No.	Elevation, m	Serial No.	Elevation, m	Serial No.	Elevation, m
Primary anemometer*	576	16.7	931	8.5	782	13.7	585	12.2
Secondary anemometer*			883	38.5				
Pressure transducer†	2366	9	225	3397	752	30	8	2841
Mercurial barometer	641	9	278	3397	961	30		
Air temperature A‡	8801	2.5	8807	1.7	7	9	703+	2.2
Air temperature B§	8802	15.3	8809	37.8	8	2.3	701+	23.2
Air temperature C‡	8	3.1	46	2.0	2	9.0	835+	2.2
Dewpoint temperature hygrometer**	8	3.1	46	2.0	1	9.0	3720	2.2

*Aerovane, Bendix, Inc., model no. 141, Baltimore, MD.
† Pressure transducer, Rosemount, Inc., model no. 1201F1b, Minneapolis, MN. Heights of all pressure sensors are given with respect to MSL.
‡Linearized thermistors, Yellow Springs Inst. Co., model no. 44212, Yellow Springs, Ohio, except at SPO.
Platinum resistance thermometer, Yellow Springs Inst. Co., model no. RTD-385, Yellow Springs, Ohio
§Thermometer, positioned at the top of the local sampling tower to facilitate an estimation of boundary layer stability.
**Hygrothermometer, Technical Services Laboratory model no. 1063, Fort Walton Beach, FL.

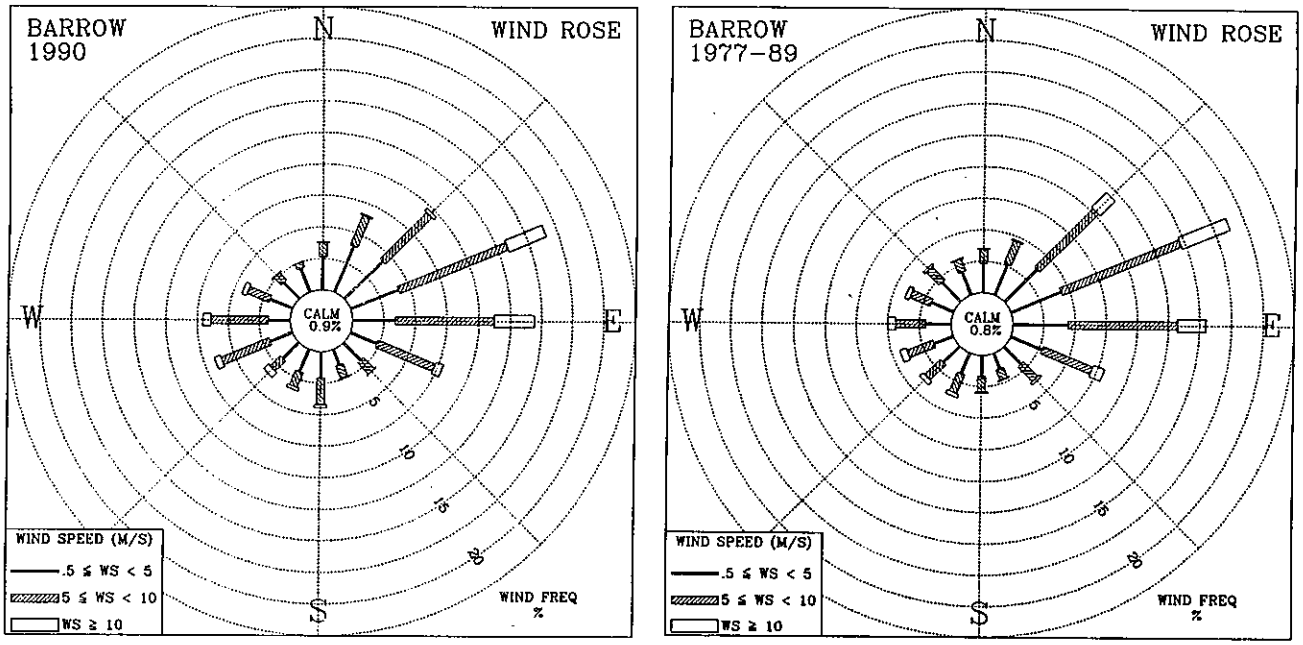

Fig. 6.1. Wind rose of surface winds for BRW for 1990 (left) and 1977-1989 (right).

TABLE 6.2. BRW 1990 Monthly Climate Summary

	Jan.	Feb.	March	April	May	June	July	Aug.	Sept.	Oct.	Nov.	Dec.	1990
Prevailing wind direction	ENE	W	NE	WSW	ESE	E	ENE	E	ENE	ENE	NE	ENE	ENE
Average wind speed (m s^{-1})	5.0	6.2	5.1	6.0	6.1	4.8	5.7	7.7	7.5	7.6	6.4	5.9	6.2
Maximum wind speed* (m s^{-1})	10	15	14	15	13	10	16	18	16	20	17	24	24
Direction of max. wind* (deg.)	69	71	203	107	86	101	236	98	78	63	238	234	234
Average station pressure (hPa)	1017.3	1017.3	1014.9	1018.8	1014.2	1009.8	1013.7	1012.9	1006.9	1007.6	1014.9	1019.7	1013.9
Maximum pressure* (hPa)	1038	1038	1041	1043	1026	1021	1025	1023	1020	1030	1039	1044	1044
Minimum pressure* (hPa)	992	1002	992	999	1003	997	1001	985	988	989	993	1000	985
Average air temperature (°C)	−30.8	−31.4	−24.4	−13.5	−3.6	1.3	4.5	2.3	−0.3	−7.9	−21.7	−26.9	−12.3
Maximum temperature* (°C)	−18	−19	−3	1	4	10	18	11	7	−1	0	−2	18
Minimum temperature* (°C)	−40	−42	−39	−30	−18	−5	−2	−2	−5	−19	−38	−38	−42
Average dewpoint temperature (°C)	−33.6	−34.7	−27.1	−15.4	−4.7	−0.3	2.9	0.8	−2.7	−9.9	−24.1	−29.5	−15.3
Maximum dewpoint temperature (°C)	−19	−21	−3	−1	0	8	15	9	3	−2	−1	−3	15
Minimum dewpoint temperature (°C)	−44	−47	−43	−32	−20	−5	−2	−4	−8	−21	−41	−42	−47
Precipitation (mm)	0	0	0	0	4	14	27	19	9	0	0	0	73

Instrument heights: wind, 16.7 m; pressure, 9 m (MSL); air temperature, 2.5 m; dewpoint temperature, 3.1 m. Wind and temperature instruments are on tower 25 m northeast of the main building.

*Maximum and minimum values are hourly averages.

distribution of the wind direction changes with the time of day. The night (downslope) period (1800-0600 LST) and the day period (0600-1800 LST) define the two regimes. The 13-year night and day wind roses illustrate the two distinct wind patterns (Figure 6.2).

Night regime. The 13-year night wind rose (Figure 6.2) shows that 91% of all winds observed had a southerly component, southsouthwest southsoutheast. The 1990 wind rose (Figure 6.3) shows only a slightly higher percentage of southerly winds (93%) than does the 13-year rose. (Note that the difference appears greater due to the difference in scales.) Storm-related winds (WS ≥ 10 m s^{-1}) with westerly and easterly components are evident in both the 1990 and 13-year night wind rose in equal proportion, 7.5% and 7.1% respectively. The upslope or northerly component winds (northnorthwest-eastnortheast), about 5% of the time, are the results of the daytime, upslope flow extending into the evening hours.

Day regime. The 13-year day wind rose (Figure 6.2) indicates that light wind speeds in the westnorthwest-eastnortheast sector were observed 59% of the time. (Only 48 hours with speeds greater than 10 m s^{-1} were reported from 1977-1989.) This represents the upslope flow attributed to the daytime heating of MLO. The 1990 day wind rose (Figure 6.3) compares well with the 13-year rose, in that northerly wind components prevail 57% of the time. The day wind rose was more uniformly distributed in the light wind classes than that of the night wind rose which was due to the occurrence of variable wind directions during the transition periods of dawn and dusk, most of which were included in this regime. The percent frequency of occurrence of wind in the 10 m s^{-1} or greater wind class was about the same for both periods since it was largely due to storm activity.

The 1990 average day-night temperature difference was 4.3°C, and the average dewpoint depression for 1990 was 5.6°C (Table 6.3). The year's maximum temperature of 18°C occurred on August 8, and the minimum of −5°C that tied the all time low occurred on March 2. The minimum temperatures occurred in conjunction with a severe snow storm when the pressure reached 762 mb equaling the low for the year. In spite of a very dry spring, the precipitation total of 1004 mm was 153% of the 1977-1989 average precipitation. Only 22 mm of precipitation were recorded from March-June.

Samoa

A comparison of SMO's 1990 wind rose (Figure 6.4) with that for the 13-year period shows a slightly higher percentage (65%) of "clean air" sector winds (northnorthwest-southwest) in 1990 than for the 1977-1989 period (58%). (If air passing over the offshore island Aunu'u is to be avoided, the southsoutheast wind sector (26%) cannot be considered in the "clean air" sector.) The peak hourly-average wind speed of 30 m s^{-1} occurred on February 4 during the passage of Typhoon Ofa.

During the encounter with Typhoon Ofa, a number of new station records were established. The anemometer was operational throughout the storm and recorded a peak gust of 46 m s^{-1}. At its minimum, the hourly-average station pressure reached 979 hPa, a new record. A total of 156 mm of

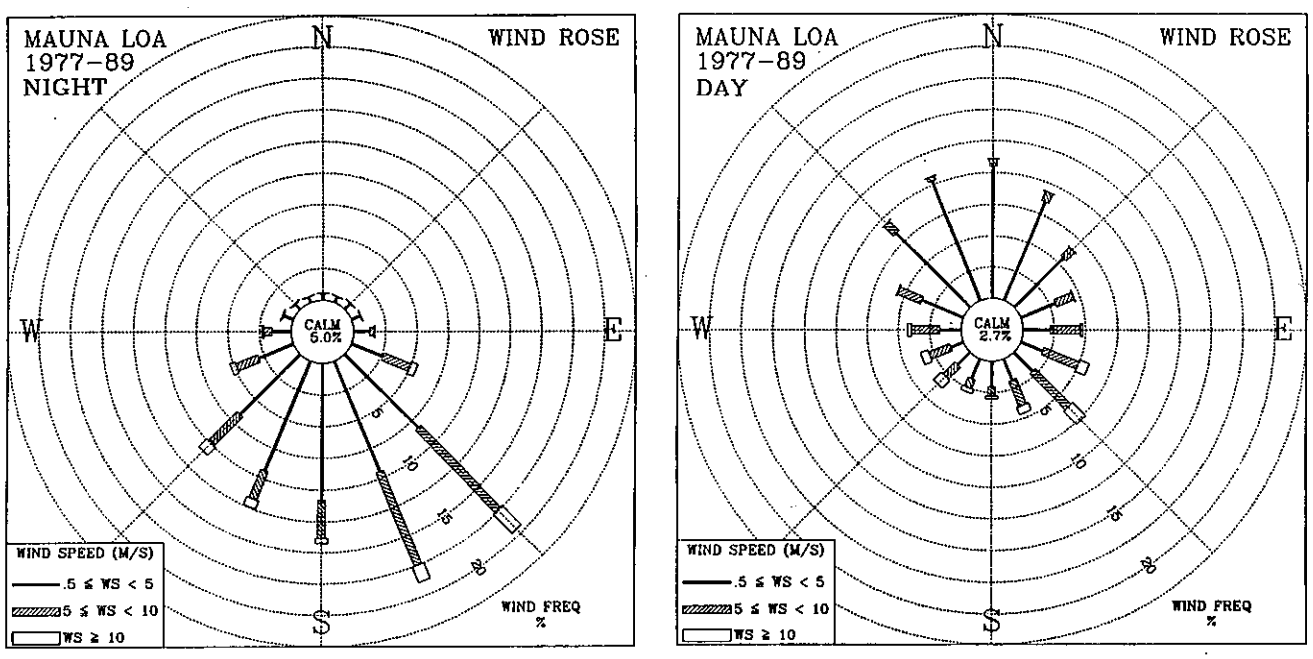

Fig. 6.2. Wind roses of the surface winds for MLO for 1977-1989 night (left) and day (right). The distribution of resultant wind direction and speed are given in units of percent occurrence for the 13-year period. Wind speed is displayed as a function of direction in three speed classes.

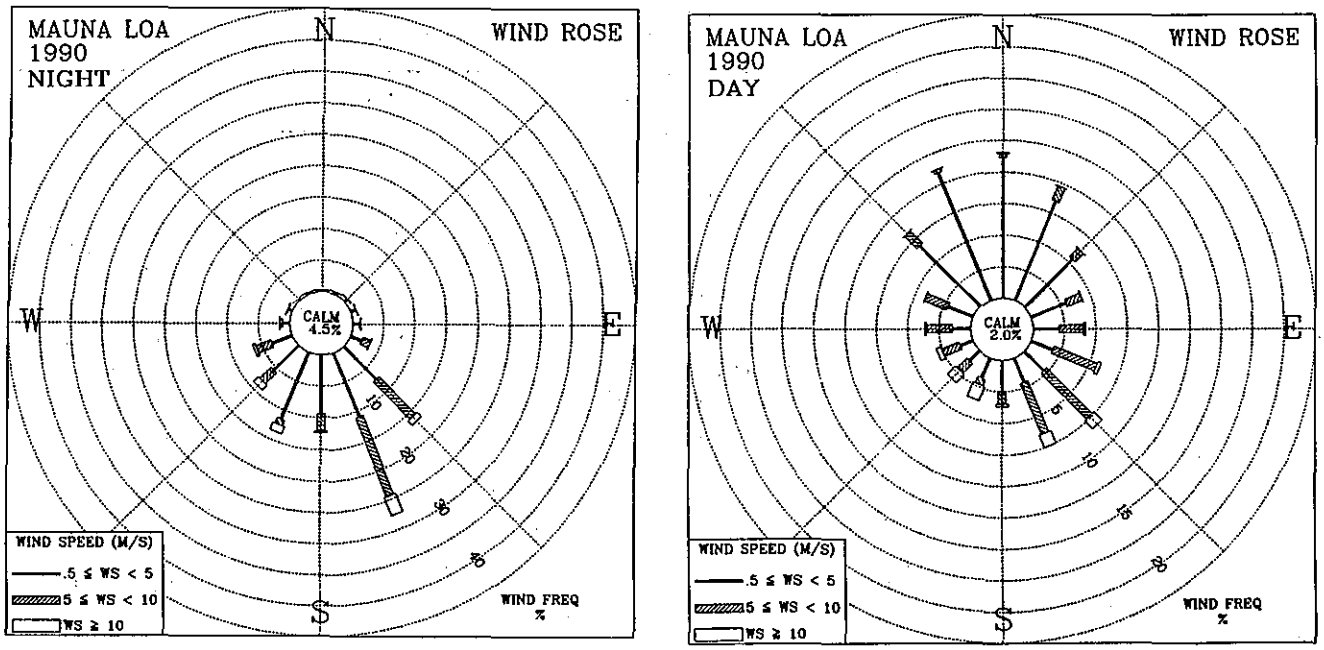

Fig. 6.3. Wind roses of the surface winds for MLO for 1990 Night (left) and Day (right). The distribution of the resultant wind direction and speed are given in units of percent occurrence for the year. Wind speed is displayed as a function of direction in three speed classes.

precipitation was reported for the storm. While considerable damage was done to the facilities, the main sampling platforms remained operational. The solar-powered uninterruptible power supply provided power throughout the storm. The only interruption to the program was the overturning of the rain gauge from which the hourly average precipitation amounts are obtained.

While a new station wind speed record was being set in February, 9 months of the monthly average values were above normal (Table 6.4). The average wind speed for the year was 1.2 m s^{-1} above normal. The average temperature for 1990 of 26.9°C is consistent with the 13-year average of 27.0°C. The average pressure of 1000.8 hPa is 1.5 hPa higher than the 13-year average. The precipitation total for the year measured 2136 mm, which was 96 mm below the 13-year normal.

Instrument heights: wind, 13.7 m; pressure, 30 m (MSL); air temperature, 9 m. Wind and temperature instruments are on Lauagae Ridge, 110 m northeast of the main building. Pressure sensors are in the main building.

South Pole

The distribution of the surface wind direction in 1990 (Figure 6.5) is nearly identical to that of the 13-year pattern with "clean air" sector winds (grid northnorthwest-east-southeast) occurring 93.9% in 1990 compared to the 13-year average of 94.1%. A slightly higher percentage of winds in the greater than 10 m s^{-1} range (6.8%) were observed in 1990 than the long-term average of 4.1%. While wind speeds were only slightly higher for the year (0.5 m s^{-1}), the average for June was 2 m s^{-1} greater than the 13-year average. The maximum hourly-average wind speed was 15 m s^{-1} on June 27.

While the 1990 annual average temperature was within 0.6°C of the 13-year average, the annual average pressure average was 2.6 hPa above normal (Table 6.5). On April 29 a new pressure of 715 hPa was recorded, surpassing the previous record by 8 hPa. Seven monthly average pressures were above normal. The average pressure for the April-July period was 5.7 hPa above normal. Of note, the monthly average pressure for May 1989 was 10 hPa below the May normal. An abnormally warm −29°C was the minimum temperature for December.

6.1.2. Data Management

During 1990 the CAMS operated 97.11% of the time, excluding the time the CO_2 CAMS in SMO was inoperative due to damage by Typhoon Ofa. Including the SMO CO_2 CAMS, which experienced a 23% data loss, the total system operated 87.76% of the year. CAMS gathers data from those sensors that operate continuously at each of the four CMDL observatories. The performance of CAMS was monitored by comparing the number of data files recorded against those expected in the year. In the case of CAMS, there are data file tapes that are regularly recorded 12 or 24 times a day. In the summary table (Table 6.6), the hourly solar radiation file was used to monitor the ASR CAMS. The hourly CO_2 data and calibration files were used for the CO2 CAMS. The count of hourly meteorological data file was used for the meteorology and ozone MO3 CAMS.

TABLE 6.3. MLO 1990 Monthly Climate Summary

	Jan.	Feb.	March	April	May	June	July	Aug.	Sept.	Oct.	Nov.	Dec.	1990
						Night							
Prevailing wind direction	SSE	WSW	SSE	SSE	SSE	SE	SSE	SSE	SSE	SSE	SSE	SSE	SSE
Average wind speed (m s^{-1})	5.9	7.1	5.3	4.3	4.2	5.8	3.9	3.8	3.5	3.5	4.3	6.3	4.8
Maximum wind speed* (m s^{-1})	15	16	13	10	14	13	13	13	10	10	16	16	16
Direction of max. wind* (deg.)	150	206	237	154	151	138	157	145	157	239	204	215	215
Average station pressure (hPa)	678.5	678.2	679.8	680.0	680.5	681.3	681.0	681.6	681.2	681.3	680.0	678.6	680.2
Maximum pressure* (hPa)	683	683	683	684	685	685	684	685	684	684	683	683	685
Minimum pressure* (hPa)	673	672	674	676	678	678	678	679	679	679	676	672	672
Average air temperature (°C)	3.5	2.0	3.4	4.9	5.4	7.2	5.2	6.5	5.8	5.5	5.1	2.8	4.8
Maximum temperature* (°C)	9	8	10	12	11	13	12	14	11	10	9	8	14
Minimum temperature* (°C)	−2	−3	−5	−2	1	2	−1	2	1	2	2	−2	−5
Average dewpoint temperature (°C)	−10.5	−13.4	−10.1	−12.0	−13.4	−13.5	−8.2	−8.0	−5.3	11.2	−1.7	−5.5	−9.6
Maximum dewpoint temperature (°C)	6	4	4	4	6	7	7	7	7	9	8	11	11
Minimum dewpoint temperature (°C)	−32	−30	−25	−26	−29	−28	−35	−30	−21	−27	−19	−26	−35
Precipiation (mm)	0	0	0	0	4	14	27	19	9	0	0	0	73
						Day							
Prevailing wind direction	SE	SW	SSE	NW	NNE	SE	N	NNE	N	NNW	SSE	SSE	SSE
Average wind speed (m s^{-1})	5.4	7.5	4.8	4.3	4.5	5.5	3.7	4.1	3.5	3.4	3.9	6.0	4.7
Maximum wind speed* (m s^{-1})	19	15	16	9	14	14	10	12	9	9	15	17	19
Direction of max. wind* (deg.)	164	230	236	145	151	149	146	155	137	114	201	148	164
Average station pressure (hPa)	678.3	678.2	679.9	680.1	680.7	681.5	681.3	681.6	681.2	681.3	680.0	678.3	680.2
Maximum pressure* (hPa)	683	683	684	684	685	685	684	685	684	684	684	684	685
Minimum pressure* (hPa)	673	672	673	675	678	678	679	679	679	679	675	672	672
Average air temperature (°C)	6.8	5.7	8.2	9.7	10.7	12.3	9.9	11.7	10.0	9.4	8.1	6.1	9.1
Maximum temperature* (°C)	15	13	15	17	16	18	16	18	14	14	13	13	18
Minimum temperature* (°C)	−2	−3	−2	−1	3	4	2	3	3	2	2	−1	−3
Average dewpoint temperature (°C)	−7.6	−9.6	−6.3	−6.1	−5.5	−6.7	−1.8	−2.2	−1.1	−1.5	−2.6	−2.7	−4.0
Maximum dewpoint temperature (°C)	7	6	7	8	7	9	9	9	9	9	10	18	18
Minimum dewpoint temperature (°C)	−31	−28	−25	−29	−28	−22	−32	−26	−23	−25	−17	−24	−32
Precipitation (mm)	146	100	9	3	1	0	21	18	34	17	125	59	533

Instrument heights: wind, 8.5 m; pressure, 3403 m (MSL); air temperature, 1.7 m; dewpoint temperature, 2.0 m. Wind and temperature instruments are on a tower 15 m southwest of the main building.

*Maximum and minimum values are hourly averages.

TABLE 6.4. SMO 1990 Monthly Climate Summary

	Jan.	Feb.	March	April	May	June	July	Aug.	Sept.	Oct.	Nov.	Dec.	1990
Prevailing wind direction	SE	S	SE	SE	SE	SE	S	SE	SSE	SSE	SE	SSE	SE
Average wind speed (m s^{-1})	6.0	7.2	6.7	5.6	6.2	6.9	5.5	6.5	5.5	5.3	6.4	5.8	6.2
Maximum wind speed* (m s^{-1})	14	30	14	13	12	14	12	11	13	15	14	17	30
Direction of max. wind* (deg.)	115	341	322	115	102	121	138	134	136	155	326	116	341
Average station pressure (hPa)	998.8	997.7	1000.2	1001.2	1002.0	1002.1	1002.5	1002.8	1002.7	1002.2	998.4	999.2	1000.8
Maximum pressure* (hPa)	1003	1005	1005	1006	1005	1006	1008	1006	1006	1005	1004	1004	1008
Minimum pressure* (hPa)	992	979	996	998	998	998	996	999	1000	999	992	994	979
Average air temperature (°C)	27.2	26.9	27.1	26.8	27.3	26.8	26.3	26.2	26.8	27.3	27.1	27.3	26.9
Maximum temperature* (°C)	31	31	30	31	32	33	32	30	33	33	31	32	33
Minimum temperature* (°C)	23	23	23	21	23	24	23	23	22	23	23	22	21
Average dewpoint temperature (°C)	23.9	23.3	24.1	24.0	23.6	23.2	21.6	21.5	22.6	23.2	23.6	23.1	23.2
Maximum dewpoint temperature (°C)	25	25	26	26	25	25	24	24	25	27	26	25	27
Minimum dewpoint temperature (°C)	21	20	21	19	20	20	18	16	18	20	20	19	16
Precipitation (mm)	209	318	226	333	50	157	68	37	99	139	266	234	2136

Instrument heights: wind, 13.7 m; pressure, 30 m (MSL); air temperature, 9 m. Wind and temperature instruments are on Lauagae Ridge, 110 m northeast of the main building. Pressure sensors are in the main building.

*Maximum and minimum values are hourly averages.

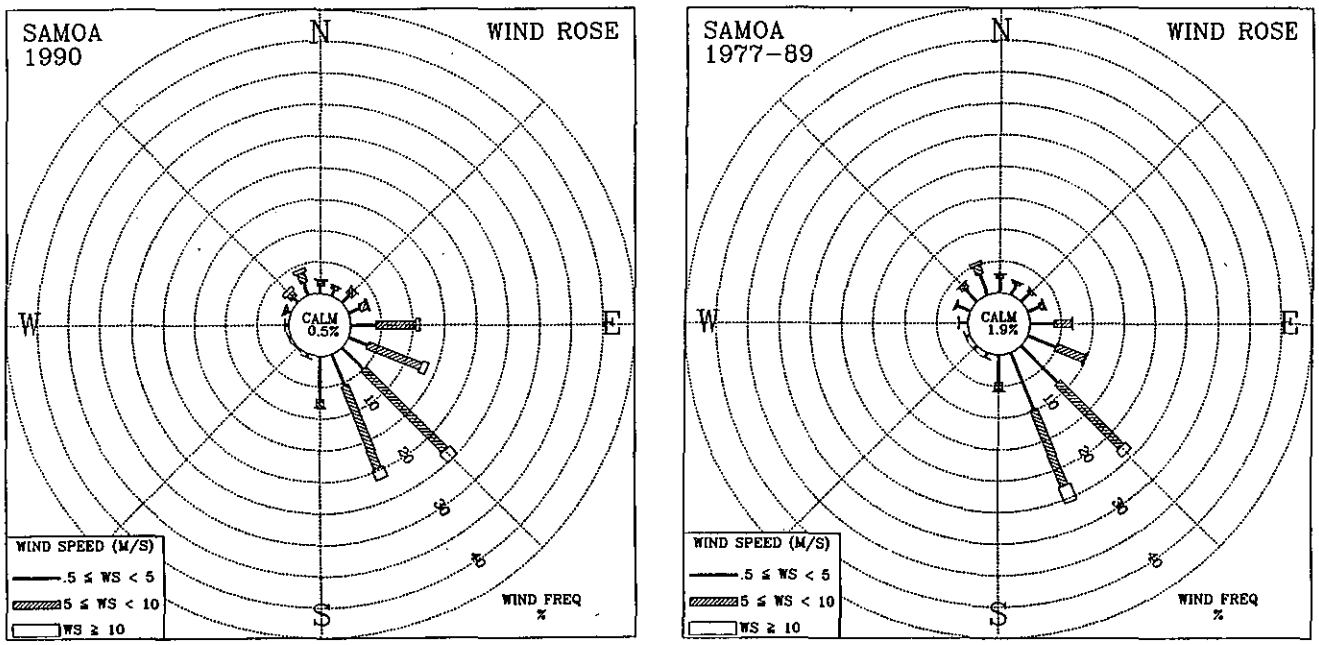

Fig. 6.4. Wind roses of the surface wind for SMO for 1990 (left) and 1977-1989 (right). The distribution of the resultant wind direction and speed are in units of percent occurrence for the year and 13-year period, respectively. Wind speed is displayed as a function of direction in three speed classes.

TABLE 6.5. SPO 1990 Monthly Climate Summary

	Jan.	Feb.	March	April	May	June	July	Aug.	Sept.	Oct.	Nov.	Dec.	1990
Prevailing wind direction	N	ENE	ENE	ENE	E	NNE	NNE	NNE	NNE	N	NNE	N	NNE
Average wind speed (m s^{-1})	4.6	4.8	5.3	5.4	5.0	7.8	6.7	5.9	6.9	6.4	6.4	5.8	5.9
Maximum wind speed* (m s^{-1})	10	9	9	12	10	15	14	13	13	14	13	11	15
Direction of max. wind* (deg.)	330	312	17	13	98	12	13	13	360	3	356	344	12
Average station pressure (hPa)	688.3	681.3	680.6	685.1	684.5	681.2	681.5	674.6	666.7	678.6	685.2	689.1	681.4
Maximum pressure* (hPa)	699	689	691	715	707	695	694	694	688	701	700	699	715
Minimum pressure* (hPa)	677	670	671	668	668	668	658	661	651	662	676	674	651
Average air temperature (°C)	−26.8	−40.6	−57.1	−58.7	−60.6	−55.6	−56.9	−60.9	−58.1	−49.0	−35.4	−23.8	−48.4
Maximum temperature* (°C)	−19	−30	−38	−39	−39	−40	−40	−45	−36	−33	−19	−19	−19
Minimum temperature* (°C)	−35	−49	−70	−74	−71	−69	−75	−74	−76	−64	−51	−29	−76
Average Dewpoint temperature (°C)	−27.7	−42.9	†	†	†	†	†	†	†	†	−38.6	−25.2	−49.3
Maximum dewpoint temperature (°C)	−19	−32	†	†	†	†	†	†	†	†	−25	−20	−19
Minimum dewpoint temperature (°C)	−36	†	†	†	†	†	†	†	†	†	†	−41	−41

Instrument heights: wind, 12.2 m; pressure 2841 m (MSL); air temperature, 2.2 m. The anemometer and thermometer are on a tower 100 m grid east-southeast of CAF. Pressure measurements are made inside CAF.

*Maximum and minimum values are hourly averages.

†Missing data

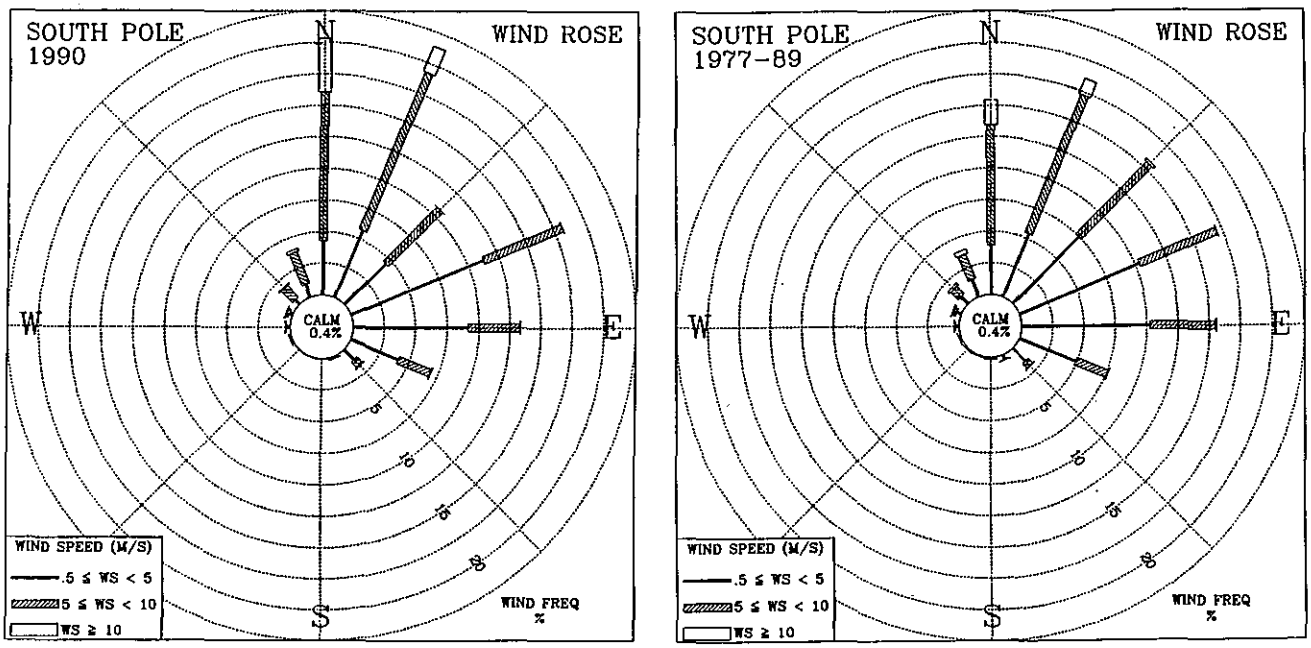

Fig. 6.5. Wind roses of the surface wind for SPO for 1990 (left) and 1977-1989 (right). The distribution of the resultant wind direction and speed are in units of percent occurrence for the year and 12-year period, respectively. Wind speed is displayed as a function of direction in three speed classes.

TABLE 6.6.*a* CMDL CAMS Operations Summary, 1990

Block Type	Description	Expected No. of Blocks 1990	Blocks Recorded and [Blocks Missing]			
			BRW	MLO	SMO	SPO
A	Hourly aerosol data	2190	2170 [20]	2179 [11]	2178 [12]	2157 [33]
B	Secondary aerosol data	2190	1924	2090	0*	2158
H	Daily aerosol data	365	361 [4]	364 [1]	363 [2]	361 [4]
S	Hourly solar radiation data	8760	8681 [79]	8714 [46]	8712 [48]	8634 [126]
T	Daily solar radiation data	365	343 [2]	363 [2]	363 [2]	360 [5]
C	Hourly CO_2 data	8396†	8292 [98]	8316 [58]	6416 [2042]	8260 [11]
D	Daily CO_2 data	365	362 [3]	365 [0]	279 [86]	365 [0]
E	Hourly CO_2 calibration data	364‡	355	343	297	490
F	CO_2 calibration report	52	51	49	41	69
M	Hourly meteorological data	4380	4377 [4]	4369 [11]	4377 [3]	4286 [94]
O	Daily surface ozone data	365	365 [0]	365 [0]	365 [0]	358 [7]
W	Daily meteorological data	365	365 [0]	365 [0]	365 [0]	358 [7]
I	Meteorological calibration	365	365 [0]	364 [1]	365 [0]	357 [8]
N	Surface ozone calibration	52	54	56	56	5

TABLE 6.6.*b* CMDL CAMS Operations Summary, 1990

Individual CAMS	Expected No. of Blocks 1990	Percent Data Capture			
		BRW	MLO	SMO	SPO
ASR	8760	99.10% [79]	99.47% [46]	99.45% [48]	98.56% [126]
CO_2	8760	98.71% [113]	98.85% [101]	76.63% [2047]	99.89% [10]
MO3	4380	99.93% [3]	99.75% [11]	99.93% [3]	97.85% [94]
Total	21900	99.11% [195]	99.28% [158]	90.42% [2098]	98.95% [230]

*Secondary aerosol channels are not used in Samoa
†Nominal block count equal to total hours in year less 52 7-hr calibration periods.
‡Nominal block count equal to 52 7-hr calibration periods.

Due to the remoteness of the observatories, power outages are common occurrences. This has been the case at SPO as the load on the generators has increased to capacity during recent years. If the board that restarts CAMS after power failures is operational, the amount of data loss is confined to the time of the outage. This board failed and was replaced in the ASR and MO3 CAMS at BRW. A memory and clock board were replaced at SMO; a memory board was replaced at SPO. The five boards that failed constitute about 4% of the system's complement.

During 1990, the CAMS data processing software was completely rewritten. The data is now stored on indexed files by block type rather than by the individual CAMS hardware it was recorded on. Data files are smaller and faster to access than before. All CAMS data from previous years (1984-present) were translated to the new file format. All such data are stored on the CMDL/VAX computer.

6.2. Reference

DeLuisi, J.J. (Ed.), *Geophysical Monitoring for Climatic Change, No. 9: Summary Report 1980*, 163 pp., NOAA Environmental Research Laboratories, Boulder, CO, 1981.

7. Nitrous Oxide and Halocarbons Group

W.T. STURGES (Editor), T. BARING, J. BUTLER, J.W. ELKINS, B.D. HALL, R.C. MYERS, S.A. MONTZKA, T.H. SWANSON, AND T.M. THOMPSON

7.1. CONTINUING PROGRAMS

7.1.1. FLASK SAMPLES

Air samples continued to be collected in pairs during 1990 and analyzed for CFC-12, CFC-11, and N_2O concentrations. Samples were collected from the CMDL baseline stations BRW, MLO, SMO, and SPO with the addition of Niwot Ridge (NWR), Colorado (see Section 7.1.2) and Alert, North West Territories (ALT). Higher pressure pumps (3 atm) were deployed at BRW, MLO, and SMO in late February to early March so that sufficient sample volume would be available for both the LEAPS and flask projects. NWR received the pump in July. SPO personnel used the new pump in 1989 and continued its use during 1990. ALT will be upgraded in 1991.

The new automated flask-analysis system was tested extensively throughout the year. Intercomparisons of flask and calibration tank results were made between the new and old GC systems. The two systems gave consistent results with no systematic differences. Routine flask analyses with the new system should begin in 1991.

The time series of monthly mean N_2O concentrations has been extended another year in Figure 7.1. Likewise, updated CFC-12 and CFC-11 data are shown in Figures 7.2 and 7.3.

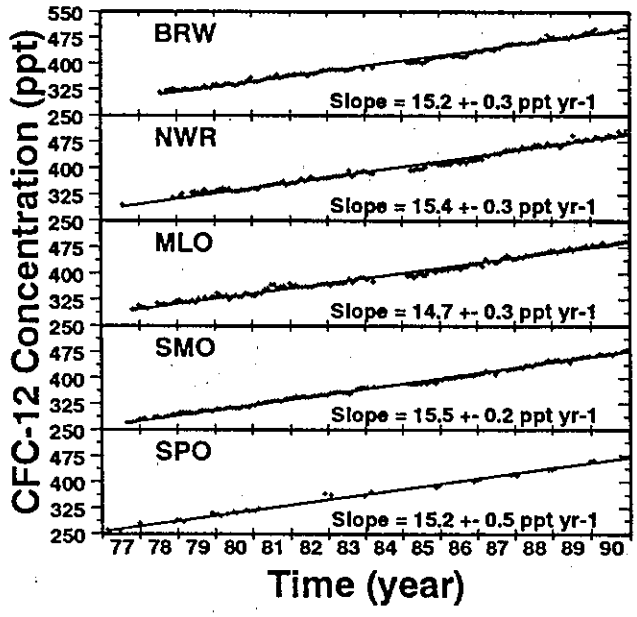

Fig. 7.2. Monthly mean dry concentrations of CFC-12 from the CMDL flask sample network. The trends and 95% confidence intervals are also shown.

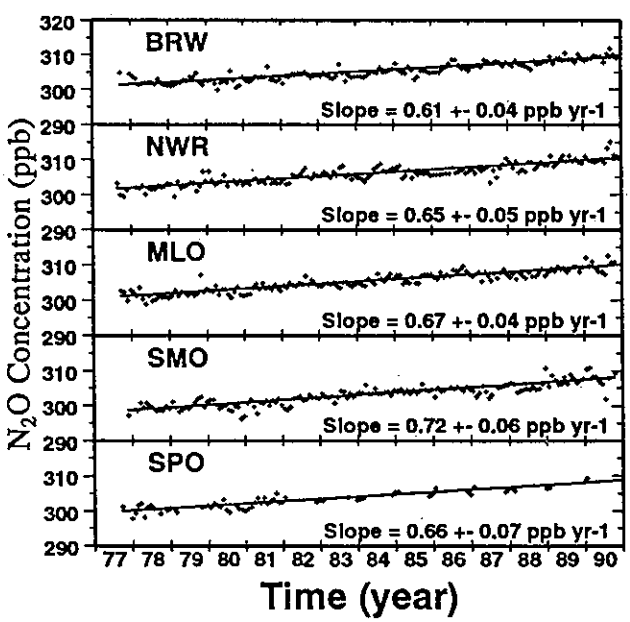

Fig. 7.1. Monthly mean concentrations of N_2O (CO_2 and H_2O corrected) from the CMDL flask sample network. The trends and 95% confidence intervals are also shown.

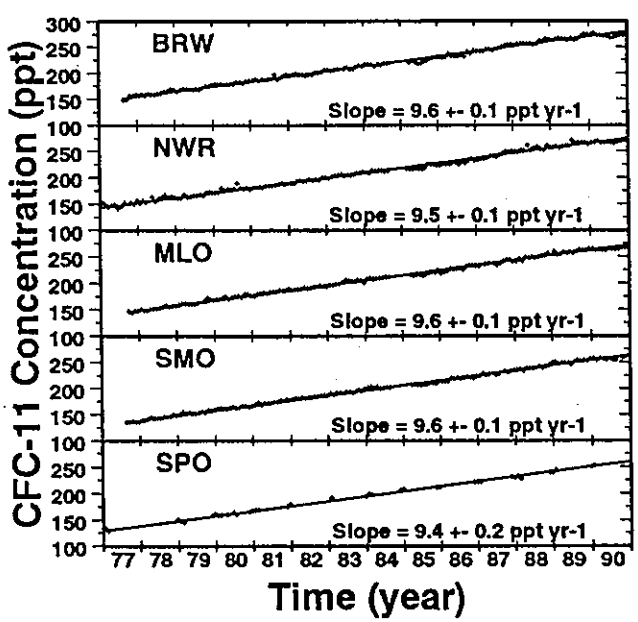

Fig. 7.3. Monthly mean dry concentrations of CFC-11 from the CMDL flask sample network. The trends and 95% confidence intervals are also shown.

ALT flask sample concentrations, which have now been measured for 3 years, are plotted in Figure 7.4. The incidence of inconsistencies between flask pairs decreased considerably at ALT in 1990.

The long record of BRW data has been analyzed for seasonality by removing the trend and fitting a locally weighted spline to the residuals. CFC-12, CFC-11, and N_2O all exhibit the same seasonal cycle (Figure 7.5) with higher concentrations in the November-February period and lowest values during May through August. This is typical of many pollutants measured in the Arctic Basin. A cold stable air mass develops in winter, bounded by the arctic front, with limited loss mechanisms from advection, mixing, deposition and photochemistry. Concentrations grow from periodic injection of polluted air masses originating at midlatitudes.

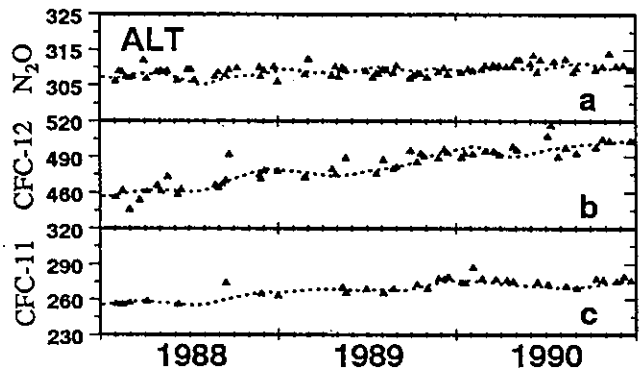

Fig. 7.4. Flask sample concentrations for (*a*) N_2O, (*b*) CFC-12, and (*c*) CFC-11 at Alert, North West Territories. The dashed lines are spline fits to corresponding BRW flask sample data, for comparison.

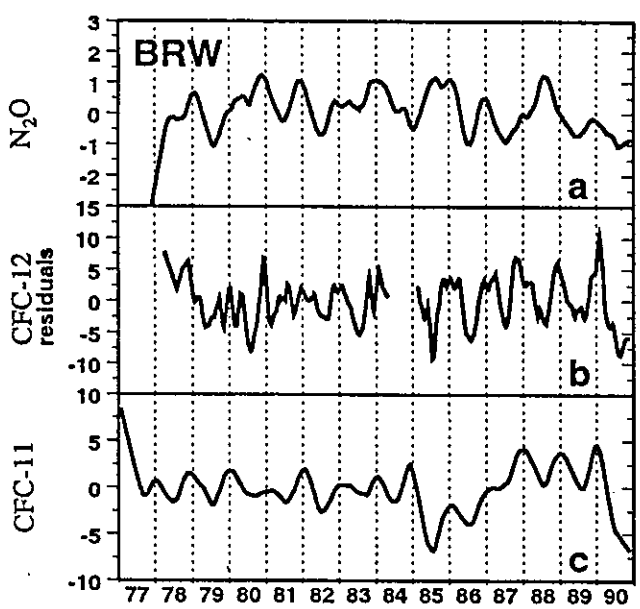

Fig. 7.5. Spline fit showing seasonal variability in the residuals of (*a*) N_2O, (*b*) CFC-12, and (*c*) CFC-11 flask concentrations at BRW.

7.1.2. RITS Continuous Gas Chromatograph Systems at CMDL Baseline Stations

In situ sampling of air continued at BRW, MLO, SMO, and SPO. Twenty-four analyses of N_2O, CFC-12, CFC-11, CFC-113, methyl chloroform and carbon tetrachloride were made every day at each station.

In February a new continuous gas sampling system was brought on line at NWR. The system is a duplicate of the GC systems at BRW, MLO, and SMO. The NWR site provides the group with continuous monitoring of nitrous oxide and halocarbons at the same site used to fill working calibration cylinders. The GC system is located in an air-conditioned unit at site C-1 of the Mountain Research Station, Institute for Arctic and Alpine Research (INSTAAR), University of Colorado. C-1 is located at 40°2′N, 105°32′W and is at an altitude of 2027 meters (9900 feet). NWR is the group's only interior continental site and provides a unique platform to analyze continental air composition. In addition, it provides a field site for testing hardware and software before installation at other, more remote, sites.

In 1990 significant improvements were made to the GC network. During the first quarter the sampling and analysis frequency was increased to once every half hour. This resulted in a significant improvement in precision, due to the decrease in lag time between sample and calibration runs. The increased frequency was achieved by the addition of an eight-port stream selection valve, which permits two air samples to be analyzed per rotation.

An upgrade of the hard drives at the stations from 15 megabytes to 20 megabytes allowed the addition of new software at each station. This included RITSPLOT, a program developed by the group, and installed at the stations in November. RITSPLOT is a complete package of plotting and database management routines written in HP-BASIC. It calculates preliminary concentrations after every air-sample run and updates a database containing 1 month of concentration values. A key feature of RITSPLOT is that it is accessible by station personnel. With a single keystroke they are able to view the previous month's data and assess the system performance. This should prove invaluable in troubleshooting.

Access to RITSPLOT was made via a new version (v. 5.1) of the NOAA data acquisition software installed in 1990. This allows RITSPLOT to be run without affecting the data collection functions of the system computer. It also has improved error handling capabilities and a routine to store preliminary concentration data in IBM-compatible ASCII format on a 720-kilobyte, 3.5-in. floppy disk for easy transfer to the station PCs. Two 1.44-megabyte data diskettes now provide room for 1216 files. Each diskette is filled with raw chromatographic data approximately every 4 days for return to the Boulder office.

To accommodate the increase in raw data received from the stations, consolidation of the processing programs at the Boulder office was implemented. Ten programs were

consolidated into four: (1) catalog and back-up incoming data diskettes; (2) reprocess raw chromatograms for area and height data; (3) calculate concentration values; and (4) plot data for visual quality control applications. The reduced data is stored on the group's UNIX network hard drive where it is available to all the group for statistical analysis.

The 3.5-year record of daily average N_2O concentrations from the in situ GCs at BRW, MLO, and SMO is shown in Figure 7.6. The annual cycle at BRW can be best seen in the 1990 data set, with a maximum in February and a minimum in August. This also illustrates the improvements brought about by the increased precision due to the higher sampling frequency. During 1989-1990 the annual growth rate was approximately 0.6 ppb yr^{-1} at all stations.

Daily average CFC-12 concentrations are shown in Figure 7.7. The annual increase remained at 19 ppt yr^{-1} for all three stations. CFC-11 daily average concentrations for BRW, MLO, and SMO are shown in Figure 7.8. The CFC-11 data confirm the cyclic nature of CFCs at BRW. Again, the improvements in precision in 1990 are evident, particularly at BRW. CFC-11 measurements from SMO before March 1989 were extremely noisy and have not been plotted. Annual growth rates at BRW, MLO, and SMO were about 7.5 ppt yr^{-1}, which is low compared to the flask data. The study period, however, is short, and experimental and calibration errors are still relatively large. A proper intercomparison of the flask and continuous data is, therefore, not possible at this stage.

Daily average carbon tetrachloride (CCl_4) concentrations are shown in Figure 7.9. The concentrations were nearly constant in 1990.

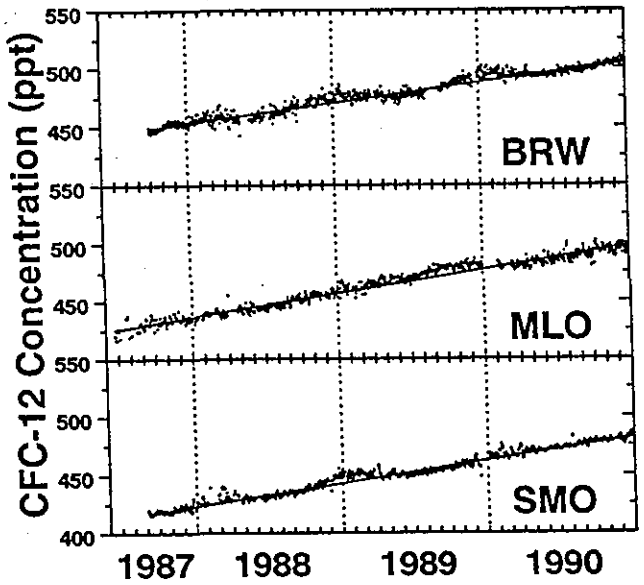

Fig. 7.7. Daily average CFC-12 concentrations at BRW, MLO and SMO obtained from the in situ GCs. The trends were generated using least squares regression analysis.

During 1990 SMO station had a large number of power outages and brownout conditions. The computer equipment that controls the sampling sequence and stores the data was protected by an uninterruptible power supply (UPS). The GCs, because of their high power load, were not protected.

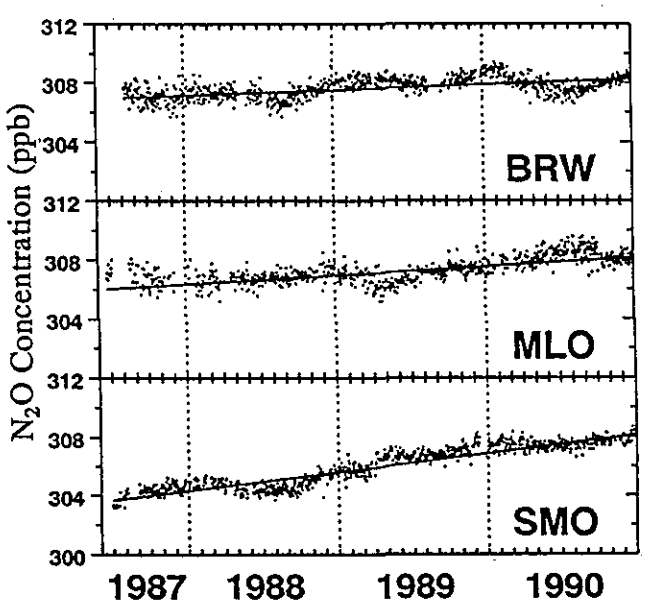

Fig. 7.6. Daily average N_2O concentrations at BRW, MLO and SMO obtained from the in situ GCs. The trends were generated using least squares regression analysis.

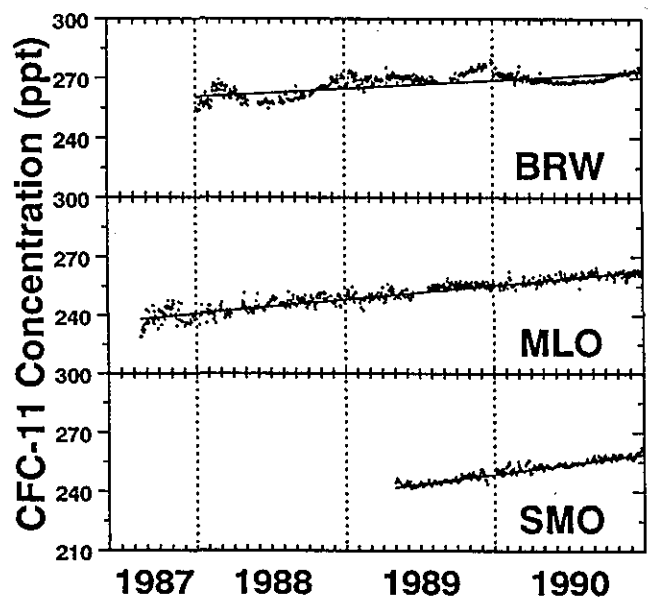

Fig. 7.8. Daily average CFC-11 concentrations at BRW, MLO and SMO obtained from the in situ GCs. The trends were generated using least squares regression analysis.

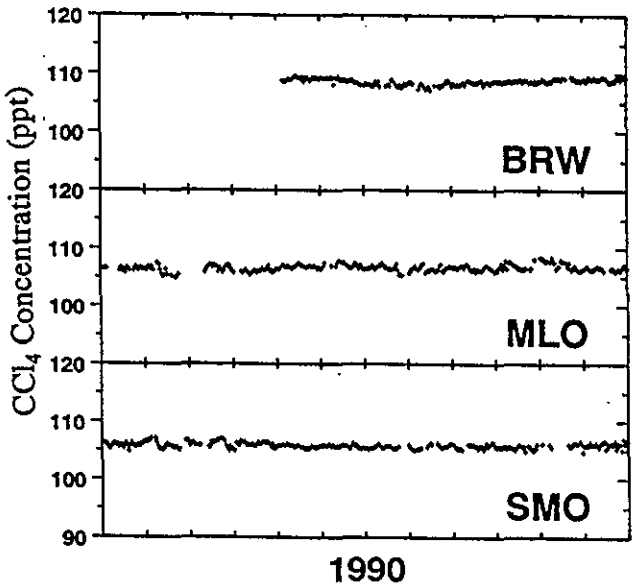

Fig. 7.9. The 1990 daily average carbon tetrachloride (CCl_4) concentrations at BRW, MLO, and SMO obtained from the in situ GCs.

An analysis of the N_2O data shows a diurnal variation (Figure 7.10) that could be due to these variations in line voltage to the GCs. Nine months of data were fitted with a spline to remove trends and seasonality. The residuals were then grouped by hour of the day and the mean and 95% confidence interval calculated. At 0400 GMT (1700 LST), N_2O concentration dropped for a few hours, rose dramatically, then dropped back to normal over the following few hours. This period corresponds to the daily increase in domestic power supply at the end of the working day, resulting in voltage fluctuations observed at the station. In 1991 a large UPS will be installed to condition the GC equipment power and a similar analysis will be done to see if the N_2O variation diminishes. Similar variations were not observed in the CFC measurements.

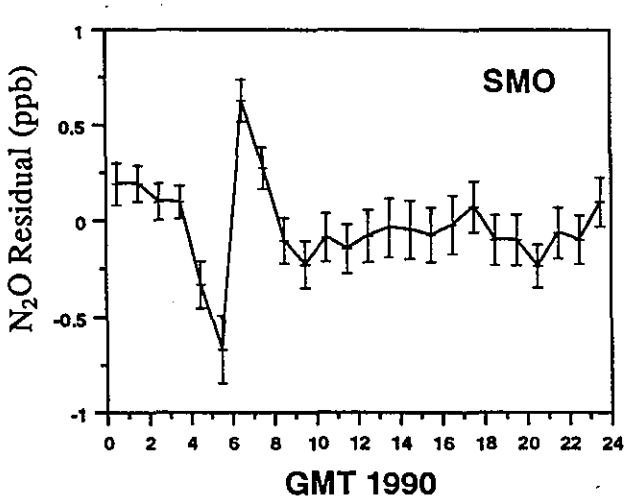

Fig. 7.10. Residual N_2O concentrations at SMO during 1990 averaged for each hour of the day. The bars show the 95% confidence intervals.

7.1.3. Low Electron Attachment Potential Species

Routine flask sampling and analysis of LEAPS gases began in mid-1989. Despite some instrumental down-time, we now have a relatively continuous record spanning 1.5 years. HCFC-22 measurements began in mid-1990. Procedures have been developed to measure HCFC-22 and the other LEAPS and CFC gases in the same sample by connecting two electron-capture detectors in series and doping the carrier stream with O_2 to 0.2% before the second detector. This enhances the HCFC-22 peak measured by the second detector while the adjacent, and potentially interfering, CFC-12 peak is reduced during passage through the first detector (Figure 7.11). Halon (brominated CFC) measurements have been made without serious problems. Although the data set spans only 1.5 years, some trends are already apparent. Data from the four CMDL observatories show a significant rate of growth for H-1301 (Figure 7.12*a*). The rate of increase varied among stations from 0.26 to 0.47 ppt yr^{-1}, with a mean of 0.36 ppt yr^{-1}, but the differences between these slopes are only marginally significant, owing to the short amount of time and relatively small number of samples. Mean concentrations at the observatories increased with increasing latitude, indicating the importance of northern hemispheric sources.

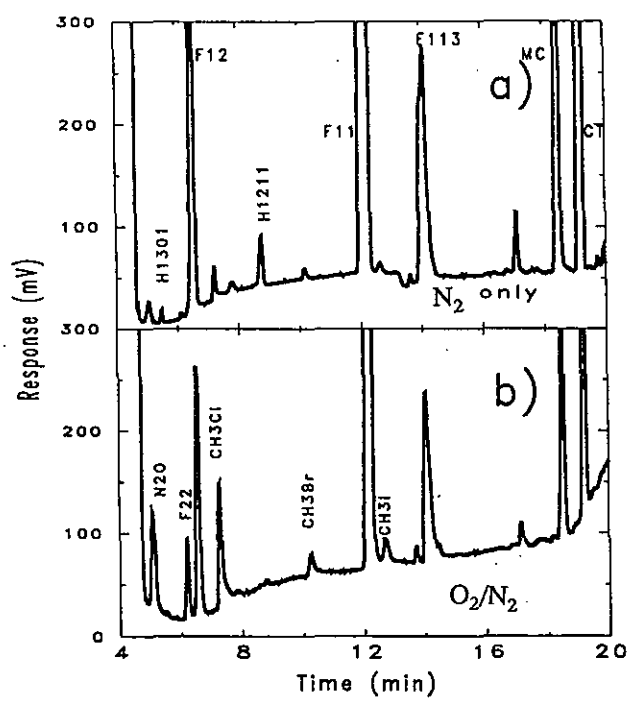

Fig. 7.11. LEAPS chromatograms of air from BRW; (*a*) N_2 carrier gas (ECD #1), (*b*) N_2 carrier gas doped with O_2 to 0.2% (ECD #2). The ECDs were connected in series.

H-1211, unlike H-1301, showed little or no growth at the four observatories during this period, and the latitudinal gradient was not significantly different from zero (Figure 7.12*b*). Production rates for H-1211 did not decline during this time, although release rates may have slowed in response to international control agreements and environmental considerations [*Halon Research Institute*, 1989]. A longer sampling record is required to determine accurately whether or not there are indeed temporal and latitudinal variations in both H-1301 and H-1211.

7.1.4. Gravimetric Standards

A total of 36 primary calibration standards were prepared during 1990 for use in the RITS, LEAPS, and special projects. A summary is given in Table 7.1. The total number of primary standards on the NOAH inventory was 223 at the end of 1990. Of these, 122 were prepared in our own standards laboratory. Twenty-five cylinders were filled with air at Niwot Ridge during the year and analyzed for use as secondary standards at the field sites and in the laboratory.

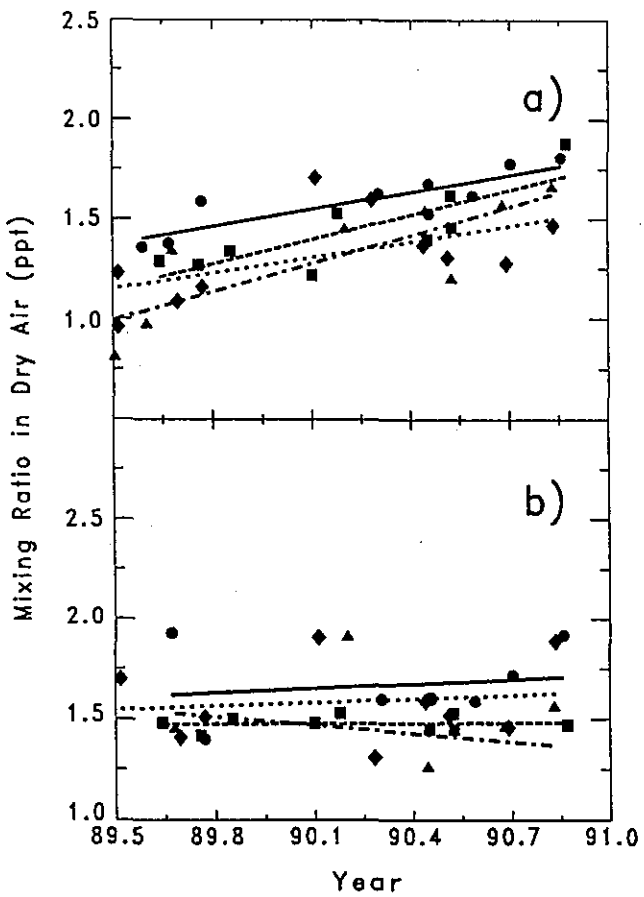

Fig. 7.12. Concentration trends in (*a*) H-1301 and (*b*) H-1211 at CMDL observatories from mid-1989 through 1990. The mean slope for all H-1301 measurements is 0.36 ppt y^{-1}. The mean slope of the H-1211 measurements does not differ significantly from zero. Stations are identified as follows: BRW, circles and solid line; NWR, squares and dashed line; MLO, triangles and broken dashed line; SMO, diamonds and dotted line.

7.2. Special Projects

7.2.1. Alternative Halocarbon Measurements

It is anticipated that by the year 2000 most CFCs will have been phased out, partly by substitution with two alternative families of compounds: HCFCs (hydrochlorofluorocarbons) and HFCs (hydrofluorocarbons). Both break down more rapidly in the atmosphere, and therefore have lower ozone depletion and global warming potentials. Apart from HCFC-22, which is already in production, the "alternative halocarbons" are not currently present in the atmosphere. They present a three-fold challenge to their analysis: very low atmospheric concentrations for at least the next two decades, poor sensitivity with the electron capture detectors (ECDs) that NOAA presently uses to routinely measure CFCs, and similar physical properties to the CFCs that they replace, making their chromatographic separation difficult in some cases.

Beginning in October 1990, we began work to develop techniques for alternative halocarbon measurements and concentration of air samples using adsorbent traps. Initially we are focussing on HCFC-22, HCFC-123, and HFC-134a. We have been unable, as yet, to obtain standards for HCFC-141b, another important alternative halocarbon candidate.

GC/Mass Spectrometer Analysis

An HP 5971A GC interfaced to a mass spectrometer detector (GC/MS) was purchased by the NOAH group to address some of the difficulties involved in measuring alternative halocarbons in the atmosphere. This instrument can sensitively detect a much wider variety of compounds than the ECD. For example, HFC-134a contains no chlorine atoms and, therefore, has almost no ECD response. HCFC-22 does contain chlorine atoms, but is weakly electrophylic and is two to three orders of magnitude less sensitive by ECD than CFC-12. Sensitivity of the GC/MS, however, is nearly equivalent for HFC-134a, CFC-12 and HCFC-22 (Figure 7.13*a*). HCFC-123, a proposed replacement for CFC-11, is also sensitively detected by GC/MS and can be easily separated from CFC-11 (Figure 7.13*b*). By collecting 1-10 dm^3 of air for a single analysis we expect to be able to detect <1 pptv of alternative halocarbons such as HFC-134a in air. This will be accomplished by either cryogenically concentrating air contained in cylinders or by using adsorbent tube pre-concentration techniques.

The GC/MS can be operated in either a full scan mode, with a wide range of compound sensitivity, or in a highly selective "single ion mode" (SIM). SIM enables quantification of coeluting compounds and also provides greater sensitivity for the selected species. Although the

Table 7.1. Summary of Gravimetric Standards Prepared in 1990

Compounds	Quantity	Concentration Range	Prepared for
N_2O	6	ppm, ppb	NOAA/RITS
CFC-12	2	ppt	NOAA/RITS
CFC-11	2	ppt	NOAA/RITS
CFC-11, CH_3CCl_3, CCl_4	7	ppm, ppb, ppt	NOAA/RITS
C_6F_{12}, C_7F_{14}, C_8F_{16}, C_9F_{18}	4	ppm, ppb, ppt	NOAA/ARL
CFC-11, CFC-113, CH_3CCl_3, CCl_4	5	ppt	NOAA/RITS
CFC-11, CFC-12, CFC-113, CH_3Cl, CH_3CCl_3, CCl_4	3	ppt	NOAA/RITS
CFC-11, CFC-113, CH_3CCl_3, CCl_4	6	ppb, ppt	NOAA/RITS
Halon-1301	1	ppt	NOAA/LEAPS

compounds presently under study have been successfully separated chromatographically, SIM may prove invaluable for other alternative halocarbons.

Because of its wide-range sensitivity and ability to identify unknowns from their ion spectra, the GC/MS will also prove useful in checking our gravimetric standards for purity. It will also be used to investigate contamination problems with sample and standard tanks; for example, acetaldehyde has been identified as a contaminant in one of our gravimetric standards, possibly originating from a sealing compound in the pressure fittings.

Adsorbent Tube Pre-Concentration

A large number of materials, including chromatography packing materials, carbon molecular sieves, and activated carbons, have been screened for their potential use as adsorbents to concentrate CFCs and alternative halocarbons from large volumes of air. This presents a significant challenge since the compounds we wish to collect are considerably more volatile, and therefore less easy to trap, than compounds normally collected with adsorbent tubes. We now have several alternative designs for multi-stage traps (see example in Figure 7.14). After sampling, trapped compounds are desorbed by heating the tube while backflushing with nitrogen. The compounds are then cryogenically reconcentrated at the head of a GC capillary column for analysis.

Adsorbent tubes offer a number of advantages over flask sampling. Due to their small size we will be able to produce a hand-portable microcomputer-controlled 32 tube sampler and desorber. Designs have also been made for an automatic aircraft sampler-desorber-GC analyzer. Tubes can be used to concentrate greater volumes: as much as tens of dm^3 compared with approximately 2.5 dm^3 for the largest flasks used in our sampling network. This is valuable where detection of ultra-low concentrations is required, or where less sensitive techniques such as GC/MS are employed.

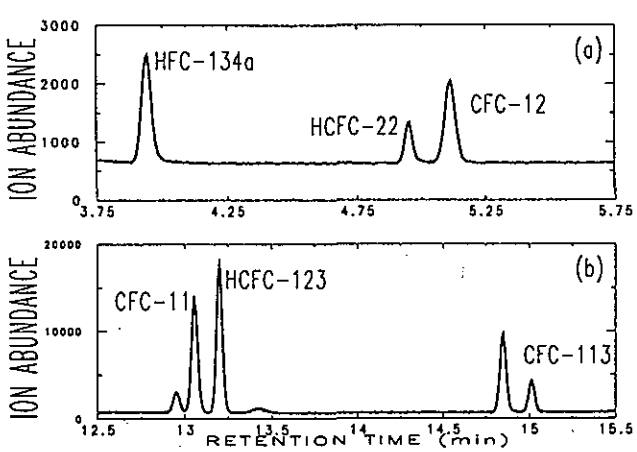

Fig. 7.13. Reconstructed selected ion chromatograms of (*a*) HFC-134a (1.3×10^{-10} dm^3), HCFC-22 (1.1×10^{-11} dm^3), and CFC-12 (2.4×10^{-11} dm^3), and (*b*) HCFC-123 (1.0×10^{-10} dm^3) and CFC-11 (1.0×10^{-10} dm^3). Sample volumes are vapor phase volumes at STP.

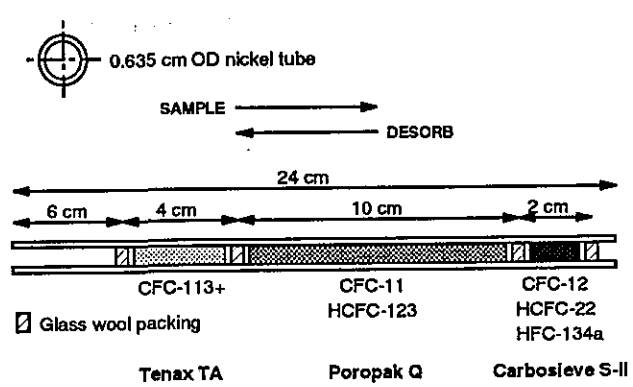

Fig. 7.14. Example of three-stage adsorbent trap designed to collect key CFCs, HCFCs and HFCs with high efficiency from 15 dm^3 of air at a flow rate of 50 cm^3 min^{-1}, and desorb all trapped compounds within 5 minutes at 220°C.

Most compounds are very stable on the adsorbents and, since the entire tube is desorbed, wall losses should not be a problem; thus some of the artifacts that plague flask samples may be overcome. The adsorbents selected are hydrophobic and other gases such as CO_2, which may cause cryo-trapping and analytical problems, are not collected. Tubes also extend the practical limits to in situ GC cryo-trapping; to directly cryo-trap the same amounts of air could take more than an hour of instrument time and undoubtedly lead to peak broadening, sample loss, and column plugging.

It is planned to send the portable tube sampler to the baseline observatories and on aircraft and ocean-cruise missions. On return it will be interfaced to the GC/MS and/or GC/ECD. Specialized ECD techniques will need to be developed, including oxygen doping, halogenation reactions, and multiple columns, to improve HCFC sensitivity and separation. In the long term, we look to placing real-time GC systems in the field to measure alternative CFCs.

7.2.2. Soviet-American Gas and Aerosol Experiment (SAGA III)

The SAGA III cruise, from February to April 1990, began in Hilo, Hawaii, and crossed the equator seven times between 20°N and 15°S before ending in Singapore. Automated in situ measurements of N_2O, CFC-11, CFC-113, CH_3CCl_3, and CCl_4 in the atmosphere and surface water were made at 40-minute intervals. The main objectives were to evaluate the spatial and temporal variability of trace gases across the inter-tropical convergence zone (ITCZ), trace the zonal movement of the ITCZ, determine halocarbon saturation anomalies and assess their use in calculating air-sea transfer coefficients, measure the flux of N_2O from equatorial waters, and compare the results at stations sampled in 1987, an El Niño year.

The most significant findings were that CH_3CCl_3 and CCl_4 were undersaturated in surface seawater for almost the entire cruise. Until now the ocean has not generally been considered to be a sink for these gases. The air-sea fluxes we calculated (Figure 7.15) are supported by recently published rates of hydrolysis for the two compounds [*Gerkens and Franklin*, 1989; *Jeffers et al.*, 1989]. Our results indicate that 5-11% of atmospheric CH_3CCl_3 and 16-35% of CCl_4 are lost to hydrolysis and mixing in the world oceans [*Butler et al.*, 1991]. This finding is particularly significant to model calculations of tropospheric OH concentration based on the lifetime of CH_3CCl_3, since it is presently assumed that CH_3CCl_3 is lost solely by reactions in the atmosphere. This suggests that current estimates of mean global OH concentration are about 5-11% too high. This in turn implies that estimates of the atmospheric lifetimes of some important atmospheric compounds that are removed by tropospheric OH, such as CH_4, CO, non-methane hydrocarbons (NMHCs), HCFCs, and HFCs, are longer than previous estimates by about 5-11%, increasing their global warming or ozone destruction potentials by the same amount.

The utility of CH_3CCl_3 and CFC-11 as tracers of atmospheric circulation was demonstrated on this cruise. Both compounds indicated that the width of the ITCZ varied from 2° to 20° of latitude, depending upon major atmospheric circulation patterns (Figure 7.16). The concentrations were also used to identify an intrusion of northern hemispheric air as far south as 14°S. This was later identified from satellite photographs as having been associated with a large storm system moving southward.

As expected, N_2O was supersaturated in equatorial surface waters, with highest saturation anomalies in the east Pacific (Figure 7.17). N_2O was found to be the most sensitive chemical tracer of upwelling, in agreement with the findings of SAGA II [*Butler et al.*, 1988, 1989]. It was also noted that atmospheric N_2O increased in response to higher saturation anomalies in the underlying water, implying either stratification within the marine boundary layer or the presence of a shallow, stable surface layer retarding vertical mixing. This is consistent with observations of CO_2 during SAGA II where atmospheric CO_2 was found to be lower over highly undersaturated waters during surface inversion conditions. One notable exception to this occurred around day 58, when atmospheric N_2O increased with the intrusion of northern hemispheric air mentioned earlier.

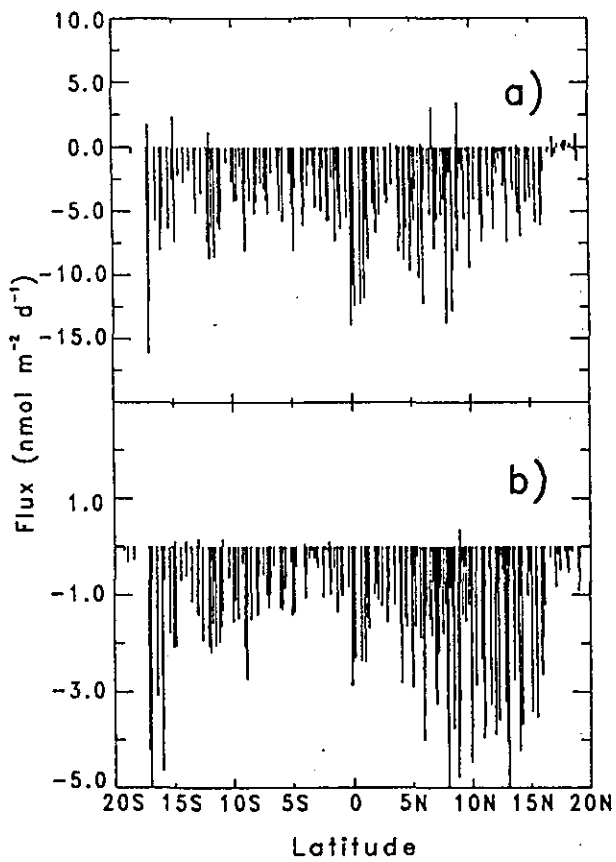

Fig. 7.15. Fluxes of (*a*) CH_3CCl_3 and (*b*) CCl_4, calculated from saturation anomalies and instantaneous air-sea transfer velocities from SAGA III, and plotted as a function of latitude. The mean flux of CH_3CCl_3 was 3.2 nmol m^{-2} d^{-1} and for CCl_4 was 0.95 nmol m^{-2} d^{-1}.

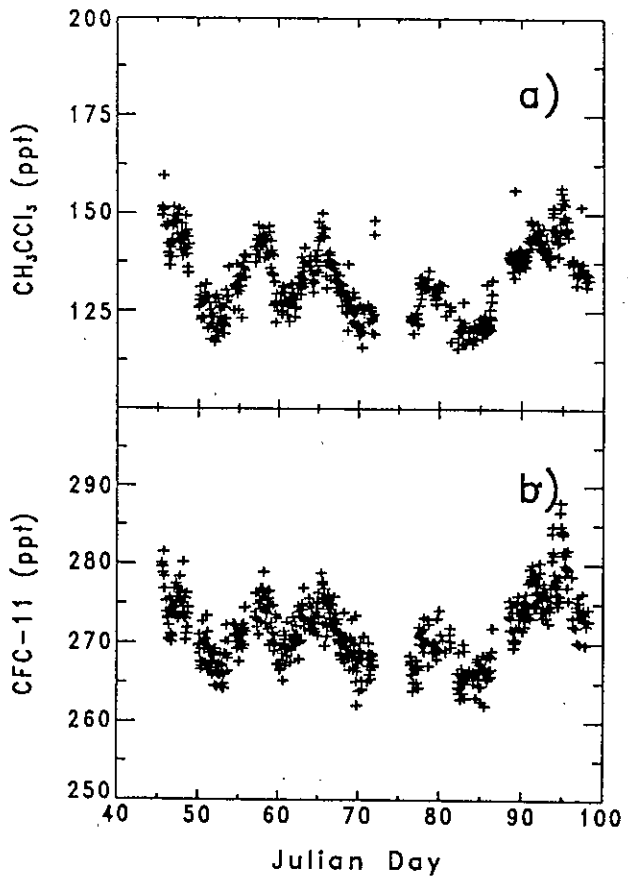

Fig. 7.16. Atmospheric dry mixing ratios of (*a*) CH_3CCl_3 and (*b*) CFC-11 during SAGA III, showing the transition between northern and southern hemispheric air masses.

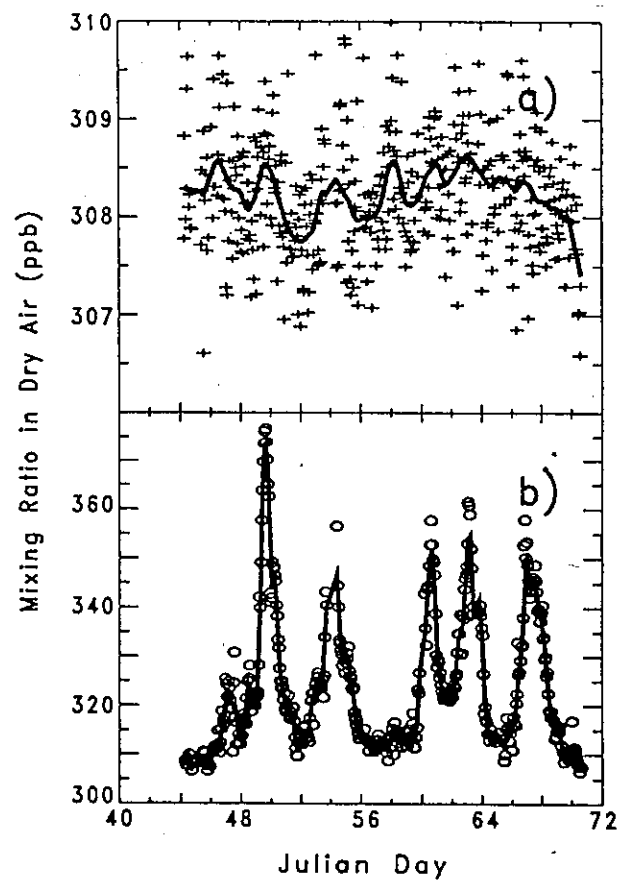

Fig. 7.17. N_2O gaseous mixing ratios in the (*a*) atmosphere and (*b*) surface water for the entire cruise. Data are fitted with a locally weighted statistical smoothing (LOWESS) function [*Cleveland*, 1988].

7.2.3. Airborne Chromatograph for Atmospheric Trace Species (ACATS)

One of the recommendations of the National Global Climate Change Program [*GCRP*, 1989] is that more measurements be made of vertical profiles of atmospherically significant trace gases. Such measurements are required as input to increasingly sophisticated and detailed atmospheric models used to predict potential global climate change. Expanding our measurements of trace gases to vertical profiles has therefore become one of the major goals of the RITS program at NOAA. In the NOAH group this is being implemented for N_2O and halocarbons by collecting flask samples for later analysis and by installing real-time GC analysis systems in aircraft. For aircraft such as the NASA ER-2 and for future pilotless drones (e.g. the Condor) with flight times of 8 hours or more, an airborne GC has the advantages of higher time resolution (up to 2 minutes per sample), smaller bulk and weight on a per-sample basis, no flask artifacts from wall losses and contamination, and immediate availability of analytical results. The greater spatial and temporal resolution achieved by the high sampling frequency may help resolve such issues as whether the polar vortex is a static or dynamic processor for ozone depletion [*Albritton et al.*, 1991].

Some of the capabilities of an airborne GC were demonstrated during flights sponsored by the California State Board of Air Quality over the San Joaquin Valley and San Jose-San Francisco metropolitan area during August 1990. The aim of the study was to examine the influence of human activities and the role of the ocean in transport of pollution into and out of the San Joaquin Valley. Northern California is one of the top ten areas of the world for the release of CFC-113, a solvent used in the production of semiconductor circuits and metal degreasing.

A commercial GC was modified for aircraft operation (Figure 7.18) to measure CFC-11 and CFC-113 once every 3 minutes. The system pressure was regulated to be unaffected by changes in cabin and ambient pressure. The most prominent feature on all flights was the high concentration of CFC-113 over San Jose ("Silicon Valley"), a major producer of semiconductor circuit boards and chips (Figure 7.19). There was also a distinct change in CFC-113 concentrations on crossing the coastline, with values over the ocean lower by about 5-10%.

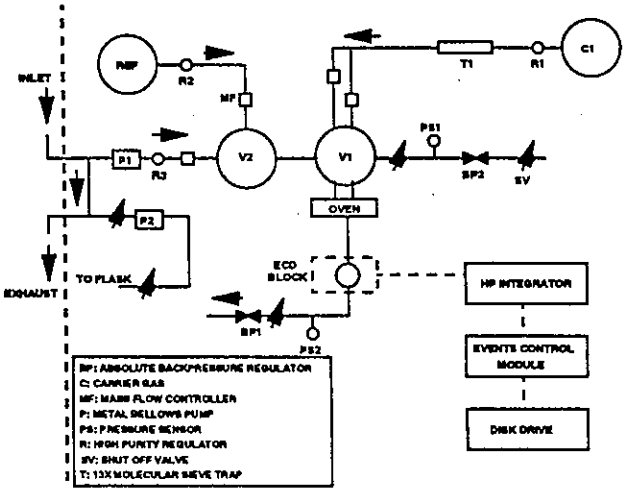

Figure 7.18. Schematic diagram of airborne gas chromatograph.

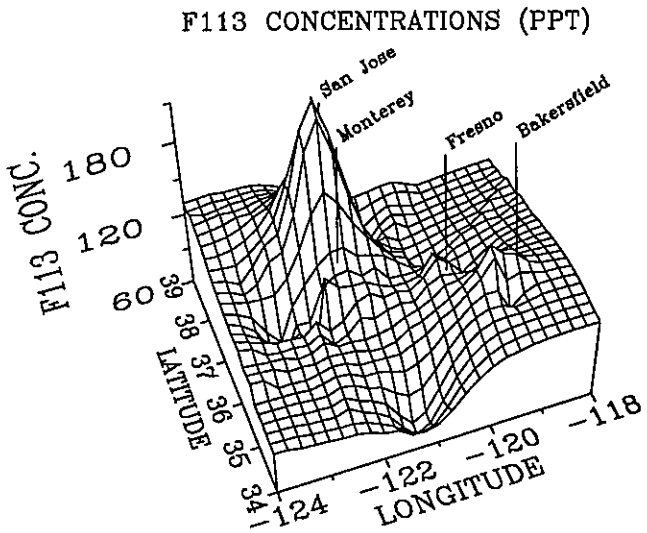

Figure 7.19. Three-dimensional display of concentration levels of CFC-113 (in ppt) over northern California measured from an airborne GC on August 22.

7.3. References

Albritton, D.L., F.C. Fehsenfeld, and A.F. Tuck, Instrumental requirements for global atmospheric chemistry, *Science, 250*, 75-81, 1990.

Butler, J.H., J.W. Elkins, C.M. Brunson, K.B. Egan, T.M. Thompson, T.J. Conway, and B.D. Hall, Trace gases in and over the west Pacific and east Indian Oceans during the El Niño Oscillation event of 1987, *NOAA Data Report ERL ARL-16*, 104 pp., NOAA Environmental Resources Laboratories, Boulder, CO, 1988.

Butler, J.H., J.W. Elkins, T.M. Thompson, and K.B. Egan, Dissolved and atmospheric nitrous oxide of the W. Pacific and E. Indian Oceans during the 1987 El Niño Oscillation event, *J. Geophys. Res., 94(D12)*, 14,865-14,877, 1989.

Butler, J.H., J.W. Elkins, T.M. Thompson, B.D. Hall, T.H. Swanson, and V. Koropalov, Oceanic consumption of CH_3CCl_3: Implications for tropospheric OH, *J. Geophys. Res.*, in press, 1991.

GCRP (Global Change Research Program), *Our Changing Planet: The FY 1990 Research Plan, The U.S. Global Change Research Program*, A Report by the Committee on Earth Sciences, pp. 118, U.S. Geological Survey, Reston, VA, 1989.

Gerkins, R.R., and J.A. Franklin, The rate of degradation of 1,1,1-trichloroethane in water by hydrolysis and dehydrochlorination, *Chemosphere, 19(12)*, 1929-1937, 1989.

Halon Research Institute, *1989 Annual Report*, Halon Research Institute, Washington, DC, 1989.

Jeffers, P.M., L.M. Ward, L.M. Woytowitch, and N.L. Wolfe., Homogenous hydrolysis rate constants for selected chlorinated methanes, ethanes, ethenes, and propanes, *Environ. Sci. Technol. 23(8)*, 965-969, 1989.

8. Director's Office

M.C. SERREZE, J.D. KAHL (*University of Wisconsin-Milwaukee*), and R.C. SCHNELL

8.1. LOW-LEVEL TEMPERATURE INVERSIONS OF THE EURASIAN ARCTIC AND COMPARISONS WITH SOVIET DRIFTING STATION DATA

8.1.1. INTRODUCTION

Results from a number of recent studies point toward the need for more detailed investigations of spatial and temporal variability in the Arctic temperature inversion. For example, the height of the inversion base can be used to estimate the geostrophic drag coefficient [*Overland*, 1985; *Overland and Guest*, 1991; *Overland and Davidson*, 1991] which, in turn, is needed as input into sea ice and coupled ice-ocean models [e.g., *Hibler and Bryan*, 1987] to simulate sea-ice motion. With regard to Arctic energy budgets, the strength of the inversion influences the magnitude of heat and moisture fluxes through leads and polynyas, and the depth of vertical mixing [*Andreas*, 1980; *Andreas and Murphy*, 1986]. *Schnell et al.* [1989*a*] recently reported that plumes of heat and condensate rising from large leads may sometimes penetrate the inversion layer to a depth of up to 4 km, suggesting that heat and moisture can be mixed through a far greater depth of the Arctic troposphere than previously thought.

Turning to other lines of research, elevated concentrations of pollution gases and aerosols from AGASP results have been observed to coincide with the top of the inversion layer [*Bridgman et al.*, 1989]. Photochemical destruction of boundary-layer ozone at Arctic sunrise recently documented by *Barrie et al.* [1988] and *Oltmans et al.* [1989], appears to involve a meteorological modulation process in which ozone-depleted air within the inversion layer is occasionally replaced by above-inversion, ozone-rich air, via a poorly understood mixing process.

Here we examine characteristics of the inversion layer using up to 12 years of twice-daily sounding data from 31 coastal and inland stations from the Eurasian Arctic and approximately 6 station-years of data from three Soviet drifting stations within the interior pack ice near the North Pole. The sounding data base we use is at least an order of magnitude larger than available for previous studies.

The sounding data were obtained from a NOAA/CIRES Arctic radiosonde data set being developed for the NOAA Climate Change Program. These data tapes contain 1.8 million Arctic soundings of up to four times daily for regularly-reporting Eurasian stations north of 60°N for the period 1976-1987, as well as aircraft, ship, and drifting ice-station data. Station locations are plotted in Figure 8.1. Pressure, geopotential height, temperature, dewpoint depression, wind direction and speed, and accompanying quality flags are given for each sounding. For this study, we use soundings for both 0000 and 1200 UTC.

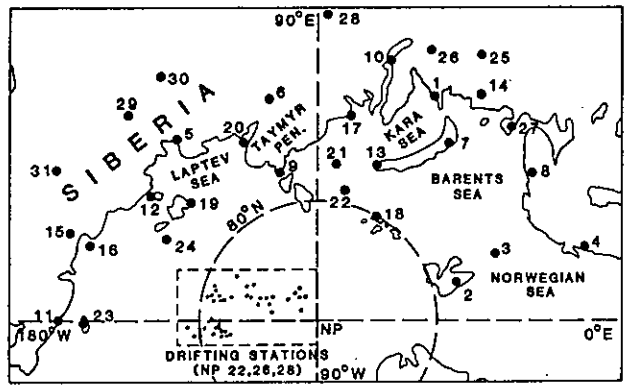

Fig. 8.1. Location of the 31 Arctic land stations and drifting station data used in this study, with drifting station positions shown at the beginning of every month that data are available.

In the present study, we are only concerned with low-level inversions defined here as those with a base below the 700 mb level. Inversions are identified using the detection algorithm developed by *Kahl* [1990]. Each temperature profile is scanned upwards from the surface to the 700 mb level to locate the first layer (if any) in which temperature increases with altitude, with the bottom of this layer defining the inversion base. The inversion top is defined as the bottom of the first subsequent layer in which the temperature decreases with altitude. Since Arctic temperature profiles often exhibit a complicated vertical structure [*Belmont*, 1957], thin negative-lapse layers are occasionally encountered in the upward scan. If these layers are thin (<100 m) and the next layer above shows an increase in temperature with altitude, the thin layer is considered to be embedded within the overall inversion layer. Examples of the technique are given by *Kahl* [1990].

8.1.2. RESULTS: SEA ICE/LAND COMPARISONS

Monthly inversion frequencies for the drifting stations are plotted in Figure 8.2, along with the estimated total cloud cover for the central Arctic, based on published data from *Huschke* [1969]. The cloud-cover data will be discussed in the next section. Other monthly statistics are shown in Figure 8.3. The top of each bar in Figure 8.3 is the median inversion top, and the bottom of each bar is the median height of the inversion base. The total length of each bar is hence approximately the median inversion depth. Also plotted on a separate scale is the median temperature difference across the inversion layer. For comparison, we plot results for station Zhigansk, located on the Siberian tundra (66.8°N, 123.4°E) (Figures 8.4 and 8.5). This station is reasonably typical of all the inland sites (Figure 8.1).

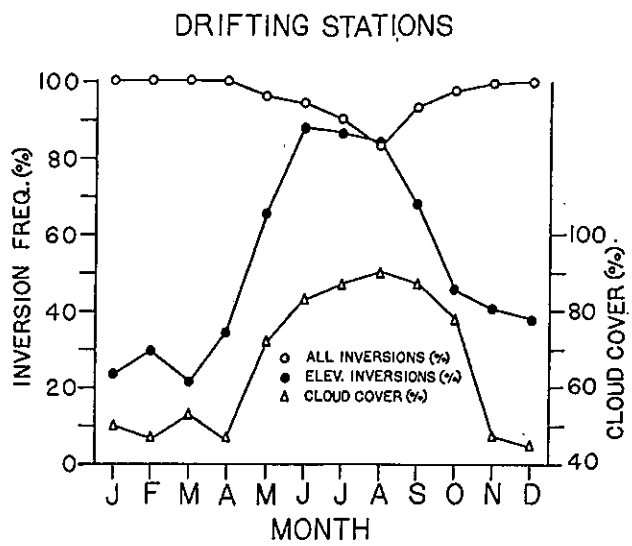

Fig. 8.2. Monthly inversion frequencies from drifting station data and sky-cover percentage for the central Arctic [cloud cover data from *Huschke*, 1969].

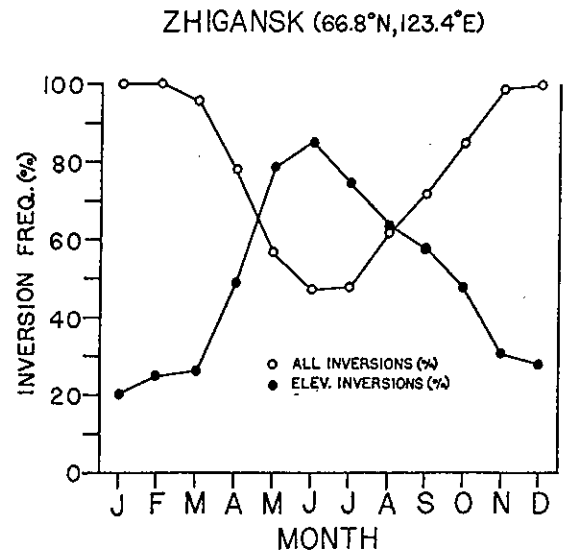

Fig. 8.4. Monthly inversion frequencies from station Zhigansk.

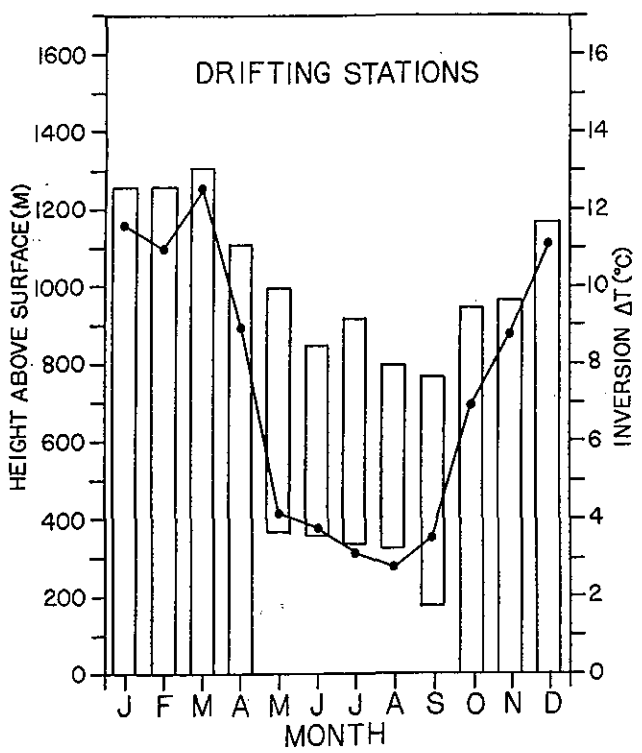

Fig. 8.3. Monthly median inversion top (top of bars), base (bottom of bars), and temperature difference (solid line) from drifting station data.

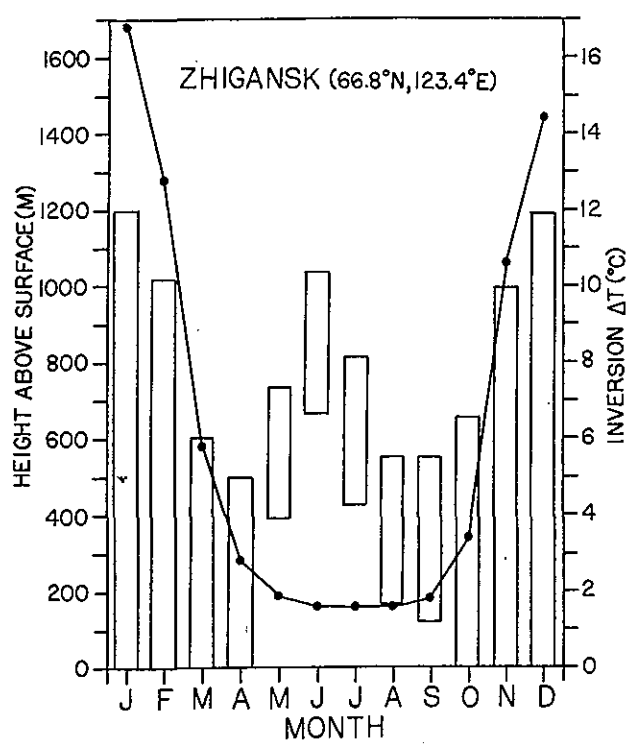

Fig. 8.5. Monthly median inversion top (top of bars), base (bottom of bars), and temperature difference (solid line) for station Zhigansk.

An initial comparison shows a strong seasonal cycle in inversion characteristics over both the pack ice and land. However, while the seasonal range in inversion frequencies over the pack ice is only 17%, it is over three times as large (53%) for Zhigansk, consistent with the stronger solar flux at the latter, more southerly station. Also, subsequent to spring snow melt, incident radiation at Zhigansk can be used to heat the atmosphere rather than to melt ice. In general, the magnitude of elevated inversions is similar at both locations.

Differences between the two sites are more apparent when Figures 8.3 and 8.5 are examined. During the winter months the temperature difference across the inversion layer is considerably higher at Zhigansk; in January it reaches 17° for Zhigansk, but only 12° for the drifting stations. While differences in cloud cover may in part be responsible for these and other differences, the contrast in ΔT during winter is consistent with the moderating influence of the heat flux through the sea-ice cover as compared to the strong radiative losses from the snow-covered land surface. Note that the effects of leads and thin ice will be absent in summer due to melting conditions.

Both the drifting stations and Zhigansk show a sharp drop in inversion ΔT during spring, but it is much more pronounced at Zhigansk, also consistent with removal of the snow cover and the stronger downwelling solar radiation at the latter location. From May through September, the temperature difference across the inversion layer is less than 2°C at Zhigansk, but from 2-4°C over the pack ice. Both sites show a mixed layer below the inversion from May to September. While it never rises above 400 m at the drifting stations, it rises to over 650 m at Zhigansk in June when potential solar radiation receipts at the surface would be maximized and strong turbulent heat transfer to the atmosphere would occur. The absence of this June peak at the drifting stations demonstrates the tendency for absorbed radiation over the sea ice to be used in melt. During autumn, surface-based inversions are again the rule at both sites with inversion ΔT also rapidly rising. By November, however, the values at Zhigansk exceed those for the pack ice, again suggestive of the moderating effect of the winter heat flux through the ice cover and stronger heat loss from land.

In Figure 8.2 cloud cover over the central Arctic exhibits a pronounced seasonal cycle. During winter, limited cloud cover can be largely understood in terms of infrequent cyclonic activity [*Serreze and Barry*, 1988] and the low moisture content of the cold, winter atmosphere. During summer, cloud cover is typically extensive (80-90%). While part of the summer increase is comprised of middle- and high-level clouds associated with increased cyclonic activity [*Serreze and Barry*, 1988], the most notable change is the development of extensive low-level Arctic stratus. According to *Herman and Goody* [1976], Arctic stratus forms when moist air masses move over the ice and condense. Once formed, it persists due to the presence of a wet, convection-limiting sea-ice surface and weak dissipative mechanisms. Since large-scale advection will be strongly associated with synoptic-scale weather systems, increased cyclonic activity in summer and the development of Arctic stratus go hand-in-hand.

Cloud cover-inversion relationships over sea ice are particularly complex during summer. When the ice surface is melting, it will be at a fixed temperature. Although the summertime surface net radiation budget is positive, the melting surface, in conjunction with advection of relatively warm air from more southerly latitudes, will tend to maintain an inversion. Persistent Arctic stratus is favored by limited mixing which implies that during summer, variations in the inversion layer will, to some extent, drive the cloud cover variations.

8.1.3. Summary and Conclusions

We believe that our study has opened several avenues for further research. For example, it may be possible to relate spatial variability in inversion features to the distinct horizontal patchiness observed in Arctic haze layers [e.g., *Bridgman et al.*, 1989]. Closer studies at shorter time scales of the spatial distribution of inversion frequencies and characteristics in winter and spring, and their relationship with synoptic activity, may be useful in identifying those locations and climatic conditions in which the inversion layer temporarily breaks down. These regions could be useful in identifying locations where boundary-layer ozone destruction [*Barrie et al.*, 1988; *Oltmans et al.*, 1989] may be most pronounced and most easily measured. Further analysis of the inversion structure over the Arctic Ocean with additional drifting station data and dropsonde data is already underway. Results may provide some guidance for the estimation of parameters needed by sea-ice modelers, and help in investigating temporal and regional variations in the potential for plumes of condensate from leads and polynyas to penetrate the inversion layer [*Schnell et al.*, 1989*a*].

Finally, possible climatic change in the Arctic as forecast by models [e.g., *Hansen et al.*, 1988] would be expected to impact cloud cover and the inversion layer. In studying the boundary-layer properties of the South Pole, *Stone and Kahl* [1991] suggest that the inversion depth, temperature difference across the inversion layer, and the bulk boundary-layer wind shear may be useful indices for monitoring climatic change since they respond to both radiative and dynamical forcings. Studies of these parameters may yield useful information in the Arctic.

8.2. Boundary Layer Ozone Fluctuations Related to Organobromine Photochemistry in the Springtime Arctic

P.J. Sheridan, R.C. Schnell and J.M. Harris

8.2.1. Introduction

Recent springtime atmospheric field experiments in the Arctic have shown episodic ground-level O_3 depletions accompanied by high levels of bromine-containing com-

pounds collected on particulate filters (FBr) [*Barrie et al.*, 1988; *Oltmans et al.*, 1989; *Sturges et al.*, 1991]. In order to further investigate the phenomenon of ground-level Arctic O_3 destruction, an airborne field experiment was performed in the eastern Arctic in the spring of 1989. During March 4-April 1, 1989, the NOAA WP-3D Orion was deployed to Bodo, Norway, in support of the CEAREX/AGASP-III mission. The aircraft was extensively outfitted for the measurement of atmospheric and meteorological parameters and for the sampling of atmospheric gases and aerosols, similar to its configuration on the 1986 AGASP-II experiment [*Schnell et al.*, 1989*b*]. The regions selected for study were the Norwegian and Greenland Seas and the ice-covered Arctic Ocean north of Spitsbergen. Aerosol sampling during these flights was concentrated in the surface inversion layer above the pack ice, specifically to address the O_3 depletion events.

The major objectives of this study were to (1) make extended measurements out over the ice in the surface inversion layer where only small fractions of a limited number of aircraft-collected aerosol samples were taken in past studies, (2) determine if O_3 destruction was occurring immediately above and downwind of large leads, which would support the hypothesis of a rapid O_3 loss mechanism, (3) extend the geographic range of the O_3 depletion observations into the Norwegian Arctic and determine whether a similar FBr/O_3 relationship is present there, and (4) determine the chemical species responsible for photolytic ground-level O_3 destruction in the springtime Arctic. Here we present bulk aerosol and trace gas chemistry data, along with meteorological information which assisted us in our interpretations of the chemistry data.

8.2.2. EXPERIMENTAL

Since the aircraft was shared among several groups with different flight requirements, only certain flights during the AGASP-III experiment were designated atmospheric chemistry flights. It was on these flights that we concentrated our sampling efforts in the surface inversion layer and free troposphere over the pack ice. Samples or measurements collected during these intensive periods included bulk aerosols and inorganic/acidic gases in three-stage filter packs, size-segregated aerosols on thin-film cascade impactor substrates, trace organic gases in grab flasks, and ozone concentrations in real time with several onboard ozone monitors. Specific details concerning the sample collection and analytical procedures used in this study, and the steps taken to minimize potential aircraft sampling artifacts, have been presented elsewhere [*Sheridan and Zoller*, 1989; *Sheridan et al.*, 1991]. Thus only a brief description of our experimental methods follows.

Sample Collection

A high-volume, aerosol filter sampling system was used to collect atmospheric particles and gases in 11-cm diameter filter packs during the AGASP-III flights. Mass flow rates through the system with the three filters in line were 350-500 standard liters per minute at the low sampling altitudes, with volume flow rates reasonably close to the mass flows (usually within ~10%). Standard conditions for our mass flowmeters were defined as 760 mm Hg and 25°C, and all concentration values were calculated using volumes corrected to standard conditions.

The aerosol sampling system collected atmospheric particles on Teflon filters in the first stage of the filter pack. The collection efficiency of the type FA Teflon filter is stated by the manufacturer to be >99.9% for 0.3 μm particles. Species which passed the particulate filter were forced through the two KOH-treated Whatman filters, which efficiently collect acidic gases. Although there is some uncertainty concerning the identity and collection efficiency of Br-containing species on base-impregnated filters, a recent survey of the literature showed general agreement that HBr, atomic Br, $BrONO_2$, and, to a lesser extent, Br_2, would be efficiently trapped [*Sturges et al.*, 1991]. Organic vapors are generally not retained on base-treated filters. Less certain are the collection efficiencies of other species, including BrO, BrNO, HOBr, and H_2OBr. The potential sampling artifacts of gas trapping by the particulate filter and volatilization of Br-containing species on the particulate filter with subsequent trapping on the base-treated filters have been discussed elsewhere [*Sturges et al.*, 1991].

Ambient air samples were collected in electropolished stainless steel 1-L flasks for subsequent GC analysis. The time required for purging and collection of a pressurized (3-atm absolute) gas sample was 1-2 minutes, depending on altitude. Details concerning sample preparation strategies and contamination precautions have been published elsewhere [*Rasmussen et al.*, 1983]. Ozone was measured with a Dasibi continuous O_3 monitor.

Analytical Procedures

INAA was used to determine the concentrations of 10-20 trace elements present on one-half of each aerosol filter sample. A few elements for which INAA is not sensitive or which showed large interferences were determined by analysis of the acid extracts of another quarter of each aerosol filter using inductively-coupled plasma atomic emission spectroscopy (ICP-AES). Concentrations of INAA-determined elements were also corroborated using this method. Major ion analysis of the filters was conducted using ion chromatography. The final one-quarter of each aerosol filter was used for these analyses, while half-filter sections of the second- and third-stage filters were used. The water soluble fraction of the aerosol was extracted with triple-distilled water in an ultrasonic bath. Ions determined using this technique included Cl^-, Br^-, NO_3^-, $SO_4^=$, Na^+, NH_4^+, and K^+.

Trace gas analysis was performed using a temperature-programmed Perkin-Elmer Model 3920B GC with an electron capture detector. Details concerning the GC column, thermal desorption steps, and other analytical procedures are reported in *Rasmussen and Khalil* [1984]. The analytical precision for the measured Br-containing trace gases is better than 2%.

Isobaric backward air mass trajectories were calculated for the purpose of estimating air parcel motion to the sampling locations. The computer model that produced these trajectories was developed by *Harris* [1982]. The primary input for the trajectory program consists of gridded wind components at mandatory pressure levels, produced by the NMCs global atmospheric model. The resolution of these data grids is 2.5° of latitude and longitude and 12 hours, with grids produced at 0000 GMT and 1200 GMT each day. Isentropic trajectories were not calculated because the model does not produce reliable trajectories near the surface in the mixed boundary layer.

8.2.3. Results

Figure 8.6 shows the approximate collection location for each of the eight AGASP-III tropospheric filter samples (A through H) and the extent of near-solid (>9/10) pack ice as of March 20 and 28, 1989 (data supplied by Norwegian Meteorological Institute). The 90% solid ice contour was within ~100 km of the ice edge everywhere in the figure except in the area southwest of Spitsbergen, where large regions of drifting ice (10-90% ice cover) were observed.

AGASP-III chemistry missions were characterized by a high-altitude ferry segment to the research area, a slow ramping descent to map the atmospheric structure at ~500 feet min^{-1} over a predetermined spot on the ice, several long duration, low-altitude sampling/measurement runs, and a rapid climb and ferry back to Bodo. Figure 8.7 shows the WP-3D descent profile for ambient temperature, O_3 concentration, and aerosol light scattering at 83°N, 10°E during flight 311. This profile featured a strong (~15°C) temperature inversion, the base of which was at 500-600 m above the ice. An isothermal layer was encountered during the descent at ~40 m radar altitude. This was the SSL over the ice on March 30 described in *Walter and Overland* [1991]. Aerosol light scattering measurements with a 3-λ nephelometer [*Bodhaine et al.*, 1991] indicated no major aerosol layers below the top of the inversion. The O_3 trace appears to show significant O_3 depletion occurring well below the top of the SSL. Allowing for the 15 second time response of the Dasibi O_3 monitor, however, the altitude at which O_3 concentrations dropped to zero was within a few meters of the top of the SSL.

Data on the concentrations of various aerosol and gas species determined from tropospheric continuous O_3 measurements, filter samples, and concurrently collected gas flasks are presented in Table 8.1. Additionally, the percentage of the sampling period for each filter that was spent in ozone-depleted (<20 ppbv O_3) air is listed. Excess filterable Br (XSFBr) is defined as the amount of Br captured on the filter in excess of the amount expected from a marine salt contribution, and was computed from the total elemental Br and Na concentrations determined by INAA. The Br/Na mass ratio used in these calculations was 0.0043, which is appropriate (correcting for Br volatilization) for aged aerosols as discussed by *Sturges and Barrie* [1988]. We

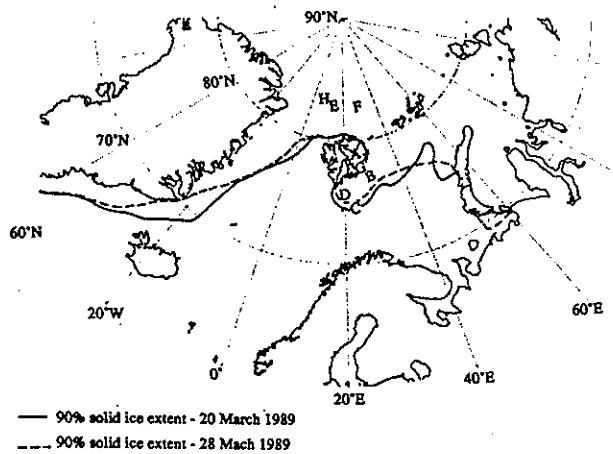

Fig. 8.6. Map of the European Arctic showing the extent of solid ice during late March 1989 and approximate collection locations of the eight AGASP-III high volume filter samples.

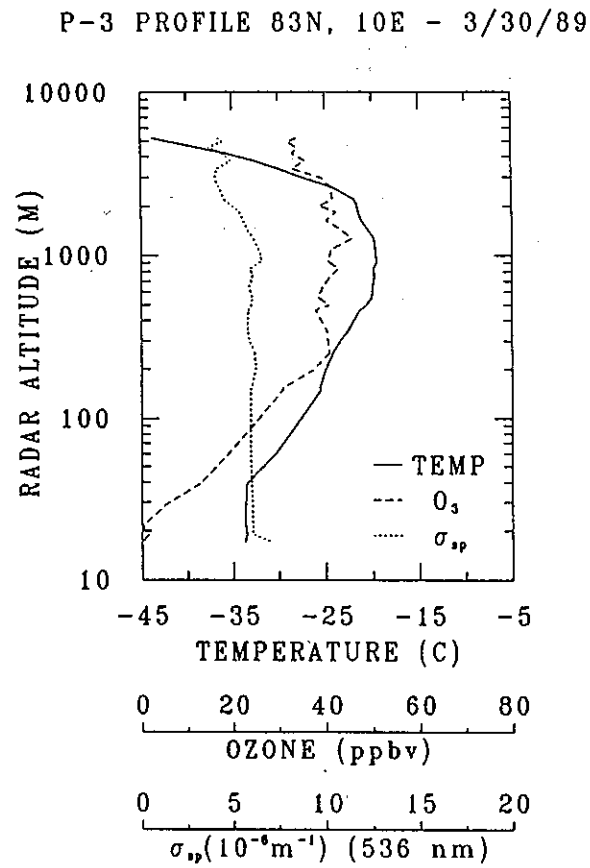

Fig. 8.7. Descent profile of ambient temperature, O_3 and aerosol light scattering for March 30, 1989, showing the atmospheric structure on flight 311. Sample collection period H was conducted under these conditions. Notice the 40-50 m deep isothermal or slightly stable layer below the strong inversion.

TABLE 8.1. Concentrations of Various Gas and Aerosol Species on Filters A-H During AGASP-III Sampling

Species	Concentrations							
	A	B	C	D	E	F	G	H
				Aerosol				
Na (ng m^{-3})	51	B	31	112	59	463	1180	34
Cl (ng m^{-3})	44	B	B	132	55	313	1230	101
Br (ng m^{-3})	4.1	2.6	1.0	5.7	6.3	35.7	6.9	11.5
XSFBr (ng m^{-3})	3.9	2.5	0.8	5.2	6.0	33.7	1.9	11.3
NH_4^+ (ng m^{-3})	400	960	620	240	280	280	180	190
SO_4^{2-} (ng m^{-3})	1490	700	1670	790	1150	940	1300	690
NO_3^- (ng m^{-3})	27	B*	B	9.1	14	<18†	92	11
				Gas Phase				
$O_{3\,avg}$(ppbv)‡	37	47	46	35	33	2.4	38	13
%T<20 (ppbv)§	1	0	0	4	12	96	0	60
CH_3Br (pptv)	23	9.6	12	NA≠	10	11	14	NA
CH_2Br_2 (pptv)	2.1	3.6	5.3	NA	4.3	5.3	4.2	NA
CH_2BrCH_2Br (pptv)	26	3.5	2.2	NA	1.7	3.3	1.8	NA
$CHBr_3$ (pptv)	2.1	1.9	4.7	NA	13	5.1	13	NA

*Value was at or below filter blank
†Value listed was instrumental detection limit
‡Mean O_3 concentration during filter sampling period
§Percentage of sampling time spent in ozone-depleted air (O_3 < 20 ppbv)
≠Data not available - flasks not collected during this period

were unable to accurately assess the motor vehicle contribution to atmospheric Br in these samples, because Pb was not detected above our instrumental ICP-AES detection limit (DL) of ~0.05 ppm. However, based on levels of other INAA- and IC-determined species, a strong anthropogenic/urban component to these samples is not expected. Total $SO_4^=$ concentrations measured on these flights (most of which were conducted specifically to find and sample Arctic haze) ranged between 700 and 1700 ng m^{-3}, which is substantially lower than past springtime Arctic haze $SO_4^=$ and non-sea salt (XS) $SO_4^=$ measurements (2-3 μg^{-3}) reported by other investigators [*Barrie and Hoff*, 1985; *Iverson and Joranger*, 1985]. Most of the filters showed XS $SO_4^=$ fractions of >0.95. The NH_4^+/XS $SO_4^=$ mole ratio for most of the samples (excluding the marine aerosol sample G) was high and ranged between 1.32 and 1.99. These values suggest an aged, background aerosol present at this time in the European Arctic, rather than a new pulse of pollution. This is consistent with visual observations of very light haze episodes during AGASP-III.

Figure 8.8 shows XSFBr concentrations from the eight tropospheric filter samples plotted against mean O_3 concentration during each sample collection period. The strong anticorrelation between these two parameters first observed at Alert [*Barrie et al.*, 1988] is again obvious. The reasons for this relationship out over the ice are probably the same as at Alert. A strong temperature inversion over the pack ice presents a barrier to O_3 mixing down to the surface from higher altitudes. The O_3 below the top of the inversion is probably destroyed through photochemical reactions involving Br radicals. A shallow surface-based SSL which was not observed at Alert limited the extent of severe ozone depletion to ~40-50 m above the pack ice surface. The PBL above this SSL showed less O_3 depletion, as would be expected with a surface source of reactant and a larger reservoir volume. Instead of shifting winds causing low-O_3, high XSFBr (onshore) and high-O_3, low XSFBr (offshore) air to flow over a stationary sampler as at Alert, the sampler in this study was mobile and collected samples and measurements in the different air masses.

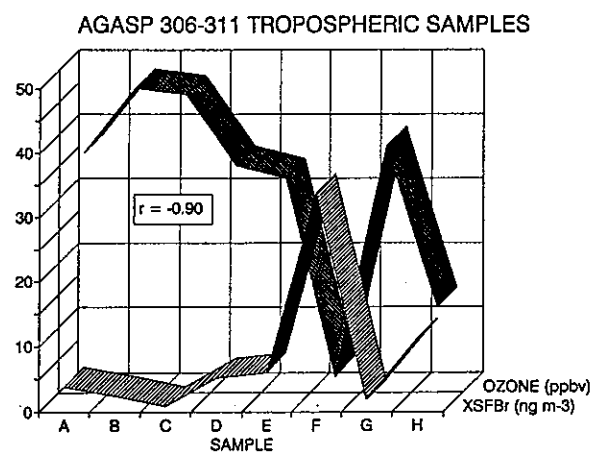

Fig. 8.8. Plot of XSFBr and mean O_3 concentration for the eight sampling periods. Samples F and H were the only ones showing severe O_3 depletion from typical tropospheric values. A linear regression least-squares fit of these data produced a correlation coefficient of r = -0.90.

While mean O_3 concentrations varied inversely with XSFBr, other O_3-related measurements also showed strong anticorrelations during this period. A linear regression fit of XSFBr plotted against the percentage of sampling time spent in O_3-depleted air (<20 ppbv O_3) yields a correlation value of r = -0.94. Similarly, a fit of the minimum O_3 concentration measured during sampling plotted against XSFBr gives a high negative correlation (>-0.8).

Observational and experimental evidence suggest a fast reaction mechanism at work in the photolytic destruction of surface O_3 over the pack ice. *Sturges et al.* [1991] have suggested a reaction rate of less than one day for the reduction of O_3 from typical well-mixed tropospheric concentrations (35-40 ppbv) to depleted values (<25 ppbv), based on the transport time from ice covered regions with exposed seawater (i.e., leads) to Barrow, Alaska. The same authors have shown in laboratory photochemical experiments that within minutes of irradiation with actinic radiation, Arctic air samples containing organobromine gases and O_3 produced significant amounts of filterable (i.e., aerosol) Br. Since we were sampling continuously in and around lead-filled regions, mixing and dilution of the air mass during transport to a remote sampler did not occur. Our AGASP-III air samples collected over solid ice (with some leads) and below the top of the SSL (samples F and H) showed almost complete O_3 destruction over large fractions of the sampling period. We believe that the concentrations of Br-containing species and O_3 in these samples are more representative of the photochemistry occurring over the pack ice than those collected a day downwind on the Arctic coast.

Two samples collected close spatially and temporally in the near-isothermal SSL were compared for evidence of catalytic O_3 destruction by gaseous Br compounds [*Sheridan et al.*, 1991]. Table 8.2 shows the concentrations of O_3, $CHBr_3$, and XSFBr for the two samples, and the respective concentration changes of these species over the 2-day period. The first sample showed no significant O_3 depletion and concentrations of $CHBr_3$ and the other Br-containing gases were similar to those reported by other researchers for springtime European Arctic conditions [*Berg et al.*, 1984; *Rasmussen and Khalil*, 1984]. The O_3 decrease (ΔO_3 = -30.6 ppbv) during the period between samples E and F was more than three orders of magnitude higher than the $CHBr_3$ reduction, suggesting a reasonably efficient catalytic cycle for O_3 destruction. $CHBr_3$ decreased in concentration by 7.9 pptv, which, assuming only one Br atom is released during photolysis, converts to a loss of 28.2 ng Br m^{-3} at STP. The observed increase in XSFBr during this period was nearly identical at 27.7 ng m^{-3}.

TABLE 8.2. Concentrations and Flucuations of O_3 and Br Species Collected North of Spitsbergen During Flights AGASP 309 and 310 (Samples E and F)

Species	Sample E Concentration	Sample F Concentration	Δ Concentration
O_3 (ppbv)	33	2.4	-30.6
$CHBr_3$ (pptv)	13	5.1	-7.9
XSFBr (ng m^{-3})	6.0	33.7	+27.7

8.2.4. Discussion and Summary

As is evident in Figure 8.8 the major O_3 destruction and XSFBr episodes were observed in the SSL during collection of filter samples F and H. It is important to identify what conditions were different in these two samples that may have contributed to the aerosol chemistry. These two samples were collected in a ~50 m deep SSL above solid pack ice with large leads present. Two other samples (D and E) were also collected in a SSL and showed no such O_3 depletion/ aerosol Br enrichment. Samples F and H were collected far to the north of Spitsbergen, but so was sample E which, as discussed above, was chemically quite different from the O_3-depleted samples. Wind direction may provide the answer in this case. Isobaric backward air mass trajectories at appropriate pressure levels arriving at the midpoint location of each filter sample were calculated. The largest O_3 depletions and XSFBr concentrations were observed during sampling north of Spitsbergen in light winds with a northerly component (filter samples F and H) [*Sheridan et al.*, 1991]. Winds for sample E were from the North Atlantic, arriving at the aircraft location from the south and southeast during the sample collection period.

Thus a few generalizations can be made concerning the geographic and meteorological conditions present during episodes of O_3 depletion in the Norwegian Arctic boundary layer. Samples F and H were the only ones showing any significant O_3 depletion, and were characterized by the following conditions: 1) sample collection over pack ice with relatively little open water (as opposed to collection near the ice edge); 2) a strong (>10°C) low level temperature inversion was present to limit mixing with free troposphere air; 3) a ~50 m thick slightly stable layer was present that acted as an additional barrier to mixing and which capped the significant O_3 destruction; 4) light winds of 5-10 m sec^{-1} or less; and 5) northerly winds transporting Arctic rather than marine air masses to the research area.

The remaining six periods when tropospheric samples were collected on AGASP-III were missing one or more of the conditions characterizing sample collection periods F and H. When sampling occurred in the free troposphere, concentrations of O_3 were relatively high and Br-containing species low. When sampling occurred in the PBL above the SSL or when the SSL was not present (i.e., the temperature profile increased continuously with altitude up to the inversion height), O_3 concentrations did not show severe depletions. In these cases, a much larger reaction reservoir (several hundred or more meters in depth) was probably responsible for the modest O_3 reductions. When marine aerosol was sampled, either because sample collection was near the broken ice edge or winds were from the direction of open water, O_3 was not severely depleted and XSFBr was relatively low. Most of the filterable Br in these samples was attributed to a bulk seawater contribution.

Concentrations of four Br-containing gases were determined by gas chromatography. None showed a persistent relationship with either O_3 or XSFBr concentration. This is probably because of the variable meteorological factors that appear to influence the efficiency of the photochemical reactions. Two samples collected spatially and temporally close in the SSL were compared for aerosol and gas composition. The first sample showed no significant O_3 depletion and concentrations of the Br-containing gases were similar to those reported by other researchers for springtime European Arctic conditions. The second sample was collected 2 days later near the same geographic location and showed a significant O_3 depletion over this time period with a concurrent $CHBr_3$ decrease and XSFBr increase. The Br released by the $CHBr_3$ losing one Br atom per molecule was nearly equal to the Br bound in XSFBr compounds. While this comparison is only as valid as the initial assumptions concerning similarity of the samples and a limited mixing scenario (i.e., few other sources and sinks) for the reacting species, the fact that Br in gaseous $CHBr_3$ and aerosols undergoes inverse and nearly equal changes in concentration over this short time period suggests that $CHBr_3$ is a key species acting to rapidly destroy O_3 over the pack ice. Unfortunately, the reaction rate for the gas phase photolysis of $CHBr_3$ is known to be far too slow to account for the concentration flucuations observed in this and other studies. This raises the possibility that heterogeneous chemical reactions involving organic Br in the particulate phase may be important. The aerosol surface area can provide a means for reacting atmospheric particles to encounter one another with greater frequency, which is a suggestion from other studies [*Sturges et al.*, 1991; *Sheridan et al.*, 1991]. More study is needed on the potential role of aerosols accelerating boundary layer O_3 destruction through heterogeneous photochemical reaction mechanisms.

Acknowledgments. The Arctic low-level temperature inversion study was supported by contracts from the NOAA Climate and Global Change Program (NA85RAHO5066), the National Science Foundation (DPP-8822472), the Electric Power Research Institute (RP2333-07), and the Office of Naval Research University Research Initiative (N00014-86-K-0695). M. Rehder (CIRES) provided valuable programming assistance. We thank the University of Washington for providing most of the aerosol analyses. We appreciate the trace gas data supplied by the Oregon Graduate Institute of Science and Technology. Thanks are also expressed to the NOAA/Aircraft Operations Center in Miami, Florida, for a well-conducted field experiment at a remote site. This study was supported through grants from NASA, ONR, and NSF.

8.3. References

Andreas, E.L., Estimation of heat and mass fluxes over Arctic leads. *Mon. Wea. Rev.*, *108*, 2057-2063, 1980.

Andreas, E.L. and B. Murphy, Bulk transfer coefficients for heat and momentum over leads and polynyas, *J. Phys. Oceanogr.*, *16*, 1875-1883, 1986.

Barrie, L.A. and R.M. Hoff, Five years of air chemistry observations in the Canadian Arctic, *Atmos. Environ. 19*, 1995-2010, 1985.

Barrie, L.A., J.W. Bottenheim, R.C. Schnell, P.J. Crutzen and R.A. Rasmussen, Ozone destruction and photochemical reactions at polar sunrise in the lower Arctic atmosphere, *Nature*, *334*, 138-141, 1988.

Belmont, A.D., Lower tropospheric inversions at ice island T-3, *J. Atmos. Terres. Phys., Special Supplement*, 215-284, 1957.

Berg, W.W., L.E. Heidt, W. Pollock, P.D. Sperry, and R.J. Cicerone, Brominated organic species in the Arctic atmosphere, *Geophys. Res. Lett.*, *11*, 429-432, 1984.

Bodhaine, B.A., N.C. Ahlquist, and R.C. Schnell, Three wavelength nephelometer suitable for aircraft measurement of background aerosol scattering coefficient, *Atmos. Environ. 25A*, 2267-2276, 1991.

Bridgman, H.A., R.C. Schnell, J.D. Kahl, G.A. Herbert and E. Joranger, A major haze event near Point Barrow, Alaska: analysis of probable source regions and transport pathways, *Atmos. Environ.*, *23*, 2537-2549, 1989.

Hansen, J., I. Fung, A. Lacis, D. Rind, S. Lebedeff, R. Rudey, G. Russell and P. Stone, Global climate changes as forecast by the Goddard Institute for Space Sciences three-dimensional model, *J. Geophys. Res.*, *93*, 9341-9364, 1988.

Harris, J.M., The GMCC atmospheric trajectory program, *NOAA Tech. Memo. ERL-ARL-116*, 30 pp., NOAA Environmental Research Laboratories, Boulder, CO, 1982.

Herman, G. and R. Goody, Formation and persistence of Arctic stratus clouds, *J. Atmos. Sci.*, *33(8)*, 1537-1553, 1976.

Hibler, W.D., III, and K. Bryan, A diagnostic ice-ocean model, *J. Phys. Oceanogr.*, *17*, 987-1015, 1987.

Huschke, R.E., Arctic cloud statistics from "air-calibrated surface weather observations," *Memorandum RM-L173-PR*, 79 pp., Rand Corporation, Santa Monica, CA, 1969.

Iverson, T., and E. Joranger, Arctic air pollution and large scale atmospheric flows, *Atmos. Environ. 19*, 2099-2108, 1985.

Kahl, J.D., Characteristics of the low-level temperature inversion along the Alaskan Arctic coast. *Int. J. Climat.*, *10*, 537-548, 1990.

Oltmans, S.J., R.C. Schnell, P.J. Sheridan, R.E. Peterson, S.M. Li, J.W. Winchester, P.P. Tans, W.T. Sturges, J.D. Kahl, and L.A. Barrie, Seasonal surface ozone and filterable bromine relationship in the high Arctic. *Atmos. Environ.*, *23*, 2431-2441, 1989.

Overland, J.E., Atmospheric boundary layer structure and drag coefficients over sea ice. *J. Geophys. Res.*, *90*, 9029-9049, 1985.

Overland, J.E., and K.L. Davidson, Geostrophic drag coefficients over sea ice, *Tellus*, in press, 1991.

Overland, J.E., and P.S. Guest, Control of minimum snow and air temperatures over Arctic sea ice during winter, *J. Geophys. Res.*, *96(C-3)*, 4651-4662, 1991.

Rasmussen, R.A., M.A.K. Khalil and R.J. Fox, Altitudinal and temporal variation of hydrocarbons and other gaseous tracers of Arctic haze, *Geophys. Res. Lett. 10*, 144-147, 1983.

Rasmussen, R.A., and M.A.K. Khalil, Gaseous bromine in the Arctic and Arctic haze, *Geophys. Res. Lett. 11*, 433-436, 1984.

Schnell, R.C., R.G. Barry, M.W. Miles, E.L. Andreas, L.F. Radke, C.A. Brock, P.J. McCormick, and J.L. Moore, Lidar studies of leads in Arctic sea ice, *Nature*, *339(6225)*, 530-532, 1989*a*.

Schnell, R.C., T.B. Watson, and B.A. Bodhaine, NOAA WP-3D instrumentation and flight operations on AGASP-II, *J. Atmos. Chem. 9*, 3-16, 1989*b*.

Serreze, M.C., and R.G. Barry, Synoptic activity in the Arctic Basin, *J. Climate*, *1(12)*, 1276-1295, 1988.

Sheridan, P.J., and W.H. Zoller, Elemental composition of particulate material sampled from the Arctic haze aerosol, *J. Atmos. Chem. 9*, 363-381, 1989.

Sheridan, P.J., R.C. Schnell, W.H. Zoller, N.D. Carlson, R.A. Rasmussen, J.M. Harris, and H. Sievering, Composition of Br-containing aerosols and gases related to boundary layer ozone destruction in the Arctic, *Atmos. Environ.*, submitted, 1991.

Stone, R.S., and J.D. Kahl, Variations in boundary layer properties associated with clouds and transient weather disturbances at the South Pole during winter. *J. Geophys. Res., 96(D3)*, 5137-5144, 1991.

Sturges, W.T., and L.A. Barrie, Chlorine, bromine and iodine in Arctic aerosols, *Atmos. Environ. 22*, 1179-1194, 1988.

Sturges, W.T., R.C. Schnell, S. Landsberger, J.M. Harris, and S.-M. Li, Chemical and meteorological influences on surface ozone destruction at Barrow, Alaska during spring 1989, *Atmos. Environ.*, submitted, 1991.

Walter, B., and J. Overland, Aircraft observations of the mean and turbulent structure of the atmospheric boundary layer during spring in the central Arctic, *J. Geophys. Res., 96(C3)*, 4663-4673, 1991.

9. Cooperative Programs

Continuous Aerosol Monitoring with the Epiphaniometer at MLO

U. BALTENSPERGER, H.W. GÄGGELER, AND D.T. JOST
Paul Scherrer Institute, CH-5232 Villigen PSI, Switzerland

An epiphaniometer has been operating at MLO since December 1989. This instrument was developed recently [*Gäggeler et al.*, 1989] and has the ability for continuous aerosol monitoring even at very low aerosol concentrations [*Baltensperger et al.*, 1991]. Due to the low flow rate of 1.0 L min^{-1}, the device consumes only 8W of power, including counting and data processing. It is, therefore, suitable for battery operation, and it has been used together with a solar panel for continuous aerosol measurements in the Swiss Alps at elevations up to 4450 m. [*Baltensperger et al.*, 1991].

The system is described in detail by *Gäggeler et al.*, 1989. Aerosols are pumped through a chamber containing radioactive lead isotopes (^{211}Pb). These single lead atoms are produced at a constant rate by the decay of a short-lived radon isotope (^{219}Rn) emanating from a long-lived actinium source (^{227}Ac). ^{211}Pb atoms attached to aerosol particles are transported through a capillary acting as a diffusion barrier for non-attached lead atoms. At the end of the capillary, the aerosol particles and with them the attached lead atoms are deposited on a filter. The resulting activity on the filter is measured continuously by a surface barrier detector via the α-decay of ^{211}Bi, the daughter of ^{211}Pb. Due to the relatively short half-life of ^{211}Pb, the device allows continuous monitoring of aerosols, without changing or transporting the filter.

Calibration experiments with artificial aerosols showed that the attachment coefficient of the ^{211}Pb atoms can be described by the Fuchs theory of coagulation [*Pandis et al.*, 1991]. Since the device delivers a signal which is proportional to the "Fuchs surface" of the aerosol particles, it was called epiphaniometer (the Greek word epiphania small aerodynamic diameters (d<100 nm) the epiphaniometer means surface of a body) [*Gäggeler et al.*, 1989]. Thus at signal is roughly proportional to the surface area of the aerosol particles. At large aerodynamic diameters (>3 μm) the signal is proportional to d. In the intermediate regime, the obtained signal is proportional to dx, with x varying between 1 and 2, depending on particle diameter. Thus the Fuchs surface of an aerosol particle can be viewed as an intermediate moment between its diameter (first moment) and its surface (second moment). Generally the epiphaniometer data alone are not sufficient for the calculation of other moments like number, surface, or volume in the same way that a CNC can provide only number concentration and not any other moments. However, for an aged aerosol usually found at remote locations good correlations are normally found between epiphaniometer signal and mass concentration [*Baltensperger et al.*, 1991]. Therefore, good agreement between epiphaniometer and nephelometer data should be expected at MLO.

During 1990, the epiphaniometer was running with very few interruptions, mainly caused by power failures. With the chosen time resolution of 30 minutes the lowest value found for this year was still nearly two orders of magnitude above the detection limit, demonstrating the excellent sensitivity of the instrument. As an example, Figure 1 shows the epiphaniometer data along with the nephelometer data (for λl = 450 nm) from MLO for July, 1990. Very good agreement is found with a correlation coefficient r =

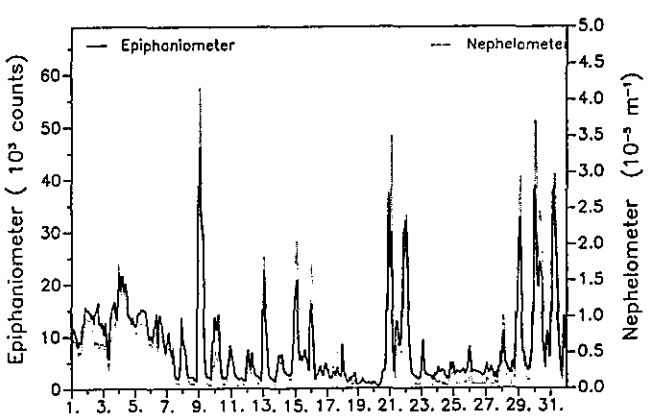

Fig. 1. Epiphaniometer and nephelometer (λ = 450 nm) data from MLO for July 1990 (GMT).

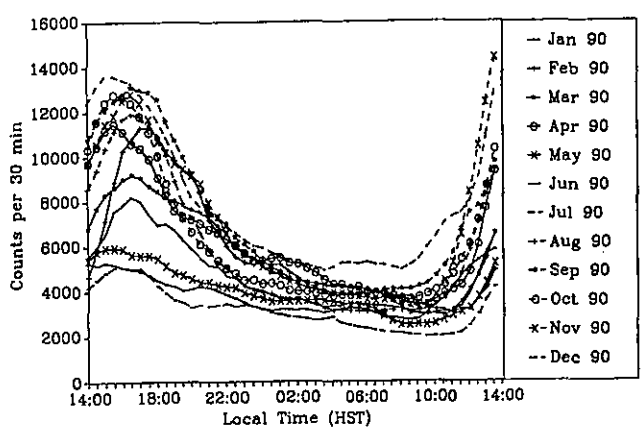

Fig. 2. Diurnal variations of the epiphaniometer signal from MLO averaged over each month of 1990.

0.955 for this month. This is true for the usual diurnal variation found at MLO (as shown, e.g. on July 9) as well as for the special episode with high aerosol concentrations between July 1 and 7. The correlation with CNC data for this month was worse (r = 0.54). During most of the period July 1 through 7, number concentrations were below 500 cm^{-3}. Thus downslope conditions along with a CNC reading of less than 500 cm^{-3} are not a secure indication for low aerosol concentrations, and nephelometer or epiphaniometer data might be used to define clean background conditions.

Figure 2 shows the diurnal variations averaged over each month of 1990. It can be seen that the minima of these variations are rather constant during the year (with the exception of July, which showed the exceptional episode described above). On the other hand, the maxima show a higher variability depending on the meteorological conditions of the corresponding month. On an average, the minima during downslope conditions (0730-0900 LST) correspond to 60 % of the annual mean. For the fine aerosol mass concentration, *Cahill et al.* [1990] found a downwind value of 80% compared to the annual average. Taking into account the concentration decrease between 0000 and 0900 LST (Figure 2), this is in reasonable agreement with our data.

Acknowledgments. We thank E. Robinson and A. Yoshinaga for their cooperation and surveillance of the epiphaniometer, and B. Bodhaine for providing the nephelometer and CNC data.

REFERENCES

Baltensperger, U., H.W. Gäggeler, D.T. Jost, M. Emmenegger, and W. Ngeli, Continuous background aerosol monitoring with the epiphaniometer, *Atmos. Environ. 25A*, 629-634, 1991.

Cahill, T.A., L.K. Wilkinson, and R.A. Eldred, Chemical resolution of fine aerosol mass at MLO: The role of organic matter, in *Climate Monitoring and Diagnostics Laboratory, No. 18: Summary Report 1989*, edited by W.D. Komhyr and R.M. Rosson, pp. 88-91, NOAA Environmental Research Laboratories, Boulder, Colorado, 1990.

Gäggeler, H.W., U. Baltensperger, M. Emmenegger, D.T. Jost, A. Schmidt-Ott, P. Haller, and M. Hofmann, The epiphaniometer, a new device for continuous aerosol monitoring, *J. Aerosol Sci., 20*, 557-564, 1989.

Pandis, S.N., U. Baltensperger, J.K. Wolfenbarger, and J.H. Seinfeld, Inversion of aerosol data from the epiphaniometer, *J. Aerosol Sci., 22*, 417-428, 1991.

Antarctic Ultraviolet Spectroradiometer Monitoring Program

C. R. BOOTH, T. LUCAS, J. MORROW, D. NEUSCHULER, J. TUSSON, AND J. YEH
Biospherical Instruments Inc., San Diego, California 92117

1. INTRODUCTION

The Antarctic Ultraviolet Spectroradiometer Monitoring Network was established by the United States National Science Foundation (NSF) in 1988 in response to predictions of increased UV radiation in the polar regions. The network consists of a number of automated, high resolution spectroradiometers placed in strategic locations in Antarctica and the Arctic (Table 1). The network makes essential measurements of UV irradiance and provides a variety of biological dosage calculations of UV exposure. Biospherical Instruments Inc. (San Diego, California), under contract to Antarctica Support Associates (ASA), directed by NSF, is responsible for providing engineering and operating support and distributing data to the scientific community.

2. METHODOLOGY

The spectroradiometer system consists of two main subassemblies: the Scanning Monochromator Detector Assembly (SMDA) and the Process Control Assembly (PCA). The SMDA collects the downwelling irradiance, and the PCA acquires and stores these data.

The SMDA contains an irradiance diffuser, monochromator, photomultiplier tube (PMT), and calibration lamps. UV irradiance passes through a Teflon diffuser and is directed by a beam splitter through a 0.1 m double monochromator to the PMT detector. Tungsten-halogen and mercury vapor lamps are used for internal calibration of the optical pathway. In order to minimize noise, the monochromator and PMT are located in individual temperature-controlled subassemblies.

A series of additional sensors are scanned simultaneously with the PMT and between the high resolution PMT scans. These provide reference data that can be used to track instrument operation and can also be used to normalize data for time varying changes in atmospheric conditions and system responsivity.

TABLE 1. Installation Sites

Site	Longitutde	Latitude	Established	Location
McMurdo	166.40°E	77.51°S	March 1988	Arrival heights
Palmer	64.03°W	64.46S	May 1988	Clean Air Building
South Pole	0	90.00°S	Feb. 1988	Clean Air Building
Ushuaia, Argentina	68°W	54.59°S	Nov. 1988	CADIC
Barrow, Alaska	156.61°W	71.32°N	Dec. 1990	

Typically this assembly is located on a building rooftop, away from obstructions. Only the irradiance collector and auxiliary sensors are located outdoors. Twice per month a calibration lamp fixture containing a Standard of Spectral Irradiance is mounted by the site operator atop the SMDA and a high resolution scan is performed. Following immediately, a scan of the internal tungsten-halogen source transfers the absolute calibration to the internal source.

The SMDA is controlled and data is acquired by the PCA. This assembly, located up to 50 feet from the SMDA, includes a personal computer and monitor, power control panel and supplies, precision voltmeter, and microcomputer-controlled peripheral interface modules. In addition to data acquisition, the computer processes UV irradiance measurements and performs intermediate calibrations automatically. Human attention is required only for data transfer, periodic manual absolute calibrations, and maintenance of the system.

3. RESULTS

The amount of short wavelength ultraviolet radiation incident on the earth is governed by several factors. Solar angle, cloud cover, and atmospheric gas concentration are the main factors. Although 1988-1990 showed considerable depletion of the ozone layer over Antarctica, the geographical distribution of the ozone hole as a function of time varies. A dramatic comparison of the impact of ozone depletion is seen in Figure 1. Here we compare spectral scans recorded at McMurdo at the same time on October 20 for 1988, 1989, and 1990. For this calendar day in 1988, the TOMS satellite reported total column ozone concentration of 386 Dobson Units (DU), a relatively high level; it was 161 DU in 1989; and 179 in 1990, with all years showing considerable temporal variation. Note that this calendar day was selected because of the wide range of readings that

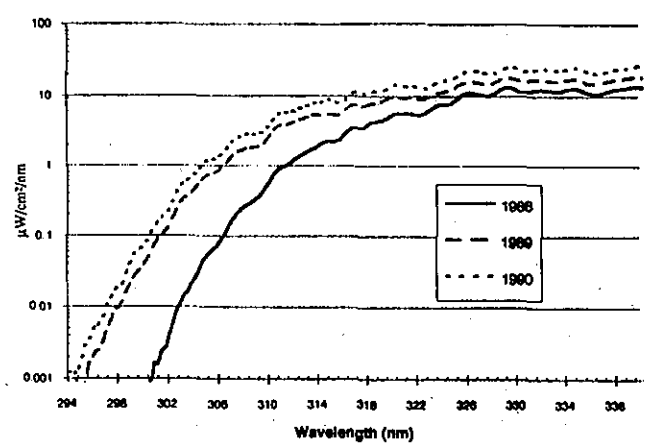

Fig. 1. Spectral irradiance as measured at McMurdo for October 20, 1988, 1989, and 1990.

occurred on this day over the 3 years. This wide range is not in itself indicative of annual trends in either ozone depletion or UV exposure at Antarctica.

To compare UV irradiances from the northern and southern polar regions, we selected data from sunrise to the solar maximum and expressed the time series in terms of the increasing solar zenith angle that is experienced during the spring as the sun progressively gets higher. This method of presentation compensates for the effect of sun angle on the measured irradiance. For the 1990-1991 "Ozone Hole Season," there are marked differences between the two example sites (Figure 2). McMurdo experienced generally larger integrated UV-B irradiances compared to Barrow as well as greater variability. This variability is indicative of the strong transient depletion in atmospheric ozone concentration experienced over McMurdo that was not experienced over Barrow. In considering the entire solar UV region of the spectrum, the observations are increasingly different as we examine shorter wavelengths.

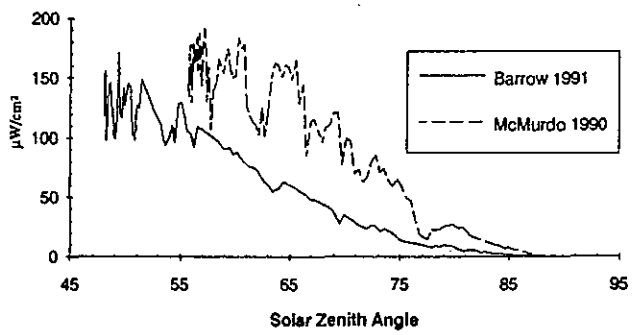

Fig. 2. Integrated UV-B irradiance (290-320nm) during the springtime for Barrow, Alaska and McMurdo, Antarctica, for a variety of solar zenith angles.

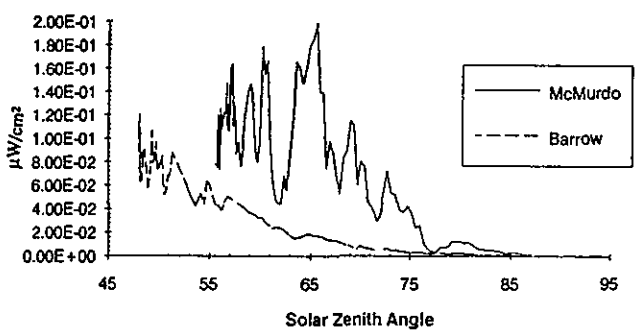

Fig. 3. Integrals (290-320nm) of DNA dose weighted irradiances [*Setlow*, 1974] for Barrow, Alaska and McMurdo, Antarctica, for a variety of solar zenith angles.

Most of the concern over ozone depletion has arisen due to the prediction that the resulting high levels of UV would have significant biological impact. The spectral expression of this impact is commonly called the dose weighting or action spectra weighting. Figure 3 shows the integral of the product of irradiance spectra as shown in Figure 1 and the DNA damage action spectra as determined by *Setlow* [1974], also as a function of solar zenith angle. The total UV dosage that an organism with a similar spectral susceptibility would receive can be expressed by this integral. For the most recent ozone-hole season, there was marked contrast in DNA dose weighted irradiance between McMurdo and Barrow for similar solar zenith angles. McMurdo experienced considerably higher DNA dose irradiances during the spring as well as significant local temporal variability as compared to Barrow.

4. Summary

The establishment of a monitoring network for UV radiation has been a critical part of the United States Antarctic Program. Its purpose is to evaluate the consequences of stratospheric ozone depletion on the health and productivity of Antarctic organisms and personnel. Data products resulting from this network include analyses of various measures of UV, including UVB, unweighted spectral integrals, and a variety of biologically weighted dosages. This monitoring network supports scientific researchers in Antarctica, and has provided independent confirmation of the role of the ozone layer in moderating UV solar irradiance.

Acknowledgments. This research and monitoring activity was funded by contract AOT00010 to Biospherical Instruments from Antarctic Support Associates (ASA). Dr. A. Kruger of NASA/GSFC provided TOMS Total Ozone data for comparison purposes. Prior to December 1990, the South Pole installation was the responsibility of NOAA personnel including J. Lowell and M. O'Neill. From December 1990 on, the system operation has been the responsibility of S. Redick of ASA. Barrow operators include Dr. D. Norton, D. Roghair, and NOAA/CMDL personnel D. Endres and C. Churylo.

Special thanks goes to Dr. Steve Kottmeier of ASA (and formerly ITT-ANS) who works with us on a daily basis to make it possible to accomplish this project in Antarctica. Data from the NSF UV Spectroradiometer Network is available to all qualified researchers. NSF grantees have priority access to these data. For more information, please contact: Dr. Polly Penhale, Division of Polar Programs, National Science Foundation, 1800 G St. N.W., Washington, D.C. 20550.

5. Reference

Setlow, R.B., The wavelengths in sunlight effective in producing skin cancer: a theoretical analysis, *Proceedings, National Academy of Science, 71(9)*, 3363-3366, 1974.

A Case Study of the Stable Lower Atmospheric Boundary Layer at Barrow, Alaska

TAK KEE CHEUNG

Institute of Marine & Coastal Sciences, Rutgers University, New Brunswick, New Jersey 08903

In late March and early April 1990, an experiment was performed at BRW. The main purpose of the experiment was to investigate what atmospheric phenomena are present under stable conditions in the Arctic and to field test, under winter conditions, the equipment that will be deployed in a future Arctic leads experiment (LEADEX) scheduled for 1992. Short time-scale atmospheric phenomena are of special interest here because the time scale of a lead is relatively short and is on the order of hours, or at the most a day or so; the spatial scale varies from meters to hundreds of meters wide and kilometers to tens of kilometers long [*Smith et al.*, 1990].

A monostatic sodar with real-time facsimile output was the primary instrument. In the monostatic (backscatter) mode, the sodar facsimile record provides a vertical profile of the intensity of small-scale temperature fluctuations [*Little*, 1969]. These fluctuations are generally associated with turbulence within regions of non-zero potential temperature gradient. Thus various atmospheric phenomena, such as temperature inversions and wave perturbations, can easily be detected by the sodar. Radiosondes were launched twice daily and were generally set to relatively low ascent rates (using 100-g balloons) to increase the vertical resolution of meteorological data. A tethered sonde system was deployed whenever conditions allowed (e.g., clearance from the local airport). The tethered balloon reached an altitude of about 1 km during its flights. Other data from the observatory tower such as wind speed and direction (at 17 m), pressure (9.5 m MSL), and air and dewpoint temperature (3 m) were averaged hourly and recorded.

The mean temperature hovered near approximately −16°C during the experiment, and daily temperature variations were between 5-12°C. This mean temperature is warmer than normal for late March and early April at BRW (e.g., the monthly mean temperature for March is −26°C from climatological records). The wind came mostly from the east or east northeast, which is the prevailing climatological wind direction. A strong temperature inversion persisted throughout this experiment. The temperature difference across the inversion varied between 8-13°C. Multiple inversion layers were observed in several soundings. With few exceptions, the stronger inversion layers were elevated. However, thin surface-based inversion layers with heights less than 150 m were frequently observed. In all soundings, major inversions seem to be confined to below 1.5 km. The temperature soundings are consistent with climatological data [*Kahl*, 1990].

A wide range of phenomena were recorded, including a solitary-like wave train similar to those observed by *Cheung and Little* 1990 (see their Figure 16). This is the only gravity wave train of this type recorded during the experiment; it is unclear whether this is an indication of the frequency of occurrence of such events in this region.

Multiple scattering layers (each at 6-10 m thick) were observed. During such time, even with a moderate wind speed near the surface, there appeared to be little perturbation of the boundary layer. The near-surface temperature was usually very cold during such occurrence. This may explain the lack of features other than the mostly unperturbed strata in an overall strongly stable stratification. Most of the visible changes were confined to within adjacent layers or within individual layers, which is another indication of strong stable stratification. Thus any shear-generated instability was at most strong enough to produce changes or mixing within adjacent layers.

The sodar also detected breaking waves as evidenced on the facsimile record by the braided structure characteristic of this type of event. High wind speed is usually observed with these breaking wave structures and is consistent with the results of similar observations. Vigorous mixing caused by continual wave breaking and turbulence generation beneath the inversion could explain the near-neutral conditions and the diffuse sodar return so often observed in the Arctic winter surface boundary layer [*Holmgren and Spears*, 1974]. A simple order-of-magnitude estimate indicates that the waves are indeed due to Kelvin-Helmholtz instability.

Additional cases as documented in *Cheung* [1991] are all just "snapshots" of the wide variety of activities that can occur during winter at BRW and probably along the Alaskan coast. Shear-generated Kelvin-Helmholtz instability seems to be the prominent mechanism in these chosen examples. In the absence of solar heating during Arctic winters, Kelvin-Helmholtz instability and the possible triggering of such instability by passing gravity waves, appear to be the dominant mechanisms in small-scale (meters to hundreds of meters) overturning and generation of centimeter-scale turbulence within the near-ground boundary layer. This mixing close to the surface may also explain why elevated inversion layers are often observed during Arctic winters. The transition from one case to another is very gradual as reported by *Holmgren and Spears* [1974].

The mesoscale or synoptic-scale activity may also influence the events described here. It is unclear if the low-level jet so often observed at BRW is associated with the processes described by *Kozo* [1980] and *Dickey* [1961]. *Neff and Hall* [1976] and *Neff* [1980] certainly claimed synoptic-scale influences for their observations in Antarctica.

Given the lack of local orography and the slowly changing synoptic conditions at BRW, it is quite surprising to find such a wide assortment of atmospheric structure and dynamics. In 1992, we plan a more comprehensive study on the pack ice 100-300 km from Prudhoe Bay as part of

LEADEX. The effects of open and newly frozen leads will be one of the primary objectives of the experiment. Besides a sodar, the radiosondes, and the tethered balloon used in the present study, further investigation of the Arctic boundary layer will encompass additional instruments, e.g. lead-site portable sodars, a UHF wind profiler with thermodynamic profiling capability (the radio acoustic sensing technique described by *May et al.*, 1989*a,b*) and a surface pressure array. Preliminary results from a pilot experiment near Prudhoe Bay in April 1991 indicated that these instruments performed well in the cold near a lead.

Acknowledgments. The author gratefully acknowledges the assistance of Scott Abbot, Catherine Russell, and Dan Wolfe in the planning, preparation, and implementation of the experiment. The BRW personnel provided invaluable logistics support for the experiment. The encouragement and support of C. G. Little and W. D. Neff made this study possible. The University Corporation for Atmospheric Research supported the research with funds supplied by the Atmospheric Directorate of the Naval Oceanographic and Atmospheric Research Laboratory, Monterey, California.

REFERENCES

Cheung, T. K., Sodar observations of the stable lower atmospheric boundary layer at Barrow, Alaska, *Boundary-Layer Meteorol.*, in press, 1991.

Cheung, T. K. and Little, C. G., Meteorological tower, microbarograph array, and sodar observations of solitary-like waves in the nocturnal boundary layer, *J. Atmos. Sci.*, *47*, 2516-2536, 1990.

Dickey, W.W., A study of a topographic effect on wind in the Arctic, *J. Meteorol. 18*, 790-803, 1961.

Holmgren, B. and Spears, L., Sodar investigation of the effect of open leads on the boundary layer structure over the Arctic basin, *AIDJEX Bulletin, 27*, 167-179, 1974.

Kahl, J. D., Characteristics of the low-level temperature inversion along the Alaskan Arctic Coast, *Int. J. Climat. 10*, 537-548, 1990.

Kozo, T. L., Mountain barrier baroclinity effects on surface winds along the Alaskan Arctic Coast, *Geophys. Res. Lett. 7*, 337-380, 1980.

Little, C. G., Acoustic methods for the remote probing of the lower atmosphere, *Proceedings, IEEE, 57*, 571-578, 1969.

May, P. T., Moran, K. P., and Strauch, R. G., The accuracy of RASS temperature measurements, *J. Appl. Meteorol.*, *28*, 1329-1384, 1989*a*.

May, P. T., Strauch, R. G., Moran, K. P., and Ecklund, W. L., Temperature sounding by RASS with wind profiler radars: A preliminary study, *IEEE Trans. Geosci. Remote Sens.*, *28*, 19-28, 1989*b*.

Neff, W. D., An observational and numerical study of the atmospheric boundary layer overlying the East Antarctic Ice Sheet, Ph.D. dissertation, University of Colorado, Boulder, 272 pp., 1980.

Neff, W. D. and Hall, F. F., Acoustic Sounder Measurements of the South Pole Boundary Layer, *Preprint Volume-17th Radar Meteorological Conference*, American Meteorological Society, Boston, 297-302, 1976.

Smith, S. D., Muench, R. D., and Pease, C. H., Polynyas and Leads: An Overview of Physical Processes and Environment, *J. Geophys. Res.*, *95*, 9461-9479, 1990.

Artificial Windshielding of Precipitation Gauges in the Arctic

GEORGE P. CLAGETT
Soil Conservation Service, Anchorage, Alaska 99501

1. INTRODUCTION

Precipitation gauges can provide good measurements of the water equivalent of snow precipitation, provided the gauge is protected or shielded from wind effects. Unfortunately, there are no standards for collecting snow precipitation. Gauges located in exposed and windy areas may be totally unshielded, partially shielded by one or more buildings, or equipped with one of several types of artificial shields. The various shielding options in common use, therefore, produce a wide range of gauge catch efficiency. Also, the various studies of artificial shields in the United States and Canada have produced a wide range of results. This must be, in part, due to the wide range of weather conditions under which the various studies have been conducted. A lingering problem is applying the results to the local conditions of Alaska's tundra regions.

2. METHODS

A study of the windshield alternatives, under the unique conditions of Alaska's Arctic coastal region, was set up at the CMDL facility at BRW during September 1989. Snowfall catches from four newly installed precipitation storage gauges were compared with that from an existing storage gauge protected by a Wyoming shield [*Hanson*, 1988]. Two of the new gauges were shielded—one with a Nipher shield [*Goodison et al.*, 1983] and the other with an Alter shield [*Alter*, 1937]—and two were unshielded. One of the unshielded gauges was serviced on an event basis, the same as the three shielded gauges. The other unshielded gauge was treated as if it were a remote gauge, allowing rime to build up and dissipate naturally to see what effects rime had on the overall catch. The four newly installed gauges are 20.3 cm in diameter × 100 cm tall, mounted with the orifice 2 m above the normal ground surface. The existing Wyoming-shielded gauge is 30.5 cm in diameter × 2 m tall, and is equipped with a Leupold-Stevens water-level recorder.

3. RESULTS

The 1990-1991 winter season, and second year of the study, was marked by a plumbing line blockage between the Wyoming-shielded precipitation gauge and the recording system. Seasonal totals were available for comparison between the Nipher, Alter, and unshielded gauges, however. Provisional results for the period October 18, 1990, to May 3, 1991, are as follows: the Nipher-shielded gauge caught a total of 39.6 mm snowfall moisture during the period. The Alter-shielded gauge caught 12.7 mm or 32% of the Nipher-shielded gauge. The unshielded but serviced gauge caught only 4.8 mm or 12% of the Nipher-shielded gauge. The unshielded and non-serviced gauge appears to have been leaking through the spring months. The results continue to confirm the unshielded and/or Alter-shielded gauges catch only one-third or less of the catches of Nipher-shielded (or Wyoming-shielded) gauges.

Acknowledgment. Appreciation is expressed to D. Endres, Station Chief, BRW, who serviced the precipitation gauges and collected the snow samples.

4. REFERENCES

Alter, S.C., Shield storage precipitation gauges, *Mon. Weather Rev.*, *65*, 262-265, 1937.

Goodison, B.E., V.R. Turner, and J.E. Metcalfe, A nipher-type shield for recording precipitation gauges, *Proceedings, 5th Symposium on Meteorological Observations and Instrumentation*, Toronto, Ontario, Canada, pp. 2-126, American Meteorological Society, Boston, 1983.

Hanson, C.L., Precipitation measured by gages protected by the Wyoming shield and the dual-gauge system, *Proceedings, 56th Western Snow Conference*, Kalispell, MT, pp. 174-177, Colorado State University, Fort Collins, 1988.

UVB Monitoring Data from Mauna Loa

DAVID L. CORRELL, CARL CLARK, RUSSELL GOODRICH, AND DOUGLASS HAYES
Smithsonian Environmental Research Center, P.O. Box 28, Edgewater, Maryland 21037

Our laboratory has been continuously monitoring surface irradiance at MLO in a series of eight 5-nm band passes in the UVB (290-325 nm) since the fall of 1984. Measurements are made with a precision, accurately calibrated, spectral radiometer [*Goldberg and Klein*, 1974; *Goldberg*, 1982]. These data are now being edited and analyzed for publication. Similar data from Rockville and Edgewater, Maryland (39°N, 77°W) for the period from 1975 through 1990 have been analyzed and submitted for publication. These Maryland data are available in archived format on floppy disks with de-archiving manual and software, for $100. Requests for data and additional information should be directed to David L. Correll, Director, at the above address.

TABLE 1. UVB Global Irradiance at MLO During Solar Eclipse July 11, 1991

Time	Filter Center Wavelength (nm)					Ratio
(LST)	304.9	310.8	314.7	320.2	325.3	04.9/320.2
0700	0.0154	0.1507	0.4109	1.0144	1.8030	0.0152
0705	0.0155	0.1440	0.3759	0.9011	1.5959	0.0168
0710	0.0142	0.1232	0.3113	0.7178	1.2416	0.0197
0715	0.0118	0.0972	0.2388	0.5349	0.9072	0.0220
0720	0.0074	0.0577	0.1374	0.3060	0.5169	0.0242
0725	0.0024	0.0172	0.0415	0.0896	0.1478	0.0264
0726	0.0014	0.0108	0.0245	0.0526	0.0874	0.0257
0727	0.0007	0.0049	0.0114	0.0242	0.0387	0.0281
0728	0.0001	0.0009	0.0020	0.0042	0.0085	0.0286
0729	0.0000	0.0000	0.0002	0.0000	0.0001	--
0730	0.0000	0.0002	0.0000	0.0000	0.0000	--
0731	0.0000	0.0001	0.0000	0.0001	0.0000	--
0732	0.0000	0.0000	0.0001	0.0006	0.0004	--
0733	0.0002	0.0014	0.0036	0.0068	0.0111	0.0336
0734	0.0011	0.0070	0.0155	0.0318	0.0510	0.0345
0735	0.0023	0.0150	0.0334	0.0685	0.1100	0.0340
0736	0.0039	0.0249	0.0545	0.1116	0.1708	0.0348
0740	0.0129	0.0816	0.1735	0.3461	0.5445	0.0374
0745	0.0321	0.1930	0.3974	0.7820	1.2404	0.0413
0750	0.0613	0.3500	0.7164	1.3957	2.1858	0.0438
0755	0.1010	0.5613	1.1242	2.1220	3.3316	0.0476
0800	0.1476	0.7994	1.5406	2.9276	4.4601	0.0504

Data are 1-minute averages. Units are J/M_2/nm/minute.

The MLO spectral radiometer was operating during the July 11, 1991, solar eclipse. Intensities in all spectral channels began to decline at 0701 LST, reached zero irradiance at 0729 LST, remained at zero values until 0732 LST, then increased to normal irradiance levels by 0830 LST. Plots of various UVB wavelength irradiance ratios did not reveal any unexpected or abnormal spectral quality shifts between 0700 and 0800. Spectral radiometer data are taken as 72 spectral scans per minute. One-minute averages are recorded on the data logger. Excerpted data from the eclipse period are given in Table 1.

REFERENCES

Goldberg, B., and W.H. Klein, Radiometer to monitor low levels of ultraviolet irradiance, *Appl. Opt.*, *13*, 493-496, 1974.

Goldberg, B., Radiometric measurements in the UV-B region of daylight, in *The Role of Solar Ultraviolet Radiation in Marine Ecosystems*, edited by J. Calkins, pp. 121-129, Plenum, New York, 1982.

South Pole Lidar

G. FIOCCO, M. CACCIANI, P. DI GIROLAMO, A. DI SARRA, AND D. FUA
Universita "La Sapienza" 00185 Roma, Italy

J. DE LUISI
NOAA, Climate Monitoring and Diagnostics Laboratory, Boulder, Colorado 80303

1. INTRODUCTION

A lidar has been operational at the Amundsen-Scott South Pole Observatory (SPO) since December 1987; it was installed as a cooperative project between the University of Rome and CMDL. The lidar is, in principle, capable of measuring vertical profiles of the volume backscattering cross-section of the atmosphere at the wavelength 532 nm in a height region extending from the boundary layer to the upper stratosphere. With these measurements it is possible to infer the molecular and aerosol concentration of air and to derive, under some conditions, other quantities such as atmospheric temperature.

The information obtained is relevant to studies of atmospheric radiation, structure and composition, and may be of particular interest in studies of the ozone hole depletion process. It is worth pointing out that in the polar night the lidar, being an active instrument, has distinct advantages when compared to other remote sensing techniques.

Possible information is categorized as follows: boundary layer aerosols; tropospheric aerosols; tropospheric clouds; stratospheric aerosols; stratospheric clouds; molecular density and stratospheric temperature; and gravity waves.

2. EXPERIMENTAL DETAILS

The system was installed in the Clean Air Facility (CAF) facing the SPO dome. A hatch, with a clear opening of approximately 0.9 m × 0.9 m, equipped with glass plates, permits zenith observations. The main characteristics of the lidar are given in Table 1. The data are stored in a binary form on a computer hard disk that is backed up periodically by minitape cartridges. During the winter compacted and formatted data, representing half-hour averages, are transmitted through the ATS-3 satellite link. The entire data set is physically carried to the University of Rome at station opening each November.

TABLE 1. Characteristics of the South Pole Lidar

Characteristics	Value
Wavelength	532 nm
Pulse energy	300 mJ nominal
Pulse duration	20 ns
Pulse repetition rate	4 Hz
Receiving telescope	0.5 m diam.
Transm. beam divergence	0.3 mrad
Filter bandwidth	1 nm
Vertical resolution	75 m
Photomultipliers	Cooled and gates 11 dynode EMI
Data acquisition	CAMAC+GPIB+286 based computer

Over the years the data acquisition system has had several changes to improve its performance and reliability. In particular, two channels for the measurement of the depolarization were added.

3. OPERATION

System operations have been taken care of by the winter-over personnel of CMDL with support from ASA personnel; during 1990 the system was operated by personnel from the University of Chicago. University of Rome personnel provide maintenance of the instrument each summer at SPO.

The system installed at SPO experienced a few unexpected problems, mostly originating from an underestimation of the temperature variability within the CAF. On more than one occasion the coolant inside the laser head froze, thus requiring major repairs involving substitution of various optical elements and realignment of the system. This job requires a degree of skill not normally available in the field. The origin of the trouble was discovered in retrospect, and during the austral summer 1990-1991, the problem was solved by improving the temperature stability inside the lidar room and rearranging the instrument so that the water pipes run as high as possible above the cold floor.

Measurements were carried out for a total of 19 days during May-October 1988, 55 days during November 1989-November 1990, and more than 50 days during the period November 1990-September 1991.

Recently, the operation of the laser has been kept at lower levels to assure conservative use of the laser, and during the current year no failures were reported to date.

4. RESULTS

In view of the reduced power levels that the system utilized, the work has concentrated on targets of relatively large cross-section. The observations have yielded significant data on polar stratospheric clouds. So far the only set of data that has been analyzed to some degree of detail are those of 1988, while the analysis of the 1989-1990 and 1990-1991 sets is in progress. The analysis has permitted completion of several studies, some already published and some in the process of review.

Fiocco et al., [1989] describes interesting correlations between peaks of the lidar backscattering profiles and relative minima of the ozone profiles.

Aerosol layers, generically identified as Polar Stratospheric Clouds (PSCs) were frequently observed in the period May-October 1988 throughout the altitude range 8-20 km. A recent paper *Fiocco et al.* [1991*a*] studied the temperature dependence of the lidar echoes from PSCs and suggested that the sensitivity of the lidar backscattering to temperature may define a criterion for cloud type identification. It was concluded that Type I PCs show a modest sensitivity to temperature and produce relatively diffuse echoes, while Type II PSCs show a larger sensitivity to temperature and produce backscattering values concentrated in sharply defined layers.

On the basis of the previous work, the behavior of the aerosol backscattering cross-section B_a has been related to the temperature T through linear fits between the two variables [*Fiocco et al.*, 1991*b*]. The resulting coefficients, namely the slope $b = dB_a/dT$ and T_c, the temperature where the onset of condensation occurs, help to classify these clouds as Type I or Type II in view of the thermodynamic properties of the condensing species. A strong dependence of B_a on T, represented by a large value of b, is interpreted as evidence of ice condensation and leads to identify the cloud at Type II, while a lower value of b, characteristic of diffuse structures, is taken as evidence for Type I clouds composed of nitric acid trihydrate. The evolution of these features is reported in a companion paper [*Fua et al.*, 1991]. Type II clouds, appearing as sharp layers of moderate vertical extent, are almost always present in the interval from June to early September. The temperature at the base of the lowest layer spans from an initial value around 198 K to a final value in September around 196 K, with a corresponding height value from around 1.5 km to 10.5 km. Layers that we identify as Type I clouds appear at higher temperatures with an onset at the beginning of the season around 200 K to a final value at mid-October around 203 K. Figure 1 shows a lidar echo for August 26, 1988. The figure also shows the temperature profile for the same day as well as the profile for the molecular echoes. Backscattering ratios are as large as 5. Large changes in the echo intensity appear to be associated with little changes in the temperature, characteristic of Type II PSCs. This is related to the large amount of condensable substance mobilized by a small change in temperature: particle sizes of several microns can be inferred. The extinction of the lidar signal after traversing the cloud layer is too small to be estimated, which is an indication of a very modest vaue for the optical thickness (<0.1).

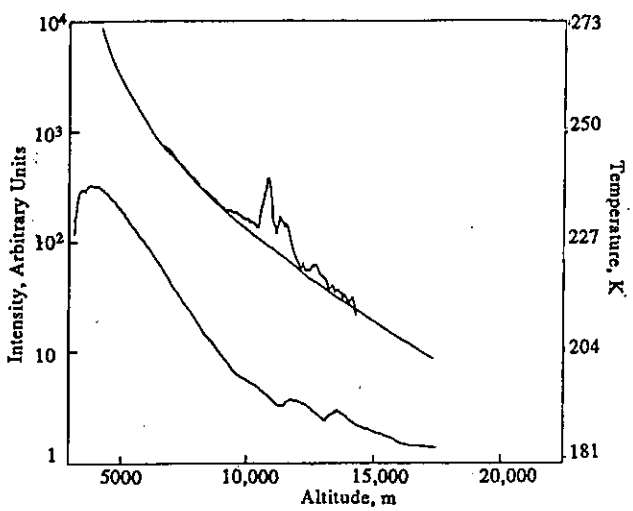

Fig. 1. Lidar echo (upper curve) superimposed to the computed molecular component of the signal, and atmospheric temperature profile (lower curve) obtained from radiosonde data for August 26, 1988.

5. References

Fiocco, G., W. Komhyr, and D. Fua, Is ozone destroyed during the Antarctic polar night in the presence of polar stratospheric clouds?, *Nature, 341*, 426-427, 1989.

Fiocco, G., D. Fua, M. Cacciani, and P. Di Girolamo, On the temperature dependence of polar stratospheric clouds, *Geophys. Res. Lett., 18*, 424-427, 1991*a*.

Fiocco, G., D. Fua, M. Cacciani, P. Di Girolamo, and J. DeLuisi, Stratospheric clouds at South Pole during winter 1988: 1) Results of the lidar observations and their relationship to temperature, submitted *J. Geophys. Res.*, 1991*b*.

Fua, D., M. Cacciani, P. De Girolamo, G. Fiocco, and A. di Sarra, Stratospheric clouds at South Pole during winter 1988: 2) Their evolution in relation to atmospheric structure and composition, submitted *J. Geophys. Res.*, 1991.

Total Nitrate Variations at Mauna Loa

B. J. HUEBERT AND G. L. LEE

University of Rhode Island, Graduate School of Oceanography, Narragansett, Rhode Island 02882-1197

1. INTRODUCTION

Much of the NO and NO_2 which is emitted into the atmosphere is converted to nitric acid vapor or aerosol nitrate before it is removed by dry or wet deposition. This conversion to nitrate is largely complete within a few days of the odd-nitrogen's emission, so that in remote areas such as at MLO, the total nitrate concentration (vapor plus aerosol) represents a fair estimate of the total odd-nitrogen concentration.

With support from NSF, we have measured nitrate concentrations at MLO for several years to help identify the important sources of odd-nitrogen compounds in remote parts of the globe. We now measure total nitrate every night from the walkup tower, in collaboration with the MLO staff.

2. MATERIALS AND METHODS

We use a Teflon/nylon filter-pack method for collecting atmospheric nitrate. Since August 1988, one filter is exposed each night, from 2000 LST to 0800 LST. Filters are returned to our URI laboratory for extraction and analysis by ion chromatography. Our final data are sorted using three criteria (wind direction, humidity, and CN count) to eliminate those samples that have been influenced by local sources on the island.

3. RESULTS AND DISCUSSION

During our intermittent MLO sampling prior to September 1988, we observed a sharp maximum in nitric acid and aerosol nitrate concentrations in the summer. The search for an explanation for this maximum continues to stimulate our science.

The daily values for 1990 are plotted in Figure 1. The lowest sustained concentrations are still evident in the winter, with a mix of high-concentration events and clean periods in the spring and late summer.

Now that our nightly sampling has completed almost 3 full years, the same trend is evident in this data. Figure 2 shows monthly averages of 2000 LST to 0800 LST total nitrate concentrations from September 1988 to July 1991. As is often the case when a data set finally spans several years, we are just beginning to see how different the annual cycle is from year to year. While the summer maximum/ winter minimum ratio was about five in 1989, it appears to be only two or three in 1991. (All the 1991 summer data is not yet included though, so this conclusion could change somewhat.) Clearly, we need to identify the climatological differences which cause this dramatic change in the annual cycle of nitrate.

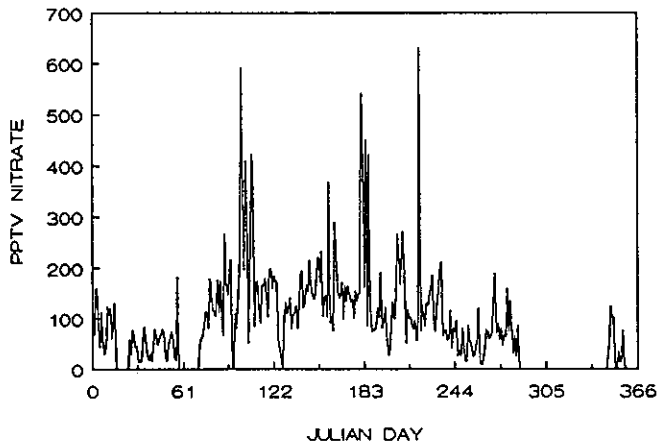

Fig. 1. Nightly concentrations of total nitrate in 1990.

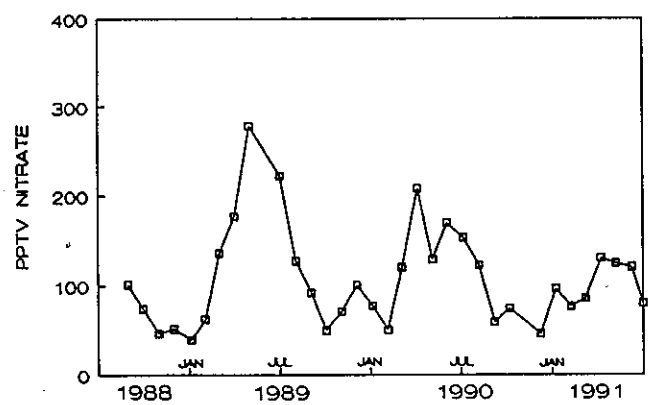

Fig. 2. Monthly average total (aerosol plus vapor) nitrate versus time.

4. ONGOING RESEARCH

We are continuing our inclusive nightly sampling from the tower, with the help of the MLO staff. Although equipment failures and bad weather (preventing filter changes on the tower) have occasionally caused brief lapses in the data, a very interesting record is emerging. We hope to identify both the frequency and source of high-nitric events during the next year or so, as well as the factors that control the form and the range of its annual cycle.

Temperature Inversions in the Canadian Arctic

JONATHAN D. KAHL
University of Wisconsin, Department of Geosciences, Milwaukee, Wisconsin 53201

MARK C. SERREZE AND RUSSELL C. SCHNELL
CIRES, University of Colorado, Boulder, Colorado 80309

1. INTRODUCTION

Here we describe one aspect of an ongoing project to acquire, assimilate and analyze all available arctic rawinsonde data dating back to the 1940s. Published results to date include studies by *Kahl* [1990], who examined temperature inversions at Alaskan Arctic stations, and *Serreze et al.* [1991], who extended Kahl's analysis to include inversions in the Eurasian Arctic. In this paper we report on our efforts to further extend our analyses of inversion characteristics to the Canadian Arctic. A full description of results are given by *Kahl et al.* [1991].

2. DATA BASE

Historical time series of rawinsonde measurements made at the thirteen Canadian Arctic stations were obtained on magnetic tape from NCAR in Boulder, Colorado. These measurements consist of vertical profiles of temperature, moisture, wind, geopotential height and pressure throughout the troposphere and lower stratosphere (typically to altitudes of 25-30 km). The station locations are shown in Figure 1. The stations provide reasonably good spatial coverage throughout the Canadian Arctic, extending from 65°N (Norman Wells) to 82.5°N (Alert) and from 133.5°W (Inuvik/Aklavik) to northwest Greenland and Baffin Bay (Alert and Clyde River).

The Canadian Arctic rawinsonde data base is summarized in Table 1. Data records of over 30 years in length are available for 9 of the 13 stations. Forty-year records were available from three of the stations (Resolute, Eureka, and Mould Bay). The remaining four stations have a minimum of 10 years of available data. Between 10,000-26,000 usable soundings are available from all stations except Arctic Bay, yielding a total of 245,070 soundings in the final analysis.

All soundings were checked for quality and completeness using procedures described by *Serreze et al.* [1991]. Application of the quality control procedures forced us to discard 10% of the approximately 270,000 original soundings.

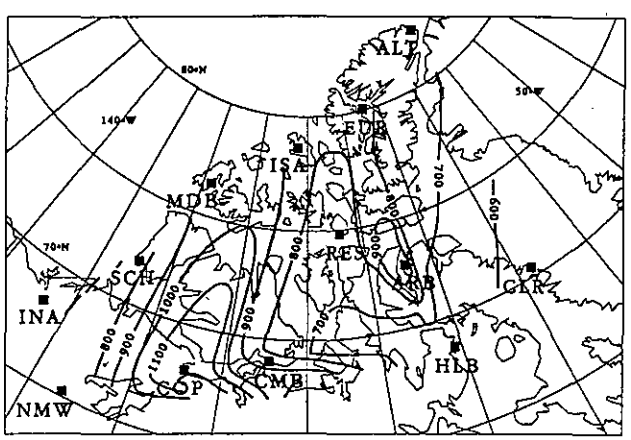

Fig. 1. Contour diagrams showing the median inversion depth (m) for February in the Canadian Arctic. Extrapolation beyond original data points has been avoided.

3. METHODOLOGY

We are concerned with low-level inversions, defined as those with a base below the 700 mb level. Inversions are identified objectively using the algorithm developed by *Kahl* [1990]. This algorithm was also used by *Serreze et al.* [1991] to examine inversions over the Eurasian Arctic. Briefly, the procedure is to scan each sounding from the surface upwards, identifying the inversion base as the bottom of the first layer in which temperature increases with altitude. The inversion top is defined as the bottom of the first subsequent layer in which the temperature decreases with altitude. Since arctic temperature profiles often exhibit a complicated vertical structure [*Belmont*, 1957], negative-lapse layers are frequently encountered in the lower levels of the sounding. If these layers are thin (with a critical thickness arbitrarily defined as 100 m), they are considered to be imbedded within the overall inversion layer. Illustrative examples of this technique are given by *Kahl* [1990]. Inversions were found in 89% of all usable soundings.

4. RESULTS

Our results consist of descriptions of the spatially-and temporally-varying features of the inversion. Because the complete analysis is presented elsewhere [*Kahl et al.*, 1991], we present only one sample result here.

Inversions are generally surface-based in winter, with maximum depths and temperature differences occurring in February or March. February is representative of wintertime conditions and was chosen for presentation because, unlike March, there is a lack of sunlight during the entire month. In February, inversions occur in at least 98% of the soundings examined at all stations. During February the median height of the inversion base is zero (i.e., surface-based) at all stations except Norman Wells, where it is 114 m. The tendency for wintertime inversions to be elevated at Norman Wells may be due to its proximity to Great Bear Lake, where ice concentrations are slightly

TABLE 1. Summary of rawinsonde data analyzed.

Station Name	Latitude (°N)	Longitude (°W)	Elevation (m msl)	Period of Record	No. of Soundings
Alert (ALT)	82.50	62.33	6*	1950-1987	23,983
Eureka (EUR)	80.22	86.18	10	1948-1987	25,480
Isachsen (ISA)	78.78	103.53	25	1948-1978	18,736
Mould Bay (MDB)	76.23	119.33	12*	1948-1987	24.927
Resolute (RES)	74.72	94.98	67*	1948-1987	25,649
Arctic Bay (ARB)	73.00	85.30	10	1948-1957	5,660
Sachs Harbor (SCH)	71.95	124.73	86*	1955-1986	19,401
Clyde River (CLR)	70.45	68.55	25*	1950-1970	13,254
Cambridge Bay (CMB)	69.10	105.13	27	1970-1987	10,637
Hall Beach (HLB)	68.78	81.25	8*	1957-1987	19,144
Inuvik/Aklavik (INA)	68.32	133.53	103	1950-1987	24,170
Coppermine (COP)	67.82	115.08	9*	1947-1970	13,489
Norman Wells (NMW)	65.28	126.80	73*	1955-1987	20,540

Total number of soundings analyzed: 245,070†

*Reported station elevation beginning January 1, 1961. Elevations reported prior to this were slightly different.
†This number is 90% of the total number of available soundings. The remaining 10% were discarded due to insufficient data quality or completeness (see text).

less than in the waters of the Canadian Archipelago [*Parkinson et al.*, 1987].

The deepest inversions (Figure 1) occur at Coppermine (median value 1177 m) and Arctic Bay (median value 926 m). The spatial gradient in inversion depth reflects the fact that the inversion is a dynamic feature controlled by a number of direct and indirect forcings, including solar and terrestrial radiation, synoptic meteorological activity (i.e. the passage of cyclones that can mix the boundary layer and break down the inversion), latent heat factors related to snowmelt, and the sea-ice cover over the Arctic Ocean, and the waters of the Canadian Archipelago.

5. SUMMARY

The spatial and temporal variability of the low-level arctic temperature inversion has been investigated using 10-40 years of rawinsonde data at 13 Canadian Arctic stations. Inversions were present in 89% of the 245,070 soundings analyzed.

As reported in detail in *Kahl et al.* [1991], our analysis of the month-to-month variability in inversion characteristics revealed:

(1) Inversions at Alert, Isachsen, and Mould Bay, three of the four northernmost stations, are primarily surface-based from autumn through midspring and elevated from midspring through summer. At all other stations the height of inversion base shows a bimodal pattern with peaks in late spring and late summer.

(2) At all stations the inversion depth peaks in February or March. Maximum median values range from 545 m at Clyde River to 1177 m at Coppermine. Minimum median inversion depths found in September, range from 212 m at Cambridge Bay to 457 m at Arctic Bay. The annual progression of inversion depth parallels the progression of clear-sky percentages.

(3) The month-to-month variability in temperature difference across the inversion is similar to that of inversion depth. Maximum median values range from 14°C at Eureka to 5°C at Clyde River. Minimum median values of 1-2°C are found between August and September at all stations.

Analysis of the spatial variability in inversion characteristics showed:

(1) Winter. Inversions are primarily surface-based at all stations. Elevated inversions are frequently found only at Norman Wells. The deepest inversions occur at the Archipelago stations Coppermine and Arctic Bay. The largest temperature inversions occur at the northern stations Mould Bay, Isachsen, and Eureka, and at the inland/coastal stations Norman Wells, Inuvik/Aklavik, and Cambridge Bay. Inversion intensity showed a similar pattern.

(2) Summer. Total inversion frequency generally increases with latitude with a local minimum observed at Arctic Bay. Elevated inversion frequency exhibits essentially the same pattern, which is expected since summertime inversions are mostly elevated. The height of inversion base shows an irregular spatial pattern. Inversion depth and temperature difference shows little spatial

variability, as inversions are characteristically weak in summer.

6. REFERENCES

Belmont, A.D., Lower tropospheric inversions at ice island T-3, *J. Atmos. Terres. Phys., Special Supplement*, 1957.

Kahl, J.D., Characteristics of the low-level temperature inversion along the Alaskan Arctic coast, *Int. J. Clim., 10*, 537-548, 1990.

Kahl, J.D., M.C. Serreze, and R.C. Schnell, Tropospheric low-level temperature inversions in the Canadian Arctic, *Atmos. Ocean*, submitted, 1991.

Parkinson, C.L., J.C. Comiso, H.J. Zwally, D.J. Cavalieri, P. Gloersen, and W.J. Campbell, Arctic sea ice, 1973-1976: Satellite passive-microwave observations, *NASA SP-489*, National Aeronautics and Space Administration, Washington, DC, 296 pp., 1987.

Serreze, M.C., J.D. Kahl, and R.C. Schnell, Low-level temperature inversions of the Eurasian Arctic and comparisons with Soviet drifting station data, *J. Clim.*, submitted, 1991.

The Historical Arctic Rawinsonde Archive

JONATHAN D. KAHL
Department of Geosciences, University of Wisconsin-Milwaukee, Milwaukee, Wisconsin 53201

MARK C. SERREZE AND RUSSELL C. SCHNELL
CIRES, University of Colorado, Boulder, Colorado 80309

1. INTRODUCTION

This document briefly describes the Historical Arctic Rawinsonde Archive, compiled under support from the NOAA Climate and Global Change Program (Grant NA85RAHO5066) and the Electric Power Research Institute (Grant RP2333-07). The archive comprises over 1.2 million vertical soundings of temperature, pressure, moisture and wind, and contains all available rawinsonde ascents from Arctic land stations north of 65°N from the beginning of record through 1987.

For most stations, the record begins in 1957 (the International Geophysical Year), but for a few stations, particularly Canadian stations, the record begins in 1948; it is in a user-friendly, ASCII format which may be easily processed by most types of computers. All data have been passed through error-checking routines. Plans are to periodically update this archive as additional data become available.

2. DATA SOURCES AND COVERAGE

Sounding data were obtained from NCAR in Boulder, Colorado, and NCDC in Asheville, North Carolina. Five original archives were used to compile our data base:

(1) Asian Arctic, 1976-1987: Soundings from Soviet and Scandinavian Arctic stations, Greenland, and "Ship M," a moored ship in the Norwegian Sea.

(2) Victor Starr, 1958-1963: This archive was compiled by Professor Victor Starr at MIT during the late 1960s, and contains soundings from 75 stations throughout the Arctic.

(3) Canadian Stations: Soundings from regularly reporting Canadian Arctic rawinsonde stations. The record for some stations begins as early as 1948, but most stations started reporting regularly in the early to mid 1950s.

(4) Alaska and Thule, Greenland: The record begins in 1947 for Barrow, Alaska; in 1952 for Barter Island, Alaska; and in 1952 for Thule, Greenland.

(5) Asian Arctic, 1962-1975: Similar to the archive (1) (described above), but in a slightly different original format and containing fewer stations. There is a considerable amount of data overlap between original sources. An effort has been made to choose the best available data from each original archive, based on error analyses and completeness of the soundings.

A list of stations for which sounding data are available is presented in Table 1. In the table, an asterisk beneath a particular year indicates that sounding data are available for at least part of that year. A total of over 1.2 million soundings are available, covering a 30-year period for most stations.

The station locations are shown in Figure 1. Note that the global, land-based coverage is relatively uniform with the exception of the lack of stations over the interior of Greenland. Depending on the station, soundings are available from one to four times daily at 0000 GMT, 0600 GMT, 1200 GMT, and 1800 GMT. Most often, reports are available at 0000 GMT and 1200 GMT. Prior to 1952, reporting times were 0800 GMT and 1400 GMT.

3. DATA COMPILATION AND ERROR CHECKING

In order to produce a consistent, single-format archive, it was necessary to perform a variety of sorting, merging, and quality-control tasks. The error-checking procedures first involved the elimination of obvious errors such as negative wind speeds. All soundings were then passed through a seasonally-adjustable limits check to screen out gross errors. We recognize that our procedure may not identify all errors and that on occasion what we flag as errors may in fact be valid data. As such, we retain the original data and give the user the option of (1) adhering to our determination of data quality; (2) adhering to the quality codes present in the five original archives (which we have included in the final

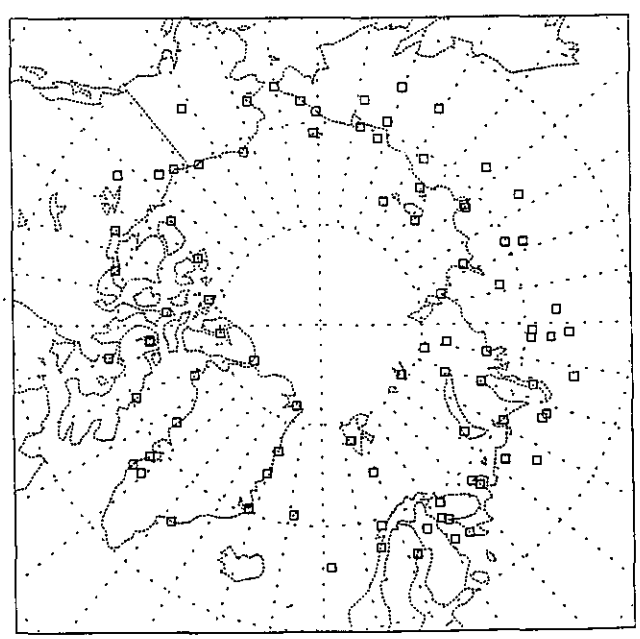

Fig. 1. Locations of rawinsonde reports contained in the Historical Arctic Rawinsonde Archive.

TABLE 1. Summary of the Soundings Contained in the Historical Arctic Rawinsonde Archive

STATION ID	NAME	COUNTRY	LAT DEG N	LON DEG E	# OF SOUNDINGS	DATA AVAILABLE
1001	JAN MAYEN	NORWAY	70.93	-8.67	15561	**********
1005	ISFJORD RADIO	NORWAY	78.07	13.63	983	***** * ***
1010	ANDOYA	NORWAY	69.30	16.12	22	***
1020			0.	0.	1237	******
1028	BJORNOVA	NORWAY	74.52	19.02	16972	**********
1030			0.	0.	2424	******
1152	BODO	NORWAY	67.28	14.42	17005	**********
2057	16LULEA/KALLAX	SWEDEN	65.60	22.10	5881	**********
2185			0.	0.	10000	**********
2836	SODANKYLA	FINLAN	67.37	26.65	25290	**********
4202	THULE AFB	GREENL	76.53	-68.75	42617	**********
4210	UPERNAVIK	GREENL	72.78	-56.17	221	*** **
4220	EGEDESMINDE	GREENL	68.70	-52.75	16727	**********
4230	HOLSTEINBORG	GREENL	66.92	-53.67	12	* ** *
4231	SDR. STROMFJORD	GREENL	67.00	-50.80	4	* *
4310	NORD	GREENL	81.60	-16.67	5512	********** * *** * ** *
4320	DANMARKSHAVN	GREENL	76.77	-18.77	15450	**********
4330	DANEBORG	GREENL	74.30	-20.22	7	***
4339	SCORESBYSUND	GREENL	70.48	-21.97	4819	********
4340	KAP TOBIN	GREENL	70.42	-21.97	11819	**********
4360	ANGMAGSSALIK	GREENL	65.60	-37.63	16452	**********
20046	OSTROV HEISA	SOVIET	80.62	58.05	20826	**********
20047			0.	0.	1649	******
20069	OSTROV VIZE	SOVIET	79.50	76.98	18358	**********
20107	BARENTSBURG	SOVIET	78.07	14.22	20289	**********
20274	OSTROV UEDINENIA	SOVIET	77.50	82.23	17337	**********
20292	MYS CHELIUSKIN	SOVIET	77.72	104.28	19396	**********
20353	MYS ZHELANIA	SOVIET	76.95	68.58	18207	**********
20406			0.	0.	2	*
20667	OSTROV BELYJ	SOVIET	73.33	70.03	8709	**********
20674	OSTROV DIKSON	SOVIET	73.50	80.23	17487	**********
20744	MALYE KARMAKULY	SOVIET	72.38	52.73	13088	****** ******** **********
20891	KHATANGA	SOVIET	71.98	102.27	16753	********** *****
21358	OSTROV ZOHOVA	SOVIET	76.15	152.83	15375	**********
21432	OSTROV KOTELNY	SOVIET	76.00	137.90	18983	**********
21504	OSTROV PREOBRAZHENIA	SOVIET	74.67	112.93	20447	**********
21647	MYS SHALAUROVA	SOVIET	73.18	143.93	18181	**********
21824	BUKHTA TIKSI	SOVIET	71.58	128.92	19476	**********
21825	OSTROV MOSTAKH	SOVIET	71.53	129.92	2	*
21908	DZHALINDA	SOVIET	70.13	113.97	4	* *
21946	COKURDAH	SOVIET	70.62	147.88	11238	**********
21965	OSTROV CHETYREKHSTOLBO	SOVIET	70.63	162.40	17650	**********
21982	OSTROV VRANGELYA	SOVIET	70.97	181.47	16430	**********
22113	MURMANSK	SOVIET	68.97	33.05	23186	**********
22165	KANIN NOS	SOVIET	68.65	43.30	1803	*****
22205	ENA	SOVIET	67.60	31.17	4	**
22217	KANDALASKSA	SOVIET	67.13	32.43	21051	**********
22271	SOJNA	SOVIET	67.88	44.13	20852	**********

TABLE 1. Summary of the Soundings Contained in the Historical Arctic Rawinsonde Archive - Continued

ID	STATION NAME	COUNTRY	LAT DEG N	LON DEG E	# OF SOUNDINGS	DATA AVAILABLE 4 5 5 6 6 7 7 8 8 9 / 8-0----5----0----5----0----5----0----5----0
22408	KALEVALA	SOVIET	65.20	31.17	2	*
22522	KEM-PORT	SOVIET	64.98	34.78	5660	**********
23022	AMDERMA	SOVIET	69.77	61.68	18284	**********
23074	DODINKA	SOVIET	69.40	86.17	2231	******* **
23078	NORILSK	SOVIET	69.32	88.22	8777	********
23130			0.	0.	6	* *
23146	MYS KAMENNY	SOVIET	68.47	73.60	18944	**********
23162			0.	0.	10	* *
23205	NARJAN MAR	SOVIET	67.65	53.02	24628	**********
23274	IGARKA	SOVIET	67.47	86.57	5356	**********
23330	SALE-KHARD (OBDORSK)	SOVIET	66.53	66.53	20461	**********
23338	POLUY	SOVIET	66.27	67.87	96	**********
23383	AGATA	SOVIET	66.93	93.47	2	*
23418	PECHORA	SOVIET	65.12	57.10	23793	**********
23472	TURUKHANSK	SOVIET	65.78	87.95	21946	**********
23552	TARKO-SALE	SOVIET	64.92	77.82	1478	********
24125	OLENEK	SOVIET	68.50	112.43	15175	**********
24266	VERKHOYANSK	SOVIET	67.55	133.38	19425	**********
24343	ZHIGANSK	SOVIET	66.77	123.40	21842	**********
25042	AYON	SOVIET	69.93	167.97	6272	****** **********
25123	NIZHNIE KRESTIY/CERSKI	SOVIET	68.80	161.28	18090	****** **********
25173	MYS SCHMIDT	SOVIET	68.92	180.52	18478	**********
25248	ILIRNEYJ	SOVIET	67.33	168.23	3	*
25282	VANKAREN	SOVIET	67.85	184.37	73	********
25399	MYS UELEN	SOVIET	66.17	190.17	7373	**********
25400	ZYRIANKA	SOVIET	65.73	150.90	13294	**********
25428	CHERBAROVO	SOVIET	65.23	160.50	13838	**********
70026	BARROW, AK	ALASKA	71.30	-156.78	27713	**********
70086	BARTER IS., AK	ALASKA	70.13	-143.63	24613	**********
70133	KOTZEBUE, AK	ALASKA	66.87	-162.63	4869	**********
70192	145UNIVERSITY EXP STA	USA	64.90	-147.90	2	*
71043	NORMAN WELLS, NT	CANADA	65.28	-126.80	23631	**********
71051	SACHS HARBOUR, NT	CANADA	72.00	-125.27	22302	**********
71072	MOULD BAY, NT	CANADA	76.23	-119.32	28243	**********
71074	ISACHSEN, NT	CANADA	78.68	-103.53	21518	**********
71081	HALL BEACH, NT	CANADA	68.78	-81.25	22020	**********
71082	ALERT, NT	CANADA	82.50	-62.33	26745	**********
71090	CLYDE, NT	CANADA	70.47	-68.62	13867	********** *
71914	NANISIVIK, NT	CANADA	72.97	-84.53	2	*
71917	EUREKA, NT	CANADA	80.00	-85.93	28437	**********
71918	ARCTIC BAY, NT	CANADA	73.03	-85.15	5697	* ******** *** *
71924	RESOLUTE BAY, NT	CANADA	74.72	-94.95	29933	**********
71925	CAMBRIDGE BAY, NT	CANADA	69.10	-105.13	13122	** * **********
71938	COPPERMINE, NT	CANADA	67.82	-115.13	14132	**********
71957	INUVIK, NT	CANADA	68.30	-133.48	19942	**********
71968	SHINGLE POINT, YT	CANADA	68.93	-137.23	7056	**********
C7M			66.00	2.00	15521	* * **********
TOTAL					1,220,713	

archive); or (3) making their own determination of data quality. The data processing and error-checking procedures are described in detail in *Serreze et al.* [1991].

4. Accessing the Archive

The data base is currently archived on 9-track magnetic tape at the National Snow and Ice Data Center at the University of Colorado in Boulder. Efforts to transfer the archive to CD-ROM media are in progress. Requests for the data base may be directed to the Data Center in Boulder.

5. Reference

Serreze, M.C., J.D. Kahl, and S. Shiotani, The historical Arctic rawinsonde archive documentation manual. In preparation (preprint available from J. Kahl, Dept. of Geosciences, University of Wisconsin-Milwaukee, P.O. Box 413, Milwaukee WI 53201), 1991.

Trajectory Forecasting for Misers Gold

JONATHAN D. KAHL
University of Wisconsin-Milwaukee, Department of Geosciences, Milwaukee, Wisconsin 53201

RUSSELL C. SCHNELL AND PATRICK J. SHERIDAN
CIRES, University of Colorado, Boulder, Colorado 80309

1. INTRODUCTION

Here we describe an experiment where a real-time trajectory forecast model was used to estimate the transport of debris associated with a large chemical explosion in the southwestern United States. The trajectory forecasts were used to vector sampling aircraft into a position favorable for intersecting the debris cloud. Full details of the experiment have been reported by *Kahl et al.* [1991].

On June 1, 1989, the U.S. Defense Nuclear Agency conducted a high explosive test at White Sands Missile Range (WSMR) in southern New Mexico. The explosive charge consisted of 2.21×10^6 kg of ammonium nitrate fuel oil slurry that provided an airblast approximately equivalent to that which would be generated by a 4 kiloton nuclear device. The program, called "Misers Gold", included 180 experiments designed to collect basic explosive environmental data and to test the performance of various systems and structures in a simulated nuclear environment [*Lutton*, 1989].

Trajectory forecasts, prepared in the field using a real-time trajectory forecast model, were used to track the position of the debris cloud after the winds had carried it beyond visual range. For the forecast trajectory model, the NOAA program for operational trajectories model [*Heffter and Stunder*, 1987] was used. The model uses archived wind data from the U.S. National Meteorological Center's Nested Grid Model (NGM). Forward or backward trajectories may be run in forecast mode using prognostic fields from the NMC forecast models, in diagnostic mode using observed data, or in a combined diagnostic/forecast mode. Both two- and three-dimensional trajectories are available at a number of vertical levels from 1000 mb to 100 mb. In this study only forward, quasi-two-dimensional (isobaric) trajectories were used. All trajectories were calculated at the 500-mb level.

Beginning 39 hours before the blast, forward trajectories were initiated at the Misers Gold detonation site at WSMR. The forecast trajectories were programmed to start at 1500 UT on June 1, 1989, to correspond as closely as possible to the planned blast time of 1500 UT (the actual blast occurred at 1530 UT). The trajectories were updated every 12 hours as new data from the NGM prognostic model became available. After the blast, trajectory forecasts originating at intermediate debris cloud positions were calculated to test the ability of the trajectory model to project the balloon and debris transport in real time using location updates.

The accuracy of the trajectory forecasts is evaluated by comparing the forecast trajectories with diagnostic (after-blast) trajectories based on observed rather than forecast meteorological data and by comparing the projected cloud position with aircraft measurements of explosion debris. The diagnostic trajectories were calculated using the isobaric model described by *Harris* [1982].

2. RESULTS AND DISCUSSION

Forecast Misers Gold debris trajectories are shown in Figure 1. The legends indicate the time, relative to the blast, that the forecasts were prepared. For example, the legend "T-39" refers to the trajectory calculated using NGM forecast winds based on meteorological observations at 0000 UT on May 31, 1989, 39 hours before the planned blast time. Trajectory forecasts were made at *T*-39 hr, *T*-27 hr, *T*-15 hr and *T*-3 hr. Also shown is the post-blast diagnostic trajectory determined from the observed wind fields.

Inspection of Figure 1 shows that the forecast trajectories predicted the diagnostic trajectory quite well. All trajectories clearly track in the correct northeasterly direction, although there are some differences in speed. Note that the forecasts improved as the trajectory initiation time approached the blast time. The position errors were small, however, all trajectories reflect the southwesterly flow at 500 mb as depicted by weather charts (not shown).

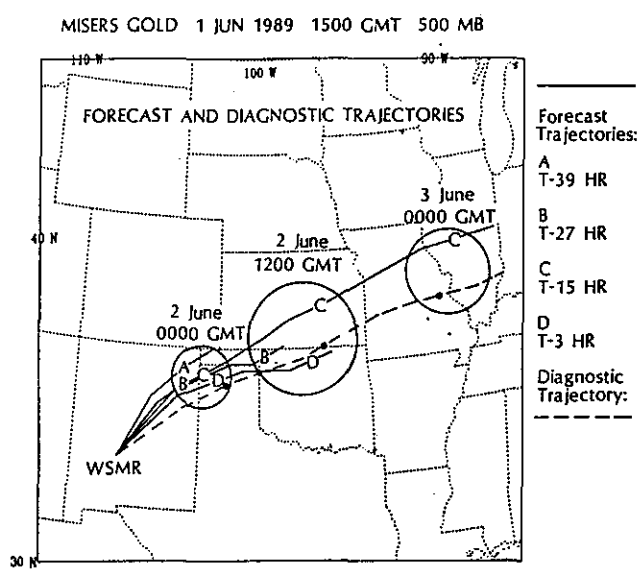

Fig. 1. Forecast and diagnostic 500 mb trajectory positions. Legends indicate the time, relative to the planned blast time of 1500 UT, June 1, that the trajectory forecasts were prepared. For example, the legend "T-39 hr" refers to the trajectory calculated using NWS forecast winds based on then-current meteorological observations available 39 hours before the blast, on 0000 UT, May 31, 1989. The symbols A, B, C, D and solid circles depict times as indicated by the large circles.

The differences in the trajectories in Figure 1 are within the numerical uncertainty limits ascribed to trajectory models [*Kahl and Samson*, 1986]. These uncertainties are related to the limited spatial and temporal resolution of the meteorological data, the dynamics of the weather situation under study, and the performance of the meteorological forecast model. Despite these unavoidable uncertainties, the forecast trajectories compared well with the diagnostic trajectory, confirming the quality of the meteorological forecast data upon which the forecast trajectories are based.

The "acid test" of any forecasting technique is a comparison of the forecast with independent observations of the variable or variables of interest. In the Misers Gold trajectory forecasting experiment, the necessary observations are downwind measurements of an indium tracer (In_2O_3) that had been placed within the explosive charge. These measurements are available as instrumental neutron activation analyses of debris samples collected by the Los Alamos National Laboratory (LANL) aircraft chase team. Descriptions of the sampling and analytical techniques are given by *Lutton* [1989] and *Mason et al.* [1990]. Chemical analyses of the samples confirm that our forecasts of the debris cloud transport were correct. In this section we describe the trajectory forecasts used to vector the aircraft into a proper sampling position.

During the Misers Gold experiment we were asked to vector the LANL aircraft to a position favorable for intercepting the debris cloud at the 500 mb level. At 2227 UT on June 1, a request was made for a June 2, 1700 UT sampling location, which would be 26.5 hours downwind of the blast at WSMR. We therefore initiated a trajectory forecast at the best visual estimate of the debris cloud position available to us at that time.

The evaluation of this forecast is shown in Figure 2. The LANL aircraft sampling took place from 1530-1700 UT rather than being centered at 1700 UT as originally scheduled. The line labeled "F" is the real-time after-blast trajectory forecast discussed above; the line labeled "D" is a diagnostic trajectory computed later using observed data. The estimated sampling location given to the aircraft crew is indicated by "M". This location, judged to be along the most probable path of the debris cloud, was assumed to be slightly to the north of the forecast trajectory (line "F").

Significant concentrations of the indium tracer were found in short (~40 km) sampling traverses centered around point "M". Figure 2 shows that the after-blast trajectory (line "F") compared favorably with the diagnostic trajectory, especially considering the fact that the trajectory crossed a region with significant convective precipitation [*Kahl et al.*, 1991]. While the forecast and diagnostic trajectories followed nearly identical paths, the forecast trajectory was somewhat slower. This difference proved fortunate, as the aircraft sampling was centered 1.25 hours earlier than the time corresponding to the trajectory position originally requested. Given the significant dispersion that would have occurred in the ~24 hour transport to this point, however , it is likely that a portion of the cloud would have been intercepted at the same location had the sampling occurred at the originally-scheduled time.

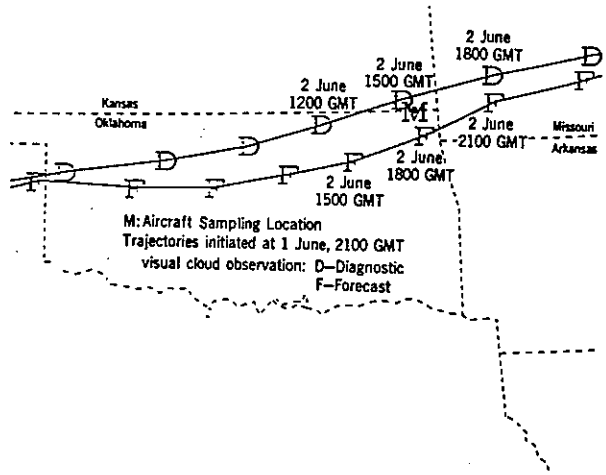

Fig. 2. Evaluation of the trajectory forecast used to vector the Los Alamos National Laboratory sampling aircraft to a cloud interception point at 1700 UT, June 2, 1989. The projected location for cloud sampling is indicated by "M"; the Misers Gold debris cloud was indeed found there. Line "F" is the after-blast forecast of the debris cloud transport pathway. Line "D" is the diagnostic trajectory calculated later using observed meteorological data.

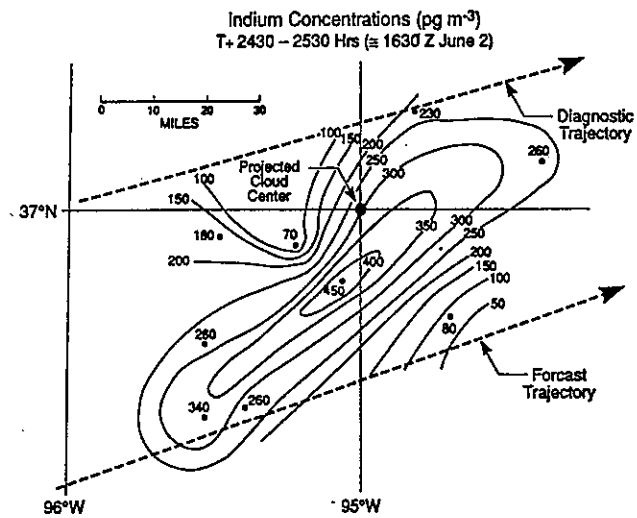

Fig. 3. Isopleths of indium concentrations (pg/standard m^3) measured by the LANL team from air samples collected between 24.5 and 25.5 hours after the blast. Portions of the forecast and diagnostic trajectories from Figure 2 are also shown.

Detailed results of the indium tracer measurements obtained by the LANL group [*Mason et al.*, 1990] are shown in Figure 3. The measurements correspond to aircraft sampling in the vicinity of point "M" in Figure 2. The peak concentrations of indium, 450 pg/standard m^3, were observed only 20 km south-southwest of point M between 24.5 and 25.5 hours after the blast. The presence of a distinct maximum in indium concentration close to the projected cloud center gives us reason to believe that the trajectory forecast did in fact direct the aircraft crew to near the center of the debris cloud at the 500 mb level.

3. CONCLUSIONS

In this case a trajectory forecast model proved to be an accurate and inexpensive means of estimating atmospheric debris transport in an operational setting. The results summarized above lead us to conclude that forecast trajectories are valuable tools for vectoring sampling aircraft in atmospheric dispersion experiments and operations. Application of these models should prove useful in the future when forecasts of atmospheric transport are needed.

4. REFERENCES

Harris, J.M., The GMCC atmospheric trajectory program, *NOAA Tech. Memo. ERL ARL-116*, Air Resources Laboratory, Silver Spring, Maryland, 30 pp., 1982.

Heffter, J.L. and B.J.B. Stunder, Program for operational trajectories (POT), *NOAA Tech. Memo. ERL ARL-157*, Air Resources Laboratory, Silver Spring, Maryland, 12 pp., 1987.

Kahl, J.D., and P.J. Samson, Uncertainty in trajectory calculations due to low resolution meteorological data, *J. Climate Appl. Meteorol.*, *25*, 1816-1831, 1986.

Kahl, J.D., R.C. Schnell, P.J. Sheridan, B.D. Zak, H.W. Church, A.S. Mason, J.L. Heffter, and J.M. Harris, Predicting atmospheric debris transport in real-time using a trajectory forecast model, *Atmos. Environ.*, *25A*, 1705-1713, 1991.

Lutton, T., Misers Gold program document, *Report POR 7350*, Defense Nuclear Agency, Washington, DC, 284 pp., 1989.

Mason, A.S., D.L. Finnegan, G.K. Bayhurst, R. Raymond, Jr., R.C. Hagan, G. Luedemann, K.H. Wohletz, Dust collection and cloud characterization, Misers Gold Symposium, Defense Nuclear Agency, Kirtland Air Force Base, New Mexico, in press, 1990.

Trace Gases Over Hawaii: Concentrations, Trends, and Vertical Gradients

M.A.K. KHALIL AND R.A. RASMUSSEN

Global Change Research Center, Oregon Graduate Institute, Beaverton, Oregon 97006

1. INTRODUCTION

For more than 10 years we have taken global measurements of trace gases at seven sites spanning latitudes from the Arctic to the South Pole. These sites are Point Barrow, Alaska; Cape Meares, Oregon; Cape Kumukahi and Mauna Loa, Hawaii; Cape Matatula, Samoa; Cape Grim, Tasmania; and the South Pole. Over the years this experiment has established the global trends of CH_4, CO, N_2O, H_2 and F-113. The experiment has included the gases that are expected to be most significant in causing global environmental changes either by the greenhouse effect or by depleting the stratospheric ozone layer (CH_4, N_2O, CCl_3F, CCl_2F_2, CO). Also included are baseline studies of gases that may contribute to global changes in lesser amounts (F-22, F-113, CH_3CCl_3, CCl_4, H_2, and the nonmethane hydrocarbons). The experiment at Hawaii is unique in that we have two sampling locations—one at sea level (Cape Kumukahi) and the other at 3.4 km above sea level (MLO). While the trends of trace gases at these sites are about the same, the average concentrations of most trace gases at Cape Kumukahi are generally significantly higher that at MLO [*Rasmussen and Khalil*, 1981; *Steele et al.*, 1987]. Here we report the results obtained at the Hawaiian sites over the past decade.

2. CONCENTRATIONS OF TRACE GASES

Samples were taken in specially prepared stainless-steel flasks, in triplicate, every week at the two sites starting in 1980 [*Rasmussen and Khalil*, 1981]. The flasks were sent to our laboratory where several gas chromatographs were used to measure the concentrations of trace gases. The results are summarized in Table 1 as annual average concentrations of 12 trace gases.

We first calculated the concentrations of trace gases during each month, then took seasonal averages. For each year, the average of the seasonal concentrations is the annual average concentration. In some years we did not have data for all seasons. In such cases interpolated estimates were used to fill the gaps. We described the concentration as:

$$C(\text{season}) = C_o + bt + \text{Seasonal Cycle} \qquad (1)$$

where "Seasonal Cycle" is the average seasonal adjustment based on all the years of data [see: *Khalil and Rasmussen*, 1990], C is the concentration at time t, C_o is the concentration in the base year, b is the rate of increase, and t is time. When there were no data in a given season, Eq. (1) was used to interpolate to obtain an unbiased annual average with all four seasons represented. When data were missing for two or more seasons, the annual average was not computed. The periods when reliable annual averages could not be calculated are indicated by "--" in Table 1.

The data in Table 1 show two features: first, there are significant increasing trends for most gases produced or affected by human activities; second, there is a difference of concentrations between Cape Kumukahi and MLO.

3. TRENDS

For the anthropogenic CFCs, CH_4, and some other trace gases affected by human activities, the trends are the most apparent component of the time series. Using the seasonal concentrations of the trace gases, we estimated the trend by two different models:

$$C = C_o + bt \qquad (2)$$

$$C = C_o \exp(\beta t) \qquad (3)$$

where β is the rate of exponential increase. The results are reported in Table 2. The value of C_o is reported only from Eq. (2) since the two methods gave very similar results. Trends estimated according to Eq. (3) are not affected by errors in absolute calibration of concentrations. Moreover, Eq. (3) provides a uniform comparison of the trends of various trace gases that differ in absolute concentrations over many orders of magnitude. On the other hand, trace gases that are at very low concentrations can appear to increase extremely rapidly when Eq. (3) is applied. This is because the base concentrations are so low. Therefore, an evaluation of increases according to Eq. (2) is needed to provide a balanced view of the trends. The results are plotted in Figure 1. In the top panel we plot the percent-per-year increases sorted by highest to lowest values according to Eq. (3). F-113, F-22, and other CFCs are increasing at faster percent-per-year rates than CH_4, H_2, N_2O, and CO. In the lower panel the results from Eq. (2) are plotted to show that CH_4, H_2, N_2O, and CO are increasing faster in terms of number of molecules per year in the atmospheric compared to the fluorocarbons.

4. VERTICAL GRADIENTS

We estimated the difference of concentrations of trace gases at sea level (Cape Kumukahi) and above the boundary layer (MLO) based on the measurements taken since 1980. The results are shown in Table 3. The differences are generally lower than found in our previous evaluation [*Rasmussen and Khalil*, 1981]. The earlier estimates were based on very few months of data, which did not reflect the long-term differences of concentrations. On the other hand, in the present evaluations, outliers have not been evaluated

TABLE 1. Annual Average Concentrations of Trace Gases in Hawaii

	H_2 ppbv	CO ppbv	CH_4 ppbv	N_2O ppbv	F-12 pptv	F-11 pptv	F-113 pptv	$CHCl_3$ pptv	CH_3CCl_3 pptv	CCl_4 pptv	F-22 pptv	CH_3Cl pptv
						Cape Kumukahi, Hawaii						
1980	--	87	1583	304	299	175	--	--	110	118	58	654
1981	--	81	1589	304	312	184	--	--	117	119	64	642
1982	--	91	1612	305	328	193	--	--	125	121	70	656
1983	--	--	--	--	--	--	--	--	--	--	--	--
1984	--	--	--	--	--	--	--	--	--	--	--	--
1985	490	89	1668	306	376	221	32	17	143	126	88	615
1986	489	84	1676	308	398	231	35	15	149	127	95	601
1987	493	84	1698	310	417	245	39	15	160	133	103	586
						Mauna Loa, Hawaii						
1980	--	75	1565	303	291	172	--	--	105	113	55	637
1981	--	72	1573	305	309	184	--	--	111	116	61	623
1982	--	77	1601	305	325	191	--	--	119	119	69	644
1983	--	80	1627	306	343	202	25	--	123	120	75	669
1984	--	73	1636	307	359	209	27	--	128	124	80	646
1985	488	81	1652	308	376	220	31	15	136	125	87	636
1986	508	78	1665	310	396	230	34	13	140	127	93	635
1987	523	75	1686	311	415	243	38	16	151	134	101	661

TABLE 2. Trends of Trace Gases in Hawaii

	H_2	CO	CH_4	N_2O	F-12	F-11	F-113	$CHCl_3$	CH_3CCl_3	CCl_4	F-22	CH_3Cl
						Cape Kumukahi						
a	482	85	1575	333	311	181	13	27	135	146	56	664
n	6	15	17	17	17	17	20	8	23	23	21	22
b/YR	1.4	0.3	17.5	0.8	16.8	9.7	3.3	–1.8	6.8	1.9	6.2	–9.9
b%/yr	0.8	0.2	1.0	0.2	4.8	4.7	9.5	–13.5	5.1	1.5	7.9	–1.6
						Mauna Loa						
a	401	76	1566	333	306	179	16	16	128	140	53	638
n	5	24	24	24	24	24	12	8	27	27	27	27
b/yr	17.4	0.3	17.2	1.0	17.4	9.8	2.8	–0.1	6.3	2.7	6.5	1.9
B%/yr	4.2	0.4	1.1	0.3	4.9	4.7	11.1	1.9	4.8	2.1	8.2	0.3

C_o = concentration in base year, n = number of months of data, b = rate of increase using a linear trend modelβ = rate of increase in percent per year using an exponential trend model.

TABLE 3. Average Difference of Concentrations of Trace Gases: Cape Kumukahi and Mauna Loa

	H_2	CO	CH_4	N_2O	F-12	F-11	F-113	$CHCl_3$	CH_3CCl_3	CCl_4	F-22	CH_3Cl
<d>	–15.6	8.1	12.9	-0.3	2.7	2.3	1.1	1.8	7.6	1.3	2.6	–18.6
n	30	50	51	50	51	51	30	30	51	51	51	48
90%cl	4.7	2.5	2.6	1.7	1.7	1.7	1.4	1.7	1.5	1.4	1.8	7.2
<%d>	–4.1	9.4	0.9	-0.4	0.6	0.6	0.7	5.0	5.4	0.7	2.2	–2.9
τ (yrs)	2	0.2	10	100	75	50	110	0.5	6	50	20	2

<d> (and <%d>) = Estimates of average difference of concentrations (or percent difference of concentration) at MLO and Cape Kumukahi, 90%cl = 90% confidence limits of <d>, Tau = average lifetime of a trace gas.

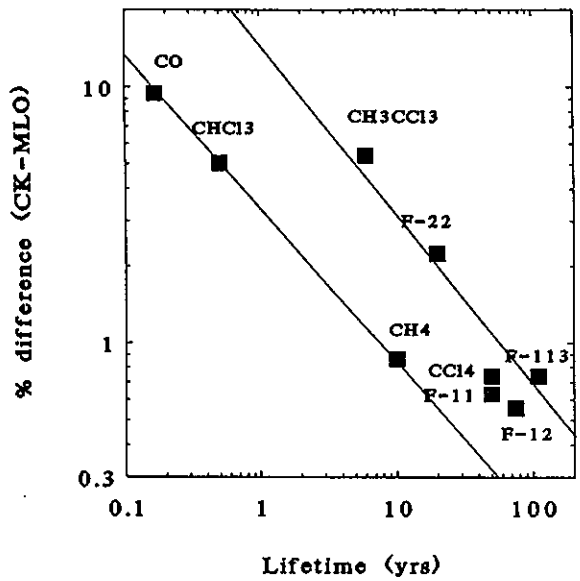

Fig. 1. Difference of concentrations in and above the boundary layer at Hawaii as a function of average tropospheric lifetimes of the trace gases.

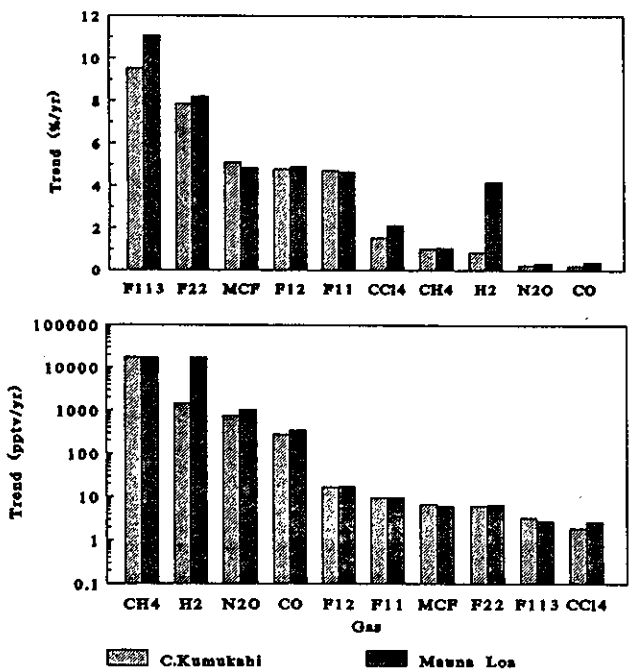

Fig. 2. Trends of trace gases in Hawaii. Trends are shown both as percent-per-year increases and increases in pptv/yr.

and such data may be contributing to the reduced average differences of concentration in and above the boundary layer.

The differences of concentrations in and above the boundary layer are plotted in Figure 2 as a function of the average atmospheric lifetimes of the trace gases. There is an inverse relationship between lifetime and the difference of concentrations as may be expected from previous work including our past publications [*Khalil and Rasmussen*, 1983; 1984; 1988].

5. Conclusions

We have reported the results of trace gas measurements at Cape Kumukahi and MLO in Hawaii taken since 1980. The difference of concentrations between the two sites is somewhat less than our previous estimates. While concentrations of most gases are higher at Cape Kumukahi compared to MLO, the patterns for H_2, CH_3Cl, and N_2O are reversed. It is possible that volcanic contributions affect the concentrations of these gases at MLO.

Acknowledgments. Samples at MLO were collected and shipped to our laboratory by NOAA/CMDL. Support for this work was provided in part by Biospherics Research Corp. and the Andarz Co.

References

Khalil, M.A.K., and R.A. Rasmussen, Gaseous tracers of arctic haze, *Environ. Sci. & Tech. 17*, 157-164, 1983.

Khalil, M.A.K., and R.A. Rasmussen, Statistical analysis of trace gases in arctic haze. *Geophys. Res. Lett. 11*, 437-440, 1984.

Khalil, M.A.K., and R.A. Rasmussen, Trace gases over the western Atlantic Ocean: Fluxes from the eastern United States and distributions in and above the planetary boundary layer, *Global Biogeochemical Cycles 2*, 63-71, 1988.

Khalil, M.A.K., and R.A. Rasmussen, Atmospheric methane: Recent global trends, *Environ. Sci. Tech., 24*, 549-553, 1990.

Rasmussen, R.A. and M.A.K. Khalil, Atmospheric halocarbons: Measurements and analyses of selected trace gases, *Proceedings of the NATO Advanced Study Institute on Atmospheric Ozone: Its Variation and Human Influences*, A.C. Aikin (Ed.), U.S. Department of Transportation, Washington, D.C., 209-231, 1980.

Rasmussen, R.A., and M.A.K. Khalil, Differences in the concentrations of trace gases in and above the tropical boundary layer, *Pure and Applied Geophysics, 119*, 990-997, 1981.

Steele, L.P., P.J. Fraser, R.A. Rasmussen, M.A.K. Khalil, T.J. Conway, A.J. Crawford, R.H. Gammon, K.A. Masarie, and K.W. Thoning, The global distribution of methane in the troposphere, *J. Atmos. Chem. 5*, 125-171, 1987.

Radioactivity in the Surface Air at BRW, MLO, SMO, and SPO

RICHARD J. LARSEN AND COLIN G. SANDERSON

U.S. Department of Energy, Environmental Measurements Laboratory, New York, New York 10014-3621

1. INTRODUCTION

Air filter samples are routinely collected by CMDL personnel at BRW, MLO, SMO, and SPO for EML's Surface Air Sampling Program (SASP). The primary objective of this program is to study the temporal and spatial distribution of specific natural and anthropogenic radionuclides in the surface air. Of the radionuclides that are analyzed by gamma-ray spectrometry, only the naturally occurring radioisotopes ^{7}Be and ^{210}Pb are still readily measured in most of the filter samples. ^{7}Be (half-life 53.2 days) is produced by cosmic-ray interactions in the upper troposphere and the stratosphere. ^{210}Pb (half-life 22 years) is a decay product of ^{222}Rn, which is a natural radioisotope emitted from soils. Because of their distinctly different source regions, these radioisotopes serve as tracers for upper and lower tropospheric sources and transport processes.

2. MATERIALS AND METHODS

Weekly air filter samples are continuously collected using Microdon filter material. The air samplers move ~1700 m^3 of air per day through a 20-cm diameter filter.

The weekly filter samples collected at BRW and MLO are analyzed by gamma-ray spectrometry using a high-purity germanium (HPGe) detector with a 1.5-cm diameter well. For each site, one-half of each of the weekly filter samples are added together to form a monthly composite sample. These composite samples are compressed into a 45-cm^3 plastic planchet, and are routinely analyzed for several

TABLE 1. Monthly Surface Air Concentrations of Radionuclides at BRW, MLO, SMO, and SPO During 1990

Site	Nuclide		Jan.	Feb.	March	April	May	June	July	Aug.	Sept.	Oct.	Nov.	Dec.
BRW	Gamma	(cpm m^{-3})	<0.01	<0.01	<0.01	<0.01	<0.01	<0.01	<0.01	<0.01	<0.01	<0.01	<0.01	<0.01
MLO	Gamma	(cpm m^{-3})	<0.01	<0.01	<0.01	<0.01	<0.01	<0.01	<0.01	<0.01	< 0.01	<0.01	<0.01	<0.01
SMO	Gamma	(cpm m^{-3})	<0.01	<0.01	<0.01	<0.01	<0.01	<0.01	<0.01	<0.01	<0.01	<0.01	<0.01	<0.01
SPO	Gamma	(cpm m^{-3})	<0.01	<0.01	<0.01	*	<0.01	<0.01	<0.01	<0.01	<0.01	<0.01	<0.01	<0.01
BRW	^{7}Be	(mBq m^{-3})	1.4	1.7	1.7	1.6	1.0	0.8	0.4	0.6	0.7‡	0.9	1.4	1.7
MLO	^{7}Be	(mBq m^{-3})	5.2	5.8	6.6	6.4	5.6	6.9	4.8	5.3	3.8	6.1	2.2	4.4
SMO	^{7}Be	(mBq m^{-3})	1.9	1.8	1.9	1.4	2.2	2.4	2.6	2.7	2.3	2.2	1.7	1.9
SPO	^{7}Be	(mBq m^{-3})	2.8	<2.4	<2.1	*	1.3‡	2.2	1.9	1.1	1.6‡	3.5	3.4	4.1
BRW	^{95}Zr	(μBq m^{-3})	<6.6	<3.3	<3.1	<2.1	<4.0	<6.8	<6.0	<4.0	<16.2	<11.8	<5.9	<9.8
MLO	^{95}Zr	(μBq m^{-3})	<10.0	<7.6	<5.2	<10.1	<8.8	<3.9	<7.9	<14.1	<17.3	<29.6	<39.8	<15.9
SMO	^{95}Zr	(μBq m^{-3})	<5.0	<5.9	<7.2	<5.4	<5.0	<10.5	<7.8	<4.5	<11.3	<14.1	<28.9	<9.9
SPO	^{95}Zr	(μBq m^{-3})	<6.2	<200.0	<178.0	*	<51.5	<52.7	<37.9	<17.6	<26.3	<13.4	<8.6	<35.7
BRW	^{137}Cs	(μBq m^{-3})	<1.6	<1.0	<0.9	<0.6	<0.8	<1.1	<1.5	<1.3	<1.1	<1.0	<0.5	<1.1
MLO	^{137}Cs	(μBq m^{-3})	<2.8	<2.6	<1.8	<2.6	<2.4	<1.0	<3.2	<2.5	<1.2	<2.3	<3.7	<1.2
SMO	^{137}Cs	(μBq m^{-3})	<1.3	<1.3	<1.5	<1.5	<1.0	<2.8	<1.7	<1.3	<1.6	<2.4	<1.8	<0.8
SPO	^{137}Cs	(μBq m^{-3})	<1.2	<1.9	<1.7	*	<1.1	<1.7	<1.4	<1.2	<2.1	<1.7	<1.3	<3.3
BRW	^{144}Ce	(μBq m^{-3})	<6.5	<3.3	<3.3	<2.4	<3.2	<3.5	<5.7	<4.7	<4.7	<3.9	<1.8	<5.3
MLO	^{144}Ce	(μBq m^{-3})	<10.7	>9.5	>7.4	>11.7	>10.5	<4.0	<10.6	<12.4	<6.3	<12.5	<21.1	<5.1
SMO	^{144}Ce	(μBq m^{-3})	<4.5	<5.0	<6.5	<5.8	<4.4	<11.3	<6.5	<5.5	<7.2	<10.7	<9.3	<4.0
SPO	^{144}Ce	(μBq m^{-3})	<4.2	<15.1	<14.0	*	<6.1	<10.6	<6.6	<4.8	<8.1	<8.0	<5.0	<12.3
BRW	^{210}Pb	(mBq m^{-3})	0.86	1.04	1.00	0.54	0.22	0.08	0.06	0.09	0.09	0.27	0.61	0.81
MLO	^{210}Pb	(mBq m^{-3})	0.19	0.27	0.38	0.48	0.39	0.55	0.33	0.26	0.19	0.26	0.08‡	0.18
SMO	^{210}Pb	(mBq m^{-3})	0.05	0.05	0.03	0.04	0.06	0.10‡	0.07‡	0.09	0.08	0.10‡	0.05‡	0.05
SPO	^{210}Pb	(mBq m^{-3})	0.03	0.02†	0.02†	*	0.01†	0.02†	0.02‡	0.01†	0.02†	0.04‡	0.03‡	0.04‡

*No data

†Uncertainty is between 50% and 100%;

‡Uuncertainty is between 20% and 50%; uncertainty for all other concentrations is <20%.

gamma-ray-emitting radionuclides using either HPGe n-type low-energy coaxial or Ge(Li) or HPGe p-type coaxial high-resolution germanium detectors. Detailed information on SASP is periodically published [*Larsen and Sanderson*, 1990].

3. Results

The results of the analyses of several radionuclides and the total gamma-ray activities for the monthly composite samples from filters collected at BRW, MLO, SMO, and SPO during 1990 are reported in Table 1. The total gamma-ray activities are reported in units of counts per minute (cpm) per standard cubic meter (15°C, 1 atm) of sampled air. The surface air concentrations of ^{7}Be and 210Pb are reported in millibecquerels (mBq) per standard cubic meter of air, and ^{95}Zr, ^{137}Cs, and ^{144}Ce are reported in microbecquerels (μBq) per standard cubic meter of air. The concentrations are reported as corrected for radioactive decay to the midpoint of the month of collection. The results of the analyses on the weekly samples from BRW and MLO are being prepared for publication as an EML report.

4. Discussion

There were no announced atmospheric nuclear weapons tests or other reported significant releases of radioactive materials into the atmosphere during 1990, and the concentrations of fission products such as ^{95}Zr, ^{137}Cs, and ^{144}Ce were at or below the lower limits of detection for the analytical and sampling techniques that we currently use to measure them.

The monthly mean concentrations of ^{7}Be nd ^{210}PB show a seasonal cycle at all CMDL sites. *Feely et al.* [1989] described the factors that cause seasonal variations in the ^{7}Be concentration in the surface air.

Acknowledgment. We wish to thank the NOAA/CMDL staff at BRW, MLO, SMO, and SPO for the collection of air filter samples for the SASP.

5. References

Feely, H.F., R.J. Larsen, and C.G. Sanderson, Factors that cause seasonal variation in beryllium-7 concentrations in surface air. *J. Environ. Radioactivity*, *9*, 223-249, 1989.

Larsen, R.J., and C.G. Sanderson, Annual report of the surface air sampling program, *EML-524*, 120 pp., U.S. Department of Energy Environmental Measurements Laboratory, New York, 1990.

Zonal Representativeness of Cape Grim CO_2 Measurements

G. I. PEARMAN, D. J. BEARDSMORE, R. J. FRANCEY
CSIRO, Division of Atmospheric Research, Victoria, Australia 3195

1. INTRODUCTION

It has long been recognized that annual average CO_2 concentrations measured in air of marine origin at Cape Grim have registered lower concentrations than comparable measurements in the southern hemisphere [*Tans et al.*, 1990]. The reasons for this have not been fully understood, with initial investigations concentrating on standard intercalibration and data selection. Recently an intercalibration between the CO_2 programs at Amsterdam Island (French, 37°S, 77°E), Baring Head (New Zealand, 41°S, 170°E) and Cape Grim (Australian, 41°S, 150°E), revealed that the calibration scale applied to the Australian results was around 0.6 ppmv too low [*Monfray et al.*, 1990].

The Australian scale is based on WMO secondary standard mixtures purchased from Scripps Institution of Oceanography and last calibrated in 1984. The lack of access to a primary standard calibration since 1984 meant that a drift in the Australian standard was not unanticipated. The purpose of this report is to establish (a) when the Australian standards began to deviate from the international scale, and (b) a history of the difference of Cape Grim CO_2 values from comparable records at similar southern latitudes.

Two flask records are used to assist in the comparisons: one from Cape Grim but measured on the NOAA/CMDL scale and one from aircraft over southeast Australia (approximately 38°S, 145°E, 4 km altitude) on the Australian calibration scale.

2. DATA RECORDS

In an attempt to determine when the scale of the WMO secondary tanks held at CSIRO, Division of Atmospheric Research, commenced to drift with respect to the WMO Primary Standard, the differences between Cape Grim monthly means and those of other programs were computed. Details of data sets used for these comparisons are: (a) Cape Grim (CSIRO, Australia) values as published to the end of 1984 [*Beardsmore and Pearman*, 1987] and, from 1985-1989 as provided for appropriate reports of the WMO Environmental Pollution Monitoring and Research Program. (b) Baring Head (DSIR, New Zealand) values to 1984 [*Manning and Pohl*, 1986] and provisional values 1985-1989 (personal communication, A. Gomez). (c) Amsterdam Island (CNRS, France) values from 1980-1988 [*Gaudry, et al.*, 1991] and provisional data for 1989 (personal communication, M. Ramonet). (d) Southeastern Australia midtroposphere (CSIRO, Australia) values as published to the end of 1981 [*Pearman and Beardsmore*, 1984] and the 1985-1989 CSIRO data currently being prepared for publication.

Since 1984, NOAA/CMDL has collected and analyzed air samples in flasks from Cape Grim. As the Cape Grim in situ values at the time of sample collection are available, these data were also obtained from 1984-1990 (personal communication, T. Conway) to provide an additional comparison.

3. INTERCOMPARISON OF DATA RECORDS

Figure 1 plots 12-month running means at six monthly intervals, of the differences between the Cape Grim monthly means of baseline CO_2 and those from the other data sets. All three graphs show similar gross features until about 1987/1988 when the differences between Cape Grim and both Baring Head and Amsterdam Island continue to rise while Gape Grim minus southeastern Australia midtroposphere falls sharply. We assume that this was the time when the Australian standards started to diverge from the true WMO 1985 Calibration Scale.

To pinpoint the start of drift more accurately, the monthly means of the differences between CMDL flasks and Cape Grim in situ (at the sampling time) were plotted (Figure 2). These data also show a divergence from about 1987. When a 24-month running mean is added (solid line), the divergence is confirmed to begin at this time after a steady mean difference of 0.37 ppmv. In view of the large scatter in the data we have assigned January 1987 as the time of commencement of drift on the basis of visual inspection of Figure 2.

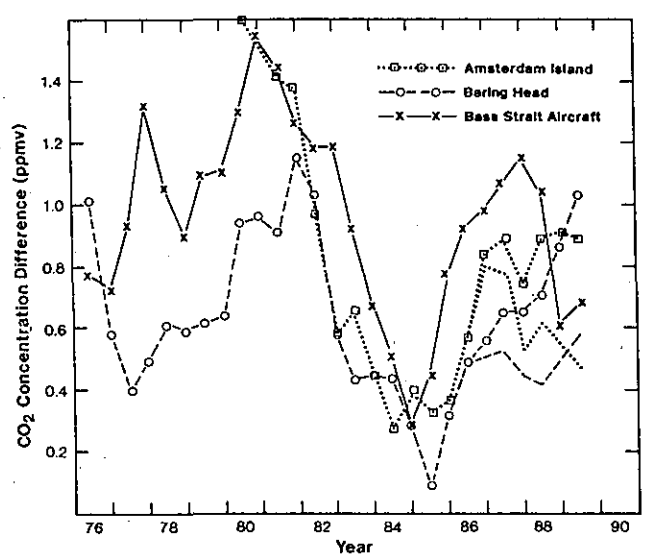

Fig. 1. Twelve month means (at six month intervals) of the monthly CO_2 concentration differences between Cape Grim and SE Australian midtroposphere (crosses), Baring Head (circles) and Amsterdam Island (squares).

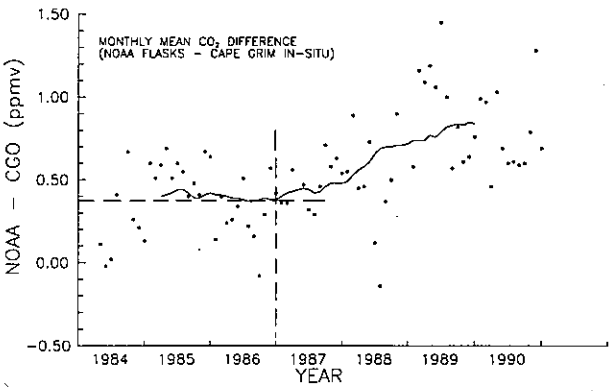

Fig. 2. Monthly mean CO_2 concentration differences between CMDL flasks, and in situ measurements at the same time, from Cape Grim. The solid line is a 24-month running mean of the data points. The 1984-1986 mean and nominal "start-of-drift" are identified by dashed lines.

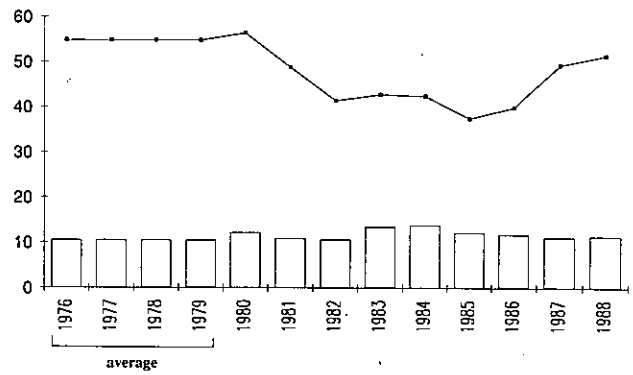

Fig. 3. Annual mean wind speed (bars, in meters per second) and frequency of occurrence of winds in the 180°-270° sector (line, in percent) at Cape Grim.

Therefore, if we take the magnitude of the drift relative to the French/New Zealand scales to be 0.63 ± 0.03 ppmv in August, 1990 [*Monfray et al.*, 1990], assume that it is linear with time, and that it started in January 1987, a correction of 0.013 ppmv/month can be computed. From the CMDL comparison alone, a smaller drift of 0.010 ppmv/month is indicated. A detailed intercomparison of CMDL and Australian scales would help to refine the actual correction.

The resulting corrected differences between Cape Grim and both Baring Head and Amsterdam Island are included in Figure 1 without symbols.

4. Interannual Variation in the Cape Grim "Deficit"

The most striking feature of Figure 1 is the coherence in interannual variation of the differences of all three other stations from Cape Grim. There is a strong implication that the Cape Grim record is influenced by a surface sink which varies in intensity on interannual time scales. For the aircraft record (on the same calibration scale as Cape Grim and effectively representative of air vertically above Cape Grim, Beardsmore, unpublished data), the difference is a maximum of 1.4 ppmv in 1980/1981 (slightly preceding the 1982-1983 Southern Oscillation Index) and a minimum of 0.3 ppmv in 1984/1985.

A possible controlling influence on the interannual variability emerges from a preliminary analysis of wind speed and direction data taken from the Australian baseline series of publications. Figure 3 shows a history of the frequency of occurrence of winds recorded in the western and southwestern "baseline sector," also the annual average wind speeds in meters per second. A significant interannual variation in the frequency of occurrence of "baseline winds" is evident, with the same phasing as the variation in "CO_2 difference from Cape Grim" in Figure 1. An independent confirmation of this behavior [*Harris et al.*, 1988], identifies the number of days of zonal westerly winds over Tasmania from 1945 to 1985 using daily surface synoptic weather charts. The number of days of westerlies peaks around 1980 at 140 days per annum, decreasing to around 70 days per annum in 1985.

Two possibilities are under investigation for explaining interannual variation in the vertical gradient over Cape Grim via changes in westerly wind frequency. One of these hypothesizes a variation in the occurrence of sea breezes, the second changes in the air-sea exchange rate. A further possible influence of interannual behavior in the Indian Ocean circulation is also being investigated.

Acknowledgments: The provision of unpublished CO_2 data from the French, New Zealand, and NOAA programs is acknowledged in the text. Staff of Cape Grim, which is jointly operated by the Bureau of Meteorology and CSIRO, played an essential role in the collection of high precision records over many years.

5. References

Tans, P.P., I.Y. Fung and T. Takahashi, Observational constraints on the global atmospheric carbon dioxide budget, *Science, 247*, 1431-1438, 1990.

Monfray, P., M. Ramonet, A. Gaudry, G. Pearman, D. Beardsmore, M. Manning and P. Pohl, An intercalibration of CO_2 measurements between France, Australia, and New Zealand, *Report to the WMO Meeting of Experts on CO_2 measurements*, Lake Arrowhead, October 1990.

Beardsmore, D.J. and G.I. Pearman, Atmospheric carbon dioxide measurements in the Australian region: data from surface observatories, *Tellus, 39B*, 42-66, 1987.

Manning, M.R. and K.P. Pohl, Atmospheric carbon dioxide monitoring in New Zealand, 1971-1985, *Report No. INS-R-350*, Institute of Nuclear Sciences, DSIR, New Zealand, 1986.

Gaudry, A, P. Monfray, G. Polian, G. Bonsang, B. Ardouin, A. Jegou and G. Lambert, Non-seasonal variations of atmospheric CO_2 concentrations at Amsterdam Island, *Tellus, 43B*, 136-143, 1991.

Pearman, G.I. and D.J. Beardsmore, Atmospheric carbon dioxide measurements in the Australian region: ten years of aircraft data, *Tellus, 36B*, 1-24, 1984.

Harris, G.P., P. Davies, M. Nunez and G. Meyers, Interannual variability in climate and fisheries in Tasmania, *Nature, 333*, 754-757, 1988.

Aerosol Constituents at American Samoa: May-June 1990

DENNIS L. SAVOIE AND JOSEPH M. PROSPERO
University of Miami, Rosenstiel School of Marine and Atmospheric Science, Miami, Florida 33149-1098

RICHARD ARIMOTO AND ROBERT A. DUCE
University of Rhode Island, Graduate School of Oceanography, Center for Atmospheric Chemistry Studies Graduate School of Oceanography, Narragansett, Rhode Island 02882-1197

1. INTRODUCTION

A major goal of our cooperative work at SMO is to define more rigorously the sources, atmospheric pathways, and fluxes of particulate nitrogen and sulfur species in the remote marine atmosphere. Toward this end, we continue to collect weekly bulk aerosol samples at SMO where past studies [e.g. *Arimoto et al.*, 1987] indicate that the transport of soil material and pollutants from continental sources is extremely low. In addition, daily samples were collected throughout November 1989 and from May 10 to June 11, 1990, in support of the First and Second Survey Flights of the NASA Global Backscatter Experiment (GLOBE). The objective of GLOBE is to assess the feasibility of a space-based lidar system that could provide vertical profiles of winds over a substantial portion of the earth. Our task in this endeavor was to place the period of the flights within a climatological framework by comparing the results obtained during the flight periods to those from our long-term record. Here we concentrate on the results from the May-June 1990 intensive; the results from the November 1989 intensive were presented by *Savoie et al.* [1990].

As with our normal weekly samples, the daily samples were collected from onshore winds by drawing air through 20×25 cm Whatman 41 filters at a flow rate of 1.1 m^3 min^{-1}. Nitrate, sulfate, and MSA in aqueous extracts of the filters were determined by ion chromatography, ammonium by automated colorimetry, and sodium by flame atomic absorption at the University of Miami; aluminum concentrations were measured by neutron activation analysis at the University of Rhode Island. Mineral aerosol was estimated from aluminum, which constitutes about 8% of the mineral aerosol mass. Nss sulfate was estimated as total sulfate minus sodium times 0.2517, the sulfate to sodium mass ratio in seawater.

2. MEAN CONCENTRATIONS

Samples included in this study were collected from May 10 through June 11, 1990. The wind was very favorable throughout this period, being in-sector almost 95% of the time. The minimum in-sector time for a given sample was 64% from May 27 to 28. The nitrate, sulfate, sodium, and MSA concentrations in the samples were all well above their detection limits; concentrations on the filters were at least 10 times higher than in the blanks and the net concentrations (total-blank) were always at least 50 times higher than the standard deviation of the blank. In contrast, the ammonium aluminum blanks accounted for a major fraction of the total concentrations of these species in most of the samples. Gross ammonium concentrations in the samples were usually only a factor of 2 higher than the blanks with most net concentrations only factors of 3-4 higher than the standard deviation of the blank. For aluminum, the gross sample concentrations were frequently within the range of the blanks and were never more than a factor of 2 higher than the average blank. Because the reported sample concentrations are based on the net sample concentration (gross minus average blank), calculated negative concentrations frequently result when the atmospheric concentrations are extremely low, as is the case for aluminum. Though the results clearly attest to the very low concentrations of ammonium and mineral dust at the site, the high relative errors for these constituents make it difficult to assess the real day-to-day variations in their concentrations.

Four of the samples were collected over 2-day (as opposed to 1-day) periods. In calculating the statistical parameters for the data set, each day of these 2-day periods was assigned the same set of concentrations, i.e. the mean concentrations for the 2-day period. The statistics calculated on this basis are presented in Table 1 along with other comparative data.

The mean nitrate concentration at SMO during May 10-June 11, 1990 (MJ90), is only about 8% higher than the long term (1983-1990) May-June mean, but 17% lower than the

TABLE 1. Concentrations of Various Species in Atmospheric Particulates for Several Time Periods at SMO

	NO_3^- $\mu g\ m^{-3}$	NSS $SO_4^=$ $\mu g\ m^{-3}$	MSA ng^{-3}	Mineral $ng\ m^{-3}$	NH4+ $ng\ m^{-3}$
May-June 1990	0.095 ±0.017	0.465 ±0.085	30.8 ±6.2	14.3 ±7.0	16.9 ±4.4
May-June 1983-1990	0.088 ±0.012	0.322 ±0.040	29.8 ±5.7	11.3 ±4.6	16.9 ±4.4
1983-1990 (All)	0.114 ±0.007	0.368 ±0.019	25.9 ±5.1	19. ±3.	16. ±4.
Nov. 1989	0.178 ±0.039	0.368 ±0.064	17.7 ±2.8	21. ±17.	26. ±6.

The data in this table were compiled from *Prospero and Savoie* [1989], *Prospero et al.* [1989], *Saltzman et al.* [1985, 1986] and *Savoie et al.* [1989*a*].

overall 1983-1990 mean. Moreover, the MJ90 mean is nearly a factor of 2 lower than that during the first GLOBE flight, November 1989. These results are consistent with the long-term nitrate seasonal cycle at SMO [*Savoie et al.*, 1989].

In contrast to nitrate, the mean nss sulfate concentration during MJ90 is substantially (44%) higher than the long-term May-June mean and about 25% higher than the overall 1983-1990 mean. These results conflict with the long-term nss sulfate seasonal cycle that showed relatively lower concentrations during this part of the year. In fact, the MJ90 mean is comparable to the highest long term monthly mean which occurs in September.

The mean MJ90 MSA concentration is nearly identical to the long-term May-June mean but about 20% higher than the overall 1983-1990 mean. However, because of the sparsity of previous MSA measurements, these comparisons must be viewed with caution. Certainly the most dramatic difference is between the MJ90 intensive and that of November 1989 with the former being about 75% higher. These results suggest the possibility of a strong seasonal cycle in MSA, in contrast to the rather constant concentrations reported by *Saltzman et al.* [1986].

Despite the extremely low levels of mineral dust at SMO, the results obtained from the MJ90 samples are consistent with those that we have obtained in the past. Hence, our results continue to support the contention that American Samoa is minimally impacted by the transport of materials from continental regions. As with nitrate, the mean MJ90 concentration is comparable to the long-term May-June mean and about 20% lower than the long-term overall mean.

Previous measurements of ammonium at SMO have been very sparse. Consequently, comparisons with the long-term data sets are of questionable value. However, it is interesting to note that the mean ammonium concentration during the MJ90 intensive is about 35% lower than that during November 1989. This difference is comparable to that for nitrate but sharply contrasts with those for nss sulfate and MSA which are both much higher during MJ90.

3. Daily Variations and Sources

The concentrations of each of the constituents exhibited substantial day-to-day variations during the MJ90 intensive (Figure 1). Nitrate varied by a factor of 6, from 0.036 to 0.21 $\mu g\ m^{-3}$. Sodium ranged from 2.0 to 7.9 $\mu g\ m^{-3}$, a factor of about 4. The sulfur species varied by factors of about 7 to 8: MSA from 8.7 to 66 $ng\ m^{-3}$; and nss sulfate from 0.112 to 0.87 $\mu g\ m^{-3}$. The variations in the concentrations of the sulfur species tend to track one another reasonably well with major peaks near the beginning and the end of the intensive. Nitrate, in contrast, exhibits a peak near mid-month with relatively low levels near the beginning of the period. The differences between the nitrate and sulfur species time series support the conclusion that a marine biogenic source is probably not the dominant source of nitrate at SMO [*Savoie et al.*, 1989*b*]. Ammonium exhibits several peaks of which two appear to coincide with those of the sulfur species and one with that of nitrate and/or mineral dust.

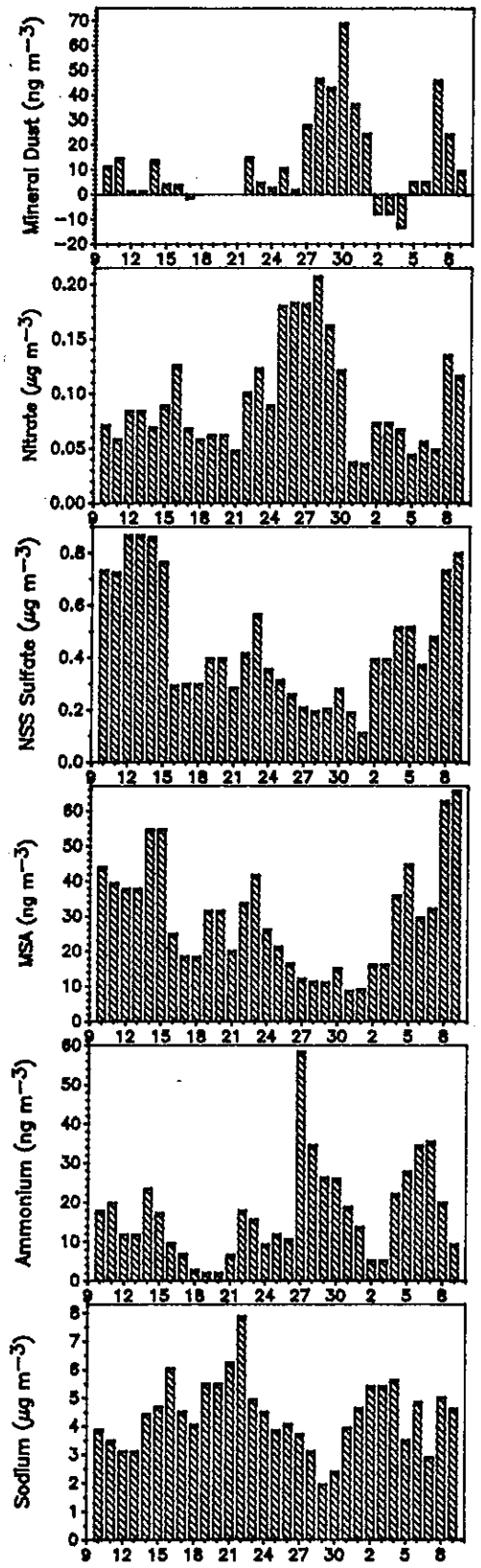

Fig. 1. Daily-average concentrations of chemical species in atmospheric particulates at SMO from May 10 to June 11, 1990.

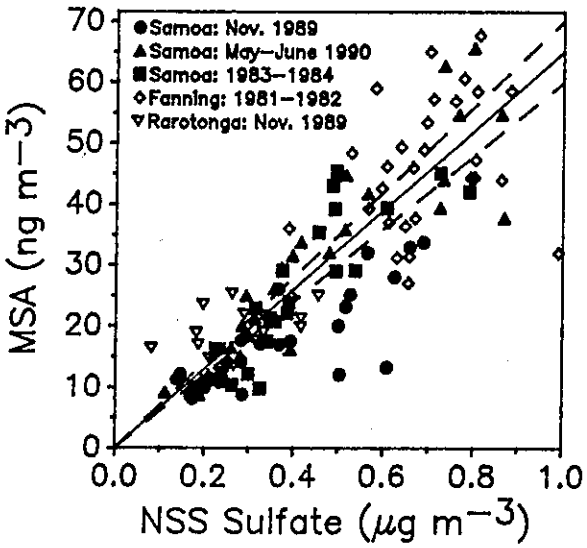

Fig. 2. Methanesulfonate (MSA) versus nss sulfate at SMO, Fanning Island, and Rarotonga for various time periods.

In an evaluation of earlier data, *Saltzman et al.* [1985] reported a reasonably consistent MSA/nss $SO_4^=$ = ratio (0.065 ± 0.005) at SMO and Fanning Island. In Figure 2, we update their original data set with the November 1989 and MJ90 data from SMO and the November 1989 data from Rarotonga. With these additions, the pattern remains reasonably consistent, supporting the conclusion that the nss sulfate at these stations is derived predominantly from the oxidation of dimethyl sulfide. With the 121 samples, the geometric mean MSA/nss $SO_4^=$ = ratio, 0.0614 ± 0.0037, is not significantly different from that obtained from the original 55. However, the ratio at SMO may vary significantly. The original 1983 and 1984 weekly samples yield a ratio of 0.0593 ± 0.0078, the November 1989 samples yield 0.0490 ± 0.0068, and the MJ90 samples yield 0.0655 0.0055. Only the November 1989 result differs significantly from the overall mean. Additional investigations will be required to assess the possible reasons for this apparent difference.

4. Other Comparisons

We have also compared our nss sulfate data with the condensation nuclei (CN) and nephelometer data acquired during these intensive periods by the CMDL personnel. Although the CN concentrations and the aerosol scattering at 500 nm are significantly correlated with the nss sulfate concentrations, there is considerable scatter in the relationship. We tentatively ascribe much of this scatter to variations in the size distribution of the nss sulfate particles, primarily as a function of relative humidity. However, other processes such as coagulation of particles and growth of particles from the absorption of reactive gases may also play important roles.

Acknowledgments. We thank T. Snowdon, Huang F., Huang T., and M. Izaguirre (all of UM) and J.D. Cullen (URI) for their technical assistance. We also thank C. Farmer and E. Wilson-Godinet (NOAA/CMDL SMO) for maintaining and operating our sampling systems. We gratefully acknowledge the cooperation of B. Mendonca and NOAA/CMDL Boulder for allowing us to continue our program at SMO. This work was supported under NASA contracts NAG8-621 and NAG8-841.

5. References

Arimoto, R., R.A. Duce, B.J. Ray, A.D. Hewitt, and J. Williams, Trace elements in the atmosphere of American Samoa: Concentrations and deposition to the tropical South Pacific, *J. Geophys. Res., 92*, 8465-8479, 1987.

Prospero, J.M., and D. L. Savoie, Effect of continental sources on nitrate concentrations over the Pacific Ocean, *Nature, 339*, 687-689, 1989.

Prospero, J.M., M. Uematsu, and D.L. Savoie, Mineral aerosol transport to the Pacific Ocean, in *Chemical Oceanography, 10*, edited by J.p. Riley, R. Chester, and R.A. Duce pp. 188-218, Academic Press, London, 1989.

Saltzman, E.S., D.L. Savoie, J.M. Prospero, and R.G. Zika, Atmospheric methanesulfonic acid and non-seasalt sulfate at Fanning and American Samoa, *Geophys. Res. Lett., 12*, 437-440, 1985.

Saltzman, E.S., D.L. Savoie, J.M. Prospero, and R.G. Zika, Methanesulfonic acid and non-seasalt sulfate in Pacific air: Regional and seasonal variations, *J. Atmos. Chem., 4*, 227-240, 1986.

Savoie, D.L, M.M. Prospero, and E.S. Saltzman, Nitrate, non-seasalt sulfate, and methanesulfonate over the Pacific Ocean, in *Chemical Oceanography, 10*, edited by J.P. Riley, R. Chester, and R.A. Duce, pp. 219-250, Academic Press, London, 1989*a*.

Savoie, D.L., J.M. Prospero, J.T. Merrill, and M. Uematsu, Nitrate in the atmospheric boundary layer of the tropical South Pacific: Implications regarding sources and transport, *J. Atmos. Chem., 8*, 391-415, 1989*b*. .

Savoie, D.L., J.M. Prospero, R. Arimoto, and R.A. Duce, Aerosol constituents at American Samoa: November 1989, in *Climate Monitoring and Diagnostics Laboratory, No. 18, Summary Report 1989*, edited by W.D. Komhyr, pp. 123-124, NOAA, CMDL, Boulder, Colorado, 1990.

Analysis of MSA and nss $SO_4^=$ at MLO

B.B. SHURTLEFF, X.Y. CAI, AND W.H. ZOLLER
University of Washington, Chemistry Department, Seattle, Washington 98195

I. INTRODUCTION

Tropospheric downslope air samples collected between January 1, 1990, through June 6, 1991, from the Mauna Loa Observatory (MLO) on the island of Hawaii were analyzed for non- seasalt sulfate (nss $SO_4^=$) and methanesulfonic acid (MSA) using ion chromatography (IC).

2. SAMPLING AND ANALYSIS

Atmospheric samples have been continuously collected at MLO utilizing the selective sampling system installed in 1979 [*Parrington*, 1983]. Originally used to collect either upslope or downslope aerosol samples, the system currently collects only downslope samples by measuring wind direction and speed, time, and condensation nuclei (CN) count for parameters on which to make a decision. Since 1989 downslope filter packs have consisted of five filters in tandem; the first, a Teflon filter, collects particulate matter, and the four subsequent filters are ^{7}LiOH treated filters which collect acidic gases. When the testing parameters did not satisfy downslope criteria (i.e. interim parameters), a single Nucleopore filter was used to sample. However, due to pump failure on November 1, 1990, interim samples are no longer collected and the previously described five-filter pack for downslope sampling remains as the only means of collection. Currently, filters are analyzed by two methods: (1) instrumental neutron activation analysis (INAA) measures particulate elements on the Teflon filters, and (2) IC measures particulate species, such as MSA, on the Teflon filters and acidic gases, such as SO_2, HCl, and HNO_3, collected on the ^{7}LiOH treated filters, and measures the residual ions left in the filters (i.e. $SO_4^=$, Cl^-, and NO_3^-).

3. DISCUSSION AND RESULTS

MSA is an oxidation product of dimethylsulfide (DMS) released by oceanic phytoplankton into the marine boundary layer; nss $SO_4^=$ comes from two main sources: continents and marine biological activity. Because MLO is 3.4 km high and the downslope air originates from an altitude of about 4 km [*Parrington et. al.*, 1984], low levels of MSA were expected from the samples. In fact, levels of MSA in the samples were found to be considerably less than marine boundary layer samples (see Table 1). However, nss $SO_4^=$ levels at MLO were found to be relatively similar to levels found at marine boundary layer stations. For MLO, the mean nss $SO_4^=$ concentration and the mean MSA concentration for the testing period are 314 ng/m^3 at STP and 2.3 ng/m^3 at STP, respectively (see Figures 1 and 2). Table 1 shows concentrations for MSA and nss $SO_4^=$ from the free troposphere (MLO) and several Pacific marine boundary layer stations. The ratio of MSA/nss $SO_4^=$ is also shown as a means of easy comparison (see Figure 3). Ratios for marine boundary layer data were calculated; they were not obtained from the actual reports or references.

Obviously, the mean concentration of MSA at MLO is very low in comparison to the boundary layer samples. The low mean concentration is due to the observatory's high altitude and downslope sampling procedure. Originating from a marine source, high concentrations of MSA cannot easily reach the 3.4 km altitude of the MLO when downslope winds are blowing. As previously mentioned, the downslope wind originates from an altitude of about 4 km; therefore, the measured MSA is from the middle troposphere (i.e. MSA which has migrated into the troposphere from the marine boundary layer).

TABLE 1. Mean concentrations of Methanesulfonic Acid (MSA) and Non-Seasalt Sulfate (nss SO_4) at Mauna Loa, Hawaii, and at Several Marine Boundary Locations in the Pacific Ocean.

Sampling Location	Year(s)	Mean nss $SO_4^=$ ng/m^3 (STP)	Mean MSA ng/m^3 (STP)	MSA/nss $SO_4^=$ Ratio
Midway	1983-1987	370-930	10-33	0.027-0.35
MLO	Jan. 1990-June 1991	314 ± 231	2.3 ±1.9	0.009
Fanning Island	1983-1987	600-740	34-60	0.057-0.081
SMO	1983-1987	360	26	0.72
New Caledonia	1983-1987	280-490	8.5-30	0.03-0.061
Norfolk Island	1983-1987	121-400	5-75	0.041-0.187
Mawson, Antarctica	Feb. 1987-Oct. 1989	90	20	0.222

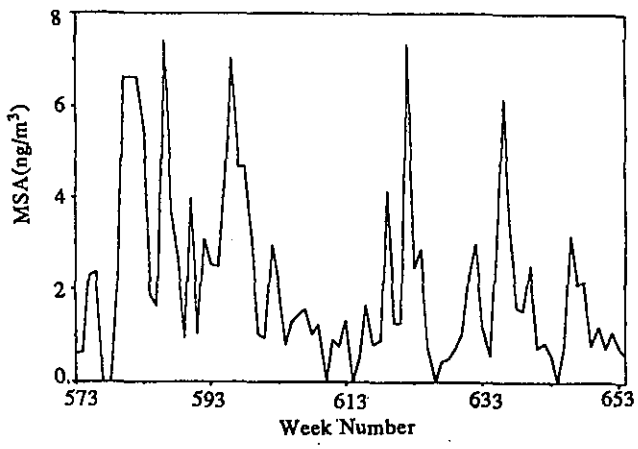

Fig. 1. Weekly methanesulfonic acid concentrations at MLO for January 1990 through June 1991.

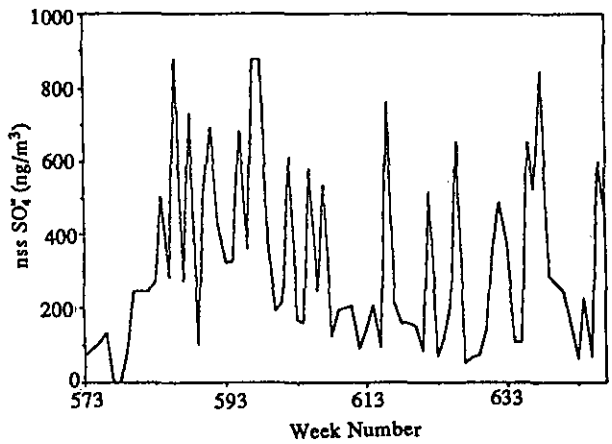

Fig. 2. Weekly non-seasalt sulfate concentrations at MLO for January 1990 through June 1991.

The mean concentration of nss $SO_4^=$ in the samples is similar to the other testing locations. However, unlike MSA, transport from Asia is the major contributor of nss$SO_4^=$ in the troposphere at MLO on an annual basis.

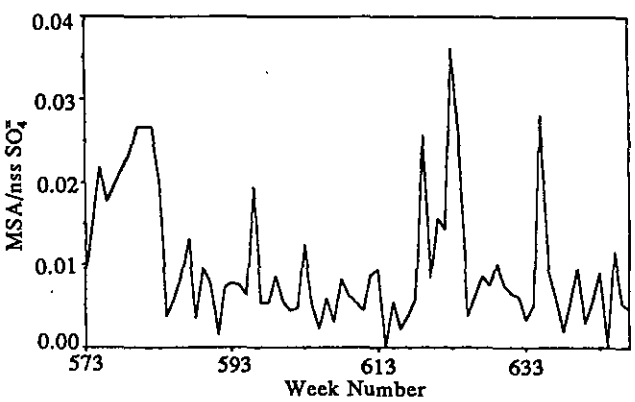

Fig. 3. Methanesulfonic acid/non-seasalt sulfate ratio at MLO for January 1990 through June 1991.

The MSA and nss $SO_4^=$ concentrations appear to follow a seasonal cycle. However, the data also contain very large random peaks. Although the peaks tend to obscure evidence of a seasonal cycle, they are very strong indicators of storm or strong wind activity mixing marine boundary layer aerosols into the troposphere near MLO.

Acknowledgments. This work was supported in part by NSF Grant 62-6955. We would like to thank the NOAA/CMDL staff at MLO for their collection the air filter samples.

REFERENCES

Parrington, J.R., The chemistry of background atmospheric particles collected at Mauna Loa Observatory, Hawaii, Ph.D. Thesis, Univ. of Maryland, 1983.

Parrington, J.R., and W.H. Zoller, Diurnal and longer-term changes in the composition of atmospheric particles at Mauna Loa, Hawaii, *J. Geophys. Res.*, *89*, 2522-2534, 1984.

Savoie, D.L., and J.M. Prospero, Comparison of oceanic and continental sources of non-sea-salt sulfate over the Pacific Ocean, *Nature*, *339*, 685-686, 1989.

Stable Lead Isotope Ratios at Barrow, Alaska

W.T. STURGES AND R.C. SCHNELL
Cooperative Institute for Research in Environmental Sciences, University of Colorado, Boulder, Colorado 80309-0449

J.F. HOPPER AND L.A. BARRIE
Atmospheric Environment Service, Downsview, Ontario M3H 5T4, Canada

1. INTRODUCTION

Measurement of stable lead isotope ratios in atmospheric particulate matter provides a means to trace the origins of pollutant aerosols where there are marked differences in the isotopic composition of regional sources [*Sturges and Barrie*, 1987]. Earlier measurements in the Canadian Arctic [*Sturges and Barrie*, 1989*a*] showed evidence for a Soviet origin of the lead. More recent measurements in Scandinavia [*Hopper et al.*, 1991] have better characterized the regional isotopic signatures in Europe and the Soviet Union, and have also shown that it is necessary to examine ratios of both Pb^{206}/Pb^{207} and Pb^{208}/Pb^{207} to properly discriminate regional sources. The latter isotope ratio was not measured in the Canadian Arctic study. We undertook sample collection at BRW, to both better characterize the origins of leaded aerosol in the Arctic, and also to compare with the isotopic composition measured at the Canadian Arctic sites, thousands of kilometers away.

2. METHODS

Atmospheric particulate matter was collected at BRW between March and April 1990. Samples were collected by filtration at about 100 dm^3 min^{-1} through 90 mm diameter Whatman 41 filters over periods of between 1 and 6 days (typically 2). Field blanks were collected in the same way as samples, but with the pump turned on for just 5 seconds. Breakthrough was assessed by placing a second filter in the filter pack. Samples were shipped and stored in heat-sealed semiconductor-grade-cleaned polyethylene bags. The samples were dry-ashed and acid-extracted for analysis by inductively coupled plasma mass spectrometry (Sciex Elan) at the Ontario Ministry of the Environment, Laboratory Services in Rexdale, Ontario (procedures described in *Sturges and Barrie*, 1989*b* and *Hopper et al.*, 1991).

3. RESULTS

Figure 1 shows the measured Pb^{206}/Pb^{207} results plotted versus atmospheric lead concentration. Only those data passing a rigorous quality control procedure have been plotted. Most of the points are clustered closely together. The highest isotope ratio was associated with snowmobile activity in the immediate vicinity of the sampler and corresponds to the ratio expected from U.S. leaded gasoline combustion. A meteorological analysis ruled out the possibility of pollution from the town of Barrow having affected the results, but we cannot rule out the chance of contamination from unreported vehicular activity close to the sampler, although the uniformity of the ratios and their mostly lower ratios argue against this.

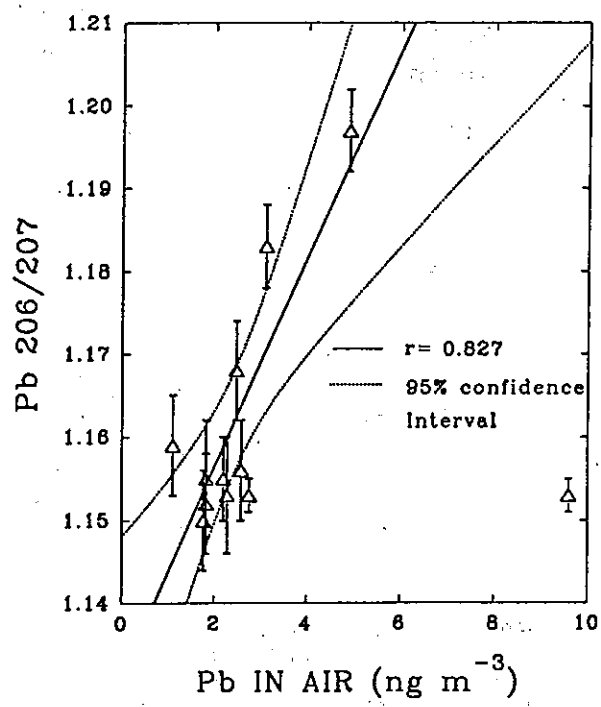

Fig. 1. Isotope ratio Pb^{206}/Pb^{207} as a function of lead-in-air concentration. The linear regression line was computed excluding the high lead concentration outlier. The dashed lines show the 95% confidence limits of the regression line. Error bars are 1 sigma analytical precisions.

The results for both isotope ratios are summarized in Figure 2 and compared with other data. The BRW results are shown as crosses, where the limbs of the crosses represent analytical uncertainties. Some of the the data are co-located and therefore not visible. The open elipses encompass the 95% confidence limits of representative ore bodies in the region, and the shaded elipses represent the 95% confidence limits of the regional isotope signatures determined by *Hopper et al.* [1991]. The shaded horizontal band represents the mean and standard deviation of the Canadian Arctic samples from *Sturges and Barrie* [1989*a*].

The measured Pb^{206}/Pb^{207} ratios were almost all very close to those from the Canadian Arctic study confirmimg that, on the time scale of days, the entire arctic basin is affected by a relatively uniform and homogeneous polluted air mass. The crosses mostly fall close to the signatures for Eastern Europe and the East (essentially the northern and central Soviet

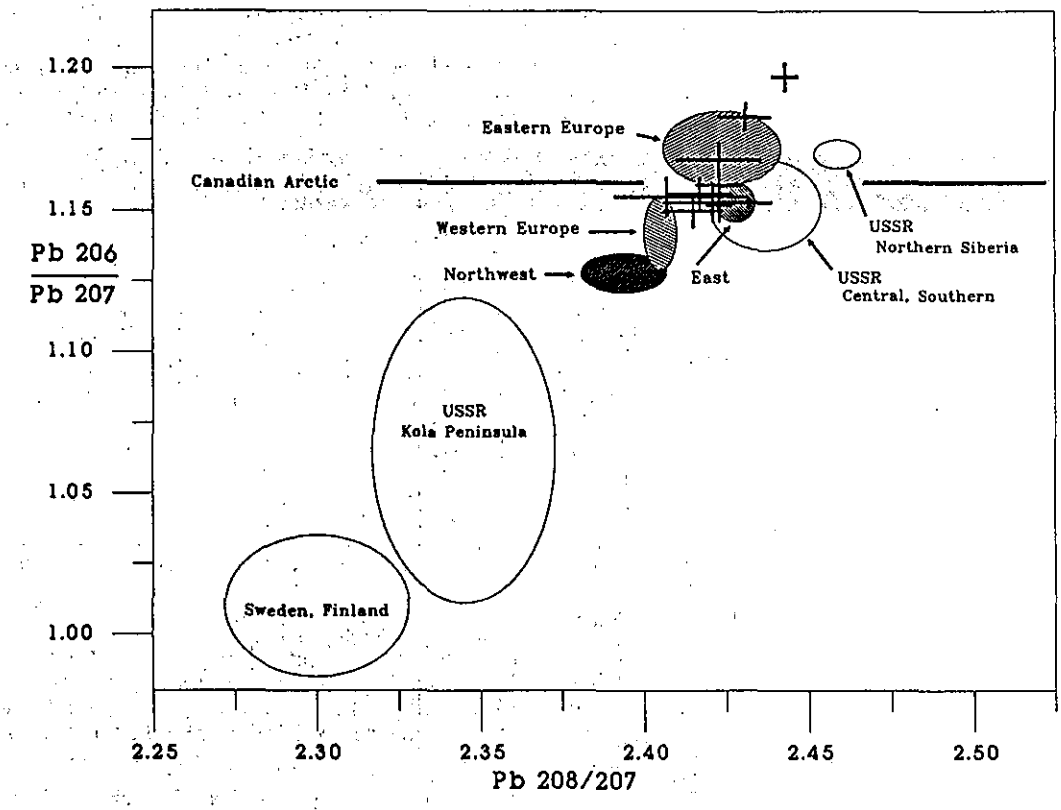

Fig. 2. Pb^{206}/Pb^{207} versus Pb^{208}/Pb^{207} for some representative lead ores (open ellipses), regional lead aerosol signatures determined by *Hopper et al.* [1991] (shaded ellipses), the mean and standard deviation of Pb^{206}/Pb^{207} ratios measured at Alert and Mould Bay from the Canadian Arctic by *Sturges and Barrie* [1989*a*] (thick horizontal line and shaded band respectively), and the results from this study at BRW (crosses, where the limbs represent 1 sigma analytical precisions).

TABLE 1. Estimated Apportionment, From This Study, of Aerosol Lead at BRW to Eurasian Sources, Compared With Similar Apportionments of Elements in Arctic Aerosol From Other Published Studies

Reference/Location	Method	Element	Apportionment (%)		
			East*	Western Europe	North America
This study BRW	Pb isotopes	Pb	67	33	?
Maenhaut et al. [1989] Ny Ålesund	Elemental ratios	Pb	63	37	<<10
Lowenthal and Rahn [1985] BRW	Elemental ratios	Trace elements	60-74	20-28	6-19
Akeredolu et al. [1991] Arctic	Transport model	Pb	~66	~33	?

*East = USSR and E. Europe

Union). They are similar to ratios in central/southern U.S.S.R., but unlike those in the huge northern metallurgical plants of northern Siberia and the Kola Peninsula.

We performed an apportionment calculation using the Pb^{208}/Pb^{207} data. These were selected since the mean Eastern European and East regional signatures were very close, and we could justify taking a mean value as representative of an undiscriminated Soviet/Eastern Europe source. We assume that only two homogeneous source regions contributed to the BRW leaded aerosol: the Soviet/Eastern Europe source and Western Europe. We then used a linear interpolation between the two mean signatures as our end points to calculate a day-by-day contribution factor from the two sources, weighted according to atmospheric lead concentration. Summing over the study period yielded the results shown in Table 1. We estimated that 67% of the lead was derived from the Soviet Union and Eastern Europe, and 33% from Western Europe. We found no evidence for a North American contribution (other than local vehicle contamination). These results are remarkably similar to those from other, quite different, analyses by other workers for BRW, Ny Ålesund, and the Arctic in general, also shown in Table 1.

Acknowledgments. WTS thanks the National Research Council for support. RCS was supported by the Office of Naval Research and the National Science Foundation under grant DPP-8822467. Thanks are due to CMDL for permission to use BRW, and we thank the station staff, especially Tim Quakenbush who set up the sampler and collected many of the samples. We also acknowledge the expertise of Mark Powell of the Ontario Ministry of the Environment who developed the technique for sensitive multiple lead isotope analysis in atmospheric aerosols.

4. REFERENCES

Akeredolu, F.A., L.A. Barrie, M.P. Olson, K.K. Oikawa, and J.M. Pacyna, The flux of anthropogenic trace metals into the Arctic from the mid-latitudes in 1979/80, *Atmos. Environ.*, in press, 1991.

Hopper, J.F., H.B. Ross, W.T. Sturges, and L.A. Barrie, Regional source discrimination of atmospheric aerosols in Europe using the isotopic composition of lead, *Tellus, 43B*, 45-60, 1991.

Lowenthal, D.H. and K.A. Rahn, Regional sources of pollution aerosol at Barrow, Alaska, during winter 1979-1980 as deduced from elemental tracers, *Atmos. Environ, 19*, 2011-2024, 1985.

Maenhaut, W., P. Cornille, J.M. Pacyna, and V. Vitols, Trace element composition and origin of the aerosol in the Norwegian Arctic, *Atmos. Environ., 23*, 2551-2569, 1989.

Sturges, W.T. and L.A. Barrie, Stable lead isotope ratios in Arctic aerosols: evidence for the origin of arctic air pollution, *Atmos. Environ., 23*, 2513-2519, 1989*a*.

Sturges, W.T. and L.A. Barrie, The use of stable lead 206/207 isotope ratios and elemental composition to discriminate the origins of lead in aerosols in Eastern Canada, *Atmos. Environ., 23*, 1645-1657, 1989*b*.

Sturges, W.T. and L.A. Barrie, Lead 206/207 isotope ratios in the atmosphere of North America: tracers of American and Canadian emissions, *Nature, 329*, 144-146, 1987.

Atmospheric Bromine Measurements at Barrow, Alaska, Using a Sequential Filter Pack and Carbon Tube Sampler

W.T. STURGES, R. C. SCHNELL, AND G. S. DUTTON
Cooperative Institute for Research in Environmental Sciences, University of Colorado, Boulder, Colorado 80309

S. R. GARCIA
Los Alamos National Laboratory, Los Alamos, New Mexico 87545

J. A. LIND
National Center for Atmospheric Research, Boulder, Colorado 80307

1. INTRODUCTION

Bromine (Br) is of interest in the arctic atmosphere because of the now well-known spring "pulse" of particulate Br that has been observed at widely separated sites throughout the Arctic [*Sturges and Barrie*, 1988; *Oltmans et al.*, 1989]. The pulse lasts for 2 to 3 months, during which time Br concentrations reach levels that are hundreds of times greater than summer and early winter values. The start of the peak is timed to the first appearance of sunlight at the particular site, suggesting a link to photochemistry. High concentrations of $CHBr_3$, and other brominated organic gases, have been observed in late winter and early spring [*Cicerone et al.*, 1988] and may be the source of the particulate Br. A strong anticorrelation between particulate Br and ozone has also been observed during the arctic spring. *Barrie et al.* [1988] conjectured that the ozone was being removed by the photochemical formation of Br atoms from $CHBr_3$, although others have suggested that inorganic Br gases such as nitryl bromide may be important [*Finlayson-Pitts et al.*, 1990].

The origin of $CHBr_3$ in the Arctic has been something of a mystery, but recently we have measured emissions of $CHBr_3$ and other volatile organic Br species from both Antarctica and Arctic ice algae [*Sturges et al.*, 1991*b*], as well as high fluxes of $CHBr_3$ out of leads and holes drilled in the ice (Sturges and Cota, unpublished data). Ice algae have been found on the underside of virtually all annual ice in the polar regions, constituting an enormous, and largely overlooked, amount of primary productivity.

It is desirable to examine the speciation of Br between particulate and gaseous phases on a diurnal basis to further our understanding of the likely mechanisms involved in the Br pulse phenomenon. There is only one record, that of *Berg et al.* [1983], of an attempt to measure a complete breakdown of Br between organic, inorganic, and particulate phases. Unfortunately, results from just four samples were reported, and no attempt was made to examine diurnal variations. Furthermore, due to collection efficiency problems, they did not differentiate organic from inorganic gaseous Br.

We have been fortunate to obtain the original sampling equipment of *Berg et al.* [1983], which we have modified for higher sampling rates. We have extended the data set at the same sampling site (Barrow, Alaska), examined day/night differences, measured inorganic gaseous Br, and also measured organic gaseous chlorine.

2. METHODS

A filter pack arrangement was used to separate and collect the different phases of Br at BRW (see *Sturges et al.* [1991a] for details). The Teflon filter pack contained a Teflon filter to collect particulate matter, followed by two absorbent filters in series to collect inorganic gaseous Br. These filters were either cellulose impregnated with potassium hydroxide (KOH) or pure Nylon 66. Following the filters were two (or three) tubes containing activated coconut charcoal, to collect organic Br gases. Using paired filters and tubes in series allowed us to measure, and correct for, collection efficiency. The charcoal was highly cleaned and vacuum fired using the procedure of *Berg et al.* [1983]; the process takes about 3 months.

The filters were extracted in ultra-pure water and analyzed at NCAR by ion chromatography (IC). Bromide, nitrate, and sulfate ions were measured. Chloride blank levels were too high for Cl measurements to be reported. The charcoal was analyzed non-destructively by neutron activation analysis (NAA) at Los Alamos National Laboratory (details in *Berg et al.* [1983]).

3. RESULTS

The carbon tube analyses of Br were most encouraging. Field blanks were below detection limit, and all samples were at least three times the detection limit. Collection efficiency was greater than 88% for all samples (mean of 96%), even for sample volumes of up to 55 m^3. This is remarkable considering that only 1.5 g of charcoal was used. Chlorine blanks were measurable, but all of the samples exceeded the blank by more than three standard deviations. Iodine could not be detected at more than one standard deviation above the blank.

A summary of all the Br data is shown in Figure 1. It is clear from this figure that inorganic gaseous Br was an almost negligible component of total Br. Particulate and organic gaseous Br contributed variable, but roughly similar amounts of Br. We are still in the process of fully examining our results, but some preliminary observations may be made as follows.

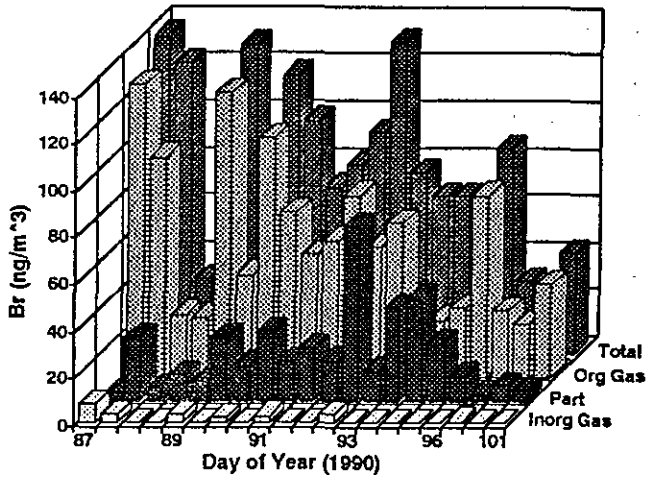

Fig. 1. Summary of Br measurements from the spring 1990 study period.

In Figure 2*a* the particulate Br results are shown. Night and day samples are identified. It should be noted that the terms "night" and "day" as used here are somewhat misleading. The day samples were taken during the working day, i.e. about 0900 to 1700 LST. The night sample covers the remaining period, and incorporates several hours of full sun and twilight. Diurnal differences will consequently be somewhat muted in this record. The few multi-day samples at the end of the experiment have not been included in this plot.

There appeared to be a tendency towards higher particulate concentrations during the day in agreement with the hypothesis of a link to photochemistry. In the next panel down (Figure 2*b*), organic gaseous Br shows some evidence for higher nighttime concentrations. Combining the two into a ratio in panel *c* indicates a diurnal variation in particulate to organic Br, with lower values at night. This again suggests photochemical loss of organic Br and formation of particulate Br.

It was unfortunate that during the field experiment there was little deviation in ozone concentrations compared to those observed during the following weeks. There was only one distinct ozone destruction "episode" towards the end of the period (Figure 2*d*). Nevertheless, it is notable that this episode coincided exactly with the large peak in the particulate to organic Br ratio (panel *c*), suggesting some influence of Br chemistry on ozone concentrations.

Figure 3 shows a plot of organic Br against particulate Br for day and night samples. This also illustrates the apparent inverse relationship between the two Br phases. The correlation coefficient r^2 was $CHBr_3$ −0.227 for all of the points, but increased to −0.667 when the two low concentration outliers were removed. The regression line in the figure is for the latter correlation calculation. Surprisingly, the relationship appeared to hold even for the night samples. It should be remembered, however, that the night sample periods did include a significant amount of daylight.

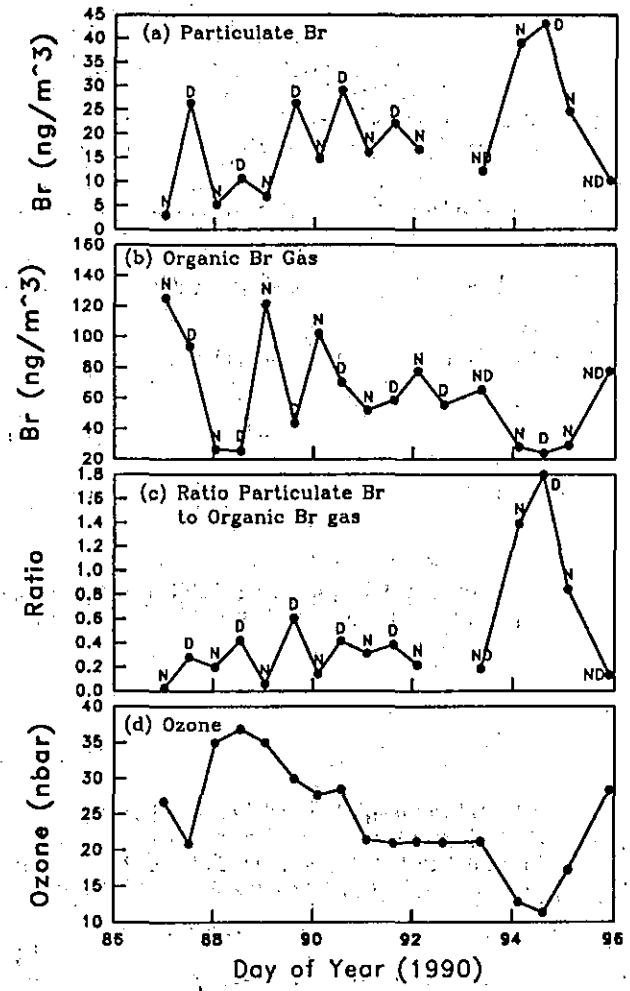

Fig. 2. Diurnal measurements of (*a*) particulate Br, (*b*) organic gaseous Br, (*c*) the ratio of particulate to organic gaseous Br, and (*d*) mean hourly ozone concentrations averaged over the corresponding Br sampling interval. N = night sample, D = day sample, ND = 24-hour sample.

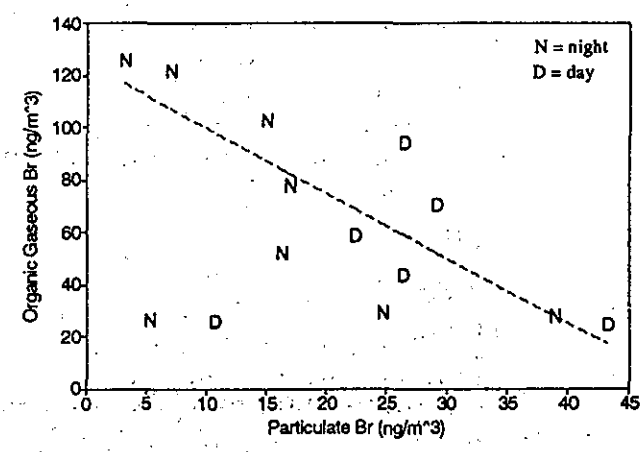

Fig. 3. Plot of organic gaseous Br against particulate Br for diurnal samples. The regression line was calculated excluding the two outlying points with low organic gaseous Br concentrations.

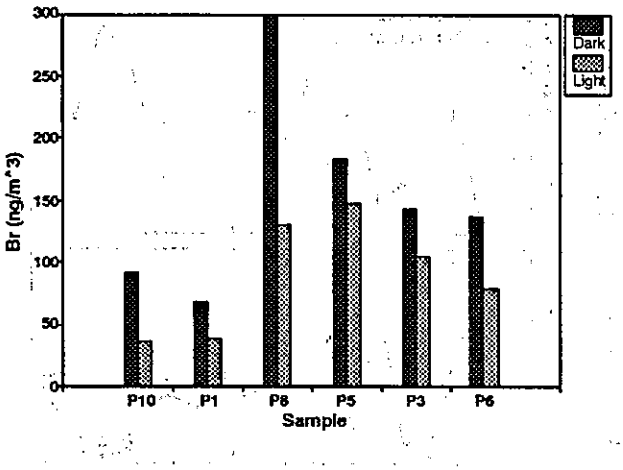

Fig. 4. Ratio of organic gaseous Br to organic gaseous Cl multipied by 1000 for diurnal samples.

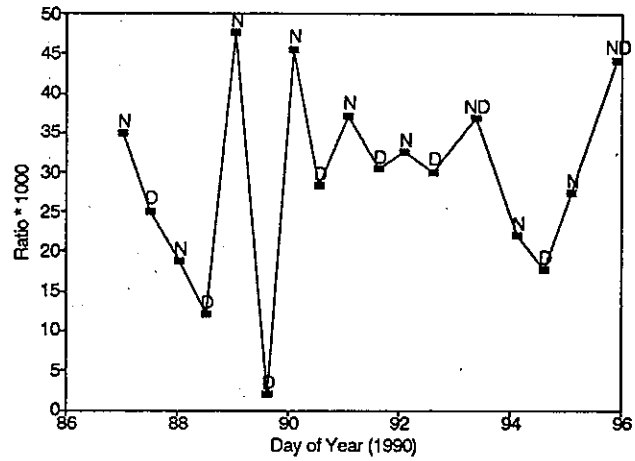

Fig. 5. Results from irradiation of nighttime air at Barrow with long wave ultraviolet light (light shaded bars) compared with a dark control chamber (dark shaded bars).

Organic Br and Cl were well correlated with an r^2 of 0.67. It seems probable that both have some similar sources from Arctic marine biological activity. The non-zero Cl intercept (825 ± 453 ng m^{-3} or 522 ± 286 ppt Cl) may be at least partly due to pollutant Cl-containing gases.

We expect to see some diurnal variation in the ratio of organic Br to Cl if they have similar source strengths and if we are correct in believing that Br gases are photolyzed in the lower troposphere, while most organic Cl gases are not, or to a much lesser degree. The ratios plotted in Figure 4 do appear to at least weakly support this hypothesis; in all cases there was a lower daytime ratio following the nighttime value.

The final evidence for the importance of photochemistry comes from an experiment conducted at BRW where nighttime air was drawn through two glass chambers. One was kept dark as a control, and the other was illuminated with long-wave ultraviolet fluorescent lights. Filter packs were used to collect the effluent from the tubes (details in *Sturges et al.* [1991*a*]). Figure 5 shows that inorganic Br was destroyed in the illuminated chamber in every experiment. Using the same equipment we were able to demonstrate loss of ozone in ambient nighttime air from 20 ppb to zero in the illuminated chamber during 30 min stop flow. In 1989, using similar equipment, we measured an irradiation time-dependent increase in particulate Br in the lit chamber [*Sturges et al.*, 1991*a*]. Regrettably, we were not able to make reliable measurements of particulate Br in the latest experiment, due to the small sample size.

The main conclusion of this study is that the results point to the existence of a rapid photolysis of organic Br gases in the arctic spring, resulting in the formation of particulate Br, and possibly accounting for the Br pulse phenomenon. There was also some supporting evidence for a link to surface ozone loss. We hope that further examination of the data, and integration with other chemical and meteorological data, including specific organic Br compounds measured by absorption tube collection and gas chromatography, will shed further light on arctic Br and ozone chemistry.

Acknowledgments. WTS was supported by the National Research Council of the National Academy of Sciences. RCS was supported by the Office of Naval Research and the National Science Foundation under grant DPP-8822467. GSD was supported by undergraduate research grants from the Colorado Commission for Higher Education, and the Undergraduate Research Opportunities Program of the University of Colorado. We thank Paul Sperry of NCAR for generously donating the NCAR sampling system. We are also indebted to CMDL for access to the BRW station and data, and to the station staff for their invaluable help.

4. References

Barrie, L.A., J.W. Bottenheim, R.C. Schnell, P.J. Crutzen, and R.A. Rasmussen, Ozone destruction and photochemical reactions at polar sunrise in the lower arctic atmosphere, *Nature, 334*, 138-141, 1988.

Berg, W.W., P.D. Sperry, K.A. Rahn, and E.S. Gladney, Atmospheric bromine in the Arctic, *J. Geophys. Res., 88(C11)*, 6719-6736, 1983.

Cicerone, R.J., L.E. Heidt, and W.H. Pollock, Measurements of atmospheric methyl bromide and bromoform, *J. Geophys. Res., 93(D4)*, 3745-3749, 1988.

Finlayson-Pitts, B.J., F.E. Livingstone, and H.N. Berko., Ozone destruction and bromine photochemistry at ground level in the Arctic spring, *Nature, 343*, 622-625, 1990.

Oltmans, S.J., R.C. Schnell, P.J. Sheridan, R.E. Peterson, J.W. Winchester, S.-M. Li, P.P. Tans, W.T. Sturges, L.A. Barrie and J.D. Kahl, Seasonal surface ozone and filterable bromine relationship in the High Arctic, *Atmos. Environ., 23*, 2431-2441, 1989.

Sturges, W.T. and L.A. Barrie, Chlorine, bromine and iodine in arctic aerosols, *Atmos. Environ., 22*, 1179-1194, 1988.

Sturges, W.T., R.C. Schnell, S. Landsberger, J.M. Harris, and S.-M. Li, Chemical and meteorological influences on surface ozone destruction at Barrow, Alaska during spring 1989, *Atmos. Environ.*, in press, 1991*a*.

Sturges, W.T., C.W. Sullivan, R.C. Schnell, L.E. Heidt, W.H. Pollock, and Hofmann, D.J., Symposium on the Tropospheric Chemistry of the Antarctic Region, edited by A. Hogan and S.L. Bowen, Cooperative Institute for Research in Environmental Sciences, University of Colorado, Boulder, Colorado, June 3-6 1991, US Army Cold Regions Research and Engineering Laboratory Special Report (Abstracts) 91-10, p. 55, 1991*b*.

Radon as a Baseline Selection Criterion at Mauna Loa Observatory

S. WHITTLESTONE
Australian Nuclear Science and Technology Organization, PMB 1, Menai, N.S.W. 2234, Australia

L.P. STEELE
CSIRO, Division of Atmospheric Research, Mordialloc, Victoria 3195, Australia

S. RYAN
NOAA, Mauna Loa Observatory, Hilo, Hawaii

1. INTRODUCTION

At the observatories studying the global changes in trace constituents of the atmosphere, knowledge of the air history in weeks prior to sampling is of great importance in the interpretation of the results. Local emissions and meteorology can significantly influence the concentrations of trace gases. *Keeling et al.* [1976] demonstrate the impact on the carbon dioxide record of the upslope winds at MLO. Because of this, it is common practice to select sampling times or flag data so that a record can be obtained under so-called "baseline" conditions [*Thoning et al.*, 1989]. In this context, baseline is usually interpreted to mean that the sample is representative of a large volume of the atmosphere. This is essential for comparing measurements to current fixed-grid model simulations of trace gas levels in the global atmosphere because the size of grid boxes is large, and the atmosphere is assumed uniform in each box at each time step of the simulation [*Fung et al.*, 1991].

While model verification and intercomparison of data from different species requires a conformity of sampling conditions, the definition of baseline is notoriously species-dependent. In practice, a minimum requirement is made that does not exclude an unacceptable amount of data, then additional criteria are added for each species. One aim of the present study is to investigate the possibility of upgrading the minimum requirement to increase the overlap of sampling conditions for different species. Thus at MLO, the present minimum requirement for baseline is non-upslope conditions to avoid local influence. However, most trace gases are perturbed by passage over land or cities. It is, therefore, suggested that the criteria for baseline selection should include indicators of recent contact with land.

Local wind speed and direction are important in determining whether atmospheric trace species measurements made at MLO are free from local Hawaiian influence. Dewpoint and temperature help to determine the extent of mixing of the free troposphere with the boundary layer. However, the local meteorological data cannot indicate where the air has been on scales of more than a few hundred km. Trajectory calculations provide a good general idea of the path the air has taken, but there are three important limitations: the information is not immediately available, so that it cannot be used to operate conditional samplers; the timing accuracy is generally no better than several hours, so the data cannot be used to select pollution episodes during periods of change; and even though air may have passed over land, it may not actually have mixed with air from the surface. Tracer techniques offer an objective, real-time criterion for baseline selection provided the tracer can be measured continuously with suitable sensitivity.

Radon has been widely used as a tracer for air masses which have recently passed over land because it is an inert gas unaffected by chemical interactions in transit, and its emanation rate from land is about one hundred times the rate from the ocean [*Wilkening and Clements*, 1975]. Its half-life of 3.8 days ensures that it does not build up in the atmosphere. It has been measured continuously at MLO since May 1989, and it has been demonstrated to be highly sensitive to the influx of air from distant continents [*Whittlestone et al.*, 1991]. *Gras et al.* [1991] have shown that CN are in some ways a better tracer than radon for polluted air masses for distances up to the order of a few hundred km from the source, but that for the longer distances involved at MLO, radon is to be preferred.

Recent CN data results from the radon program at MLO were measured by the CN counter incorporated into the radon detection system. Radon is correlated with CN and other gases, CO_2, chlorofluorocarbons, N_2O, and CH_4, and evaluated for inclusion with other criteria in defining the aged baseline condition at MLO.

2. RADON, CN AND AIR MASS TRAJECTORIES

In selecting data, it was necessary to exclude samples perturbed by local radon sources. Wind direction and speed are strong indicators of the likelihood of local contamination, and the value of requiring winds to be non-upslope is well established. However, it is reasonable to expect some contamination in air in the non-upslope sector for a short time after a change in conditions from upslope. To avoid this, the meteorological baseline condition can be required to be established for some time before sampling. A period of 2 hours has been employed in the subsequent analysis. This extended local meteorological baseline criterion resulted in three groups of data: about half in the baseline group, a quarter in the locally affected upslope group, and the group whose members did not fit into the first two.

For the study of interrelationships between radon, CN, and 10-day isobaric back trajectories ending at MLO, we have selected from throughout 1990 a number of periods (totalling 66 days) from all seasons. For each of these days, back trajectories were obtained for air parcels at both the 500 hPa and 700 hPa pressure levels, for arrival times at MLO of 0000 and 1200 hours GMT. To account for timing uncertainties in the calculation, both the radon and CN baseline

data have been averaged over the 12-hour period centered on the calculated time of arrival of the air parcels. We have then used the local meteorological data to classify the air masses as either "free troposphere" (FT) or "boundary layer" (BL). When the local dewpoint was less than -10°C, the air mass was classified as FT, and the 500 hPa trajectory was used to examine the relationships. For dewpoints above -10°C, the classification was boundary layer (BL) and the 700 hPa trajectory used. The data included in this BL category represent times when strong synoptic flows lead to mixing between the midtroposphere and the boundary layer. The fraction of the time that the dewpoint lay in the -5° to -15°C range was small, so the analysis is not sensitive to the exact demarcation point chosen to separate the categories.

A procedure was devised to test the extent to which radon and CN concentrations correlated with trajectories passing over land. Frequency distributions of FT radon and CN concentrations were formed for the selected trajectory classes (Figure 1). In the case of radon there is a strong bias towards high radon concentrations when the trajectory path started over land. The median concentrations of both radon and CN for all trajectories were calculated and used as convenient reference levels. The fractions of radon and CN concentrations less than these reference levels were determined for the land and sea trajectory groups. For our FT category, 71% of the radon concentrations for land trajectories exceed the reference level, clearly indicating that the high radon is associated with trajectories over land. As expected in the group associated with sea trajectories, a lower fraction of the radon concentrations, 33%, are above the reference level. A separation factor, S, was obtained by dividing the land fraction (71%) by the sea fraction (33%) for FT radon, yielding a value of 2.2 for S. This procedure was carried out for both radon and CN in the FT and BL categories (Table 1).

For the BL category, both CN and radon distributions are strongly separated according to whether or not the trajectories have passed over land. This is also true for FT radon; but for FT CN, the trajectories provide no separation, as the CN concentration distributions are the same for land and sea trajectories (Figure 1). Evidently passage over land often is accompanied by some vertical mixing between the BL and the FT. It appears that during or shortly after mixing, processes such as precipitation (which results in the low dewpoint of FT air) remove CN but not radon.

TABLE 1. Performance of Trajectory Calculations in Separating High Radon and CN Concentrations From Low Values

Sample Category	Separation factor	
	Radon	CN
Upslope	1.5	1.1
Boundary layer	2.1	1.8
Free troposphere	2.2	1.0

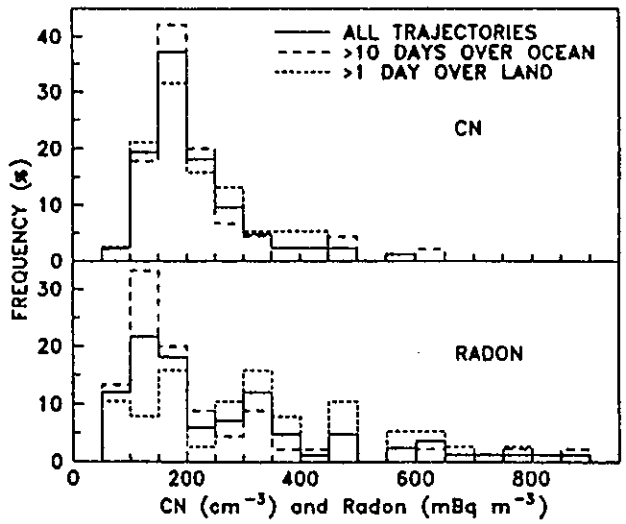

Fig. 1. Normalized frequency distributions of radon and CN concentrations in free tropospheric air.

Upslope air is considered for completeness. It is BL air with added radon and CN uncorrelated with the air mass origin. As expected, the separation factors are less than for the non-upslope BL samples.

3. Comparison of CN and Radon

In this section CN are evaluated as a tracer of continental influence using radon as the baseline criterion taking hourly data from July 1989 through June 1990. The extended meteorological baseline selection criterion was applied as in Section 2, yielding upslope, BL, and FT data groups. Not only is the sample larger than was possible with the trajectory analyses, but the timing uncertainty has been removed. Since there are considerable seasonal changes of CN [*Gras*, 1990)] and radon, the data have been put into summer and winter groups.

The upslope dependence of CN on radon is only moderate (Figure 2) because the fetch over land is so short that paths by a CN source may not always pass over deep soils emanating radon. Also, the highest radon concentrations are from distant land while the main CN sources are local. In the non-upslope samples, the distributions have no dependence on radon below 0.1 Bq m^{-3}. This is similar to the results reported by *Gras et al.*, [1991] at Cape Grim (Tasmania, 41°S, 145°E) and Macquarie Island (55°S,159°E) and supports the use of 0.1 Bq m^{-3} as a baseline criterion for radon.

To allow comparison to the analysis based on the trajectories, the tentative 0.1 Bq m^{-3} baseline criterion has been used as a reference level to separate the CN distributions in a similar fashion to that done in Section 2. The values are 2.4 upslope, 1.6 boundary layer, and 1.5 free troposphere which should be compared to the values in Table 1 for CN selected by trajectory of 1.1, 1.8 and 1.0 respectively. It is expected that the separation factors should be greater in the upslope winds using the radon criterion because a high proportion of the CN and radon in this sector

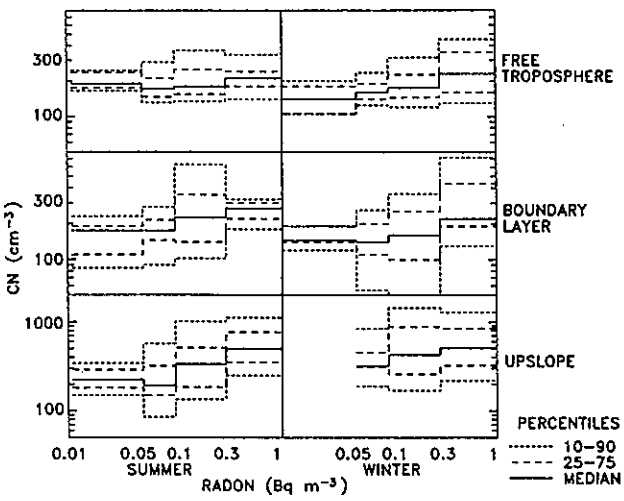

Fig. 2. CN concentration frequency distributions versus radon concentrations at MLO in 1989-1990.

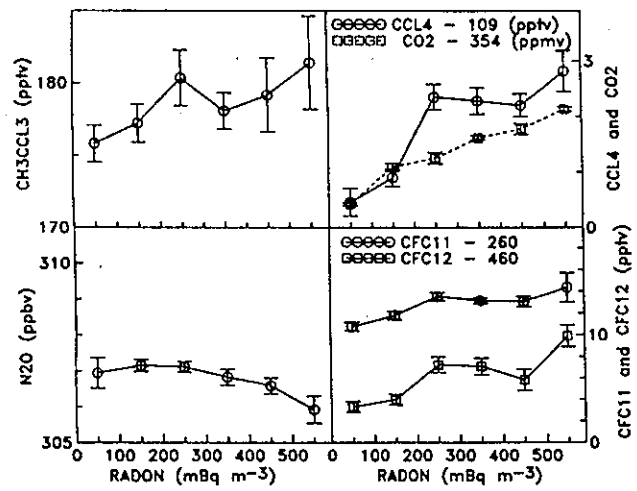

Fig. 3. Trace gases versus radon at MLO in non-upslope winds.

is local and independent of the long range path. What is more surprising is the relatively high separation factor in the free troposphere. In the events selected for trajectory analysis, it appeared that no CN survived the vertical mixing which raised radon to the FT. A study of CN, radon, and trajectories to resolve this apparent inconsistency may help to understand the conditions under which vertical transport of reactive species is favored.

4. Radon Applied to Selection of Trace Gases at MLO

This is a preliminary examination of the value of including radon in the definition of baseline conditions for sampling CO_2 (measured during January 1991), CH_4 (July 1989 through June 1990), N_2O, CFC-11, CFC-12, CCl_4, and CH_3CCl_3 (all for November 1989). In all cases hourly data are used.

For simplicity of interpretation, the gases were selected using the extended meteorological baseline criterion to eliminate local influence. During the short data period studied, CO_2, CFC-11, CFC-12, CCl_4, CH_3CCl_3, and N_2O all exhibited strong dependence on concurrent radon concentration. The data being grouped into radon bins 50 mBq m^{-3} wide centered on the data points is shown in Figure 3. The error bar indicates one standard deviation of the mean for each bin. It is notable that the correlations are positive for all species except N_2O. This reflects the fact that of the six gases, N_2O is the only one for which oceanic sources can predominate (*IPCC*, 1990).

To illustrate the power of radon in characterizing air masses, the CH_4 data have b1,3 placed in four groups defined by range of radon concentration and monthly averages have been obtained (Figure 4). It is clear that during much of the year, radon and CH_4 are strongly positively correlated. Selection of CH_4 using the 0.1 Bq m^{-3} baseline criterion yields a well-defined seasonal cycle with an amplitude of about 25 ppbv and high period from September through February. A marked feature of the "baseline" group is the small size of the standard deviations. We are investigating the implications of the results suggesting that the selection of CH_4 during periods of low radon may offer a more realistic seasonal cycle with which to compare the model simulations of *Fung et al.*, [1991].

5. Conclusions

Meteorological data are primary indicators of the upslope air which is subject to local land influence. Once upslope air is identified and removed from the analysis, dewpoint and wind direction provide no clues to the degree of recent land

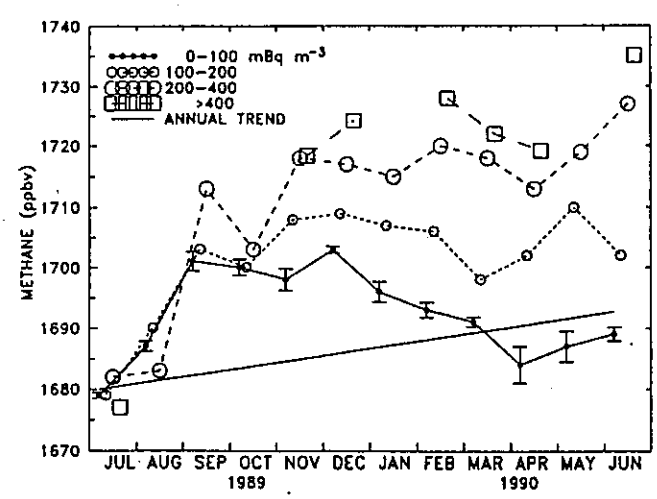

Fig. 4. Monthly averages of methane selected by radon concentration range at MLO. Samples during upslope conditions have been excluded.

influence. Analysis using air trajectories shows that radon correlates strongly with passage over land (Table 1), while in the case of CN the correlation is not consistent. This supports the use of radon as a principal indicator of potential perturbation of the trace gas records at MLO caused by the recent passage of air masses over land.

The application of radon as a selection criterion for other trace gases has demonstrated that the data from the MLO radon instrument provide a powerful means of gaining insights into the variability of these trace gas records. In particular, there is a strong indication that CH_4 selected from times at which the radon is below 100 mBq m^{-3} is much better matched to the output of global models than the full record. It is, therefore, likely the radon baseline criterion is necessary for verification of models for any gas influenced by passage over land.

Acknowledgments. The authors are grateful to CMDL for providing the laboratory space and technical support for the MLO work and its staff members, P. Tans for the CO_2 data, J. Elkins for other trace gas data, G. Herbert for the meteorological data, and J. Harris for the trajectories. The work would not have been possible without the support of technical staff at CSIRO and ANSTO.

6. References

Gras, J.L., Baseline atmospheric condensation nuclei at Cape Grim 1977-1987, *J. Atmos. Chem.*, *11*, 89-106, 1990.

Gras, J.L., and S. Whittlestone, *Radon and CN: Complementary tracers of polluted air masses at coastal and island sites*, MARC-II conference of the American Nuclear Society (ANS), April 22-26, 1991, LaGrange, IL, 1991.

Fung I., J. John, J. Lerner, E. Mathews, M. Prather, L.P. Steele, and P.J. Fraser, Three-dimensional model synthesis of the global methane cycle, *J. Geophys Res.*, *96*, 13,033-13,065, 1991.

IPCC, *Climate Change, the IPCC Scientific Assessment*, edited by J.T. Haughton, G.J. Jenkins, and J.J. Ephraums, Cambridge University Press, Cambridge, pp. 7-40, 1990.

Keeling, C.D., R.B. Bacastow, A.E. Bainbridge, C.A. Ekdahl, P.R. Guenther, L.S. Waterman, and J.F.S. Chin, Atmospheric carbon dioxide variations at Mauna Loa Observatory, Hawaii, *Tellus*, 28,538-551, 1976.

Miller J.M., A five-year climatology of back trajectories from the Mauna Loa Observatory, Hawaii, *Atmos. Environ.*, *15*, 1553-1558, 1981.

Thoning, K.W., P.P. Tans, and W.D. Komhyr, Atmospheric carbon dioxide at Mauna Loa Observatory, 2, Analysis of the NOAA GMCC data, 1974-1985, *J. Geophys. Res.*, *94*, 8549-8565, 1989.

Whittlestone, S., E. Robinson, and S. Ryan, Radon at the Mauna Loa Observatory: Transport from distant continents, *J. Atmos Res.*, in press, 1991.

Wilkening, M.H., and W.E.Clements, Radon 222 from the Ocean surface, *J. Geophys. Res.*, *80*, 3828-3830, 1975.

Seasonal Amplitude Variations in CO_2 in the Northern Hemisphere

T. P. WHORF AND C. D. KEELING
Scripps Institution of Oceanography, La Jolla, California 92093-0220

1. INTRODUCTION

Cooperative programs of CO_2 measurements at Point Barrow, Alaska (BRW), and Mauna Loa, Hawaii (MLO), between Scripps Institution of Oceanography (SIO) and CMDL continued during 1990. Air samples were collected in 5-L glass flasks on approximately a weekly basis since 1960 at MLO and since 1974 at BRW. In addition, SIO continued to monitor atmospheric CO_2 concentrations at MLO on a continuous basis using the NDIR gas analyzer installed on site in 1958.

Recently, data at these two sites, as well as a third northern hemisphere site at SIO, were interpreted in order to look for recent changes in the amplitude of the seasonal cycle in CO_2 concentration. Such changes were observed previously in the MLO continuous record [*Bacastow et al.*, 1985], as well as at Ocean Station P, which was discontinued in 1981 [*Keeling et al.*, 1985]. Air samples were collected on the Scripps Pier since 1969 and are supplemented by two several-year periods of continuous CO_2 measurements. Together these three sites provide the longest available records of CO_2 concentration in the northern hemisphere, where the variations are mainly attributable to the metabolic activity of land vegetation [*Keeling et al.*, 1989, p 175].

2. DATA AND ANALYSIS

All flask samples were first evacuated at the Scripps laboratory and then later returned from the field to be analyzed for their CO_2 concentration with an NDIR gas analyzer of the same design as that installed at MLO. Calibrations have continued with reference gases similar to those used at MLO [*Keeling et al.*, 1986].

Air samples were rejected if pairs did not agree within 0.40 ppm (singlets rejected also) or if found to be outliers having a residual greater than three standard deviations from a smooth curve fit describing the seasonal and interannual variations. The function chosen in the fitting process uses a sum of four harmonics to describe the seasonal variations and a cubic spline [*Reinsch*, 1967] to describe the interannual variations. A gain factor is used to model an approximately linearly increasing seasonal amplitude variation [*Keeling et al.*, 1989, pp 167, 176]. This simple model of increasing annual CO_2 cycles was introduced when it became clear in our longer CO_2 records that there were significant increases in the seasonal amplitude of CO_2 concentration.

Figure 1 shows the results of such fits made to the CO_2 observations collected from all of our northern hemisphere stations. BRW data were augmented to include continuous CO_2 data measurements made by *Kelley*, 1969 during the period 1961-1967, so as to show possible variations in the seasonal amplitude of CO_2 over a longer period. Data at three additional sites are shown in the figure: Alert, N.W.T (82°N, 62°W); Cape Kumukahi, Hawaii (19°N, 155°W); and Christmas Island (2°N, 157°W). A cooperative program at Alert between SIO and the Atmospheric Environment Service of Canada has existed since 1985 and at Cape Kumukahi between SIO and CMDL since 1979. Both the Alert and Cape Kumukahi CO_2 records are, however, relatively short and can thus provide only supporting evidence to the results from the longer stations. The location of Christmas Island near the equator makes it more useful for observing the large local fluctuations due to changes of pCO_2 in equatorial seawater [*Keeling et al.*, 1989, pp. 202-208].

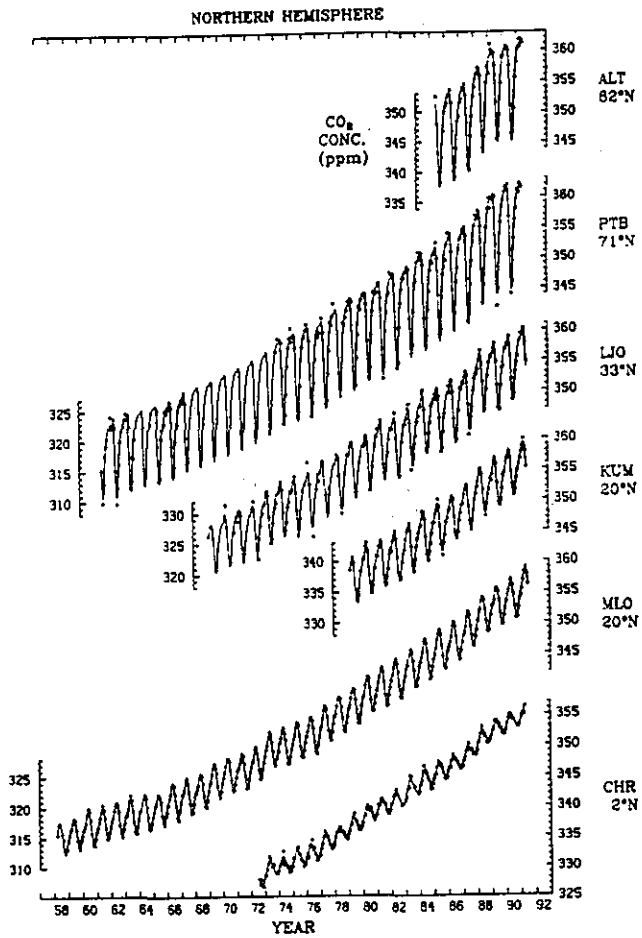

Fig. 1. Monthly average CO_2 data at current SIO northern hemisphere stations fit by the function described in text. Early BRW data from *Kelley*, 1969; MLO data are from continuous record and Christmas Island data (1977-1991) include Fanning Island data (4°N) from 1972 to 1983.

3. RESULTS

Figures 2-5 show seasonal amplitudes computed annually by least-square fitting an annual factor times the same set of four harmonics derived in the overall fit, but for each year independently. The harmonic function is thus phase locked by the fit to the overall data set. An overall gain factor "A" for the entire record is also computed where the annual factor is assumed to vary linearly with time by the expression, "1 + At," where t denotes time, here expressed relative to January 1, 1980. A linear fit made to the set of independent annual amplitudes for a given station gives approximately the same gain factor. Note that in the figures the annual factors are computed for times relative to the midpoint of the record (i.e., the amplitudes are relative to the mean annual cycle). Also, for each station the most recent annual amplitude is preliminary since the year is not complete. Table 1 lists the gain factors for each of the three northern hemisphere stations shown in Figures 2-5, as well as at Ocean Station P where a solid estimate was obtained up to 1980. Standard error estimates for the computed gain factors are also listed. These range from 4% to 26%. MLO seasonal amplitudes are shown separately for the continuous CO_2 data and the CO_2 data derived from flask samples. The latter data set is, of course, noisier than the continuous record because of obvious differences in sampling and smoothing, but it is useful nonetheless to see how well the records agree, since most of the data at other stations are derived from air sampling by flasks. Smoothing of the MLO continuous record results from omitting CO_2 data that appear to be contaminated by local sources or sinks, whereas in the case of flask sampling it is not always so clear what local effects may be present, even if conditions seem adequate for sampling. By sufficiently frequent sampling, however, and omitting flask data that have fit residuals greater than three standard deviations, these effects were minimized. The distribution and quantity of data throughout any given year will necessarily impact the seasonal amplitude for that year, so that in some years the computed amplitudes may be unreliable. One such year, 1976, was omitted in the case of the La Jolla amplitudes. Generally a good quality of data at the La Jolla station has been maintained as long as care was taken in choosing sampling times, despite the proximity of local sources. Recently, maintenance of a continuous record has been quite helpful in achieving this goal.

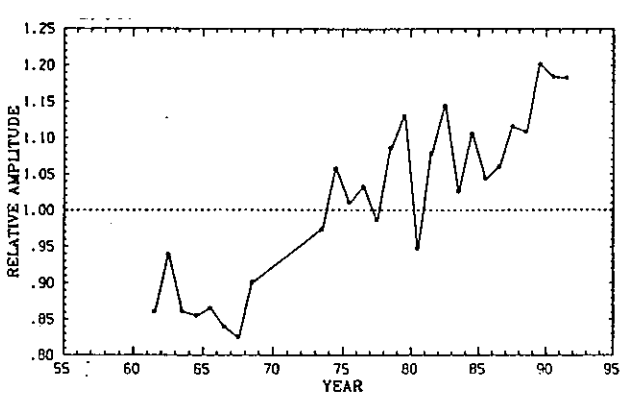

Fig. 2. Relative amplitudes of the seasonal cycle in atmospheric CO_2 at BRW where time is relative to the midpoint of the record (also true for Figures 3-5).

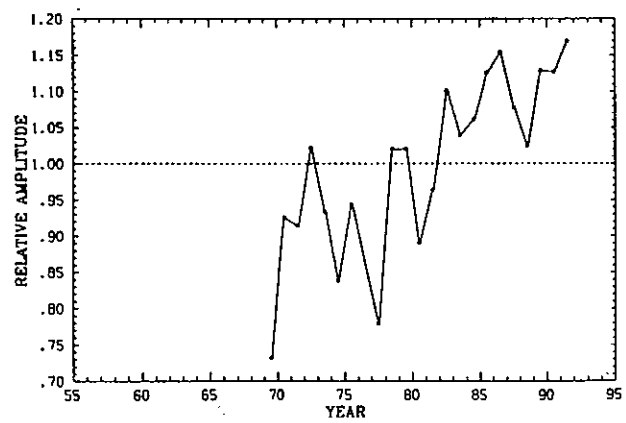

Fig. 3. Relative amplitudes of the seasonal cycle in atmospheric CO_2 at La Jolla Pier.

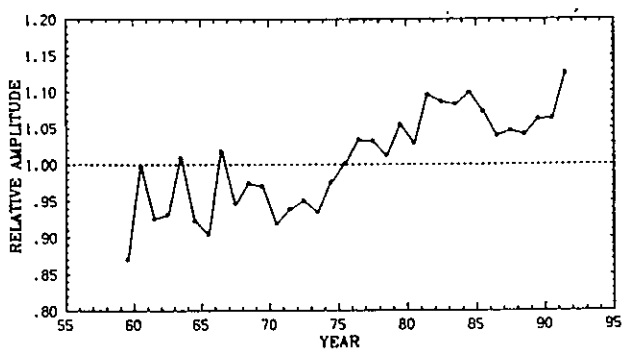

Fig. 4. Relative amplitudes of the seasonal cycle in atmospheric CO_2 at MLO. Data used in fitting are weeklies averaged from continuous record.

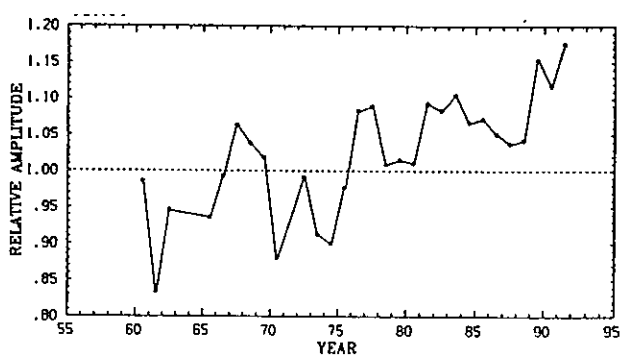

Fig. 5. Relative amplitudes of the seasonal cycle in atmospheric CO_2 at MLO. Data are from flask samples.

TABLE 1. Annual Rate of Increase in the Amplitude of the Seasonal Oscillation of Atmospheric CO_2 at Various Locations

Location	Approx. Latitude	Inclusive dates of observations	Rate of increase* (%)
BRW	71°N	July 1961-Sept. 1967 Jan. 1974-April 1991	1.04 ± 0.070
Station P	50°N	May 1969-June 1981	0.738 ± 0.259
La Jolla	33°N	Jan. 1970-June 1991	1.247 ± 0.200
MLO (continuous)	20°N	March 1958-June 1991	0.535 ± 0..042
MLO (flasks)	20°N	March 1960-June 1991	0.750 ± 0.121

*With reference to January 1, 1980.

In addition to short-term or local influences on CO_2, there are interannual changes usually related to El Niño events [*Keeling et al.*, 1989, p. 180]. These changes significantly affect the computed annual values of seasonal amplitude since the involved frequencies overlap. Comparison of seasonal amplitude plots, with plots showing the correlation of El Niño events with interannual variations in CO_2, reveal that the influence of one on the other is small, except for Christmas Island that lies close to the equator in the Pacific Ocean. Though separation of the two modes of variation is mathematically possible by subtraction of the interannual variation preceding computation of the annual seasonal amplitudes, it is not discussed here.

4. Conclusions

The above analyses and plots suggest that seasonal amplitudes of CO_2 concentration in the northern hemisphere may be on the upswing again after nearly a decade with little apparent variation. All three of the long-term northern hemisphere records analyzed here suggest that this is the case. Previously, it appeared that the seasonal CO_2 amplitudes had reached a maximum in the early 1980's and had declined to some extent since then, but it now appears that this may merely be a temporary pause in an overall rising trend in seasonal amplitudes.

Results from Station Alert, available only since 1985, tend to confirm the existence of a recent upturn in seasonal amplitude, as suggested by the fact that the average amplitude for the first half of the record relative to the mean is 0.97 while the average of the last three years is 1.05. A linear fit to the annual CO_2 amplitudes yields a gain factor of 1.52% per year with an error of 0.71% per year. Cape Kumukahi data show a relatively constant or slightly declining seasonal amplitude over the years 1980-1989, as do MLO continuous data, but due to somewhat noisier data recently, are inconclusive as to the existence of a recent upturn. Further measurements at these, and other such sites, should serve to verify whether or not a continuing rise in seasonal CO_2 amplitudes is occurring now.

5. References

Bacastow, R. B., C.D. Keeling, T.P. Whorf, Seasonal amplitude increase in atmospheric CO_2 concentration at Mauna Loa, Hawaii, 1959-1982, *J. Geophys. Res.*, *90*, 10,529-10,540, 1985.

Keeling, C. D., T.P. Whorf, C.S. Wong, R.D. Bellagay, The concentration of atmospheric carbon dioxide at ocean weather station P from 1969 to 1981, *J. Geophys. Res.*, *90*, 10,511-10,528, 1985.

Keeling, C. D., P.R. Guenther, and D.J. Moss, Scripps reference gas calibration system for carbon dioxide-in-air standards: Revision of 1985, *Report No. 4 of the Environmental Monitoring Programme of the World Meteorological Organization*, Geneva, 34 pp. and Addendum, 43 pp., 1986.

Keeling, C. D., R.B. Bacastow, A.F. Carter, S.C. Piper, T.P. Whorf, M. Heimann, W.G. Mook, and H. Roeloffzen, A three-dimensional model of atmospheric CO_2 transport based on observed winds: 1. Analysis of observational data, in *Aspects of Climate Variability in the Pacific and the Western Americas*, edited by D. H. Peterson, Geophysical Monograph American Geophysical Union, *55*, 165-236, Washington, DC, 1989.

Kelley, J. J., Jr., An analysis of carbon dioxide in the arctic atmosphere near Barrow, Alaska 1961 to 1967, *Contract N00014-67-A-0103-0007 NR 307-252*, 172 pp., Scientific Report of the United States Office of Naval Research, 1969.

Reinsch, C. H., Smoothing by spline functions, *Numerische Mathematik*, *10*, 177-183, 1967.

10. International Activities, 1990

In February the Soviet research ship *Akademik Korolev* was in port for 4 days to load a number of U.S. scientists and their equipment before embarking on the third SAGA cruise directed toward research on atmospheric and oceanic interactions.

In August Tom DeFoor was invited to visit several laboratories in the U.S.S.R., especially the principal lidar developmental facility at Obninsk, near Moscow. This U.S.S.R. visit also included attendance at the International Lidar Conference in Tomsk, Siberia. Two papers, co-authored with other CMDL staff, were presented in the U.S.S.R. In Obninsk, Tom DeFoor presented a report entitled "Stratospheric Aerosol Measurements at Mauna Loa Observatory 1974-1990: The Normalization and Calibration Problem." At the Lidar Conference in Tomsk, U.S.S.R., a poster paper was presented by Tom DeFoor entitled: "Uncertainties in the Application of Lidar for Observing Stratospheric Aerosol Optical Thickness."

B. Bodhaine participated in the Chemistry of the Global Atmosphere, the Seventh International Symposium of the Commission on Atmospheric Chemistry and Global Pollution, held 5-11 September in Chamrousse, France. He presented a paper entitled "Long-range transport and annual cycles in aerosol data at background stations."

L. Waterman visited CSIRO Division of Oceanography in Hobart, Tasmania, on June 18. Contact was made with D. Mackey whose group is developing an automated system for the underway measurement of pH, salinity and chlorophyll in surface ocean waters to calculate the air-sea exchange of CO_2. The apparatus is designed for deployment on both research and commercial vessels. Contacted also was R. Bailey, who heads the CSIRO "ships of opportunity" program, which is utilizing 11 commercial vessels to obtain ocean temperature profile measurements.

On June 21-22, L. Waterman visited the CGBAPS at Smithton and Cape Grim, Tasmania, to discuss with station personnel the collection of air samples in 2.5-L two-valve flasks with the new MAKS sampler. The CSIRO Division of Atmospheric Research at Aspendale was visited on June 25. Contacts were made with all staff involved with the cooperative Australian/USA air sampling at Cape Grim and the CMDL baseline observatories. The Trace Gases Group was briefed on CMDL Carbon Cycle Group activities.

On July 2, L. Waterman met with Ng Swee Khoon, Operations Manager, C.F. Sharp Shipping Agencies in Singapore for more discussions on a program to collect air samples in the South China Sea from the Chevron vessel *M/V Carla Hills* [*CMDL Summary Report 18*, 1989].

P. Tans participated in a workshop organized by the International Union of Pure and Applied Chemistry in Petten, The Netherlands, July 4-6, on the "Assessment of Uncertainties in the Projected Concentrations of Carbon Dioxide in the Atmosphere."

L. Waterman visited TRANET Station 558, Mahè, Seychelles Islands, July 4-7, and met with New Mexico State staff members L. Bradford and C. Garcia. Training was provided on the operation of the MAKS and regular collection of air samples with the new equipment was initiated. Sampling problems associated with tropical climate were identified and discussed. Three sites used for the collection of air samples under different wind regimes were inspected.

En route from the Seychelles to Boulder, L. Waterman visited J. Young Scientific Glassware Ltd. (Acton, England) on July 9; Blue Star Management Ltd. (London) on July 10; and the British Antarctic Survey (Cambridge) on July 11. J. Young manufactures the O-ring valves used on the NOAA flasks. A tour of the shop was provided, and quality control problems associated with valve breakage were discussed. Contact was made with Capt. W. Houghton Boreham at Blue Star who was briefed on the success of the *M/V Southland Star* sampling. Information was obtained on the operation of large container vessels circumnavigating the southern oceans at high latitudes, and the possibility of air sampling on one of these carriers, the *M/V ACT 7*. L. Waterman also met with S. Morrison of the British Antarctic Survey (BAS) to discuss the air sampling at Bird Island, South Georgia, and Halley Bay, Antarctica. Problems of sampling in extreme cold weather were discussed and possible solutions were suggested. Plans were made for BAS personnel to visit Boulder.

S. Morrison, S. Colwell, and J. Cooper, of the BAS, visited Boulder August 15-21 to receive a briefing on the NOAA sampling network operations and training with the MAKS. Colwell is assigned to Halley Bay and Cooper to Bird Island for the 1991-1992 tour of duty. Two MAKS units were hand-carried to BAS to take to the stations.

P. Tans chaired the WMO Meeting of Experts on Carbon Dioxide Concentration and Isotopic Measurement Techniques, on October 14-19, Lake Arrowhead, California.

Y.S. Chung, Korea National University of Education, visited Boulder on November 13 and received training with the MAKS unit and 2.5-L two-valve flasks. The establishment of a sampling site on the Tae-ahn Peninsula (TAP) on the west coast of South Korea was discussed. Chung hand-carried a MAKS to Korea and the first samples were collected at TAP on November 24.

Under the auspices of the WMO, calibration checks were conducted on 15 foreign Dobson ozone spectrophotometers calibrated in the past by NOAA-CMDL scientists. The work was performed July 21-August 9, 1990, at Arosa, Switzerland (see Section 5.1.5). Three additional foreign Dobson instruments were calibrated for the first time. While enroute to the Arosa Dobson instrument comparisons, French Dobson instrument 49 was calibrated at Haute Provence, France.

J. Harris traveled to Seoul and Cheongwon, South Korea, in September to present two seminars concerning trajectory models and the transport of air pollution and trace gases. These were given at the Korea National University of Education and the Korean National Institute of Environmental Research. Discussions were held to determine areas for collaborative research.

In November S. Oltmans traveled to Bermuda to calibrate the AEROCE network surface ozone monitor.

J. Butler, J. Elkins, T. Swanson, and B. Hall participated on Legs 1 and 2 of the third Soviet-American Gas and Aerosol Experiment (SAGA III), conducted from February through April 1990, on the Soviet research vessel *Akademik Korolev*. James Butler met with collaborating Soviet scientists in Seattle during August 1990 and in San Francisco during December 1990. J. Butler also gave talks on SAGA III results at NOAA/PMEL and at the AGU meeting in San Francisco.

J. Elkins was an invited participant in the European Workshop on Nitrous Oxide Emissions held in Lisbon, Portugal, June 6-8.

J. Elkins gave an invited presentation at the 7th International Symposium of the Commission on Atmospheric Chemistry and Global Pollution (CACGP) held in Chamrousse, France, September 5-11.

J. Elkins worked with P. Fraser of CSIRO on installing a new GC system and on making measurements from ice cores.

11. Publications and Presentations by CMDL Staff, 1990

Bodhaine, B.A., Aerosol instrumentation on the NOAA WP-3D during the third Arctic gas and aerosol sampling program, paper A51B-10 presented at the American Geophysical Union Fall Meeting, San Francisco, December 3-7, 1990.

Bodhaine, B.A., and J.M. Harris, Long-range transport and annual cycles in aerosol data at background stations, paper presented at the Seventh International Commission on Atmospheric Chemistry and Global Pollution, Chamrousse, France, September 5-11, 1990.

Bodhaine, B.A., and M.K. Shanahan, Condensation nucleus and aerosol scattering extinction measurements at the South Pole Observatory: 1979-1988, *NOAA Data Rep. ERL CMDL-1*, NOAA Climate Monitoring And Diagnostics Laboratory, Boulder, CO, 148 pp., 1990.

Bodhaine, B.A., J.J. DeLuisi, J.F. Boatman, M.J. Post, and J.M. Rosen, The front range lidar, aircraft, and balloon experiment, *NOAA Data Rep. ERL CMDL-2*, NOAA Climate Monitoring and Diagnostics Laboratory, Boulder, CO, 27 pp., 1990.

Butler, J.H., Global warming and ozone depletion, paper presented at Back to the Future: A Workshop on Change, Denver Museum of Natural History, Denver, CO, November 28, 1990.

Butler, J.H., Global warming, ozone depletion, and trace gases in the ocean and atmosphere, paper presented at Humboldt State University, Arcata, CA, September 6, 1990.

Butler, J.H., Measurement of CFC-22, CFC-113, and Halons 1211 and 1301 in the atmosphere, paper presented at the 1990 Johnson Conference, Our Changing Atmosphere: Challenges in Measurement Technology, sponsored by the American Society for Testing Materials Committee D-22 on Sampling and Analysis of Atmospheres, Johnson, VT, July 8-13, 1990.

Butler, J.H., J.W. Elkins, T.J. Conway, B.D. Hall, T.H. Swanson, and T.M. Thompson, Reflections of surface-ocean trace gas concentrations in the atmospheric boundary layer: Implications for air-sea exchange and atmospheric transport, *EOS, 71(43)*, 226, American Geophysical Union Fall Meeting, San Francisco, December 3-7, 1990.

Butler, J.H., J.W. Elkins, B.D. Hall, T.H. Swanson, and T.M. Thompson, Measurement of N_2O and halocarbons on the third Soviet-American Gas and Aerosol Experiment (SAGA III), presented at a bilateral meeting of U.S. and Soviet scientists at NOAA/PMEL, Seattle, WA, August 27-31, 1990.

Bodhaine, B.A., R.C. Schnell, and P.J. Sheridan, Aerosol instrumentation on the NOAA WP-3D during the third Arctic Gas and Aerosol Sampling Program, *EOS, 71(43)*, 1262, 1990.

Church, T.M., R. Arimoto, L.A. Barrie, F. Dehairs, F. Dulac, T.D. Jickells, L. Mart, W.T. Sturges, and W.H. Zoller, The long-range atmospheric transport of trace elements: A critical evaluation, in *The Large Scale Atmospheric Transport of Natural and Contaminant Substances*, edited by A.H. Knapp and M.S. Kaiser, NATO ASI Series, Kluwer, Dordrecht, 321 pp., 1990.

Conway, T.J., L.P. Steele, P.M. Lang, and L.S. Waterman, The NOAA/GMCC carbon dioxide and methane measurements at Cape Grim, in *Baseline 88*, edited by S.R. Wilson and G.P. Ayers, 1990.

Conway, T.J., L.P. Steele, and P.C. Novelli, Measurements of CO_2, CH_4, and CO during AGASP III, paper presented at the American Geophysical Union Fall Meeting, San Francisco, December 3-7, 1990.

DeFoor, T.E., J.J. DeLuisi, D.U. Longenecker, and W. Chu, Aerosol measurements at Mauna Loa Observatory 1974-1990: The normalization and calibration problem, a report presented at the Soviet-American Conference on Lidar Intercomparison in Obninsk, U.S.S.R., August, 1990.

DeLuisi, J.J., T.E. DeFoor, D.U. Longenecker, and W. Chu, Uncertainties in the application of lidar for observing stratospheric aerosol optical thickness, a poster paper presented at the 15th International Laser Radar Conference in Tomsk, Siberia, U.S.S.R., August 1990.

Dutton, E.G., Annual forcing of the surface radiation balance diurnal cycle measured from a high tower near Boulder, Colorado, *J. Climate, 3*, 1400-1408, 1990.

Dutton, E.G., Comments on major volcanic eruptions and climate: A critical evaluation, *J. Climate, 3*, 587-588, 1990.

Elkins, J., CFCs and nitrous oxide measurements, paper presented at the CSIRO Annual Meeting in Melbourne, Australia, November 29-30, 1990.

Elkins, J.W., J.H. Butler, B.D. Hall, T. Swanson, J. Harris, and G. Herbert, Measurements of atmospheric halocarbons during SAGA-3: analysis of trajectories, meteorology, and comparison with other long-lived tracers, *EOS, 71(43)*, 1229, American Geophysical Union Fall Meeting, San Francisco, December 3-7, 1990.

Elkins, J.W., B.D. Hall, and J.H. Butler, Laboratory and field investigations of the emissions of nitrous oxide from biomass burning, presented at the Chapman Conference on Global Biomass Burning: Atmospheric, Climatic and Bioshperic Implications, Williamsburg, VA, March 19-23, 1990.

Elkins, J.W., T.M. Thompson, J.H. Butler, and B.D. Hall, The global budget of atmospheric nitrous oxide inferred from measurements obtained at NOAA/CMDL stations, in natural waters, and during combustion studies, presented at the Seventh International Symposium of the Commission on Atmospheric Chemistry and Global Pollution (CACGP), Chamrousse, France, September 4-11, 1990.

Hall, B.D., J.W. Elkins, J.H. Butler, and T.M. Thompson, Improvements in nitrous oxide and halocarbon measurements at the South Pole, *Antarctic J. U.S., 25(5)*, 1990.

Harrison, R.M., W.T. Sturges, A.-M.N. Kitto, and Y. Li, Kinetics of the evaporation of ammonium chloride and ammonium nitrate aerosols, *Atmos. Environ., 24A*, 1883-1888, 1990.

Herbert, G.A., Secular changes in tropospheric temperatures in the northern hemispheric polar region, presented at the International Conference on the Role of the Polar Regions in Global Change, University of Alaska, Fairbanks, Alaska, June 11-15, 1990.

Herbert, G.A., B.J. Stunder, R.C. Schnell, B.A. Bodhaine, and S. J. Oltmans, Meteorological conditions during the AGASP-III flights, March 1989, presented at the Fall 1990 American Geophysical Union Meeting, San Francisco, December 7, 1990.

Jickells, T.D., R. Arimoto, L.A. Barrie, T.M. Church, F. Dehairs, F. Dulac, L. Mart, W.T. Sturges, and W.H. Zoller, The long-range atmospheric transport of trace elements: Four case studies, in *The Large Scale Atmospheric Transport of Natural and Contaminant Substances*, edited by A.H. Knapp and M.S. Kaiser, NATO ASI Series, Kluwer, Dordrecht, 321 pp., 1990.

Komhyr, W.D., and R.M. Rosson (Eds.), *Climate Monitoring and Diagnostics Laboratory, No. 18: Summary Report 1989*, 141 pp., NOAA Climate Monitoring And Diagnostics Laboratory, Boulder, CO, 1990.

Komhyr, W.D., and R.D. McPeters, Dobson spectrophotometer 83.0 A standard for ground-based and satellite total ozone measurements, in *Digest of Topical Meeting on Optical Remote Sensing of the Atmosphere, 1990, 4*, 398-401, Optical Society of America, Washington, DC, 1990.

Komhyr, W.D., J.A. Lathrop, and D.P. Opperman, ECC ozonesonde and Dobson Umkehr observations during STOIC 1989, in *Digest of Topical Meeting on Optical Remote Sensing of the Atmosphere, 1990, 4*, 441-444, Optical Society of America, Washington, DC, 1990.

Komhyr, W.D., J.A. Lathrop, V.N. Arbuzova, V.U. Khattatov, V.I. Pilipenko, and V.V. Radakov, ECC ozonesonde observations at Mirny, Antarctica, during 1989, *NOAA Data Rep. ERL CMDL-4*, 84 pp., NOAA Climate Monitoring And Diagnostics Laboratory, Boulder, CO, 1990.

Komhyr, W.D., E.A. Crozer, J.A. Lathrop, and M.A. Winey, ECC ozonesonde observations at South Pole, Antarctica, during 1989, *NOAA Data Rep. ERL CMDL-5*, 247 pp., NOAA Climate Monitoring and Diagnostics Laboratory, Boulder, CO, 1990.

Komhyr, W.D., S.J. Oltmans, R.D. Grass, and R.K. Leonard, Possible influence of long-term sea surface temperature anomalies in the tropical Pacific on global ozone, paper presented at the Antarctic Ozone Conference, Universidad International Menendez Pelayo, Santander, Spain, July 30, 1990.

Komhyr, W.D., R.D. Evans, R.D. Grass, G.L. Koenig, J.A. Lathrop, and D.M. Quincy, Dobson spectrophotometer, ECC ozonesonde, and ground-based NOAA SBUV-2, S/N-2 satellite instrument comparison ozone observations, *NOAA Data Rep. ERL CMDL-6*, 17 pp., NOAA Climate Monitoring and Diagnostics Laboratory, Boulder, CO, 1990.

Lang, P.M., L.P. Steele, R.C. Martin, and K.A. Masarie, Atmospheric methane data for the period 1983-1985 from the NOAA/GMCC global cooperative flask sampling network, *NOAA Tech. Memo. ERL CMDL-1*, 90 pp., NOAA Climate Monitoring and Diagnostics Laboratory, Boulder, CO, 1990.

Lang, P.M., L.P. Steele, and R.C. Martin, Atmospheric methane data for the period 1986-1988 from the NOAA/CMDL global cooperative flask sampling network, *NOAA Tech. Memo. ERL CMDL-2*, 108 pp., NOAA Climate Monitoring and Diagnostics Laboratory, Boulder, CO, 1990.

Li, S.-M., J.W. Winchester, J.D. Kahl, S.J. Oltmans, R.C. Schnell, and P.J. Sheridan, Arctic boundary layer ozone variations associated with nitrate, bromine, and meteorology: A case study, *J. Geophys. Res., 95(D13)*, 22,433-22,440, 1990.

Lipschultz, F., S. C. Wofsy, B. B. Ward, L. A. Codispoti, G. Friedrich, and J. W. Elkins, Bacterial transformations of inorganic nitrogen in the oxygen-deficient waters of the Eastern Tropical South Pacific Ocean, *Deep-Sea Res., 37(10)*, 1513-1541, 1990.

Montzka, S.A., Oxygenated hydrocarbon measurements in rural Alabama, presented at the American Geophysical Union 1990 Fall Meeting, December 3-7, 1990, San Francisco, 1990.

Montzka, S.A., B.M. Hybertson, R.M. Barkley, and R.E. Sievers, Low temperature oxidation of $YBa_2Cu_3O_6.0$ with nitrogen dioxide, *J. Mater. Res., 6*, 891, 1991.

Novelli, P.C., J. W. Elkins, and L. P. Steele, Carbon monoxide standards for atmospheric measurements., *EOS, 71(43)*,1249, American Geophysical Union Fall Meeting, December 3-7, San Francisco, 1990.

Parungo, F., C.T. Nagamoto, P.J. Sheridan, and R.C. Schnell, Aerosol characteristics of Arctic haze sampled during AGASP-II, *Atmos. Environ., 24A*, 937-949, 1990.

Parungo, F., C.N. Nagamoto, P. Sheridan, and R. Schnell, Individual particle analysis of aerosol samples collected during AGASP-III, *EOS, 71(43)*, 1262, 1990.

Robinson, E., and T.E. DeFoor, Recent stratospheric aerosol lidar observations at Mauna Loa Observatory, Hawaii, presented at the American Geophysical Union Fall Meeting in San Francisco, December 3-7, 1990.

Ryan, S.C., Diurnal CO_2 exchange and photosynthesis of the Samoa tropical forest, *Global Biochem. Cycles, 4*, 69-84, 1990.

Ryan, S.C., Diurnal CO_2 exchange and photosynthesis of the Samoa tropical forest, presented at the American Geophysical Union Spring Meeting, Baltimore, MD, April, 1990.

Savoie, D. L., J. M. Prospero, R. Arimoto, R. A. Duce, and B. Bodhaine, Concentrations of particulate nitrogen and sulfur species and mineral dust in the near-surface atmospheric boundary layer over the Pacific Ocean during the GLOBE survey flights, paper A41C-9 presented at the American Geophysical Union Fall Meeting, San Francisco, December 3-7, 1990.

Sheridan, P.J., Analytical electron microscope analysis of aerosol sampled over White Sands Missile Range, New Mexico, December 11-15, 1989, Final report to the U.S. Army Atmospheric Sciences Laboratory, NOAA-Cooperative Institute for Research in Environmental Sciences, Boulder, CO, 37 pp., 1990.

Sheridan, P.J., R.C. Schnell, W.H. Zoller, J.J. Zieman, and R.A. Rasmussen, Composition of Br-containing aerosols and gases related to boundary layer ozone destruction in the Arctic, *EOS, 71(43)*, 1265, 1990.

Sheridan, P.J., R.C. Schnell, and J.F. Boatman, Wintertime black carbon aerosol measurements over the southwestern United States, December 1989, in *Climate Monitoring and Diagnostics Laboratory No. 18: Summary Report 1989*, edited by W.D. Komhyr and R.M. Rosson, pp. 77-80, NOAA Climate Monitoring And Diagnostics Laboratory, Boulder, CO, 1990.

Stone, R., E.G. Dutton, and J.J. DeLuisi, Surface radiation and temperature variations associated with cloudiness at the South Pole, *Ant. J. U. S., 24*, 230-232, 1990.

Sturges, W.T. and B.E. Taylor, Atmospheric concentrations of chlorinated solvents around a nuclear processing plant in Colorado, *Environ. Technol., 11*, 1063-1070, 1990.

Sturges, W.T., New insight into chemical reactions of tropospheric ozone and bromine at polar sunrise in the Alaskan Arctic, invited presentation to Atmospheric Environment Service, Environment Canada, Toronto, 1990.

Sturges, W.T., Bromine and ozone atmospheric chemistry in the Arctic, paper presented at the International Conference on the Role of the Polar Regions in Global Change, Geophysical Institute, University of Alaska at Fairbanks, June 11-13, 1990.

Sturges, W.T., R.C. Schnell, S. Landsberger, S.J. Oltmans, J.M. Harris, and S.-M. Li, Chemical and meteorological influences on surface ozone destruction at Barrow, Alaska, during Spring 1989, American Geophysical Union 1990 Fall Meeting, San Francisco, 1990.

Sturges, W.T., New insight into chemical reactions of tropospheric ozone and bromine at polar sunrise in the Alaskan Arctic, invited paper presented to the Air Quality and Monitoring Group of Atmospheric Environment Service in Toronto, Canada, on July 17, 1990.

Tans, P.P., K.W. Thoning, W.P. Elliott, and T.J. Conway, Error estimates of background atmospheric CO_2 patterns from weekly flask samples, *J. Geophys. Res., 95*, 14063-14070, 1990.

Tans, P.P., I.Y. Fung, and T. Takahashi, Observational constraints on the global atmospheric CO_2 budget, *Science 247*, 1431-1438, 1990.

Tans, P.P., The contemporary global carbon cycle from the perspective of an atmospheric scientist, presented at the Annual Meeting of the American Society of Plant Physiologists, Indianapolis, July 29, 1990.

Tans, P.P., An observational strategy for assessing the role of terrestrial ecosystems in the global carbon cycle: scaling down to regional levels, presented at the Meeting on Scaling Processes Between Leaf and Landscape Levels, Snowbird, UT, December 2-5, 1990.

12. Acronyms and Abbreviations

ACR	active cavity radiometer
ADVR	Advanced Very-High-Resolution Radiometer
AEM	analytical electron microscope
AEROCE	Atmosphere/Ocean Chemistry Experiment
AES	Atmospheric Environment Service, Canada
AGASP	Arctic Gas and Aerosol Sampling Program
AGL	above ground level
ALT	Alert Observatory, Canada
ANL	Argonne National Laboratory
ANSTO	Australian Nuclear Science and Technology Organization
AOML	Atlantic Oceanographic and Meteorological Laboratory, Miami, Florida (ERL)
AQG	Air Quality Group, Boulder, Colorado (ARL)
ARL	Air Resources Laboratory, Silver Spring, Maryland (ERL)
ARM	Aerosols and Radiation Monitoring Group, Boulder, Colorado (CMDL)
ASA	Antarctic Support Associates, Inc.
ASASP	Active Scattering Aerosol Spectrometer Probe
ASCII	American Standard Code For Information Interchange
ASL	above sea level
ATS	Application Technology Satellite
BAO	Boulder Atmospheric Observatory
BAS	British Antarctic Survey
BSRN	Baseline Surface Radition Network
BRW	Barrow Observatory, Barrow, Alaska (CMDL)
CADIC	Centro Austral de Investigaciones Cientificas, Argentina
CAF	Clean Air Facility
CAMS	Control and Monitoring System
CD-ROM	compact disk/random only memory
CEAREX	Coordinated Eastern Arctic Experiment
CFC	chlorofluorcarbon
CFC-11	trichlorofluoromethane
CFC-12	dichlorodifluoromethane
CIRES	Cooperative Institute for Research in Environmental Sciences, University of Colorado, Boulder, Colorado
CMDL	Climate Monitoring and Diagnostics Laboratory, Boulder, Colorado (ERL) (formerly GMCC)
CN	condensation nuclei
CNC	condensation nucleus counter
COR	correlation coefficient
CSIRO/DAR	Commonwealth Scientific and Industrial Research Organization/Division of Atmospheric Research, Australia
DB	direct-beam [irradiance]
DMS	dimethyl sulfide
DNA	Deoxyribonucleic acid
DSIR	Department of Scientific and Industrial Research, New Zealand
DU	Dobson units
ECC	electrochemical concentration cell
ECD	electron capture detector
EC-GC	electron capture-gas chromatograph
ECMWF	European Centre for Medium Range Weather Forecasts
EKTO	[a commercial name for a prefabricated building]
EML	Environmental Measurements Laboratory
ENSO	El Niño/Southern Oscillation
EPA	Environmental Protection Agency
ERBE	Earth Radiation Budget Experiment
ERL	Environmental Research Laboratories, Boulder, Colorado (NOAA)
FRLAB	Front Range Lidar, Aircraft, and Balloon experiment
FSSP	Forward Scattering Spectrometer Probe
FTIR	Fourier transform infrared (spectroscopy)

GC	gas chromatograph
G.E.	General Electric
GSFC	Goddard Space Flight Center
GLOBE	Global Backscatter Experiment
GRIB	"Gridded in Binary" format for ECMWF-TOGA analyses
HP	Hewlett-Packard
HST	Hawaii standard time
IC	ion chromatography
IR	infrared
ISWS	Illinois State Water Survey
ITT	International Telephone and Telegraph
JPL	Jet Propulsion Laboratory
LEAPS	Low Electron Attachment Potential Species
LORAN	LOng Range Aid to Navigation
LST	local standard time
LW	longwave
LWD	longwave downward irradiance
LWRF	longwave radiative forcing
MAKS	Martin and Kitzis Sampler (portable sampler)
MLO	Mauna Loa Observatory, Hawaii (CMDL)
MLOPEX	MLO Photochemical Experiment
MRI	Meteorology Research, Inc.
MSL	mean sea level
NADP	National Atmospheric Deposition Program
NASA	National Aeronautics and Space Administration
NCAR	National Center for Atmospheric Research
NDIR	non-dispersive infrared analyzer
NESDIS	National Environmental Satelite, Data and Information Service (NOAA)
NIP	normal incidence pyrheliometer
NIST	National Institute for Standards and Technology (formerly NBS)
NMC	National Meteorological Center
NOAA	National Oceanic and Atmospheric Administration
NOAH	Nitrous Oxide And Halocarbons Group, Boulder, Colorado (CMDL)
NRBS	non-Rayleigh backscatter
NSF	National Science Foundation
NSO	National Solar Observatory
NWR	Niwot Ridge, Colorado
NWS	National Weather Service
OGIST	Oregon Graduate Institute of Science and Technlogy
PBL	planetary boundary layer
PC	personal computer
PDB	pee dee belemnite
PESA	proton elastic scattering analysis
PIXE	Proton-Induced X-ray Emission
PMEL	Pacific Marine Environmental Laboratory, Seattle, Washington (ERL)
PMOD	Physikalisch-Meteorologisches Observatorium Davos [World Radiation Center]
PMT	photomultipier tube
PSC	Polar stratospheric cloud
PSP	precision sunphotometer
P^3	Portable Pressurizer Pack (air sampler)
QBO	quasi-biennial oscillation
RITS	Radiatively Important Trace Species
RSD	residual standard deviation
SAGE	Stratospheric Aerosol and Gas Experiment
SASP	Surface Air Sampling Program
SBUV	solar backscattered ultraviolet (satellite ozone instrument)
SC	sky cover
SEAREX	Sea-Air Exchange Experiment

SEASPAN	SEAREX South Pacific Aerosol Network
SERI	Solar Energy Research Institute
SIO	Scripps Institution of Oceanography
SMO	Samoa Observatory, American Samoa (CMDL)
SOI	Southern Oscillation Index
SOLRAD	Solar Radiation
SPO	South Pole Observatory, Antarctica (CMDL)
SRF	spectral response function
SRM	standard reference material
SSL	slightly stable layer
SST	sea-surface temperature
TECO	Thermal Electron Company
TEM	transmission electron microscope
TOGA	Tropical Ocean Global Atmosphere
TOMS	Total Ozone Mapping Spectrometer
TSI	Thermo Systems Incorporated
TSL	Technical Services Laboratory
TSP	total suspended particulate
UCI	University of California, Irvine
URAS	[a commercial CO_2 analyzer]
URI	University of Rhode Island
USDA	United States Department of Agriculture
USGS	United States Geological Survey
UT	universal time
UV	ultraviolet
UVB	ultraviolet B spectral band
WMO	World Meteorological Organization
WPL	Wave Propagation Laboratory, Boulder, Colorado (ERL)

☆U.S. GOVERNMENT PRINTING OFFICE: 1992-674-362